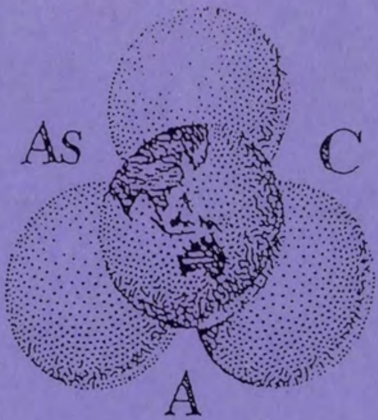

AsCA'95

Program and Abstracts

Thai
Thai Airways International

AsCA'95

2nd Conference of the
Asian Crystallographic Association

Chulalongkorn University

Bangkok, Thailand

22-24 November 1995

Program and Abstracts

Organising Committees

International Organising Committee

W.T. Robinson	New Zealand	(Chairman)
S. Hall	Australia	
K. Kannan	India	
C. Kennard	Australia	
K. Nishikawa	Japan	
A. H. Othman	Malaysia	
P. Phavanantha	Thailand	
J. Simpson	New Zealand	
M. Tokonami	Japan	
T. Uragami	Japan	

Secretariat (New Zealand)

Ward Robinson
Jim Simpson
Jan Wikaira

International Program Committee

Y. Ohashi	Japan	(Chairman)
S. Chang	Taiwan	
R. Chidambaram	India	
T. Hambley	Australia	
G. Jameson	New Zealand	
E.N. Maslen	Australia	
K. Ohsumi	Japan	
T. Tsukihara	Japan	
Z. Zhang	China	

Local Organising Committee

Phathana Phavanantha (Chairman)
Narongsak Chaichit
Chaisingh Poorakkiat
Tawee Tangasiri
Pongchan Thinapong
Ahpisit Ungkitchanukit
Sajec Wongchaiboon
Chaveng Pakawatchai
Achara Prichavudhi
Srinuan Thanomkul
Wimonrat Trakarnpruk
Siri Varothai

General Information

Conference Venue and Accommodation

The map inside the front cover of the Abstract Book shows the locations of the University Halls, Krit Thai Mansion, Novotel Siam Square, Siam Intercontinental Hotel, Florida Hotel and the Asia Hotel in relation to the Conference Venue. The venues for the Welcoming Reception and the Farewell Banquet are also indicated.

Registration/Information Desk

Prior to the opening of the conference, a Registration/Information Desk will be located at Vittaya Nives Hall and will be open from 18.30 to 19.30 on both Monday 20th and Tuesday 21 November. From 08.30 on Wednesday November 22, the Registration/Information Desk will be situated outside the Main Lecture Hall in the Institute Building III and will remain open for the remainder of the Conference.

The Conference Venue

The Conference will be held in Institute buildings II and III shown on the map. Poster sessions will be on the ground floor of Institute Building III, the main lecture hall is on the 1st floor and one other lecture room is on the 2nd floor. The trade exhibitions and the other 2 lecture rooms will be in adjacent rooms on the 1st floor of Institute building II.

Name Badges

Name badges will be issued to all registrants in their conference satchels. Participants are kindly requested to wear their badges throughout the meeting. For the purpose of easy identification the following colour scheme will be used

Active participants	Green
Accompanying Persons	Yellow
Local Organising Committee	Red
Exhibitors	Blue
International Organising Committee, Secretariat and AsCA Council Members	Purple

Mail and Messages

Mail for conference participants will be available from Vittaya Nives Hall or from the Registration Desk

Telephones

Telephones for outgoing International calls are available in the rooms at SASA International House and the Krit Thai Mansion (an additional charge is levied for International calls). International card-phones are available on the University Campus

Meals and Refreshments

Morning and afternoon coffee

Morning and afternoon coffee will be provided for all full and student participants at the conference venue.

Lunch

Lunches are provided free of charge for all full and student participants at the conference venue. Conference badges must be worn.

Poster sessions

Light refreshments will be provided during the poster sessions sponsored by ***Mac Science.***

Social Events

Welcoming Reception

A welcoming reception and get together will be held at the Thai Pavilion from 19.30 to 21.30 on Tuesday November 21 for all registrants (full student and accompanying persons). Refreshments and snacks will be served. The reception is sponsored by ***Siemens***

Farewell Banquet

A farewell banquet for all registrants (full student and accompanying persons) will be held in Sasapata Sala on Thursday November 23; 19.30 for 20.00. Dress is informal. The banquet is sponsored by ***Rigaku.***

Local Tours

Participants are reminded that tours of Bangkok and district can be arranged daily at the Registration/Information Desk. A group tour is planned for Saturday 25th November at a cost of $US40 per person.

Opening Ceremony

The opening ceremony for AsCA'95 will be held in the main lecture theatre in Institute Building III from 8.30-8.45 on Wednesday November 22nd. The speakers will be:

Professor Ward T. Robinson,	President, Asian Crystallographic Association
Professor Philip Coppens,	President, International Union of Crystallography
Professor Dr Supachai Yavaprabhas,	Vice President for International Affairs, Chulalongkorn University
Conference announcements: Professor Phathana Phavanantha	Chairman, Local Organising Committee

Society Meetings

Asian Crystallographic Association

Wednesday 22 November , SASA International House

18.30 International Organising Committee
19.00 Council Meeting

Sponsors of AsCA'95

The Asian Crystallographic Association wishes to thank the following professional bodies and institutions for their contributions towards the organisation and funding of AsCAuote 95

The International Union of Crystallography
The Crystallographic Society of Japan
The Society of Crystallographers in Australia
The Crystallography Group of the New Zealand Institute of Chemistry
Chulalongkorn University
The Thai Crystallographic Association

The Asian Crystallographic Association also wishes to gratefully acknowledge generous financial support from the following companies:

Enraf-Nonius (Columbia Trade Company)
Mac Science
Marresearch
Rigaku
Siemens
Thai Airways International
Xray Research

Scientific Programme

The overall programme is shown in the following Table. Coffee, tea and fruit juice will be served at the times stated in the programme. Participants giving poster presentations are reminded that they should be at their posters for the last two hours of the poster session

	22 (Wed)	**23 (Thu)**	**24 (Fri)**
8:30 - 8:45	Official Opening *(S. Yavaprabhas)*		
9:00 - 9:45	Plenary lecture *(M. Ando)*	Plenary lecture *(T. Matsuzaki)*	Plenary lecture *(B. O'Connor)*
9:45 - 10:30	Plenary lecture *(Hai-fu Fan)*	Plenary lecture *(G. Desiraju)*	Plenary lecture *(Y. Wang)*
10:30 - 11:00	Coffee Break	Coffee Break	Coffee Break
11:00 - 12:30	**Microsymposium** A B C MS02 MS17 MS01 (1A1 1B1 1C1)	**Microsymposium** A B C MS06 MS05 MS08 (2A1 2B1 2C1)	**Microsymposium** A B C MS18 MS07 ——
12:30 - 13:45	**Lunch**	**Lunch**	**Lunch**
13:45 -15:15	**Microsymposium** A B C MS09 MS17 MS01 (1A2 1B2 1C2)	**Microsymposium** A B C MS10 MS12 MS04 (2A2 2B2 2C2)	**Microsymposium** A B C MS11 MS14 —— (3A2 3B2)
15:15 -15:30	Coffee Break	Coffee Break	Coffee Break
15:30 -17:45	**Poster Session** (1P01 - 1P60)	**Poster Session** (2P01 - 2P60)	**Poster Session** (3P01 - 3P60)

- Invited lecture by Prof P Coppens (3PL3) is held in MS18
- Seating capacities of the rooms, A: 250; B; 40; C: 30
- All of the Plenary lectures are given in room A

MS-01 Diffraction theory and phase problem (*Prof. S. -L. Chang*)
MS-02 Synchrotron radiation (*Prof. E. N. Maslen*)
MS-04 Neutron diffraction (*Dr. A. S. Sequeira*)
MS-05 Recent development of Powder diffraction (*Prof. T. Yamanaka*)
MS-06 Methods in biological crystallography (*Dr. G. Jameson*)
MS-07 Crystal growth and characterisation (*Prof. T. Ohachi*)
MS-08 New Instrumentation (*Prof. H. Hashizume*)
MS-09 Mineral and inorganic compounds (*Prof. K. Ohsumi*)
MS-10 Organic and organometallic compounds (*Prof. Y. Kai*)
MS-11 Structural biology (*Prof. T. Tsukihara*)
MS-12 Interface, films and surfaces (*Prof. O. Nittono*)
MS-13 Phase transformation (*Prof. T. R. Welberry*)
MS-14 Organic crystal engineering (*Prof. F. Iwasaki*)
MS-17 Data bases and software (*Prof. S. R. Hall*)
MS-18 Charge density (*Prof. K. Tanaka*)

Scientific Programme

[illegible]

Program Schedule

November 22 Room A

Plenary Lecture 1PL1 (*Prof. S. Wilkins*) 9:00-9:45

1PL1 Synchrotron Radiation Science in Crystallography — Present and Future — by *Ando, M.*

Plenary Lecture 1PL2 (*Prof. T. Ashida*) 9:45-10:30

1PL2 Direct Methods - New Developments Outside The Traditional Field by *Fan, H.-F.*

Coffee Break 10:30-11:00

MS02 Synchrotron radiation (*Prof. E.N. Maslen*) 11:00-12:30

1A11 Single Crystal X-ray Diffraction Using SR in Material Science by *Ishizawa, N.*
11:00

1A12 Microcrystallography by Synchrotron Radiation by *Ohsumi, K.*, Hagiya, K.,
11:18 Miyamoto, M. & Ohmasa, M.

1A13 Multiple-Detector System for Powder Diffractometer Using Synchrotron Radiation
11:36 and High-Resolution Diffraction Data Obtained with It by *Toraya, H.*, Hibino, H. & Ohsumi, K.

1A14 Electron Density Imaging with Synchrotron X-radiation by Maslen, E.N. & *Streltsov, V.*
11:54 *A.*

1A15 Texture Study on Synchrotron Radiation by *Abovian, E.S.*, Grigorian, A.H. &
12:12 Trouni, K.G.

Lunch 12:30-13:45

MS09 Mineral and inorganic compounds (*Prof. K. Ohsumi*) 13:45-15:15

1A21 Modulated Structures in the $Nb_2Zr_{x-2}O_{2x+1}$ and $Ta_2Zr_{x-2}O_{2x+1}$ ($7.1 \leq x \leq 12$)
13:45 Solid Solution Fields by *Schmid, S.*, Futterer, K., Thompson, J. G., Withers, R. L. & Ishizawa, N.

1A22 X-ray Analysis of 4f-Electron Density in CeB_6 crystals by *Tanaka, K* & Ohnuki, Y.
14:05

1A23 A Joint X-Ray and Electron Diffraction Study of MgO by Abramov, Y. A., Avilov, A.S.,
14:25 Belokoneva, E.L., Rushdi, K., Feil, D., Tsirelson, V.G. & *Okamura, F.P.*

1A24 Crystal Structure and Magnetic Properties of the Linear Homo or Hetero Trinu-
14:45 clear Metal Complexes of Bis(2-pyridyl)amide Ligand by Lin, C.-C., Yang, E.-C., Lee, G.-H. & *Peng, S.-M.*

Coffee Break 15:15-15:30

Poster Session15:30-17:45

November 22 Room B

MS17 Data bases and software I (*Prof. S. R. Hall*) 11:00-12:30

1B11 CIF as the Common Language of Crystallography by *McMahon, B.*
11:00

1B12 The Brookhaven Protein Databank by *Sussman, J. L.*
11:30

1B13 Xtal_GX: CIF-Entry Graphics for Geometry Analysis by *Hall, S.*, Boukay, D. D.,
12:00 Hester, J. & Grossie, D.

1B14 Maximum Entropy Deconvolution in X-ray Diffraction by *Kalceff, W.*, Armstrong, N.
12:15 & Cline, J.P.

Lunch 12:30-13:45

MS17 Data bases and software II (*Prof. S. R. Hall*) 13:45-15:45

1B21 The Macromolecular CIF Dictionary Version 1.0 by *Bourne, P. E.*
13:45

1B22 The Nucleic Acid Database Project by Berman, H. M., Clowney, L., Gelbin, A.,
14:15 Hsieh, S. H. & *Westbrook, J.*

1B23 TITAN: A Molecular Graphics Program to Aid Structure Solution and Refinement
14:45 with the SHELX Suite of Programs. by Hunter, K. A. & *Simpson, J.*

1B24 MOLDRAW: Molecular Graphics For MS-Windows by Ugliengo, P., Chiari, G. &
15:00 *Viterbo, D.*

Coffee Break 15:15-15:30

Poster Session15:30-17:45

November 22 Room C

MS01 Diffraction theory and phase problem (*Prof. S.-L. Chang*) 11:00-12:30

1C11 X-Ray Phase Recovery: Mapping of Two-Dimensional Crystal Lattice Strains with
11:00 Nanometre Depth Resolution by *Nikulin, A.Y.*, Gureyev, T.E., Hashizume, H., Stevenson, A.W. & Wilkins, S.W.

1C12 X-ray Polarization Analysis of Allowed and Forbidden Reflections of Iron Pirite,
11:20 FeS_2. by Yazawa, I., Nagano, T., Kurasawa, T., *Ishida, K.*, Tsuji, E., Kumazawa, S., Sasaki, S., Mori, T. & Kishimoto, S.

1C13 Use of Harker sections of Patterson Function as Constraint of Density Modification
11:40 for Direct Phase Determination by *Shiono, M.*

1C14 Phase Extension Using X-ray Multiple Diffraction & Maximum Entropy Method
12:00 by Wang, C.-M. & *Chang, S.-L.*

Lunch 12:30-13:45

MS13 Phase transformation (*Prof. T. R. Welberry*) 13:45-15:45

1C21 Diffuse X-ray Scattering and Phase Transitions of Urea Inclusion Compounds. by
13:45 *Welberry, T.R.* & Mayo, S.C.

1C22 Atomic Short-Range Order in Nickel-Platinum Alloys by Saha, D.K. & *Ohshima, K.*
14:00

1C23 Crystallographic Studies of C_{60} and C_{70} by a Single Crystal X-ray Diffraction by
14:15 *Horiuchi, H.*, Mitsuki, T., Li, J., Kino, N. & Kitazawa, K.

1C24 High Pressure Polymorphs of ZrO_2 by *Ohtaka, O.*, Yamanaka, T., Yagi, T. &
14:30 Shimomura, O.

1C25 Isosymmetric Structural Phase Transitions and Crossovers : Phenomenology, Ex-
14:45 amples and Implications by *Christy, A. G.*

1C26 Nucleation and Growth Model of Martensitic Phase Transition by *Abe, H.* & Ohshima, K.
15:00

Coffee Break 15:15-15:30

Poster Session15:30-17:45

November 22 Poster Session 15:30-17:45

Poster Session (*MS01,02,09,13,17*) 15:30-17:45

1P01 Normal Mode Analysis of Incommensurate Modulations and Its Relation to the Atomic Debye-Waller Factors of the Normal Phase by *Achiwa, N.*, Machida, M. & Yamauchi, Y.

✓ **1P02** Atomic Anisotropic Displacement Parameters For Silicates and Oxides: A lattice-Dynamical Derivation From Empirical Potentials by *Pilati, T.*, Demartin, F. & Gramaccioli, C. M.

1P03 The Anomalous Scattering Factor Obtained from Rocking Curve Measurements of Ge Single Crystal by Kuribayashi, M., Kanamaru, T., Inoue, A., *Katoh, H.* & Ishida, K.

1P04 X-ray Study of Defects Produced by MeV Ion Implantation into Si Perfect Crystal by *Kuribayashi, M.*, Inoue, A., Kanamaru, T., Katoh, H., Ishida, K., Tomimitu, H., Aizawa, K. & Kazumata, Y.

1P05 Measurements of X-Ray Diffraction Intensities from Uniformly Bent Single Crystals by *Takama, T.* & Itoh K.,

1P06 Observation of Defects without Directly Reflected Wave in Bragg Case by *Uragami, T.*, Kobayashi, H. & Orii, D.

1P07 The Grazing Incidence Diffraction of X-Rays with Wave Front Amplitude Periodically Varying along the Crystal Entrance Surface (Symmetrical Laue Case). by *Bezirganyan, A.P.* & Bezirganyan, S.E.

1P08 Density of the p3 Close Packing of Identical Ellipses by *Matsumoto, T.* & Tanemura, M.

✓ **1P09** The Use of The Diffractometer at the Australian National Beamline at the Photon Factory for Unusual Experiments by *Creagh, D.C.*

✓ **1P10** In-situ study of structural defects in materials using Synchrotron radiation by *Yeritsian, G.N.*, Sahakian, A.A. & Nickogosian, S.K.

✓ **1P11** Investigations on Solid State Physics and Crystallography Using Synchrotron Rafiation at Yerevan Physics Institute by *Egikian, D.L.*

1P12 RIKEN Contract Beamlines for Structural Biology at SPring-8 by *Iwasaki, H.*

1P13 The Bio-Crystallography (MIR-OAS) Beamline at the SPring-8 by *Kamiya, N.*, Ueki, T., Iwasaki, H., Tanaka, N. & Miki, K.

✓ **1P14** Electron Density Distribution in Pyrite-Type MnS_2 by Ueki, M., *Ishizawa, N.* & Marumo, F.

✓ **1P15** Size Dependancy of the c/a Ratio of Tetragonal Barium Titanate Micro-Crystals Using SR by *Suda, K.*, Kataoka, M., Ishizawa, N., Marumo, F. & Ohsumi, K.

✓ **1P16** Structure Analysis of $CaYAlO_4$ Small Crystal Using SR by *Morita, K.*, Suda, K., Ishizawa, N., Kodama, N. & Yamaga, M.

✓ **1P17** Single Crystal X-Ray Diffraction and EXAFS Analysis of $(Y_{0.2}Zr_{0.8})O_{1.9}$ Fluorite-Type Compound by *Matsushima, Y.*, Hayashi, M., Suda, K., Ishizawa, N. & Oyanagi, H.

1P18 Structural Study on the Defect-Perovskite-Type Compounds $La_{1/3}MO_3$ (M=Ta,Nb) by *Tanabe, K.*, Suda, K., Ishizawa, N., Sohn, J.-H. & Itoh, M.

1P19 X-ray Diffuse Scattering Study of Magnetite by The Valence-Difference Contrast Method. by *Toyoda, T.*, Sasaki, S. & Tanaka, M.

1P20 Structural Changes of $(Pb,Cu)SrLaCuO_{5+\delta}$ on Oxygen Introduction into Block Layers by *Khasanova, N.R.*, Izumi, F., Shida, M., Chakomakos, B., Ohahima, E., Kikuchi, M. & Syono, Y.

1P21 Neutron Diffraction Study of the Improved Chemical Stability of Cation Substituted '123' Superconductor $Y_{0.6}Ca_{0.4}Ba_{1.6}La_{0.4}Cu_3O_{7-d}$ by Sequeira, A., *Rajagopal, H.*, Ganguly, R. & Yakhmi, J.V.

1P22 The Inverse Problem in Multiple Small-angle Scattering by *Mazumder, S.* & Sequeira, A.

1P23 SANS from SDS Micellar Solutions in Presence of Amines and Ammonium Salts by Kumar, S., Aswal, V.K., Goyal, P.S. & *Kabir-Ud-Din,*

1P24 Microphase Separation in Adsorbed Paraffin Mixtures by *Gilbert, E.P.*, Reynolds, P.A. & White, J.W.

1P25 Vanadium and Vanadium-Bearing Micas by *Bekenova, G.K.*

1P26 The Crystal Structures of Dehydrated Fully Cd^{2+}-Exchanged Zeolite X and of its Carbon Monoxide Sorption Complex by Jang, S., Kwon, J., Kim, U., *Kim, Y.* & Seff, K.

1P27 Structural investigation of high- and low-symmetry vesuvianite by *Ohkawa, M.*, Takeno, S. & Yoshiasa, A.

1P28 Synthesis and Characterization of Alkali-Metal Tin(IV)Arsenates: $ASnOAsO_4$ (A=K and Rb), $Cs_2Sn_3As_6O_{22}$ and $CsSn_2As_3O_{12}$ by *Lin, K.-J.* & Lii, K.-H.

✓ **1P29** Crystal Structure Studies of $CeAlO_3$ by Synchrotron Radiation by *Tanaka, M.*, Horiuchi, H., Shishido, T. & Fukuda, T.

1P30 canceled

1P31 Sodium Magnesiosilicates with the Carnegieite, or "Stuffed Cristobalite" Structure by Lobo, C.J., Schmid, S., *Thompson, J.G.*, Withers, R.L. & Stranger, R.

1P32 Cation Distribution and Crystal Chemistry in $Y_3Al_{5-x}Ga_xO_{12}$ $(0 \leq x \leq 5)$ Garnet Solid-Solutions by *Nakatsuka, A.*, Yoshiasa, A. & Yamanaka, T.

1P33 The Crystal Structure of Vesuvianites From Taiwan by *Yu, S.C.*, Lee, J.S. & Wang, C.P.

1P34 Charge Density Study of Nonlinear Optical Crystals of LBO and KB5 by *Sheu, H.-S.* & Wang, Y.

1P35 Structural Change of $Ca_2(Mg,Fe)Si_2O_7$ By Heat Treatment by *Hagiya, K.*, Kusaka, K., Haga, N., Ohmasa, M. & Iishi, K.

✓ **1P36** Structure and Residual Density of $CaFeO_3$ with Fe^{4+} by *Morimoto, S*, Yamanaka, T. & Tanaka, M.

1P37 Structure and Twinning of a Small Crystal of Mawbyite $PbFe_{1-x}Zn_x(AsO_4)_2(OH)_{1-x}$, $x = 0.06$. by Kharisum,, Taylor, M. R. & *Rae, A.D.*

1P38 Comparison of Crystal Structures between Li-Doped and Undoped Superconductor of the Type $Bi_2Sr_2CaCuO_8$. by *Kitahama, K.*, Horiuchi, T. & Kawai, T.

1P39 Synthesis and crystal structures of zirconolite Polytypes by *Ono, Y.*

1P40 Superstructure of $Ba_{6-3x}Sm_{8+2x}Ti_{18}O_{54}$ (x=0.71) by *Ohsato, H.*, Kato, H., Mizuta, M. & Okuda, T.

1P41 Intramolecular Interactions Observed in Four Bis(phthalocyaninate)lanthanoid(III) Complexes by *Koike, N.*, Uekusa, H. & Ohashi, Y.

1P42 Structure Analysis of $(NH_4)_3H(SO_4)_2$ at 150K by *Noda, Y.*, Fukuchi, S. & Tamura, I.

1P43 Incommensurate-Commensurate Phase Transition of Intramolecular Hydrogen-bonded Material d-BrHPLN by *Tamura, I.*, Noda, Y., Kuroiwa, I., Mochida, T. & Sugawara, T.

1P44 Observation of Anomalous Diffuse Rod below 200K in $Ba_2NaNb_5O_{15}$ by *Shobu, T.*, Noda, Y. & Uesu, Y.

✓ **1P45** Structure Change Investigation of Perovskite-Type $(Nd,Sm)AlO_3$ by X-ray Powder Diffraction by *Yoshikawa, A.*, Horiuchi, H. & Tanaka, M.

✓ **1P46** Structural Phase Transitions Among Complex Metal Oxides With Perovskite Type Structure: Studies by Precise X-Ray Powder Diffractometry by *Sergey, I.* & Zhurov, V.

1P47 A Single Crystal X-ray Diffraction Study of the low Temperature Phase of RbCN by *Yoshimura, Y.*, Shinohara, S., Tsuda, N. & Iwasaki, H.

1P48 Single-Crystal X-Ray Diffraction Study of $AgGaS_2$ Under High Pressures by *Kitahara, H.*, Ishizawa, N. & Noda, Y.

1P49 Structure of Pyridinium Tetrafluoroborate and Its Phase Transition Observed by a New Diffractometer by *Nemoto, T.*., Ohashi, Y., Hanaya, M. & Oguni, M.

1P50 BUNYIP: A New Approach to Detecting Errant Symmetry by *Hall, S.* & Hester, J.

1P51 A Flexible Four-Circle Diffractometer Control System For BL14A at the Photon Factory by *Vaalsta, T.P.* & Ishizawa, N.

1P52 Analysis of Metallic and Related Compounds Using ICDD Metals & Alloys Indexes by Dann, J.N., *Huang, T.C.*, McClune, W.F., Mueller, M.H., Robert, A.C. & Wallace, P.L.

1P53 TITAN: A Molecular Graphics Program to Aid Structure Solution and Refinement with the SHELX Suite of Programs. by Hunter, K. A. & *Simpson, J.*

1P54 Organo-Template Control of Inorganic Structures : A Sheet Aliminophosphate of Low Symmetry $3[NH_3CHMeCH_2NH_3][Al_6P_8O_{32}][H_2O]$ by *Williams, I. D.*, Lin, Z., Gao, Q., Chen, J. & Xu, R.

1P55 Structural Changes in Modified Smectites: Li^+ Diffused Montmorillonite Case by *Mulaba-Bafubiandi, A.*, Helsen, J., Maes, A., Langouche, G. & Prost, R.

November 23 Room A

Plenary Lecture 2PL1 (*Prof. T. Baker*) 9:00-9:45

2PL1 Crystallography-based Drug Design by *Matsuzaki, T.*

Plenary Lecture 2PL2 (*Prof. W. Robinson*) 9:45-10:30

2PL2 Strong and Weak hydrogen bonds in Crystal Engineering by *Desiraju, G. R.*

Coffee Break 10:30-11:00

MS06 Structural biology I (*Dr. G. Jameson*) 11:00-12:30

2A11 Crystal Structure Analysis of a Large Membrane Protein with the Molecular Weight
11:00 of 400K Da at 2.8 Å Resolution by Aoyama, H., Yamashita, E., *Tsukihara, T.*, Tomizaki, T., Yamaguchi, H., Shinzawa-Itoh, K., Nakajima, Y. & Yoshikawa, S.

2A12 Crystal Structure Determination of a Form of Human Apo-Lactoferrin with Both
11:30 Lobes Open by Molecular Replacement by Faber, H.R., *Anderson, B.F.*, Baker, H.M. & Baker, E.N.

2A13 Protein Sequence-Structure Alignment Based on Mutant Profile From Mean Force
11:50 Field Potential by *Lai, L.U.* & Wang, Y.

2A14 Crystal Strucutre of Bovine β-Lactoglobulin at 1.9Å Resolution by *Bewley, M.C.*,
12:10 Kingston, R., Baker, H. & Baker, E.N.

Lunch 12:30-13:45

MS10 Organic and organometallic compounds (*Prof. Y. Kai*) 13:45-15:15

2A21 Crystalline-State *trans-cis* Photoisomerization of Cobaloxime Complexes by *Ya-*
13:45 *mada, T.*, Uekusa, H. & Ohashi, Y.

2A22 Crystal Structure of Bicyclomangostin : The New Acid-Catalyzed Cyclization Prod-
14:03 uct from Mangostin by *Pakawatchai, C.*, Malabusarakam, W., Wiriyachitra, P., Taylor, W.C. & Skelton, B.W.

2A23 The γ and δ Structural Effects of Silicon and Tin by *Green, A. J.* & White, J. M.
14:21

2A24 Comparison of Fe(II)-P and Fe(0)-P Lengths : Structure of $[(\eta^5\text{-}C_5H_5)Fe(CO)C(O)\text{-}$
14:39 $Me](\mu\text{-}\eta^1{:}\eta^1\text{-}dppe)\text{-}[(\eta^4\text{-}MeC_5H_5)Fe(CO)_2]$ by *Liu, L.-K.* & Luh, L.-S.

2A25 Structures of Novel Metal-carbene Complexes Derived from Hypervalent Tetraaza-
14:57 thiapentalenes by *Iwasaki, F.*, Manabe, N., Shimamoto, S., Yasui, M. & Matsumura, N.

Coffee Break 15:15-15:30

Poster Session15:30-17:45

November 23 Room B

MS05 Recent developemt of Powder diffraction (*Prof. T. Yamanaka*) 11:00-12:30

2B11 11:00 Laue Classes of α- and β-Quartz and Their Patterson Functions Evaluated with Powder Diffraction Data by *Ohmasa, M.*, Ohsumi, K. & Taraya, H.

2B12 11:18 X-Ray Quantitative Analysis without Standards Using Rietveld Methods with High Accuracy by *Kuo, C.-L.* & Liu, H.-C.

2B13 11:36 XRD Determination of the Mineral Structural State Characteristics by *Slusarev, A.P.*

2B14 11:54 Profile Analysis for Lattice Deformation and Crystallite Size under Compression by *Yamanaka, T.*

Lunch 12:30-13:45

MS12 Interface, films and surfaces (*Prof. O. Nittono*) 13:45-15:15

2B21 13:45 Roughness Estimation of Polycrystal Metal Surfaces with Use of X-ray Glancing Scattering by *Fujii, Y.*, Yoshida, K. & Yoshida, K.

2B22 14:05 X-Ray Scattering from Microcrystallinity in the Thermally Oxidized SiO_2 Thin Films on Si(110) Surfaces by *Shimura, T.*, Kojima, R., Misaki, H. & Umeno, M.

2B23 14:25 Determination of electron density profile from x-ray reflectivity data using Distorted Wave Born Approximation. by *Sanyal, M.K.*, Datta, A. & Banerjee, S.

2B24 14:45 Electron Density Maps for Clean and Adsorbed Silicon Surfaces Calculated with the Maximum-Entropy Technique by *Hashizume, H.*, Carvalho, C.M., Yokota, O., Stevenson, A.W. & Robinson, I.K.

Coffee Break 15:15-15:30

Poster Session15:30-17:45

November 23 Room C

MS08 New Instrumentation (*Prof. H. Hashizume*) 11:00-12:30

2C11 Development of CCD-based X-Ray Detectors with a Beryllium-windowed Image
11:00 Intensifier for Diffraction Studies. by *Amemiya, Y*

2C12 The Optimization of Parameters of Bragg-Fresnel Lenses by *Haroutunyan, L.* &
11:18 Trouni, K.G.

2C13 The Theoretical and Experimental Study of X-Ray Diffraction Focusing Phenomena
11:36 on the Two-Block Crystalline System with Missorientated Blocks by *Trouni, K.G.*
& Grigoryan, A. H.

2C14 Recent Developments of X-Ray crystal Structure Analysis by New Diffractometer
11:54 and Cooling Equipment by *Uekusa, H.* & Ohashi, Y.

2C15 X-ray Wiggler Beamlines at SRRC by *Jean, Y.-C.*, Lee, C.-H., Tsang, K.-L.,
12:12 Hung, H.-H., Chan, J.-R., Hsu, C.-H., Jang, L.-Y., Tang, M.-T., Lee, H.-Y.,
Sheu, H.-S., Dann, T.-E., Lee, J.-F., Wang, J.P. & Chang, S.-L.

Lunch 12:30-13:45

MS04 Neutron diffraction (*Dr. A.S. Sequeira*) 13:45-15:15

2C21 Hydrogen in Metals: Neutron Diffraction Studies of the Crystal Structures of Zr_2NiD_x
13:45 by Elcombe, M.M., *Howard, C.J.* & Campbell, S.J.

2C22 Nuclear Density Distribution and Anharmonic Thermal Vibration of SnO_2 by the
14:00 Maximum Entropy Method by *Kumazawa, S.*, Ishida, K., Takata, M., Sakata, M.,
Ishii, Y. & Morii, Y.

2C23 Recent Neutron Studies of High Tc Superconductors by *Sequeira, A*, Sharma, R.
14:15 & Rajagopal, H.

2C24 A New Aspect of the Reaction Mechanism of Cobaloxime Complexes by Neutron
14:30 Diffraction by *Ohgo, Y.*, Ohashi, Y., Klooster, W.T. & Koetzle, T.F.

2C25 Neutron Diffraction Investigation of Phase Transition in $LiNaGe_4O_9$ by *Iwata, Y.*,
14:45 Wada, M. & Sawada, A.

2C26 Single Crystal Neutron Study of Structural Phase Transition in $(Ba/Ca)TiO_3$ by Sas-
15:00 try, P.U.M., *Sequeira, A*, Dasannacharya, B.A., Rajagopal, H. & Ramasamy, P.

Coffee Break 15:15-15:30

Poster Session15:30-17:45

November 23 Poster Session 15:30-17:45

Poster Session (*MS04,05,06,08,10,12*) 15:30-17:45

2P01 The Effect of Ending Angle on the Structural Parameters and Profile Agreement Indices in Rietveld Refinement by *Kuo, C.-L.* & Liu, H.-C.

2P02 Crystal Structure and Data On $Bi_4(SiO_4)_3$ by X-ray Rietveld Analysis by *Kuo, C.-L.* & Liu, H.-C.

2P03 Crystal Structure Analysis of Alkaline Protease (M-Protease) Forml Crystal. by *Shirai, T.*, Suzuki, A., Yamane, T., Asjoda, T., Kobayashi, T. & Ito, S.

2P04 Crystal Structure of an Acyl-Enzyme Intermediate of Guanidinohexanoyl-Trypsin by *Nitanai, Y.*, Noguchi, S., Satow, Y., Sasaki, C. & Matsuzaki, T.

2P05 Visualisation of the 3D-Structure of Calotropin DII A Plant Thiol Protease at 3Å Resolution by Ghosh, S., Mukhopadhyay, B. P., Pal, A., Seal, A., Bera, A., Dey, I., Sinha, N.K. & *Banerjee, A.*

2P06 Crystal Structure of a Complex of Wheat Germ Trypsin Inhibitor II-5 with Bovine Trypsin by Kibushi, E., *Suzuki, A.*, Shirai, T. & Yamane, T.

2P07 Structure of a Kunits-type Chymotrypsin Inhibitor Protein from Winged Bean Seeds at 2.95Å Resolution by *Dattagupta, J.K.*, Podder, A., Chakrabarti, C., Sen, U., Dutta, S.K. & Shingh, M.

2P08 Crystal Structure of Macrocyclic Inhibitor for Elastase and Structural Comparison between Non-binding and Binding States by *Kinoshita, T.*, Tada, T., Yasuda, T., Fujita, H. & Hatanaka, H.

2P09 Ligand-induced conformational changes of 3-isopropylmalate dehydrogenase from *Themus thermophilus* by *Moriyama, H.*, Kadono, S., Sakurai, M., Oshima, T. & Tanaka, N.

2P10 Crystallization and Preliminary X-Ray Crystallographic Study of Streptomyces Olivaceoviridis E-86 β-Xylanase by Fujimoto, Z., *Mizuno, H.*, Kuno, A., Yoshida, S. & Kusakabe, I.

2P11 Ability of Some Specific Natural Structures to Interact Concurently Contrary to Dioxin. ESR Study. by *Nguyen, V. T.*, Vung, P. T. & Thai, D. P.

2P12 X-ray Crystallography of Methionyl-tRNA Synthetase from *Thermus thermophilus* HB8 by *Sugiura, I.*, Ugaji, Y., Maeda, S., Konno, M., Nureki, O. & Yokoyama, S.

2P13 Crystallographic Studies of Hammerhead Ribozymes. II. by *Chatake, T.*, Matsumoto, O., Chen, Y., Tsunoda, M, Imaizumi, N., Takenaka, A., Ohta, A., Komatsu, Y., Koizumi, M. & Ohtsuka, E.

2P14 On Refinement of Protein Structures by Means of SHELXL93 by *Jameson, G.B.* & Edwards, R. A.

2P15 Measurements of the Faraday effects and X-ray birefringence at Co K-edge with the X-ray polarimeter. by *Amemiya, Y*

2P16 Crystal and Molecular Structure of a 1:1 Complex of Phathylyl Sulphathiazole and Salicylic Acid by *Verma, A. K.* & Tiwari, R.K.

2P17 Structure Characterization of Constituents from *Bridelia ovata* Dense and From *Davalia Solida* Sw. by *Haller, K. J.*, Petson, A., Roengsumran, S., Lertpratchya, P., Boonyaratavej, S., Thongkon, N. & Phaopongthai, J.

2P18 Syntheses and Crystal Structures of Group 6 metal Carbonyls Containing Polyphosphine Ligands by *Ueng, C.-H.*, Horng, D.-N., Luo, T.-T. & Shieh, M.-H.

2P19 Aperiodic Crystal Structure in Vegetable Fibres by *Nguyen, V. T.*, Thang, N. V. & Vung, P. T.

2P20 Outer-sphere Coordination of Phenanthroline in Aquachlorotri(*p*-chlorophenyl)Tin · 1,10-Phenanthroline Dimer by *Weng, N. S.* & Kumar Das, V.K.

2P21 Novel polychalcogen-pnicogen chromium compounds by *Chen, W*, Goh, L. Y. & Wong, R.C.S.

2P22 Structure Analysis of Unstable Crystals Using Rapid X-Ray Measurement System by *Watanabe, T.*, Manabe, N., Nashiyama, H., Yasui, M. & Iwasaki, F.

2P23 Structure of $\{[(Ph_2NCH_2PPh_2)Au]_3S\}Cl\cdot H_2O$ by *Wang, J.-C.* & Lion, L.-S.

2P24 Crystal Structure of Binuclear 1:1 Silver(I) 2-Hydroxy-3,5-dinitrobenzoate: Triphenylphosphine Complex by *Othman, A. H.*, Kimia, J., White, E. & White, A. H.

2P25 Crystal Structure of [4-[w-(cholesteryloxycarbonyl)hexyloxycarbonyl]phenyl]ferrocene by *Nakamura, N.* & Takayama, T.

2P26 Solvant Influence on Crystallization of Phenyl Carbamidonitrile by *Yang, Q.-C.*, Huang, D.-M., Chen, H.-Y. & Tang, Y.-Q.

2P27 Crystal Structure of cis[-5-(2-Dimethlaminoethyl)-3-hydroxy-2-(4-methoxyphenyl)-2,3-dihydro-1,5-benzothiazepine](±) by *Kumaradhas, P.*, Nirmala, K.A. & Sridhar, M.A.

2P28 Crystal Structure of cis[1,5-Benzothiazepine-4(5H)-one-1-oxide-3-(acetoxy)-2,3-dihydro-2-(4-methoxyphenyl)](±) by *Nirmala, K.A* & Kumaradhas, P.

2P29 Crystal Structures of Tin xanthates by *Mohamed-Ibrahim, M.I.*, Shawkaraly, O. B., Fun, H.-K. & Sivakumar, K.

2P30 Carbon Nanotubes on the Top Surface of Cathode Deposit at DC Arc-Discharge by *Ando, Y.*, Zhao, X., Ohkohchi, M. & Wang, M.

2P31 Crystal Structures of Group 15 Mixed Ligand Derivertives of $Ru_3(CO)_{12}$ by *Shawkataly, O B.*, Lee, S.-T., Parameswari, M., Fun, H.-K. & Sivakumar, K.

2P32 Structure of 1-[4,5-Dihydro-1-H-imidazol-2-yl]-imidazolidine-2-thione hydrobromide by *Wattanakanjana, Y.*, Pakawatchai, C., Skelton, B.W. & White, A.H.

2P33 Structural and Conformational Studies of Triterpenoids : 19-Epimers of Lupenes by *Kiyotani, T.*, Masuda, K. & Ageta, H.

2P34 Syntheses, Characterisation and Crystal Structure of Triosmium Alkylidyne Carbonyl Cluster Containing Chiral Auxiliaries by Wong, W.-Y. & *Wong, W.-T.*

2P35 Molecular Structure of Organic Lanthanide Complexes having Ethylene Polymerization Activity by *Kanehisa, N.*, Hashimoto, H., Yamagashira, M., Kai, Y., Nodono, M., Ihara, E. & Yasuda, H

2P36 Crystal Structure of 2,10-dichloro-6-(2,4-dimethyl phenoxy)-Dibenzo [*d,g*][1,3,6,2]-dioxathiaphosphocin-6-sulfide by *Kumar, N.J.*, Krishnaiah, M., Reddy, B.S. & Reddy, C.D.

2P37 X-ray Structural Studies on Substituted Thioures Derivatives. by *Sivakumar, K.*, Akilan, R., Subramanian, K. & Fun, H.-K.

2P38 'Sheet with Holes' Structure of Lead(II) Iodide — N-methylethylenediamine(3/2), $(PbI_2)_3(Me\text{-}en)_2$ by *Miyamae, H.*, Ito, T. & Hihara, G.

2P39 Structures of furo and thieno derivatives of 5-amino-8-methyl-1,2-dihydro[2,3h][1,6]-Naphthyridines by *Kingsford-Adaboh, R.*, Kashino, S. & Sasaki, K.

2P40 X-ray Investigation on Structural Phase Transition in $HOOC(CH_2)_4COOH$ by *Machida, M.* & Nishimoto, S.

2P41 Very Rapid Photoisomerization of 1-Cyanoethyl Group in Cobaloxime Crystals by *Inthapanya, P.*, Ohgo, Y. & Hashizume, D.

2P42 Crystalline-state Racemization of Chiral Methoxycarbonylethyl Group in Cobaloxime Complexes by *Saitoh, M.*, Hashizume, D., Uekusa, H. & Ohashi, Y.

2P43 A Chiral N-Methylbenzamide by *Yamaguchi, K.*, Azumaya, I., Okamoto, I., Kagechika, H. & Shudo, K.

2P44 Asymmetric Photoisomerization of (2-Cyanoethyl)(2-butylamine)cobaloxime Complexes in The Solid State by *Koura, T.*, Kogo, H. & Ohashi, Y.

2P45 Structure of A Briarein Diterpenoid :(1S*, 2S*, 5Z, 7S*, 8R*, 9S*, 10S*, 11Z, 14S*, 17R*)-2,14-diacetoxy-8,17-epoxy-9-hydroxy-briara-5,11-dien-18-one^{++} by *Lee, T.-J.*, Wang, A., Sheu, J.-H., Sung, P.-J. & Kun, F.-H.

2P46 Grazing-Induced Diffraction of X-rays on Single Crystal with Near-Surface Lattice Distortion by *Haroutyunyan, V.S.*

2P47 Model-Independent Determination of Electron Density Profiles for Al-C Multilayers Using Anomalous-Dispersion X-Ray Reflectometry Data by *Ohkawa, T.*, Yamaguchi, Y., Sakata, O., Hashizume, H., Datta, A. & Sanyal, M.K.

2P48 In-plane Structure of Arsenic-deposited Silicon Surfaces Studied Using Grazing-angle X-ray Standing Waves by *Sakata, O.*, Kumano, S., Nikolaenko, A.M. & Hashizume, H.

2P49 Micromolphology of Polished Silicon Surfaces Studied by X-Ray Reflectometry by *Yamaguchi, Y.*, Nakanishi, M., Sakata, O., Hashizume, H., Nakano, M. & Bennett, J.M.

2P50 Dislocation of Some Industrial Aluminum Alloys After Rolling by *Thang, T. Q.*

2P51 Structure of Microcrystalline Ag-based Amalgam Alloys by *Do, M. N.*, Ha, C. T., Dzan, N. V. & Dzuong, L.

2P52 Common Features of P-type and N-type Porous Silicon Layers with Visible Photoluminescence by *Nittono, O.* & Takemoto, K.

November 24 Room A

Plenary Lecture 3PL1 (*Prof. T. Yamanaka*) 9:00-9:45

3PL1 Advances in the Use of Rietveld Analysis for Materials Characterisation by *O'Connor, B.*

Plenary Lecture 3PL2 (*Prof. E.N. Maslen*) 9:45-10:30

3PL2 Charge Density Studies and Characterization of Chemical Bonds by *Wang, Y.*

Coffee Break 10:30-11:00

Plenary Lecture 3PL3 (*Prof. K. Tanaka*) 11:00-11:45

3PL3 Charge Density Studies Revisited by *Coppens, P.*

MS18 Charge density (*Prof. K. Tanaka*) 11:45-12:30

3A11 11:00 Topological Analysis of Experimental Electron Density of LiF Crystal by *Abramov, Y. A.*, Zavodnik, V.E., Feil, D. & Tsirelson, V.G.

3A12 11:45 Electron Density in $YTiO_3$ by *Hester, J. R.*, Okamura, F.P., Tomimoto, K. & Akimitsu, J.

Lunch 12:30-13:45

MS11 Structural biology II (*Prof. T. Tsukihara*) 13:45-15:15

3A21 13:45 Crystal Structure of Chimers in B-form Show that RNA can Exist as B-RNA by *Sundaralingam, M.*, Chen, X. & Ramakrishnan, B.

3A22 14:15 X-ray Structure Determination of Abrin-a. by *Lu, T.-H.*, Tahirov, T. H., Liaw, Y.-C., Chen, Y.-L. & Lin, J.-Y.

3A23 14:45 Three-Dimensional Structure of the Pseudomonas BphC Enzyme Having Polychlorinated Biphenyl (PCB)-Degrading Activity by Narita, H., Sugimoto, K., Senda, T., Kimbara, K., Fukuda, M. & *Mitsui, Y.*

3A24 15:00 Crystal Structure of Pea-Seedling Amine Oxidase by *Kumar, V.*, Freeman, H.C., Guss, J.M., Zubak, V.M., Dooley, D.M. & McGuirl, M.A.

Coffee Break 15:15-15:30

Poster Session15:30-17:45

November 24 Room B

MS07 Crystal growth and characterisation (*Prof. T. Ohachi*) 11:00-12:30

3B11 The Effect of Copper Dopant on the Growth and Properties of Potassium Sodium
11:00 Strontium Barium Niobate Crystals by *Chen, H.C.*, Jiang, Q.Z. & Lu, X.L.

3B12 Single Crystal Growth and Growth Mechanism of YNi_2B_2C Superconductors by
11:20 Floating Zone Technique by *Takeya, H.*, Kadowaki, K., Hirano, T. & Togano, K.

3B13 Anomalous Density Variation of Silicon Melt and Melt Flow in Cz Process by
11:40 *Terashima, K.*, Sasaki, H., Togawa, A., Kawanishi, S., Izunome, K. & Kimura, S.

3B14 Etching Studies of Solution-Grown Crystals : (100) Faces of Mixed KDP:ADP -
12:00 $(K_{1-x}NH_{4x}H_2PO_4)$ Crystals. by SenGupta, S. & *SenGupta, S.P.*

Lunch 12:30-13:45

MS14 Organic crystal engineering (*Prof. F. Iwasaki*) 13:45-15:15

3B21 The Attempt to Design Solid State Reaction by Reaction Cavity by *Hashizume, D.*
13:45 & Ohashi, Y.

3B22 Study on Complexes of Alkylammonium Salt-Aromatic Additive by *Vongbupnimit, K.*,
14:00 Noguchi, K. & Okuyama, K.

3B23 Diverse Mode of Crystal Structures in the Host-Guest Comlexes of Diols by *Kai, Y.*,
14:15 Suzuki, H., Kanehisa, N., Tanaka, K. & Toda, F.

3B24 Extended Molecular Networks Incorporationg the 1,4-Bis(imidazol-2-yl)but-2-yne
14:30 Ligand by *Slizys, D. A.*, Hoskins, B. F. & Robson, R.

3B25 Dynamic Behavior of N-(2,4-Dinitrophenyl)-o-anisidine Crystals by *Yasui, M.*,
14:45 Taguchi, K. & Iwasaki, F.

3B26 Modelling and Refinement of Disordered Structures from Single Crystal X-ray Data
15:00 by *Fun, H.-K.*, Shivakumar, K. & Yip, B.-C.

Coffee Break 15:15-15:30

Poster Session15:30-17:45

November 24 Poster Session 15:30-17:45

Poster Session (*MS07,11,14,18*) 15:30-17:45

3P01 On Cross-Sectional Transmission Electron Microscopy Study of Carbon Nanotubules by Hu, G., Zhang, X.F. & *Zhang, Z.*

3P02 Local Structure Around Magnesium in $CaMgSi_2O_6$ Glass by Oxygen K-Edge EXELFS Analysis by *Tabira, Y.*, Ishizawa, N. & Matumo, F.

3P03 Optimization of Prolyl endopepidase Crystal Growth by *Kagawa, Y.*, Kawauchi, Y., Sato, T., Yamashita, E., Tsukihara, T., Sazaki, G. & Komatsu, H.

3P04 Use of DLS to Compare Crystallinities of SSB and Ribosome by Nakagawa, A., *Kawauchi, Y.*, Sato, T., Tsukihara, T., Sazaki, G. & Komatsu, H.

3P05 Single Crystal Growth of Vacancy Defect Type Sulfide Spinel Compounds Using Bridgman Technique by *Ohachi, T.*, Ohmuro, Y., Asahi, K. & Taniguchi, I.

3P06 Crystal Structure of the C-terminal Domain of Rabbit Serum Haemopexin at 1.8Å Resolution. by *Baker, E.N.*, *Baker, H.M.*, Faber, H.R., Groom, C.R., Morgan, W.T. & Smith, A.

3P07 Crystal Structure of L-2-Haloacid Dehalogenase from *Pseudomonas* sp. YL at 2.5Å Resolution by *Hisano, T.*, Hata, Y., Fujii, T., Kurihara, T., Esaki, N. & Soda, K.

3P08 Crystal Structure of 3-Isopropylmalate Dehydrogenase from Facultative Thermophile, *BACILLUS COAGULANS* by *Tsuchiya, D.*, Matsumoto, O., Takenaka, A., Murakami, T., Sekiguchi, T. & Nosoh, Y.

3P09 Structure of Substrate-Complexed G4-Amylase Inactivated by Mutation of Catalytic Residues by *Hasegawa, K.*, Yamaguchi, H., Yoshika, Y., Matsuura, Y. & Kubota, M.

3P10 X-Ray Structural Analysis of the Five Isoleucine to Valine Mutants of Human Lysozyme: Contribution of Hydrophobic Residues to the Stability by *Fujii, S.*, Yamagata, Y., Kaneda, H., Takano, K. & Yutani, K.

3P11 Crystal Structure of Acidic Phospholipase A_2 from the Venom of *Agkistridon Halys Pallas* at High Resolution by *Wang, X.Q.*, Yang, J., Gui, L.L., Lin, Z.J. & Zhou, Y.C.

3P12 Crystallization and Preliminary X-ray Studies of Phophpenolpyruvate Carboxylase from Escherichia Coli by *Nagara, Y.*, Inoue, T., Suzuki, Y., Ohtsuka, R., Fukuhara, K., Nishiura, S., Kitagawa, R., Nakanishi, H., Hayashi, M., Inoue, M., Sugimoto, S., Kai, Y. & Izui, K.

3P13 Crystal Structure of Ferredoxin from a Thermoacidophilic Archaeon by *Fujii, T.*, Hata, Y., Oozeki, M., Moriyama, H., Wakagi, T., Tanaka, N. & Oshima, T.

3P14 The Refined Crystal Structure of Bence Jones Protein Pav at 2.4Å and its Domain-Domain Associations by *Hsiao, C.D.*, Rose, J., Swaminathan, S., Furuen, W. & Wang, B.-C.

3P15 Structure of Bovine Cytochrome c Oxidase at 2.8 Å Resolution by Tsukihara, T., *Aoyama, H.*, Yamashita, E., Tomizaki, T., Yamaguchi, H., Shinzawa-Itoh, K., Nakajima, R., Yaono, R. & Yoshikawa, S.

3P16 PII: The Structure of a Signal Transducing Protein by *Ollis, D,* Cheah, E., Carr, P. & Suffolk. P.,

3P17 The Utility of 4-Aminobenzoic Acid in the Promotion of Hydrogen Bonding in Crystallization Processes by *Smith, G.*

3P18 MAD Analysis of Rat Liver Macrophage Migration Inhibitory Factor by *Suzuki, M.*, Sugimoto, H., Nakagawa, A., Tanaka, I., Fujinaga, M. & Nishihira, J.

3P19 Crystal Structure of VHR, A Dual-specific Phosphatase by *Yuvaniyama, J.*, Saper, M.A., Denu, J.M. & Dixon, J.E.

3P20 Crystal Structure of the Active-Site Mutants of *Escherichia Coli* Aspartate Amino Transferase by *Miyahara, I,* Okada, K., Hosomi, K., Hirotsu, K. & Kagamiyama, H.

3P21 Unique Polymorphism and Inclusion Complex Formation of Dianilinegossypol. by *Ibragimov, B.T.*, Beketov, K.M. & Talipov, S.A.

3P22 The Attempt to Design Solid State Reaction by Reaction Cavity by *Hashizume, D.* & Ohashi, Y.

3P23 Study on Complexes of Alkylammonium Salt-Aromatic Additive by *Vongbupnimit, K.*, Noguchi, K. & Okuyama, K.

3P24 Diverse Mode of Crystal Structures in the Host-Guest Comlexes of Diols by *Kai, Y.*, Suzuki, H., Kanehisa, N., Tanaka, K. & Toda, F.

3P25 Extended Molecular Networks Incorporationg the 1,4-Bis(imidazol-2-yl)but-2-yne Ligand by *Slizys, D. A.*, Hoskins, B. F. & Robson, R.

3P26 Dynamic Behavior of N-(2,4-Dinitrophenyl)-o-anisidine Crystals by *Yasui, M.*, Taguchi, K. & Iwasaki, F.

3P27 Modelling and Refinement of Disordered Structures from Single Crystal X-ray Data by *Fun, H.-K.*, Shivakumar, K. & Yip, B.-C.

3P28 canceled

3P29 Structure Analysis of N-(2,4-Dinitrophenyl)-o-anisidine at High Temperature by *Takada, K.*, Watanabe, T., Taguchi, K., Yasui, M. & Iwasaki, F.

3P30 Crystal Structures of TEMPO Radicals Showing Ferromagnetic Interaction by *Yamamoto, H.*, Yoshikawa, H., Mitsuda, H., Takada, K., Yasui, M., Ishida, T., Nogami, T. & Iwasaki, F.

3P31 The Central C-C Bond Length in the Bi(anthracene-9,10-dimethylene) Photoisomer: Unusual Elongation and Crystalline State Reactions by Harada, J., *Ogawa, K* & Tomoda, S.

3P32 Crystal Structures of Copper Complexes Showing Ferromagnetic Interaction by *Ishikawa, Y.*, Yasui, M., Iwsaki, F., Ishida, T. & Nogami, T.

3P33 Crystalline-state Racemization of Bulky Groups on Exposure to Visible Light by *Ohashi, Y.*, Sato, H., Arai, Y. & Ohgo, Y.

3P34 Cyclic O—H...N/C—H...O H-Bond Coupling in the Design of Supramolecular Assemblies by *Pedireddi, V.R.*, Jones, W., Cambridge, A.P. & Docherty, R.

3P35 Layered Structures of Antiferroelectric Mesogens by *Okuyama, K.*, Kawano, N., Uehori, S., Noguchi, K., Okabe, N., Suzuki, Y. & Kawamura, I.

3P36 Complex Formation of Surfactant Molecules with Aromatic Compounds in a Mortar by *Sawada, K.*, Ohashi, Y., Imura, N. & Hirata, H.

3P37 Generation of Asymmetry in the Crystalline State Photoisomerization of Cobaloxime Complex by *Yoshimiya, T.*, Sekine, A. & Ohashi, Y.

3P38 Chemical Bond and Atomic Displacements in $Ba_{0.87}K_{0.13}BiO_3$ Crystal by *Abramov, Y. A.*, Reznik, I.M. & Tsirelson, V.G.

3P39 HRTEM Characterization of Homologous Series of Super Conductors $GaSr_2Ca_{n-1}Cu_nO_{2n+3}$ (n=3 and 4) by Ramirez-Castellanos, J., *Matsui, Y.*, Takayama-M., E. & Isobe, M.

3P40 Analysis of Quasicrystal Structures by Use of Powder Neutron and Single Crystal X-ray Data by *Yamamoto, A.*, Kajitani, T. & Morii, Y.

3P41 A New Barium Copper Oxychloride, $Ba_2Cu_3O_4Cl_2$: Its Synthesis and Crystallographic Characterization by *Zou, Z..*, Tachikawa, O. & Horiuchi, H.

3P42 Synchrotron Radiation Imaging of the Deformation Electron Density in $LiNbO_3$ and $LiTaO_3$. by *Hsu, R.*, Maslen, E.N., Streltsov, V.A. & Ishizawa, N.

3P43 Topological Study On The Electron Density Distribution of Bis(diiminosuccinonitrilo)Nickel, $Ni(C_4N_4H_2)_2$ by *Hwang, T.-S.* & Wang, Y.

3P44 Electron Density Studies of Cobalt(II) Octaaza Bis-α-diimine Macrocyclic complex $[Co(C_{10}H_{20}N_8)(H_2O)_2]^{2+}[ClO_4]_2^{2-}$ by *Lee, J.-J.*, You, Y.-S., Lee, G.-H. & Wang, Y.

3P45 Effect of Magnetic Field on Ni-Pt Alloys by *Saha, D.K.*

3P46 Atomic Radii from Electron Densities by Maslen, E.N. & *Etschmann, B.*

3P47 Crystal Structure Refinement of Silk Fibroin: *Bombyx mori* by *Takahashi, Y.*

3P48 Physicochemical Investigations on Natural Spinels($MgAl_2O_4$) by *Udawatte, C.P.*, Gunawardena, R.P. & Annersten, H.

3P49 Structural Studies on α- and β- Forms of Poly (Tetramethylene succinate) by *Noguchi, K.* Igarashi, Y., Okuyama, K., Ichikawa, Y., Imaizumi, M. & Moteki, Y.

3P50 On the Interpretation of Small Angle Scattering Data by *Sabine, T.M.*, Bertram, W.K. & Aldridge, L.P.

3P51 Three-Dimensional Structure of the Pseudomonas BphC Enzyme Having Polychlorinated Biphenyl (PCB)-Degrading Activity by Narita, H., Sugimoto, K., Senda, T., Kimbara, K., Fukuda, M. & *Mitsui, Y.*

3P52 Crystal Structures of the Copper Complexes Toward the Functional Model Compound of Dopamine β-Hydroxylase by *Li, C.*, Kanehisa, N., Kai, Y., Itoh, S., Kondo, T., Komatsu, M., Ohshiro, Y. & Fukuzumi, S.

Scientific Abstracts

1PL1

SYNCHROTRON RADIATION SCIENCE IN CRYSTALLOGRAPHY – PRESENT AND FUTURE –

Masami Ando, Photon Factory, KEK, Oho 1-1, Tsukuba 305, Japan

Since the advent of synchrotron x-radiation in early 1970's, mostly because of its quite brilliant nature, its parallelity, wavelength tune ability and selectivity of polarization, a number of its applications to crystallography have been intensively attempted; most of their challenges have been achieved and further some new methods are in development. Of typical examples are simultaneous observation of dynamic solid-state phase transformation, crystal growth by means of high spatial resolution x-ray topography, production of massive good quality film-based data such as in proteins and enzymes, a challenge to crystal structure analysis of nanometer scale crystals, as other major applications are XAFS which can relatively easily bring information about first neighbour atoms and some new tools for composite determination of complexes such as ternary alloys. It will be important to describe about any sciences in crystallography which could have been brought only with synchrotron radiation, such as magnetic scattering; that had been hardly observable due to its low signal level based on very weak interaction of synchrotron radiation with magnetic electrons. This has brought a new tool to survey magnetic solid-state.

Also Mossbauer scattering can lead us to various applications covering from solid state physics to x-ray optics which is also a part of crystallography. Pulse structure synchrotron radiation can reveal hyperfine structure of condensed matters and liquid phase. Further owing to a very very narrow bandwidth of most Mossbauer nuclei radiation with a very long temporal coherence length from them are now routinely available.

Together with a high spatial coherence which comes from a nature of third-generation light sources such as the SPring-8, APS and ESRF one can proceed more research which needs more coherence. Preparation of an extremely brilliant third generation light source using the main ring at KEK for some experiments in this autumn which may give us a good idea to see what a fourth generation light source should be will be also given in a talk.

With a help of doing synchrotron radiation science using third generation sources advent of x-ray laser light will be seen in the next century along with development of linear accelerators capable of extremely low emittance and specially designed insertion devices for that purpose.

1PL2

DIRECT METHODS - NEW DEVELOPMENTS OUTSIDE THE TRADITIONAL FIELD

Fan Hai-fu, Institute of Physics Chinese Academy of Sciences Beijing 100080, P.R. China

During the last ten years, the application of direct methods has been extended from the traditional field to new areas. Important progress was made along the following lines:

- * from single crystals to polycrystalline materials;
- * from small molecules to biological macro-molecules;
- * from ordinary structures to modulated structures;
- * from X-ray crystallography to electron microscopy.

Details on the last three topics will be given.

1. In principle, the combination of direct methods with the infomation from single isomorphous replacement (SIR) or one-wavelength anomalous scattering (OAS) will simplify the process of protein structure analysis. Significant contributions in this area were made by different groups on the world. The method developed in our group has been successfully tested with experimental data from known proteins of moderate size.
2. Incommensurate modulated/intergrowth structures are often found in solid state materials. They do not have three-dimensional periodicity but can be considered as the three-dimensional hypersection of a higher-dimensional periodic structure. Based on this, multi-dimensional direct methods have been established, with which incommensurate modulated/ intergrowth structures have been solved without relying on an assumed model.
3. Many solid state materials are composed of small and imperfect crystals . They are difficult to analysis by X-ray diffraction but are suitable for electron microscopic observation. However an electron micrograph needs special processing before it can reveal the true structure image of the sample. Direct-method procedures have been developed for image processing in high resolution electron microscopy combining infomation from electron micrographs and the corresponding electron diffraction pattern. The method has been used in ab-initio structure analysis of minute crystalline samples.

1A11

SINGLE CRYSTAL X-RAY DIFFRACTION USING SR IN MATERIALS SCIENCE

Nobuo Ishizawa, Research Laboratory of Engineering Materials, Tokyo Institute of Technology, Nagatsuta Yokohama 226, Japan

The high brilliance and tunability of synchrotron radiation (SR), when utilized on the four-circle diffractometer, are powerful tools for the single crystal diffraction studies of inorganic compounds generally. It is impossible to review all work of importance in materials science comprehensively. Several topics for recent studies on the horizontal-type four-circle diffractometer (Satow & Iitaka, 1989) at the 14A vertical wiggler line, Photon Factory, KEK, will therefore be presented.

It is most important when measuring the electron-density in a crystal unambiguously and precisely to reduce extinction experimentally as far as possible. we recently succeeded in obtaining almost extinction-free diffraction data from a small rectangular $CaYAlO_4$ crystal with volume 864 μm^3. The specimen was studied using focused 0.75 Å X-rays. The structure refinement revealed not just a slight deviation from stoichiometric composition, but also a slight but significant shift of the Ca position from that of the Y atom. The latter result contrasts profoundly with earlier understanding. The crystal was previously considered to be a mid member of the K_2NiF_4-type solid solution with Ca and Y atoms replacing the crystallographically-unique K site in a disordered form.

It can be stated quite generally that the stage has been reached where thermal and positional parameters for two different elements at the "same" structural sites can be determined independently, with reasonable accuracy. The aspherical electron redistribution of bonding electrons and small compositional fluctuations can also be detected. With the help of EXAFS analysis, slight deformation of the local structure around a solute atom in a solid solution is detectable even though it is superimposed on the host structure. Physical properties are often sensitive to local deformation caused by the solute atom, which in most cases, were undetectable previously.

Examples on the fluorite-type superionic conductors will be shown.

Satow, Y. & Iitaka, Y. (1989) Rev. Sci. Instrum. **60** [7], 2390-93.

1A12

MICROCRYSTALLOGRAPHY BY SYNCHROTRON RADIATION

Ohsumi,K.(Photon Factory, Natl. Lab. for High Energy Physics, KEK), Hagiya,K.(Dept. of Life Sci., Himeji Inst. of Tech.), Miyamoto, M. (Miner. Inst.,Univ. Tokyo) and Ohmasa, M.(Dept. of Life Sci.,Himeji Inst. of Tech.)

For crystallographic studies of a submicrometer-sized crystal particle or micrometer-sized area of larger specimen, an equipment and software system has been developed employing the Laue method with polychromatic synchrotron radiation (Ohsumi et al.(1991), Ohsumi et al.(1995). The micro-area Laue method(ML) may be important in the field of material science, because crystallographic information is obtained from the exact same area of samples as is probed by optical microscopy, EPMA or micro Raman spectroscopy.

Due to the limited space around the beamline, micro-beams are produced by using micro-pinholes of which diameters are 2.4, 3.5 and 8μm full width at the half maximum. An imaging plate was employed as a two dimensional detector and covers -60 to 165 degrees in two-theta with a cylindrical camera radius of 100 mm.

The software system includes (a) assignment of indices, (b) simulation of Laue pattern, (c) refinement of crystal orientation, (d) calculation of integrated intensities, (e) absorption correction and (f) structure refinement based on intensities of Laue spots.

The recent application of ML to unknown carbonaceous material in a thin section of the meteorite(ureilite) is briefly introduced in below.

Laue pattern from a crystal with dimension of 2x1 μm was obtained for 60 min. exposure. By assignment of indices and subsequent simulation of the Laue pattern, the unknown material is determined to be diamond. Refinement of an isotropic temperature factor gave 0.19(3) A^2 based on twelve Laue intensities.

Ohsumi,K., Hagiya,K. & Ohmasa,M.(1991). *J.Appl.Cryst.***24**,340-348.
Ohsumi,K., Hagiya,K., Uchida,M., Suda,N., Miyamoto,M., Kitamura,M. & Ohmasa,M.(1995). Rev.Sci.Instrum.**66(2)**,1448-1450.

1A13

Multiple-Detector System for Powder Diffractometer Using Synchrotron Radiation and High-Resolution Diffraction Data Obtained with It

H. Toraya and H. Hibino, Ceramics Research Laboratory, Nagoya Institute of Technology, Asahigaoka, Tajimi 507, Japan and K. Ohsumi, Photon Factory, National Laboratory for High-Energy Physics, Ohho, Tsukuba 305, Japan

A new powder diffractometer for synchrotron radiation with six detector arms has been constructed. Five detector arms compose a multiple-detector system. They are set radially at the interval of 25° on the 2θ-axis of goniometer. Five scintillation counters coupled with a flat Ge crystal analyzer on respective arms can record simultaneously the whole powder pattern divided into five segments with an equal 2θ span. The optics design is based on the flat-specimen-reflection geometry using parallel-beam. A 2θ-step-scanning technique is used for data collection in the asymmetric diffraction at a fixed incident angle. Thus a rapid diffractometer scan at step intervals of 0.001 to 0.004° could be realized. A sixth detector arm can be used for multi-purpose, and it can equip various kinds of analyzers such as long horizontal parallel slits, a flat or channel-cut crystal analyzer, a receiving slit, a solid state detector. This arm can be operated in the conventional single-arm-scanning mode.

Test operations of diffractometer were conducted at the BL-4B experimental station at the Photon Factory in Tsukuba. Monochromatic beam with a wavelength of 1.5416 Å was obtained from a water-cooled double-crystal Si (111) monochromator. The diffractometer scan, for example, of the (111) reflection from Si using a multiple-detector system recorded the full-width at half-maximu of 0.022° and the peak maximum intensity of more than 40,000 counts per second. The whole powder pattern of Mg_2SiO_4 could be step-scanned at a step interval of 0.004° in 2θ just within 4 hours.

1A14

ELECTRON DENSITY IMAGING WITH SYNCHROTRON X-RADIATION

E. N. Maslen and V. A. Streltsov, Crystallography Centre, University of Western Australia, Nedlands, WA 6907, Australia

Historically electron difference densities ($\Delta\rho$) were measured using X-ray diffraction with tube sources. Because of unreliable extinction corrections and high noise due to limited intensity, the reproducibility of those experiments was often mediocre. The resulting $\Delta\rho$ maps were poor representations of the electron density due to chemical bonding. Property predictions were inaccurate. Because of its excellent qualities, the electromagnetic radiation emitted by transversely accelerated relativistic electrons or positrons has become a very powerful tool for exploring basic properties of materials that were previously inaccessible. High precision diffraction using synchrotron radiation (SR) has now overtaken X-ray tube diffraction imaging because it provides less noisy images with lower distortion by extinction errors. Here we review some recent studies of the electron density with SR. The high accuracy $\Delta\rho$ images measured at the Photon Factory in Japan allows the reorganisation of the electron density in the atoms that form crystalline solids to be depicted unambiguously, sometimes with surprising conclusions.

For the birefringent carbonates $CaCO_3$, $MgCO_3$ and $MnCO_3$ the $\Delta\rho$ density correlates with optical anisotropy to a degree consistent with a cause and effect relationship between electron density and refractive index. That index is large where locally antisymmetric components dominate the electron density. The metal-CO_3 interaction has a significant effect on the $\Delta\rho$ density near the CO_3 group, the moiety responsible for optical anisotropy.

Electron densities are perturbed significantly by non-bonded interactions. Metal-metal interactions strongly influence SR electron densities for α-Al_2O_3 and for α-Fe_2O_3, a theme that continues in the orthoferrites: $YFeO_3$ and $SmFeO_3$, and the C-type sesquioxides: Y_2O_3, Dy_2O_3 and Ho_2O_3. The cation electron densities are deformed more strongly by interaction with other cations than with O atoms except where the cation's O-coordination crystal field includes a low symmetry component. These metal-metal interactions are beyond the normal range of chemical bonds. When spin-dependent they must play important roles in magnetic ordering and structural transitions.

The topography of SR images indicates that valence electron density overlapping cations' closed inner subshells is repelled by exchange towards regions of lower electrostatic potential more remote from the nuclei. The transferred density retains the cation's symmetry. That is consistent with the observed regularity of cation arrays - which often exceeds that of the anions.

1A15

TEXTURE STUDY ON SYNCHROTRON RADIATION

E.S.Abovian, A.H.Grigorian and K.G.Trouni Department of Solid State Physics, Yerevan State University, A.Manoukyan 1, Yerevan, 375049, Armenia.

A systematic study is carried out with the purpose to demonstrate the potentialities of application of the continious spectrum of synchrotron radiation for express study of textured state of various materials.

The experiments are carried out on the special diffractometer placed on the Yerevan electron accelerator "Arous". The simple geometry of "direct" exposure was realized, which enabled to register diffraction pattern on nuclear photoplates located behind the specimen, perpendicular to the incident beam.

As the objects to be investigated the Al and Cu foils having the texture of rolling, as well as the wires of Ag,Cu and Pt.

For quantitative analysis of obtained data there is carried out the study of texture by the X-ray energy-dispersive diffractometry technique. Energy-dispersive diffractograms are obtained for Al-foil when the rolling plane is perpendicular to the incident beam.

In comparison to the classic method of texture study by monochromatic radiation with the use of special textures of goniometric heads in the given work the necessary bulk of information is obtained in a few minutes. The impotrant fact is the revealing of K-edge of absorption on the diffraction pattern. Thus, the use of monochromatic synchrotron radiation together with energy-dispersive diffractometry proves to be rather promising thechnique in studies of textured materials.

Buras B. et al. J.Appl. Cryst., 1977, v.10, p.431-438.

1A21

MODULATED STRUCTURES IN THE $Nb_2Zr_{x-2}O_{2x+1}$ AND $Ta_2Zr_{x-2}O_{2x+1}$ ($7.1 \leq x \leq 12$) SOLID SOLUTION FIELDS

Siegbert Schmid , Klaus Fütterer, John G. Thompson and Ray L. Withers, Research School of Chemistry, The Australian National University, Canberra ACT 0200, Australia, and Nobuo Ishizawa, Research Laboratory of Engineering Materials, Tokyo Institute of Technology, Nagatsuta, Midori-ku, Yokohama 226, Japan

At the ZrO_2-rich end of both the $ZrO_2 . Nb_2O_5$ and $ZrO_2 . Ta_2O_5$ systems, wide range solid solutions of the type $M_2Zr_{x-2}O_{2x+1}$ (M = Nb, Ta) are observed. The widths of these solid solutions, when synthesized via solid state reaction, have been reported as $7.1 \leq x \leq 10.3$ (Thompson *et al.*, 1990), however x is beyond this range when the syntheses are carried out via a flux method. It has been shown that such systems are best described as composite modulated structures rather than homologous series M_nO_{2n+1} ($x = 2n$) of closely related phases.

X-ray intensity measurements from a $Nb_2Zr_{x-2}O_{2x+1}$, $x = 12$ single crystal were carried out at BL14-A of the Photon Factory, Tsukuba, Japan. Data were collected at 1458 and 8 eV below the Zr *K* absorption edge. The enhanced scattering contrast between the neighbouring metals close to the Zr *K* absorption edge enables refinement of potential metal atom ordering. The displacive modulation wave amplitudes obtained from these refinements (Fütterer *et al.*, 1995) are in remarkable agreement with those obtained from a Fourier decomposition of the previously published, conventional superstructure refinement of the member $x = 8$ (Galy & Roth, 1973).

The refinements in the $Nb_2Zr_{x-2}O_{2x+1}$ system will be compared with the results for $Ta_2Zr_{x-2}O_{2x+1}$, $x = 8$, both in terms of displacive modulation waves as well as metal atom ordering patterns!

Fütterer, K., Schmid, S., Thompson, J. G., Withers, R. L., Ishizawa, N. & Kishimoto, S. (1995). Acta Cryst. B**51** (in press).
Galy, J. & Roth, R. S. (1973). J. Solid State Chem. **7**, 277-285.
Thompson, J. G., Withers, R. L. , Sellar, J., Barlow, P.J. & Hyde, B. G. (1990). J. Solid State Chem. **88**, 465 - 475.

1A22

X–RAY ANALYSIS OF 4f–ELECTRON DENSITY IN CeB_6 CRYSTALS

K. Tanaka. Chemistry Department, Nagoya Institute of Technology, Gokiso–cho, Showa–ku, Nagoya, 466, Japan, and Y. Ohnuki, Physics Department, Osaka University, Machikaneyama–cho, 1–1, Toyonaka 560, Japan.

4f–electron densities have been measured by several researchers. However they have not been analyzed quantitatively with scattering factors which take into account the aspherical 4f–electron distribution. Ce atoms in the CeB_6 crystals locate in the O_h crystal field. In the limit of the crystal field theory, the 4f–orbitals are clearly defined in this case. Therefore CeB_6 is a very good compound to begin the 4f–electron density analysis. Since f–electrons locates closer to the nucleus and the distinction between the 4f–electron density and the anharmonic thermal vibration of Ce was expected to be difficult, the structure factors were measured at 100 K and 165 K. Further the ratio of the numbers of f–electrons to that of the total electrons is very small, special care was taken in the measurement. First the temperature variation at the sample position with ω and χ was measured in advance and the intensity was measured where the temperature of the sample position is stable. Second the multiple diffraction effect was also avoided with the Ψ–scan. The deformation densities around the Ce atom reveal the sharp peaks along [100], indicating the existence of a f–electron on the triply degenerate $f_{x^3-xr^2}$, $f_{y^3-yr^2}$ and $f_{z^3-zr^2}$ orbitals. For the calculation of the scattering factors of each f–orbital, 4f atomic orbital were calculated with the Dirac–Slater method using the program HEX.1) The refinement assuming this 4f–electron configuration reduced the peak heights by half. The following anharmonic thermal vibration analysis further diminished peaks by half. The tendency are the same for experiments at both temperatures. These results show that the peaks around the Ce atom are due to both the aspherical distribution of 4f electrons and the anharmonic thermal vibration of the Ce atom.

1)Liberman, L.A., Cromer, D.T. & Waber, J. T. (1971). *Comp. Phys. Commun.*, **2**, 107.

1A23

THE JOINT X-RAY AND ELECTRON DIFFRACTION STUDY OF MGO

Yu.A. Abramov*, A.S. Avilov[#], E.L. Belokoneva[&], Kitaneh Rushdi[$], D. Feil[%],
V.G. Tsirelson[$] and F.P. Okamura*

* National Institute For Research in Inorganic Materials, Tsukuba, Japan
# Institute of Crystallography , Moscow, Russia
& Moscow State University, Moscow, Russia
% University of Twente, Enschede, the Netherlands
$ Mendeleev University of Chemical Technology, Moscow, Russia

The results of study of electrostatic potential (EP) and some physical properties of MgO crystal by accurate electron and X-ray diffractometry are presented. The polycrystal thin film in the transmission electron diffraction and single crystal sample in the X-ray diffraction have been used. An agreement within 5% for the EP distributions, reconstructed from diffraction data, have been achieved. A good agreement of those with the results of theoretical calculation by the Hartree-Fock method for bulk MgO crystal was observed as well. This allows to be sure that details of EP distribution are available for the experimental study with a good degree of accuracy. The diamagnetic susceptibility and static electronic polarizability were calculated from X-ray and electron kinematic structure amplitudes for MgO. Those are in good agreement with independent experimental values. The analysis of the MgO X-ray electron density was given in terms of Bader's quantum-topological theory. The gradient field and Laplacian of the electron density have been calculated by using the obtained multipole model parameters. The bond (3,-1) critical point on the Mg-O internuclear vector was found and "sizes" of atoms bonded in the crystal were determined. The near spherical shape of bonded O atoms was revealed. The corresponding average radius equals 1.27 A. This value as well as the distance from the Mg atom to the bond critical point ,0.936 A, are in good agreement with Shannon and Prewitt's ionic radius values of 1.26 A and 0.86 A for O^{-2} and Mg^{+2} ions, respectively. The Laplacian value at the bond critical point is positive as is usual for the case of ionic bonding. A (3,+1) critical point was found at the centre of the (001) plane.

Support of this research by the Netherlands Organization for Scientific Research (NWO) and International Scientific Foundation (Grant U1G000) is gratefully acknowledged.

1A24

Crystal Structure and Magnetic Properties of the Linear Homo or Hetero Trinuclear Metal Complexes of Bis(2-pyridyl)amido Ligand

Cheng-Chen Lin, En-Che Yang, Gene-Hsiang Lee, and Shie-Ming Peng
Department of Chemistry,
National Taiwan University
Taipei, 10764, Taiwan ROC

Polynuclear metal chain complexes have received considerable interest because of their spin interaction and the nature of the metal-metal bonding. The bis(2-pyridyl)amido ligand in the syn-syn conformation allows each nitrogen atom to coordinate with a separate metal ions.

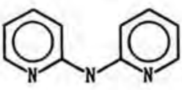

syn-syn

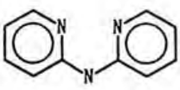

anti-anti

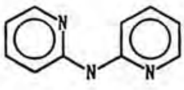

anti-syn

Here we report the syntheses, crystal structures and magnetic properties of a series of quadruply bridged trinuclear metal complexes, $[M_2M'_1(\mu_3\text{-dpa})_4L_2]^{n+}(PF_6)_n$, where M = Co^{II} or Ni^{II}, M' = Co^{II}, Ni^{II}, Pd^{II}, dpa = bis(2-pyridyl)amido, L = Cl^-, NCS^-, CH_3CN etc.

The representative structure of this family is $[Co_2Pd(\mu_3\text{-dpa})_4Cl_2]^0$ which shown in the Figure and a structural comparison of this series are presented. The magnetic interaction of these trinuclear metal complexes will also be discussed.

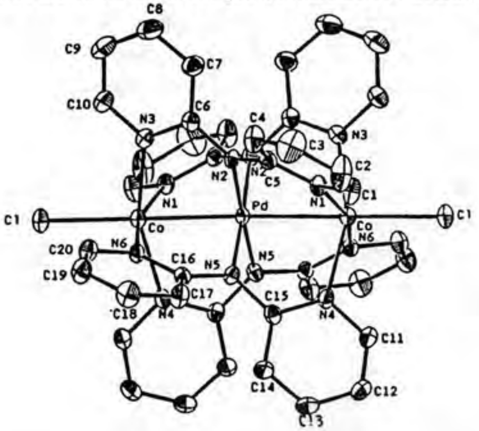

1B11

CIF AS THE COMMON LANGUAGE OF CRYSTALLOGRAPHY

Brian McMahon, International Union of Crystallography, 5 Abbey Square, Chester CH1 2HU, England

Within a scientific discipline, the efficient interchange of experimental data and derived information relies on the existence of an established protocol for representing the concepts and measurables of that discipline. The International Union of Crystallography has been vigorous in its sponsorship of suitable protocols, including the Standard Crystallographic File Structure (SCFS) (Brown, 1983) and its successor, the Crystallographic Information File (CIF) (Hall, Allen & Brown, 1991).

Although SCFS had little impact on the discipline, CIF has become established as the working language of small-molecule crystallographers, owing to its promotion by Acta Crystallographica as the preferred submission format to Section C of the journal, and to the growth of a substantial number of programs for generating, analysing and visualising CIFs. They offer an error-free route from refinement package, through submission to the journal, publication and deposition in crystallographic databases.

Together with a simple syntactic structure, CIF offers a detailed glossary of crystallographic terms, formalised in the Core Dictionary for small molecules, and new extension dictionaries for powder diffraction and macromolecular applications. Additional dictionaries for modulated structures and general symmetry definitions are also under development. Hence the CIF protocol offers a grammar and vocabulary for formal data activities; and guidelines drawn up by the Acta editorial office (IUCr, 1995), together with discussion lists and collaborative software projects undertaken by software developers, help to define the usage and idiom of what is increasingly the language of crystallography.

References

Brown, I. D. (1983). Acta Cryst. A39, 216-224.

Hall, S. R., Allen, F. H. & Brown, I. D. (1991). Acta Cryst. A47, 655-685.

IUCr (1995). A Guide to CIF for Authors. Available from the Managing Editor, IUCr, 5 Abbey Square, Chester CH1 2HU.

1B12

THE BROOKHAVEN PROTEIN DATA BANK

Joel L. Sussman, Protein Data Bank, Brookhaven National Laboratory, Upton, NY 11973, USA

The Protein Data Bank (PDB) at Brookhaven National Laboratory (BNL) is an archive of experimentally determined three dimensional structures of biological macromolecules, serving a global community of researchers, educators, and students. The challenges presented by the enormous growth in data over the past several years have been met by the PDB staff and management, which now provides an up-to-date archive, while simultaneously expanding network access (Stampf et al., 1995) and building strong world-wide collaborations (Peitsch et al., 1995). Even larger challenges are at hand, as the deposition rate continues to rise along with the expectations of the consumers of these data. We are enhancing the capabilities of the PDB and transforming it into a new biological Three-Dimensional Macromolecular Structure Database, while retaining many of the features of the PDB, for compatibility.

Over the course of the next few years, we plan to:

- Ensure that the archive remains current, correct, and relevant
- Provide a rapid and painless automated deposition system, using internationally agreed-upon CIF standards
- Enhance data validation tools
- Build a relational database to store and provide flexible access to the information
- Integrate the PDB with complementary biological and chemical databases through semantic links and schema sharing
- Provide easy access, through the Internet, to the PDB at BNL and other deposition and distribution sites worldwide

References

Peitsch, M. C., Stampf, D. R., Wells, T. N. C. & Sussman, J. L. (1995). The Swiss 3D-Image Collection and Brookhaven Protein Data Bank Browser on the World-Wide Web. Trends in Biochemical Sciences 20, 82-84.
Stampf, D. R., Felder, C. E. & Sussman, J. L. (1995). PDBBrowse - a Graphics Interface to the Brookhaven Protein Data Bank. Nature 374, 572-574.

1B13

XTAL_GX: CIF-ENTRY GRAPHICS FOR GEOMETRY ANALYSIS

Syd Hall and Doug du Boulay, Crystallography Centre, U. Western Australia, Nedlands, Australia 6009 *[syd@crystal.uwa.edu.au]*, James Hester, NIRIM, Namiki 1-1, Tsukuba, Ibaraki 305, Japan *[jrh@nirim.go.jp]*, and David Grossie, Chemistry, Wright State University, Dayton OH, USA *[dgrossie@chem.wsu.edu]*.

A new software package *Xtal_GX* has been developed to display and analyse structural data stored in CIF format. It is supplied gratis by ftp as executable modules for major operating systems supporting X11 graphics, and for a PC/MS-DOS. *Xtal_GX* is specifically designed to process and validate CIF data but it will handle other entry data. It was originally intended to test *Acta Crystallographica* C submissions and is suitable for checking geometry, additional symmetry and for preparing publication plots. It will not process diffraction data.

The package performs the following calculations:

- Read and validate, or write, data in CIF format
- Display and manipulate molecular structure interactively
- Generate ellipsoid plots which have been oriented with PIG
- Generate Newman molecular projection plots
- Search for non-space-group symmetry elements
- Search for additional unit cell settings
- Calculate full range of molecular geometry data
- Calculate least square plane equations and deviations
- Enter non-CIF cell, symmetry and coordinate data
- Interactively adjust/insert text in ORTEP or NEWMAN plots
- Output ORTEP or NEWMAN plots as PostScript or HPGL

These calculations are a small sub-set of the new *Xtal 3.4 System* due to be released in November. A WWW server may be used to obtain further *Xtal* information *(http://www.unige.ch/crystal/axtal/xtal.html)*.

Xtal_GX will be available in July by anonymous ftp (130.95.232.12 in directory *free*). A README file describes the various versions. The PC version can also be obtained by floppy from the last named author. Documentation and an example input command file with test CIF are also supplied.

MAXIMUM ENTROPY DECONVOLUTION IN X-RAY DIFFRACTION ANALYSIS.

W. Kalceff and N. Armstrong, Department of Applied Physics, University of Technology, Sydney, PO Box 123, Broadway, NSW 2007, Australia, and J.P. Cline, Ceramics Division, National Institute of Standards and Technology, Gaithersburg, MD 20899, USA.

The removal of instrumental contributions k from a measured profile g in the presence of noise n to find the specimen function f is known as the "inverse problem" and requires the solution over some range of the integral equation,

$$g(x) = \int k(x,\xi) f(\xi) d\xi + n(x) \qquad (1).$$

In this paper we discuss a C++ implementation of a maximum entropy (MaxEnt) algorithm for solving this equation and show its application in the determination of profile functions for size/strain broadened x-ray diffraction data from various specimens.

The maximum entropy method can be formulated in terms of a Lagrangian function Q (Skilling and Bryan, 1984),

$$Q(f,\lambda) = S(f) - \lambda C(f) \qquad (2),$$

where $S(f)$ is the entropy function, $C(f)$ is the constraint statistic, f is the profile function and λ is an unknown Lagrangian multiplier. In order to determine the profile function, $S(f)$ must be maximised with respect to $C(f)$ for some λ. The standard approach to solving a non-linear equation such as (2) is to apply Newton's Method or the steepest descent method. However, this has been found to be unsuccessful, because (2) is not only non-linear, but it cannot be expressed as a quadratic model, as required to ensure convergence of the solution.

The Skilling-Bryan algorithm we have used determines the MaxEnt solution by forming a subspace spanned by a number of vectors. A quadratic model of the entropy and constraint functions can then be constructed and a solution determined within the subspace.

Skilling, J. and Bryan, R.K. (1984). *Mon. Not. R. Astr. Soc.*, **221**, 111-124.

1B21

THE MACROMOLECULAR CIF DICTIONARY VERSION 1.0

Phil E Bourne, San Diego SuperComputing Center, PO Box 85608, San Diego CA 92186-9784, USA.

Version 1.0 of the macromolecular Crystallographic Information File (mmCIF) dictionary is complete and it is anticipated that it will be published close to the time of the meeting. The dictionary represents a major reference work in describing the crystallographic experiment and the resultant structure. Moreover, since the dictionary and the Dictionary Definition Language (DDL) used to describe it are self defining and rigorous in their implementation, new opportunities exist for developing software where the semantics are identical for all applications. This is possible since the semantics are described by the ONE dictionary and not the many different programs. Details of the DDL, the contents of the dictionary, and the emerging software tools that work with mmCIF will be described.

1B22

THE NUCLEIC ACID DATABASE PROJECT

Helen M. Berman, Lester Clowney, Anke Gelbin, ShuHsin Hsieh, and John Westbrook, Department of Chemistry, Rutgers University, Piscataway NJ 08855, USA

The Nucleic Acid Database (NDB) (1) contains information about the structures of more than 350 nucleic acid containing crystals. In addition to the coordinates, primary experimental information and derived features of these structures are stored. Several methods of access are provided including a forms based interface that is available via the World Wide Web. We will present some of the many types of reports that can be retrieved as well as the queries that are possible using this resource.

In addition, the standard dictionaries that have been created by the NDB for use in validation and refinement of nucleic acids will be described.

Funding for this project is provided by an NSF grant BIR 9305135

1. "The Nucleic Acid Database: A Comprehensive Relational Database of Three Dimensional Structures of Nucleic Acids," Helen M. Berman, Wilma K. Olson, David Beveridge, John Westbrook, Anke Gelbin, Tamas Demeny, ShuHsin Hsieh, A.R. Srinivasan and Bohdan Schneider, Biophysical J., 63:751-759, 1992.

1B23, 1P53

TITAN: A MOLECULAR GRAPHICS PROGRAM TO AID STRUCTURE SOLUTION AND REFINEMENT WITH THE SHELX SUITE OF PROGRAMS.

Keith A. Hunter and Jim Simpson, Department of Chemistry, University of Otago, P.O. Box 56, Dunedin, NEW ZEALAND

TITAN is a Windows based molecular graphics program designed to be used in conjunction with SHELXS-86[1] for structure solution and SHELXL-93[2] and/or SHELX-76[3] for structure refinement. The program facilitates the on-screen assignment of peaks from the direct methods E-map or Patterson map to individual atom designations. Once these designations are completed, a file is written that can be input directly to the SHELXL-93 refinement program without further modification. *TITAN* can also be used in the location of additional atoms in series of least-squares and difference Fourier cycles and as an aid to the inclusion of hydrogen atoms into the refinement using the HFIX and/or AFIX commands.

TITAN runs in the Windows environment and requires a 386 or preferably 486 processor with a minimum of 4Mb memory. Hard-copy plots can be obtained using any Windows compatible printer.

As *TITAN* was written specifically for use with the SHELXS-86/SHELXL-93 suite of programs this combination is strongly recommended. *TITAN* will also read all results files produced by SHELX-76 to allow display and plotting of data produced using that program. However some minor intervention will be required to produce input files using *TITAN* that can be used by SHELX-76.

A demonstration of the operation of the *TITAN* program will be given as part of this poster presentation.

---

[1] Sheldrick, G.M. (1986) SHELXS-86 'A program for the solution of crystal structures from diffraction data.' University of Göttingen, Federal Republic of Germany

[2] Sheldrick, G.M. (1995) SHELXL-93 J. Appl. Cryst. in preparation

[3] Sheldrick, G.M. (1976) SHELX-76 'Program for crystal structure determination', University of Cambridge, England

MOLDRAW: MOLECULAR GRAPHICS FOR MS-WINDOWS

P. Ugliengo+, G. Chiari* and D. Viterbo+

+Dipartimemto di Chimica Inorganica, Chimica Fisica e Chimica dei Materiali, Università, Via P. Giuria 7, I-10125 Torino, Italy.
*Diparimento di Scienze Mineralogiche e Petrologiche, Università, Via Valperga Caluso 37, I-10125 Torino, Italy

MOLDRAW [1] is a program for the graphical manipulation of molecules on personal computers, which can be used to analyze the conformation of molecules resulting both from diffraction techniques or from theoretical calculations, and to study the detailed structure of crystalline materials.

More recently we have undertaken the porting of the code under MS-WINDOWS, in order to take full advantage of the facilities offered by this system. The "look & feel" features of all WINDOWS applications are preserved and all operations are menu, mouse or event driven; these features make this new version of MOLDRAW very easy to learn and use.

Graphic resolution and performance are entirely determined by the WINDOWS driver. With last generation graphic boards, molecular structures may be rendered as on more costly graphic workstations. The resulting images can be printed on any WINDOWS defined printer and pasted to the clipboard or saved as bitmap files to be used by Paintbrush, Word, etc. for desktop publishing.

The improved memory menagement of WINDOWS allows to overcome the memory limits imposed by MS-DOS and the program may thus be extended to handle very large systems (biological macromolecules).

All features present in the MS-DOS version have been improved and some new facilities have been introduced. The format of the input files has been preserved.

We are currently involved in setting up a much easier interface to the crystallographic data bases and programs (CSD, ICSD, SHELX, CRYSTALS, SIR92, etc.), to the computational chemistry packages (GAUSSIAN, AMPAC, etc.) and to other molecular graphics systems (Alchemy, Biosym, etc.).

We are also engaged in the setting up of the following new facilities:

a) simulation of powder diffraction patterns;
b) representation of polyhedra;
c) generation of a complete unique molecule from the given coordinates and symmetry operators.
d) animation of molecular vibrations as computed by GAUSSIAN.

---

[1] P. Ugliengo, D. Viterbo & G. Chiari, Z. Kristallogr., 207 (1993),9-23

1C11

X-RAY PHASE RECOVERY: MAPPING OF TWO-DIMENSIONAL CRYSTAL LATTICE STRAINS WITH NANOMETRE DEPTH RESOLUTION

A. Yu. Nikulin, T. E. Gureyev, School of Physics, University of Melbourne, Parkville, Vic. 3052, Australia, H. Hashizume, Research Laboratory of Engineering Materials, Tokyo Institute of Technology, Nagatsuta, Midori, Yokohama 226, Japan, and A. W. Stevenson and S. W. Wilkins, CSIRO Division of Materials Science & Technology, Private Bag 33, Rosebank MDC, Clayton, Vic. 3169, Australia.

A model-independent method of mapping two-dimensional (2D) strain profiles in near-surface region of crystals has been developed for the crystals with 1D periodic superstructure modulations. The algorithm is based on an application of the solution for the 1D inverse problem to the Fourier-components of the strain profile.

The method relies on high-resolution x-ray diffractometry. Peak intensities of 1D crystal truncation rods (CTRs) are measured for the fundamental Bragg and individual satellite reflections. Spatial resolution is determined by the range of angles over which the data is collected. Each CTR has a different intensity distribution along the direction in reciprocal space parallel to the surface normal of the crystal. A Hilbert transform formalism is applied to retrieve the phase information for the individual CTR intensities (Petrashen, 1989). This procedure actually determines the phases of the Fourier harmonics of the 2D distribution of complex dielectric susceptibility of the distorted crystal.

The relative phases of the individual harmonics are indeterminate. Since all harmonics are independent within the framework of kinematic approximation, each harmonic has an ambiguity of constant phase shift. For laterally symmetric displacements it is possible to reduce the ambiguity to the choice of signs. The sign selection is made according to the sequential trial or minimum energy criteria.

The method was applied to a number of silicon single crystals with a laterally periodic surface oxide mask patterns and ion-implanted through such mask. The x-ray diffraction experiments were performed at the Photon Factory synchrotron source in Japan. The profiles obtained show localised strains with 10 to 50 nm depth and 0.2-0.3 µm in-plane lateral resolutions (Nikulin et al., 1994, 1995). Test scans demonstrated that a 1 nm depth resolution is achievable.

Petrashen, P.V. et al., Sov.Phys.Dokl. **34**, 957 (1989).
Nikulin, A.Yu. et al., J.Appl.Cryst. **27**, 338 (1994).
Nikulin, A.Yu. et al., J.Appl.Cryst. **28**, 57 (1995).

1C12

X-RAY POLARIZATION ANALYSIS OF ALLOWED AND FORBIDDEN REFLECTIONS OF IRON PYRITE, FeS_2.

I.Yazawa, T.Nagano, T.Kurasawa, E.Tsuji, S.Kumazawa and K.Ishida, Dept. of Phys. Science Univ. of Tokyo. Noda, Chiba 278, Japan, S.Sasaki, Research Lab. of Eng. Mater. Tokyo Inst. of Tech. Nagatsuda, Yokohama 227, Japan and T.Mori and S.Kishimoto, PF. KEK. Tsukuba, Ibaraki 305, Japan.

Usually, X-ray susceptibility is treated as a scalar, since the anisotropy of the susceptibility of the crystal is very small in the X-ray region. But the anisotropy might become large at an X-ray wavelength near the absorption edge of a constituent atom. Indeed, X-ray dichroism and birefringence were observed in several crystals at the absorption edges.[1),2)] Moreover, it should be noticed that, in the visible light region, dichroism and birefringence are not observed in a cubic crystal but, in the X-ray region, they are observed even in a cubic crystal. This fact indicates that X-ray dichroism and birefringence have great posibility to study local electronic structures of the crystal atoms and/or ions. The purpose of the present work is to elucidate the relation between the polarization and the anisotropic tensor of the structure factor (ATS).[3)] For the purpose , we carried out polarization analysis of allowed and forbidden reflections of an iron pyrite single crystal with linearly polarized SR. The SR measurements were carried out using four axis diffractometes at BL-3A and 4C of PF of KEK in Tsukuba. A polarization analyzer equipment was mounted on the counter arm of the diffractometer. $BaF_2(333)$ reflection which has Bragg angle of 46.94 ° at the Fe K-absorption edge was used for the analyzer crystal. In the arrangement of the present work, the polarization of the incident beam was σ. Because of the symmetry of iron pyrite, (002n+1) reflections are forbidden. For an allowed Bragg reflection, (002n), the polarization of the diffracted beam was σ. But for a forbidden reflection, (001), the polarization was π. The dependence of azimuthal angle on the polarized beam was also measured. The result was in good agreement with the theory which took into account of the anisotropic tensor of the structure factor. The off diagonal components of the tensor were also determined.

1) David H. Templeton and Lieselotte K. Templeton. (1980) Acta Cryst.A**35**, 237-241

2) A.Petcov, A.Kirfel and K.Fischer. (1990) Acta Cryst.A**46**, 754-763

3) V. E. Dmitrienko. (1983) Acta Cryst.A**39**, 29-35

1C13

USE OF HARKER SECTIONS OF PATTERSON FUNCTION AS CONSTRAINT OF DENSITY MODIFICATION FOR DIRECT PHASE DETERMINATION

M. Shiono, Department of Physics, Faculty of Science, Kyushu University, Higashi-ku, Fukuoka, 812, Japan.

Success of direct phase determinations based on either reciprocal or real space technique depends on the starting point. Conventional direct methods employ multi-solution procedure for overcoming this problem.

A real space direct phase determination procedure which is based on density squareing and eliminating negative density has been developed and applied to small proteins (Shiono *et al.* (1992) Acta Cryst. A48, Refaat *et al.* (1993) Acta Cryst. A49). This method uses multi-solution procedure and can produce *ab initio* solutions of small and middle size structures (IUCr XVI Congress, Beijing). The real space method, however, is time consuming and needs some criterion for selecting good starting points in order to be competitive with reciprocal space methods. For above reason, Harker Sections of Patterson map are used as a filter of the electron density. This density masking considerably improves power of the procedure in early stage of phase refinement.

The method has been applied to phase determination of Ribonuclease Ap1 (Space group $P2_1$). Firstly, Harker section is extracted from Patterson function. Secondly, the Harker section is contracted to 1/4 in area and then 4 pieces of them are placed in the original size of plane. We thus get a section which includes 4 contracted Harker sections. By using this section as 2-dimensional filter of electron density map, we can get phase sets with weighted mean phase error 75°. 20 trials from random phases have been made and 16 sets are of this quality.

1C14

PHASE EXTENSION USING X-RAY MULTIPLE DIFFRACTION AND MAXIMUM ENTROPY METHOD

C.-M. Wang and S.-L. Chang, Department of Physics, National Tsing Hua University Hsinchu, Taiwan, 300, R.O.C.

We report the extension of the phases of the structure factors of the organic crystal $C_{25}H_{25}NO_2$ from 77 starting individual phases using the maximum entropy method. These starting phases were determined from 90 experimental triplet phases calculated from 215 measured ψ-scan 3-beam and 4-beam diffraction profiles obtained with a rotating-anode x-ray source, where the ψ-scans were around the reciprocal lattice vectors of the (001), (002), and (003) reflections. The extension of the structure factors with phase values was carried out using the maximum entropy method for 2040 measured 2-beam Bragg diffraction intensities with 77 starting phases and the symmetry of space group as the constraints. The likelihood criterion was applied to the maximum entropy extrapolation to discern the best extrapolated phase sets which can be used as the new constraints for the next step of generating new phases. With this phase extension procedure, more than one hundred phases were determined.

DIFFUSE X-RAY SCATTERING AND PHASE TRANSITIONS OF UREA INCLUSION COMPOUNDS.

T.R.Welberry and S.C.Mayo, Research School of Chemistry, Australian National University, Canberra, ACT 0200, Australia.

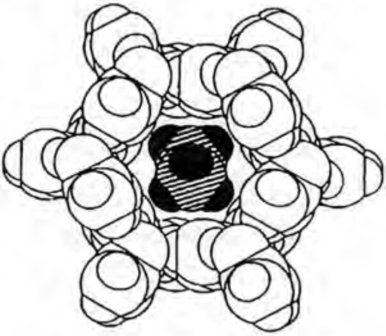

Diffuse X-ray scattering studies have been carried out on the long chain alkane/urea inclusion compounds Hexadecane-Urea (HD-Urea) and 1,10-Dibromo-n-decane–Urea (DBrD-Urea). In both examples the guest species are thought to occupy the hexagonal tunnels in the host urea structure with the alkane chains able to rotate about their long axis and switch between six energetically favourable orientations. At room temperature there is thought to be very little correlation between the orientation of molecules in adjacent tunnels or (in the case of HD-urea) in their relative positions along the channels. The guests thus form a 1D crystal and this gives rise to planes of diffuse scattering normal to the tunnel direction. In the case of HD-Urea the 1D repeat is almost commensurate with the c-axis repeat of the urea framework, but for DBrD-Urea the diffuse planes occur with a repeat distance incommensurate with that of the urea. As well as these sharp planes of scattering other distinctive diffuse scattering features are observed which are associated with the orientational ordering of the alkanes and the flexing of the urea framework.

Although the diffuse scattering in these materials has been noted by other workers (see for example Harris & Thomas, 1990), the resolution of our position-sensitive detector (PSD) X-ray system has allowed us to collect high quality diffuse diffraction data at a range of different temperatures, and investigate the changes that occur as the crystals undergo a series of phase transitions at temperatures below 150K, which are thought to correspond to the orientational ordering of the alkane chains(see for example Harris, 1993). The highly structured diffuse scattering patterns have been modelled using Monte Carlo methods which simulate both the orientational ordering of the alkane chains and the flexing of the urea tunnels about them.

Harris, K.D.M. and Thomas, J.M. (1990) J. Chem. Soc. Farad. Trans. **86**, 2985.
Harris, K.D.M. (1993) J. Solid State Chem. **106**, 83.

1C22

ATOMIC SHORT-RANGE ORDER IN NICKEL-PLATINUM ALLOYS

D. K. Saha, Atomic Energy Centre, P. O. Box - 164, Dhaka 1000, Bangladesh and K. Ohshima, Institute of Applied Physics, University of Tsukuba, Tsukuba 305, Japan.

The electron and x-ray diffraction patterns were observed from four different alloys of the x=0.25, 0.35, 0.44 and 0.50 in $Ni_{1-x}Pt_x$ to understand the existence and shape of diffuse intensity, which gives us the information about structural fluctuations. A peculiar shape of diffuse scattering has been observed at 100, 110 and their equivalent positions on the patterns where the shape of 100 position diffuse intensity changes with Pt content in the alloys. The shape of diffuse intensity at 100 position for the x=0.25 alloy is a rod-like but the shape is nearly spherical for the x=0.50 alloy. The short-range order (SRO) diffuse intensities were measured from the x=0.50 single crystal alloy at room temperature and the Warren-Cowley SRO parameters were determined after analyzing the data. A correlation length has been deduced to be about 19 Å from estimating the inverse of the full width at half maximum (FWHM) values of the diffuse peak.

1C23

CRYSTALLOGRAPHIC STUDIES OF C_{60} AND C_{70} BY A SINGLE CRYSTAL X-RAY DIFFRACTION

H. Horiuchi and T. Mitsuki, Mineralogical Institute, Graduate School of Science, University of Tokyo, 7-3-1 Hongo, Bunkyo-ku, Tokyo 113, Japan,
J. Li, Institute of Metallurgical Physico-Chemistry and Materials, Central South University of Technology, Changsha, Hunan, China,
N. Kino, and K. Kitazawa, Department of Applied Chemistry, Faculty of Engineering, University of Tokyo, 7-3-1 Hongo, Bunkyo-ku, Tokyo 113, Japan.

Crystallographic properties such as stacking faults, twinning, and phase transition behaviors were investigated for C_{60} and C_{70} crystals by means of single crystal X-ray diffraction methods. Used crystals were prepared by a vapor growth which is the same technique as that reported by Li *et al.*[1]. The structure of C_{60} is based on *fcc* and twinning by <111> axes is frequently observed. The occurrence of these type twins is due to stacking faults on {111}. Although some specimens morphologically show complex habits, they are always twinned by <111> without exceptions. The structure of C_{70} observed in this investigation is mainly based upon *hcp*. However, stacking faults in the C_{70} structure are much more abundant than C_{60}, and diffuse streaks along the c^* are much remarkable in the X-ray diffraction patterns. Weak diffraction maxima corresponding to · ·ABCABC · · stacking are sometimes observed in the above diffuse streaks depending on the specimen. In the case of C_{70}, a unique twinning by (-1 0 2) is also observed after phase transition at around 340K. This twinning can geometrically interpret by that the long principal axes of C_{70} molecule ellipsoids which is parallel to the *c*-axis before phase transition change their directions into one of $2\boldsymbol{a_1}+\boldsymbol{a_2}$, $\boldsymbol{a_1}+2\boldsymbol{a_2}$ or $-\boldsymbol{a_1}+\boldsymbol{a_2}$ after phase transition. Where, $\boldsymbol{a_1}$ and $\boldsymbol{a_2}$ are lattice vectors of the parent crystal. In order to occur this phenomenon, C_{70} molecule must achieve free rotation in the structure. This can be explained not only by precessional motion of C_{70} molecules but also by an anisotropic thermal vibration of C_{70} molecules.

[1] J.Li et al.,Physica C, 195, 205(1992).

HIGH PRESSURE POLYMORPHS OF ZrO_2

O. Ohtaka, T. Yamanaka, Earth and Space Science, Osaka University, Toyonaka 560, Osaka Japan, T. Yagi, ISSP, University of Tokyo, Minatoku 106, Tokyo, Japan and O. Shimomura, PF-KEK, Tsukuba 305, Ibaraki, Japan

ZrO_2 is one of the major components of modern ceramic materials. Recently, phase transition of ZrO_2 under high pressure has gathered much interest in both material and geophysical researches. Because the toughening mechanism of ZrO_2 ceramics is explained by a stress induced phase transition, the phase transition at high pressure is to be studied from a microscopic view point. The investigation of high pressure polymorphism of ZrO_2 is also important in geophysical implications as the polymorphic structure of ZrO_2 might be a possible candidate for the high pressure form of SiO2. ZrO_2 has a monoclinic symmetry at ambient conditions and three high pressure polymorphs of orthoI, orthoII and tetragonal have been reported. Because of the experimental difficulties, these studies of ZrO_2 under high pressure have mainly been made at room temperature or, at most, a few hundred degree. The phase relation at elevated temperature is still unknown.

The present authors have performed a series of synthesis experiments and in situ observation in order to reveal the phase relation and the crystal structure of ZrO_2 high-pressure and -temperature polymorphs. Synthesis experiments were undertaken with a cubic and a split sphere type high pressure device. Stable region of orthoI and orthoII, which are quenchable phases, were determined. Two kinds of in situ observations were performed. Combining a diamond anvil cell and a laser heating system, ZrO_2 was heated above 1000C under high pressures above 20GPa. Thermally quenched samples were investigated by using x-ray diffraction under high pressure and confirmed to have a hexagonal symmetry. Using a cubic anvil type device and synchrotron radiation, diffraction data in the temperature range from R.T. to 900C at 9GPa were collected. The results indicated that another high pressure phase appears under these P-T conditions.

1C25

ISOSYMMETRIC STRUCTURAL PHASE TRANSITIONS AND CROSSOVERS: PHENOMENOLOGY, EXAMPLES & IMPLICATIONS

Andrew G. Christy, Research School of Chemistry, The Australian National University, Canberra, ACT 0200, Australia.

Isosymmetric structural phase transitions are those in which significant changes of unconstrained atomic coordinates and cell parameters occur, while atoms remain on the same Wyckoff sites and the overall space group symmetry remains unchanged. A simple phenomenological model indicates that these transitions are necessarily first-order. The transition line extrapolates through a critical point into a 'crossover' or 'diffuse transition' across which physical properties change fast but continuously. The location of the crossover is precisely defined as that of a minimum in d^2G/dQ^2, where G is the free energy and Q is the order parameter characterising the transition. Second derivatives of free energy such as thermal expansivity exhibit a corresponding maximum (Christy, 1995).

Examples of isosymmetric transitions and crossovers are found in systems where the transition is driven by a change in coordination number (KNO_3), framework collapse ($KTiOPO_4$), competition between different order parameters of the same symmetry ($NaAlSi_3O_8$), and change in compression mechanism at high pressure ($MgSiO_3$).

Anorthite ($CaAl_2Si_2O_8$) and ferrosilite ($FeSiO_3$) are mineralogically imporatant systems each exhibiting several different phases. Both systems show a transition from a lower symmetry structure with doubled unit cell at ambient to a higher symmetry structure with both increasing pressure and increasing temperature. For both systems, the high-P and high-T phases are formally the same structure; however, there are significant differences between them in energetics and in structural detail, implying that they are separated by a crossover or isosymmetric transition. It is shown that the low symmetry phase in both systems is an ordered intergrowth of high-T and high-P forms. Therefore, coupling between the non symmetry-breaking order parameter and a zone boundary order parameter is responsible for stabilising the low-P, low-T phases in these systems (primitive anorthite and the pigeonite form of $FeSiO_3$ respectively). The crossover in the high-symmetry phase extrapolates into the stability field of the low-symmetry phase in these systems. Modelling of the behaviour of the low-symmetry phase relative to a high-symmetry reference state should take into account the consequent non-monotonic variation in free energy derivatives of the reference state (Christy & Angel, 1995).

Christy, A.G. (1995). *Acta Cryst.* **B51**, in press.
Christy, A.G. & Angel, R.J. (1995). *Phys. Chem. Minerals* **22**, 129-135.

NUCLEATION AND GROWTH MODEL OF MARTENSITIC PHASE TRANSITION

H. Abe, National Defense Academy, Yokosuka 239, Japan, and
K. Ohshima and T. Suzuki, Institute of Applied Physics,
University of Tsukuba, Tsukuba 305, Japan.

A two-dimensional idealized nucleation and growth (2D-ING) model is considered, in order to understand the experimental results relating to martensitic phase transition of In-Tl alloys (Abe et al., 1994). It is an extension of the Kakeshita model(1993) for nucleation probability derived from a nucleation barrier. We extend the Kakeshita model to an ideal growth process by introducing the concept of a dynamic embryo and a frozen nucleus. A dynamic embryo is a "non-classical" nucleus in the non-equilibrium state. Domains in the low-temperature phase are assumed to develop gathering frozen nuclei. The results of a computer simulation based on the above model show the presence of an incubation time, which is one of the essential properties of the first-order phase transition, and display the cooperative formation of domains and the fractal distribution of their size. The fractal dimension is obtained to be 1.80 for the final domain distribution at 256.7K of In-23 at.% Tl alloy. The experimental results on the kinetics of the martensitic phase tarnsition in In-Tl alloys have been interpreted in terms of the present simulation results.

Abe,H., Ishibashi,M., Ohshima,K., Suzuki,T., Wuttig, M. &
Kakurai,K. (1994). Phys. Rev. B50, 9020-9024.
Kakeshita,T, Kuroiwa,K., Shimizu,K., Ikeda,T., Yamagishi,A.
& Date,M. (1993). Mater. Trans., JIM 34, 423-428.

2PL1

CRYSTALLOGRAPHY-BASED DRUG DESIGN

Takao Matsuzaki, Mitsubishi Chemical Corporation,
Kamoshida, Aobaku, Yokohama 227, Japan

Protein crystallography suggested its potential ability to directly observe drug action from the very beginning era. In 1965, D.C. Philips et al. revealed the complex structure of lysozyme with substrate analog inhibitors. Since the middle of 1980's, protein crystallography has shown its power in drug design field through a great number of structure determinations of protein drug complexes, in addition to new structures which constitute drug targets.

In the course of anticoagulant development, we found several new facts in protein-drug complex structures. MQPA which is the first synthetic thrombin inhibitor in clinical application, binds to trypsin in a new binding mode, despite of its structural similarity to BPTI, a natural trypsin inhibitor. The X-ray structure revealed the mechanisms of the selective inhibition observed with synthetic inhibitors towards trypsin-like proteases: thrombin, factor Xa, plasmin and trypsin. X-ray structures also clarified the role of interaction energies in complex formation; electrostatic vs. van der Waals energy, and the importance of good complementarity of the surface structures between a protein and a drug.

A new drug design method has been developed based on the knowledge obtained from X-ray structures. We have tried to count up all skeleton structures of potentially active compounds. Present results suggest the ability of producing new skeleton structures of 35 non-hydrogen atoms with an rms deviation of 0.7 Å. The method will be introduced together with a review on other drug design methods.

2PL2

STRONG AND WEAK HYDROGEN BONDS IN CRYSTAL ENGINEERING

Gautam R.Desiraju, School of Chemistry, University of Hyderabad,
Hyderabad 500 046, India

Crystal engineering is the understanding of intermolecular interactions in the context of designing new solids with desired physical and chemical properties. Crystal engineering is concerned with the systematic architecture of crystal structures. Crystals are recognised as being the supramolecular equivalents of molecules and therefore, crystal engineering is the supramolecular equivalent of organic synthesis. The goal of crystal engineering is to be able to manipulate intermolecular interactions in the same way that the covalent bond is manipulated in molecular synthesis. Ideally one would like to identify connections between molecular and crystal structure which would make crystal structure design reliable and practical.

The hydrogen bond has been recognised as the master-key for molecular recognition and as such is of major importance in crystal engineering methodologies. Surprisingly, not only strong hydrogen bonds such as O-H...O and N-H...O but also weaker hydrogen bonds such as C-H...O, C-H...N, O-H...π and N-H...π are reliable agents of crystal structure design especially when they are incorporated into schemes involving multi-point recognition. In this context and especially because of the conceptual similarity between crystal engineering and classical organic synthesis, it is helpful to define supramolecular synthons as designed groups of interactions in which are encoded the chemical and geometrical attributes of molecular recognition. Supramolecular synthons are substructural motifs which are of the greatest importance in developing systematic strategies of crystal engineering.

2A11

STRUCTURE OF BOVINE CYTOCHROME C OXIDASE AT 2.8Å RESOLUTION.

Hiroshi Aoyama[1], Eiki Yamashita[1], Takashi Tomizaki[1], Hiroshi Yamaguchi[1], Tomitake Tsukihara[1], Kyoko Shinzawa-Itoh[2], Ryosuke Nakajima[2], Rieko Yaono[2] and Shinya Yoshikawa[2]

[1]Institute for Protein Research, Osaka University, 3-2 Yamada-oka, Suita 565, Japan, Department of Life Science, [2]Himeji Institute of Technology, Kamigohri Akoh, Hyogo 678-12, Japan.

Bovine heart cytochrome *c* oxidase is a membrane protein complex with molecular weight of 200 KDa containing 13 different polypeptide subunits, 2 hemes A, two redox active copper sites, one zinc, one magnesium and possibly some phospholipids as the intrinsic constituents. This enzyme is one of the most intriguing biological macromolecules in the cell, since it reduces O_2 to H_2O at the active site with the four redox active transition metals coupling with proton pumping across the mitochondrial inner membrane. This enzyme have been explored most extensively among the enzymes involved in biological oxidation, ever since this enzyme was discovered. However, in spite of these extensive efforts, lack of the crystal structure at atomic resolution limits seriously understanding of the reaction mechanism of this enzyme.

Electron density distribution of oxidized bovine cytochrome *c* oxidase at 2.8 Å resolution indicated a dinuclear copper center with a novel structure similar to [2Fe-2S] type iron-sulfur center and the O_2 binding site containing heme a_3 iron and copper atoms (Cu_B) with an inter-atomic distance of 4.5 Å without any detectable bridging ligand between iron and copper atoms, in spite of a strong antiferromagnetic coupling between them. A hydrogen bond between a hydroxyl group of the long alkyl side chain of heme a_3 and a phenol OH of a tyrosine located near an imidazole group bonded to Cu_B and a phenyl alanine sandwiched between the heme a_3 and an imidazole liganded to the other heme (heme *a*) could either provide intra-molecular electron transfer pathways or induce the redox coupled conformational change.

2A12

CRYSTAL STRUCTURE DETERMINATION OF A FORM OF HUMAN APO-LACTOFERRIN WITH BOTH LOBES OPEN BY MOLECULAR REPLACEMENT

H.R. Faber B.F. Anderson, H.M. Baker and E.N. Baker, Department of Chemistry and Biochemistry, Massey University, Palmerston North, New Zealand.

Lactoferrin, a protein of the transferrin family (Mr = 80,000, ≈691 residues) reversibly binds two Fe^{3+} and two $CO_3{}^{2-}$ ions. This process is known to be accompanied by large changes in conformation. Previous work (1) has shown that the protein consists of two lobes, each with an Fe^{3+} and associated anion bound deep within clefts between the two domains which form each lobe. The structure of apo-lactoferrin (2) shows the second domain of the N-lobe has rotated open by 54° whereas the C-lobe, although empty, remains closed, possibly due to crystal packing interactions.

We have now analysed a second form of human apo-lactoferrin in which both lobes are open. The crystals (a = 80.8, b = 116.4, c = 227.0 Å, SG = $P2_12_12_1$, z = 4) diffract weakly and only a 3.5 Å data set could be collected with synchrotron radiation at the Photon Factory, Japan. Molecular replacement studies using various models has positioned two similar 3 domain fragments (N-lobe open, C1) satisfactorily in the cell. A series of maps, calculated with domain C2 of molecule I rotated by different amounts, and quantified by calculating the average electron density for each lobe has placed this domain with a rotation of 15°. A similar exercise with molecule II has as yet not been successful. Refinement is continuing and with 7 of the 8 domains now placed the current R value for the 3.5 Å data is 0.27.

1. Anderson, B.F., Baker, H.M., Dodson, E.J., Norris, G.E., Rumball, S.V., Waters, J.M. and Baker, E.N. (1987). *Proc. Nat. Acad. Sci. USA* **84**, 1769-1773.
2. Anderson, B.F., Baker, H.M., Norris, G.E., Rumball, S.V. and Baker, E.N. (1990). *Nature* **344**, 784-787.

2A13

PROTEIN SEQUENCE-STRUCTURE ALIGNMENT BASED ON MUTANT PROFILE FROM MEAN FORCE FIELD POTENTIAL

Luhua Lai, Yanli Wang, Department of Chemistry, Peking University, Beijing 100871, China

Along with the rapid development of DNA and protein sequencing techniques, the gap between the number of known protein sequences and three dimensional structures derived by X-ray crystallography or nuclear magnetic resonance spectroscopy is expanding quickly. The rate of sequence determination is assumed to be at least 50-fold higher than the rate of structure determination. One possible way to fill this gap is to develop efficient protein structure prediction methods. Despite of the success in homology modeling, protein structure prediction remains challenging in case that only distant homology can be found between the sequence of the target protein and those with known structures. From the analysis of known protein structures, it is believed that the number of distinct protein structural folds is relatively small, perhaps no more than 1,500. When all the folds are known, the task for protein structure prediction will be turned into the problem of finding an appropriate fold for a given sequence. We worked on the protein sequence-structure recognition problem by mean force field potential method. A new potential was developed by introducing main chain characteristics into the mean force field. Based on this potential, a position-dependent protein mutant profile was constructed and converted into a 20xL scoring matrix. A protein sequence-structure alignment method was developed by modifying the dynamic programming alignment to use the 20xL scoring matrix. Both sequence-structure recognition search against sequence database and structure-sequence recognition process against an independent dataset of known structures were carried out. The method can not only pick out proteins with high sequence homology, but also can find out the similarities among proteins with sequence identity. From the analysis on sequence-structure and structure-sequence recognition results, structure candidates for a hypothetical protein and a GTP pyrophosphokinase were suggested. The possible applications of this method in protein structure prediction will be discussed.

2A14

CRYSTAL STRUCTURE OF BOVINE β-LACTOGLOBULIN AT 1.9Å RESOLUTION.

M.C. Bewley, R. Kingston, H. Baker & E.N. Baker. Dept. Chem. & Biochem., Massey University, Palmerston North, New Zealand.

β-lactoglobulin is the major protein of the whey fraction of milk. Although its function is unclear, there is evidence to suggest that that it is a transporter of lipid-soluble molecules (Iametti *et al.*, 1995). β-lactoglobulin exists as a dimer at neutral pH and tends to dissociate into monomers when the pH is lowered. The change in pH from a high to a low value is thought to bring about a conformational change in the protein which is implicated in altering the flavour of the milk during industrial processing.

Bovine β-lactoglobulin has been crystallised at pH 7.3 by the vapour diffusion method. The crystals have space group $C222_1$ with unit cell dimensions a=55.5Å, b=82.8Å, c=66.7Å and diffract to a resolution of 1.9Å. The structure has been determined by MIR (2 heavy atom derivatives). The FOM for the MIR map was 0.7 to 3.0Å resolution. The phases have been improved by solvent flattening and histogram matching and extended to 1.9Å. The current model is being refined using X-PLOR.

The refined structure and its biological implications will be reported.

Iametti S. *et al.*, (1995). *J. Agric. Food. Chem.* 43, 53-58.
Papiz M.Z. *et al.*, (1986). *Nature* 324, 383-385.

2A21

CRYSTALLINE-STATE *TRANS-CIS* PHOTOISOMERIZATION OF COBALOXIME COMPLEXES

Taro Yamada, Hidehiro Uekusa and Yuji Ohashi
Department of Chemistry, Tokyo Institute of Technology,
O-okayama, Meguro-ku, Tokyo152

A new type of crystalline-state photoisomerization, *trans-cis* conversion of the 2-butenyl group bonded to the cobalt atom, has been found in some cobaloxime complexes. Recently we prepared the crystals of (*trans*-2-butenyl)cobaloxime complexes with pyridine, **1**, 4-bromopyridine, **2**, 3-chloropyridine, **3**, and dimethyl sulfide, **4**. X-ray analysis of these crystals showed that the *trans*-2-butenyl groups take disordered structures in the four crystals. The crystals of **1** and **2** have essentially the same structure and the molecules lie on crystallographic mirror planes. The crystals of **3** and **4** have no mirror symmetry although the *trans*-2-butenyl groups have disordered structures similar to those of **1** and **2**. Crystals of **1** and **2** changed their unit cell dimensions during the irradiation with a Xe lamp. X-ray analysis showed *trans-cis* transformation of 2-butenyl group took place with retention of the crystallinity by the irradiation. The irradiation for two hours brought about 66% conversion for the crystal **1**, on the other hand for the crystal **2** only 48% conversion was observed after the irradiation for a day. The crystals **3** and **4** showed no reactivity on exposure to a Xe lamp. The reaction cavities of **1** and **2** have similar shape to each other and fairly wide void space around the *trans*-2-butenyl group. The *cis* isomers produced occupy the void space. The reaction cavities of **3** and **4** are small and have not enough void-space. This is a reason why the crystals 3 and 4 showed non-reactivity.

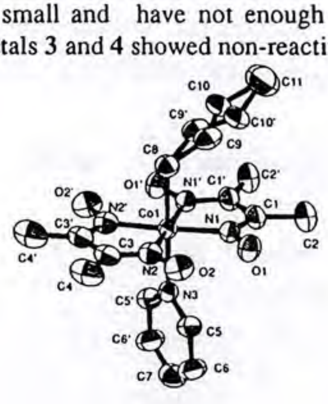

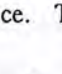
1

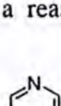

2

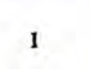

3

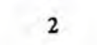

4

2A22

CRYTAL STRUCTURE OF BICYCLOMANGOSTIN : THE NEW ACID-CATALYZED CYCLIZATION PRODUCT OF MANGOSTIN

C. Pakawatchai and W. Malabusarakam, Department of Chemistry, Prince of Songkla University, Hat Yai 90112, Thailand, and P. Wiriyachitra, Department of Pharmacognosy, Chiang Mai University, Chiang Mai 50200, Thailand, and W. C. Taylor, Department of Organic Chemistry, Sydney University, NSW 2006, Australia, and B. W. Skelton and A. H. White, Department of Chemistry, University of Western Australia, Nedlands 6907, Australia.

Three cyclization products, 3-isomangostin, 1-isomangostin and bicyclomangostin, were obtained from the treatment of mangostin with *p*-toluenesulfonic acid. Bicyclomangostin was found to be a new cyclization product. Its structure has been determined by single crystal X-ray diffraction methods. The structure is almost planar. There is a strong intermolecular hydrogen bond between hydroxyl group and carbonyl group, O - H ---- O = C, 1.4 Å, this hydrogen atom being located in a final difference map.

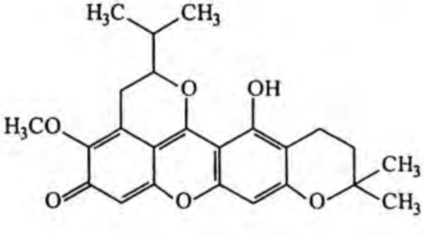

Fig 1. Bicyclomangostin.

Crystal data : $C_{24}H_{26}O_6$ monoclinic, space group *C*2/*c*(No. 15)
a 15.956(7), *b* 14.423(17), *c* 18.482(7) Å, *β* 104.92(3)°.

2A23

THE γ ,AND δ STRUCTURAL EFFECTS OF SILICON AND TIN

Alison J. Green and Jonathan M. White
Department of Chemistry, University of Melbourne, Parkville, Victoria 3052

We have been examining the effect on the length of the R-OX bond of a silicon or tin substituent four (γ) and five (δ) bonds away, where OX represents a leaving group.

Silicon and tin substituents can have a profound effect on the reactivity of the R-OX bond. eg, an ester will be solvolysed more readily if there is a $SiMe_3$ or $SnMe_3$ substituent 4[1]or 5[2] bonds away. These phenomena are known as the silicon and tin γ- and δ- effects respectively and are based on the ability of silicon and tin to stabilise a carbocation at these positions. The silicon effects have been studied more extensively, although the tin effects are more dramatic. These effects have demonstrated a conformational dependence, ie they require favorable overlap between the donor (Si or Sn) and the leaving group, and are thought to be stereoelectronic in origin. Most evidence supports the involvement of hyperconjugation in the mechanisms. This ought to be reflected in observable ground state effects, which can be manifest as changes in the C-OX bond length and, less prominently, as changes in the C-Si/Sn bond length.

A structural study was undertaken in order to examine the extent of such effects. Several nitrobenzenesulfonate esters have been prepared, with a $SiMe_3$ or $SnMe_3$ group at the γ- and δ- positions. Their structures were determined using low temperature X-ray diffraction. The results of the study will be presented in this paper.

1: Si: V.J. Shiner Jr; M.W. Ensinger Jr; R.D. Rutkowske: *J. Am. Chem. Soc.* **1986**, 108, 842; Sn: Davis, D. D. ; Black, R. H. *J. Organomet. Chem.* **1974**, 82, C30-C34; Fischer, W.; Grob, C. A. *Helv. Chim. Acta* **1978**, 61, 1588-1608.

2: W. Adcock; V.J. Shiner Jr; J. Coope; N. Trout: *J. Org. Chem.* **1990**, 55, 1411; W. Adcock; A.R. Kristic, P.J. Duggan, V.J. Shiner Jr; J. Coope, M.W. Ensinger: *J. Am. Chem. Soc.* **1990**, 112, 3140-3145.

2A24

COMPARISON OF Fe(II)-P AND Fe(0)-P LENGTHS: STRUCTURE OF $[(\eta^5\text{-}C_5H_5)Fe(CO)C(O)Me](\mu\text{-}\eta^1{:}\eta^1\text{-dppe})[(\eta^4\text{-}MeC_5H_5)Fe(CO)_2]$

Ling-Kang Liu and Lung-Shiang Luh, Institute of Chemistry, Academia Sinica, Nankang, Taipei, Taiwan 11529 and Department of Chemistry, National Taiwan University, Taipei, Taiwan 10767, ROC

In 1:1 molar ratio, $(\eta^5\text{-}C_5H_5)Fe(CO)_2Me$ proceeds with a dppe-assisted [dppe = $PPh_2(CH_2)_2PPh_2$] methyl migratory-insertion to yield the uni-dentate complex $(\eta^5\text{-}C_5H_5)Fe(CO)C(O)Me(\eta^1\text{-dppe})$, in addition to the bridging product $[(\eta^5\text{-}C_5H_5)Fe(CO)C(O)Me]_2(\mu\text{-}\eta^1{:}\eta^1\text{-dppe})$. Since the former is an intermediate towards the latter, the reaction of $(\eta^5\text{-}C_5H_5)Fe(CO)_2Me$ with dppe in 2:1 molar ratio easily proceeds to the bridging complex. At -78°C, the 1:1 mixture of $(\eta^5\text{-}C_5H_5)Fe(CO)_2I$ and the uni-dentate $(\eta^5\text{-}C_5H_5)Fe(CO)C(O)Me(\eta^1\text{-dppe})$ in THF reacts with MeLi to produce a novel complex $[(\eta^5\text{-}C_5H_5)Fe(CO)C(O)Me](\mu\text{-}\eta^1{:}\eta^1\text{-dppe})[(\eta^4\text{-}MeC_5H_5)Fe(CO)_2]$ in which a dppe links two isomeric, methylated $[(C_5H_5)Fe(CO)_2]$ units, one end being in the form of $(\eta^5\text{-}C_5H_5)Fe(CO)C(O)Me$ and the other end $(\eta^4\text{-}exo\text{-}MeC_5H_5)Fe(CO)_2$. The X-ray structure of the title complex exhibits a dppe-bridged *pseudo*-octahedral Fe(II)/*pseudo*-square pyramidal Fe(0) complex with no metal-metal bonding. The embedded structural parameters of Fe(II) and Fe(0) give evidence to a smaller Fe(II) radius than Fe(0), as suggested by the Fe(II)-P length of 2.178(2)Å simultaneously present with that of Fe(0)-P, 2.212(1)Å. The shortening of 0.034Å is significant as it represents a difference greater than 10 esds.

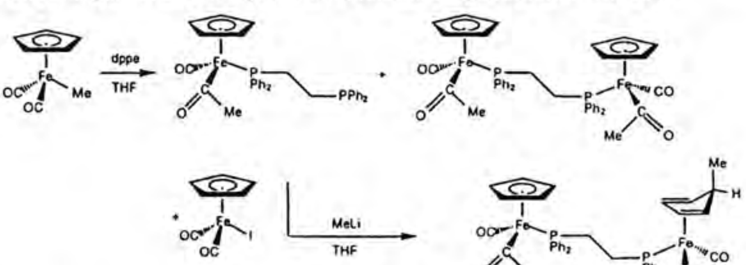

$[(\eta^5\text{-}C_5H_5)Fe(CO)C(O)Me](\mu\text{-}\eta^1{:}\eta^1\text{-dppe})[(\eta^4\text{-}MeC_5H_5)Fe(CO)_2]$, crystal data: $C_{42}H_{40}Fe_2O_4P_2$, P-1, a 11.967(2), b 12.066(1), c 14.855(4)Å, α 106.51(1), β 97.84(2), γ 108.20(1)°, V 1893.1(6)$Å^3$, FW = 782.42, Z = 2, F(000) = 811.88, ρ_{calc} = 1.373g/cm^3, μ = 0.89mm^{-1}, Mo-K_α λ = 0.7093Å, CAD-4, $2\theta \le 50^o$, transmission factors 0.935 - 0.999, 90 atoms, 451 parameters, 4052 observations $[I_o > 2.5\sigma(I_o)]$, R = 0.031, R_w = 0.037, GOF = 1.81, Δ/σ = 0.020.

2A25

STRUCTURES OF NOVEL METAL-CARBENE COMPLEXES DERIVED FROM HYPERVALENT TETRAAZATHIAPENTALENES

F. Iwasaki, N. Manabe, S. Shimamoto, H. Nishiyama and M. Yasui, Dept. of Applied Phys. and Chem., The Univ. of Electro-Comm., Chofu-shi, Tokyo 182, Japan, and N. Matsumura, Dept. of Applied Chem., College of Eng., Univ. of Osaka Prefecture, Sakai-shi, Osaka 591, Japan

6a-Thiatetraazapentalene derivatives (**1**) (Iwasaki, et al., 1991; Matsumura, et al., 1986) which contain the hypervalent sulfur atom have been found to give novel metal-carbene complexes by reaction with $Pt(PPh_3)_4$, $Pd(PPh_3)_4$ and $RhCl(PPh_3)_3$ (Matsumura, et al., 1995). In the case of **1a**, X-ray investigations revealed that the central sulfur atom in **1a** was substituted by a metal atom and that thiocarbonyl groups on one or both sides were rotated to form metal-sulfur bonds in the resulted metallapentalene framework (**2**, **3**, **4**) . In the case of **1b** the carbonyl group remained without coordinating metal atom (**5**, **6**). The reaction of $RhCl(PPh_3)_3$ with **1c** gave a Rh complex (**7**) of a different type. Frontier electron densities were calculated on these tetraazathiapentalenes using MO calculations in order to investigate the difference of reactivity among **1a**, **1b**, and **1c**. In this paper, structures of these novel calbene complexes with metallapentalene frameworks and the effects of the side groups will be reported. From the results of the structures of complexes and MO calculations the mechanism of the formation of these metal-carbene complexes will also be discussed.

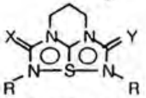

1a X=S, Y=S
1b X=S,Y=O
1c X=O,Y=O

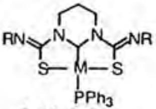

2 M=Pt,Pd
R=Me, Et, p-Cl-Ph

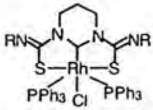

3 R=p-Cl-Ph

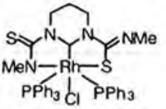

4

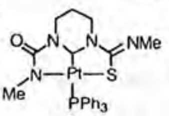

5

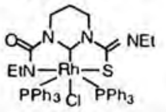

6

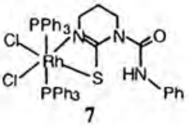

7

Iwasaki, F., Murakami, H., Yamazaki, N., Yasui, M., Tomura, M. & Matsumura, N. (1991). *Acta Cryst.*, C47, 998-1003.
Matsumura, N., Kawano, J., Fukunishi, N., Inoue, H., Yasui, M. & Iwasaki, F. (1995). *J. Am. Chem. Soc.*, 117, 3623-3624.
Matsumura, N., Tomura, M., Yoneda, S. & Toriumi, K. (1986). *Chem. Lett.*, 1047-1050.

2B11

LAUE CLASSES OF α- AND β-QUARTZ AND THEIR PATTERSON FUNCTIONS EVALUATED WITH POWDER DIFFRACTION DATA

M. Ohmasa, Department of Life Science, Himeji Institute of Technology, Kanaji 1479-1, Kamigori, Akogun, Hyogo 678-12, Japan, K. Ohsumi, Photon Factory, National Laboratory for High Energy Physics, Oho 1, Tsukuba, Ibaraki 305, Japan, and H. Toraya, Ceramics Research Laboratory, Nagoya Institute of Technology, Asahigaoka, Tajimi 507, Japan

There are two possible Laue classes, holohedral and hemihedral ones, for the crystal systems with trigonal symmetry or symmetries higher than trigonal. Recently Ohmasa & Ohsumi (1995) indicated that the available informations obtained from powder diffraction data can be regarded as *a composite reciprocal lattice* when the data are demonstrated in the three dimensional reciprocal space, and the Patterson function obtained by Fourier transform of the composite diffraction pattern represents a set of vectors corresponding to *a composite vector set.* Hemihedral Laue classes can then be distinguished from holohedral ones based on the concentration of Patterson peaks. The present studies have been carried out to apply the method to the powder X-ray diffraction data of the α- and β-quartz and to demonstrate how the difference of the Patterson functions of both phases is. The sample crystal used for the present studies was grown by the Toyotushinki Ltd. The profiles of α- and β-quartz were measured with conventional diffractometers at 293K and 893K respectively. The profiles were analysed with the program WPPF (Toraya, 1986). The lattice parameters are a=4.91296(2), c=5.40442 (3)Å for α-quartz and a=4.9947(2), c= 5.4585(2)Å for β-quartz. Significant difference of heights of the peaks in both $P(u0w)$'s was observed and ascertained to be consistent with their Laue symmetries.

Ohmasa, M. and Ohsumi, K. (1995). *Acta Cryst.* A**51**, 87-91.
Toraya, H. (1986). *J. Appl. Cryst.* **19**, 440-447.

X-RAY QUANTITATIVE ANALYSIS WITHOUT STANDARDS USING RIETVELD METHODS WITH HIGH ACCURACY

Changlin KUO and Hongchao LIU, Shanghai Institute of Ceramics, Chinese Academy of Sciences, Shanghai 200050, P. R. China

In quantitative phase analysis using the Rietveld method, weight fractions of crystalline phases can be calculated directly from scale factors. Various corrections were introduced in the Rietveld method to get correct intensities data. However, less attention was paid to the microabsorption effect. This leads the quantitative analysis give unreliable results. The diffraction data can be corrected for microabsorption effect in two ways. For the linear correction of microabsorption by Sparks that represents an empirical statement for strong absorption, the following function is used

$S_r = P_s + 2\Theta C_s$ (P_s and C_s adjustable parameters) (2)

For the use of Hermanns model,

$S_r = 1 - P_0 - C_\tau/\sin\Theta(1-\tau/\sin\Theta)$ (3)

where P_0, C and τ are adjustable parameters . This model is valid exactly for weak absorption and low surface roughness degree.

Expressions (2) and (3) can be incorporated into DBWS 9600-PC Rietveld program. Equation (4) is used to calculated the relative abundance of phase A.

$W_A = S_A(MV)_A/\sum S_t(MV)_t$ (4)

Where, M are the number and mass of unit cell; V is the volume of unit cell. The summation is over all t crystalline and identified components. If an internal standard phase s has been added to the mixture prior to data collection, then the amount of amorphous and minor phases may be estimated using the follow equation.

$W_{\text{amorph and minor phases}} = 1 - \sum W_r$ (5)

Where Wr is determined by equation (6).

$W_r = W_s S_r(ZMV)_r/S_s(ZMV)_s$ (6)

The subscript s and r refer to standard phase and each phase in the mixture.

Practical analysis proved that new correction can give more precise results.

2B13

XRD DETERMINATION OF THE MINERAL STRUCTURAL STATE CHARACTERISTICS

A.P.Slusarev, Institute of Geological Sciences NAS RK, Almaty, Kazakhstan

Investigations of the XRD structural criterions reveal relationships between structural features and alteration of minerals during geological process their evolution in sediment rocks or weathering complexes. The numerous quantitative and statistical criterions: index of crystallinity, coefficient of variation of basal spacing, integral half height breadth of diffraction reflex, crystallochemical properties of clay minerals, content of dispersive subamorphous components, total iron content were used as probable indicators for evatuating of forming conditions, direction and degree of diagenesis and rate of weathering of rocks and minerals. Numerical estimations of characteristics, describing clay minerals structural state were obtained: type of interlayer cation, degree of hydration, layer charge, expandable layers content, tetrahedral and octahedral cation substitutions, type of layers, their nature and contents, order of stacking mixed-layered minerals. The XRD criterions determined from diffraction pattern of powder, randomly and preferentially oriented samples, treated samples, or by results of special X-ray diffraction measurements were used for structural state of mineral description.

2B14

PROFILE ANALYSIS FOR LATTICE DEFORMATION AND CRYSTALLITE SIZE UNDER COMPRESSION

Takamitsu YAMANAKA Department of Earth and Space Science, Faculty of Science
Osaka University 1-16 Machikaneyama Toyonaka Osaka 560 Japan

In the last two decades structural investigations by X-ray diffraction studies under non ambient condition have been interested in order to comprehend their elastic properties and pressure-induced polymorphic transition. It has been known that the lattice deformation and lessening of the grain size under static compression bring about the line broadening of diffraction profile and that the peak position is directly related to the compressibility or bulk modulus.

Profile analysis has been made using energy dispersive diffraction spectra of NaCl, which were taken under hydrostatic pressures up to 12GPa with high pressure apparatus MAX90 in Photon Factory, Tsukuba. Pseudo-Voigt function, linear equation of Gaussian and Lorentzian function, is applied for the profile fitting concerning strain energy and grain size, which are changed with increasing pressure. The full width at half maximum (FWHM) Γ_L of the Lorentzian profile continuously increases with pressure in comparison with Γ_G of Gaussian. The Lorentzian component η parameter of pseudo-Voigt function is raised with pressure. Integrated half width β(hkl) is basically expressed by β=B+b, where B is related to the lattice deformation and size effect and b is instrumental broadening. Mean crystallite size <Da> and mean squares-strain $<e^2>$ are derived from the observed β(hkl). A smaller crystallite size makes a larger β_L. On the other hand the dislocation density and intrinsic strain in the lattice enhance β_G.

Pressure-induced amorphization of hydrates $Ca(OH)_2$ has been observed using diamond anvil pressure cell at pressures higher than 6.5GPa. With increasing pressure the peak profile becomes gradually broadened and finally no peaks are observed. The amorphous state is reversibly changed to the original hydrate structure without dehydration reaction in the course off depression. The amorphization corresponds not to the size effect but to the lattice deformation. Crystallite size estimated from B of hkl peaks is a little change with pressure but a significant change of the strain energy . The individual hkl diffraction peaks show the anisotropic lattice deformation under hydrostatic pressure. Peak shift assigned to O-H bond of the Raman spectra observed at various pressures indicates the increase in hydrogen bond character. The trend of the peak shift is continued even in the amorphous state.

2B21

ROUGHNESS ESTIMATION OF POLYCRYSTAL METAL SURFACES WITH USE OF X-RAY GLANCING SCATTERING

Yoshikazu FUJII, Kenji YOSHIDA and Kentaroh YOSHIDA,
Department of Mechanical Engineering, Kobe University, Rokkodai, Nada, Kobe 657, Japan

At glancing angle incidence of x-ray beam on a solid surface, most of the x-ray are scattered at only shallow region near the surface. For suitably chosen geometries, the scattered x-ray intensity is sensitive to surface morphology. Using these nature of x-ray glancing scattering we tried roughness estimation of polycrystal metal surfaces. The experiments were performed with use of Cu-Kα characteristic x-ray with λ=1.54Å from 18kW rotating-anode x-ray source. At several glancing angle incidence of the x-ray beam on a polycrystal silver surface, angular distributions of the scattered x-ray intensity were measured. This angular distributions reveal the surface roughness. Unlike electron diffraction, for x rays multiple scattering is negligible except very close to a bulk Bragg peak, then the observed intensity of the scattered x-ray can be computed by use of kinematical theory. The angular distributions of the scattered x-ray intensity were simulated with use of simple model of rumpled surface. Based on these result we propose new method of roughness estimation of surface.

2B22

X-RAY SCATTERING FROM MICROCRYSTALLINITY IN THE THERMALLY OXIDIZED SiO_2 THIN FILMS ON Si(110) SURFACES

T.Shimura, R.Kojima, H.Misaki, and M.Umeno, Department of Material and Life Science, Osaka University, 2-1 Yamadaoka, Suita, Japan

Very weak peaks were observed in the X-ray diffraction from the thermally oxidized thin films on Si(001) surfaces by Iida et al. (1991) . They claimed that these peaks were Bragg peaks originated from small crystallites which coexisted with the amorphous phase having some epitaxial relationship with the Si substrate. A pseudo-cristobalite structure was proposed as a possible model, in which the atomic arrangement is similar to that of the cristobalite structure, while the unit cell is tetragonal so as to match the lateral lattice spacing with that of the Si substrate. Takahashi it et al. (1993) extended this study so that the crystallites were found to locate not only at the interface between the Si substrate and the amorphous layer, but also widely in the amorphous layer, preserving the epitaxial relation with the substrate. The volume fraction of such crystallites was estimated to be a few percent of the whole volume of the amorphous layer.

In this paper we show that similar Bragg peaks are observed from the oxide layers on Si(110) surfaces, indicating the existence of crystallites having epitaxial relationship with the Si substrate. The samples were prepared by oxidizing Si wafers at 950°C in a dry oxygen atmosphere. The thicknesses of the oxide layers were 760Å and 230Å. In the X-ray diffraction patterns from these samples, similar peaks were observed just on the lower angle side of the CTR (crystal truncation rod) scattering around the 111 Bragg point, of which position is approximately 0.45 0.45 0.00 in reciprocal space. The peak intensity depends on the thickness of the oxide layer, while the peak is not observed in the etched sample. A high resolution measurement of the profile of the peak using a synchrotron radiation source revealed that the profile had Laue-function-like oscillation fringe pattern, of which period corresponded to the inverse of the film thickness.

From these results it was concluded that these peaks were Bragg peaks originated from the crystallites which coexisted in amorphous SiO_2 having some epitaxial relationship with the Si substrate.

The authors thank to Prof. J.Harada of The University of Electro-communications and Dr. I.Takahashi of Nagoya university for discussions and encouragement.

Iida, Y., Shimura, T., Harada, J., Samata, S., & Matsushita, Y. (1991) Surf. Sci. 258, 235-238.

Takahashi, I., Shimura. T., & Harada, J., (1993) J.Phys.: Condens. Matter 5, 6525-6536.

2B23

DETERMINATION OF ELECTRON DENSITY PROFILE FORM X-RAY REFLECTIVITY DATA USING DISTORTED WAVE BORN APPROXIMATION

Milan K. Sanyal, Alokmay Datta, and Sangam Banerjee Saha Institute of Nuclear Physics, 1/AF Bidhannagar, Calcutta 700 064, INDIA.

X-ray reflectivity measurement of a multilayer system in principle provides us an independent determination of thicknesses, electron densities and interfacial roughnesses of different sublayers of the film. But, due to the well-known "phase problem", determination of the electron density profile from the x-ray reflectivity data is not trivial [1]. We present here a scheme to extract electron density profiles from x-ray reflectivity data using Distorted Wave Born Approximation (DWBA). We illustrate the scheme using both simulated and measured data.

In this scheme,the electron density profile across a multilayered thin film is approximated by thin slices of fixed electron densities. Difference amplitudes of the electron densities of these slices from an average electron density of the film are determined by fitting them to x-ray reflectivity data using a DWBA formalism [1]

[1]. M. K. Sanyal et. al., Europhys. Lett, vol. 21, pp. 691, (1993)

2B24

Electron Density Maps for Clean and Adsorbed Silicon Surfaces Calculated with the Maximum-Entropy Technique

H. Hashizume, C.M. Carvalho[1], O. Yokota, A.W. Stevenson[2]
and I.K. Robinson[3]

Res. Lab. Eng. Mater., Tokyo Institute of Technology, Nagatsuta, Yokohama 226, Japan. 1) Inst. de Fisica, Univ. de Sao Paulo, Brazil, 2) CSIRO Div. of Mater. Sci. & Tech., Australia, 3) Dept. of Phys., Univ. of Illinois, USA.

Maximum-entropy (ME) electron density maps have been calculated for two-dimensional reconstructed surface structures using X-ray and electron diffraction data. Clean Si(111) 7×7 and arsenic-adsorbed Si(001) 1×2 surfaces are studied. Experimentally determined structure-factor magnitudes for in-plane reflections from these surfaces are assigned phases from refined models and then used as a constraint in a maximization of Shannon-Jaynes entropy. Surface diffraction data feature missing integer-order reflections which overlap the bulk reflections and are experimentally inseparable from them. The maps calculated for the Si(111) 7×7 surface using 84 fractional-order X-ray reflections with a maximum 1.135 Å resolution clearly resolve all the 102 atoms of Takayanagi's dimer-adatom-stacking fault model. Electrons are concentrated on the atomic sites, showing peaks at the adatom locations more than twice as high as the mean of the other atomic peaks, where third-layer atoms exist immediately below. The atomic coordinates determined from the map are in good agreement with those from a least-squares refinement [1], confirming the *p*6*mm* symmetry assumed in the latter refinement. The electron diffraction (ED) data offered by R. Twesten include 193 reflections, whose intensities are evaluated by averaging symmetry-equivalent reflections to minimize dynamical effects [2]. Higher-order reflections contained in the ED data give more round shapes to the atomic peaks and more clearly show bonding electrons for the Si(111) 7×7 surface atoms in ME maps. We will also discuss ME maps calculated for the Si(001):As 1×2 surface, which are believed to show nonspherical electron distributions around the non-reconstructed surface atoms.

The ME technique has a tendency to underfit large structure factors, often associated with low-angle reflections. To avoid adverse effects on bonding electron densities [3], we do not stop iteration calculations at $\chi^2 = 1.0$, but go to $\chi^2 \ll 1$ for several sets of $|F(\mathrm{obs})|$ data obtained by randomly fluctuating individual $|F(\mathrm{obs})|$ data within the experimental variances. Features common to the fluctuated maps are real ones and others are attributed to noise.

[1] I.K. Robinson et al., Phys. Rev. B 37, 4325 (1988).
[2] R.D. Twesten and J.M. Gibson, Ultramicroscop. 53, 223 (1994).
[3] G. Jauch, Acta Cryst. Acta. Cryst. A 50, 650 (1994).

2C11

DEVELOPMENT OF CCD-BASED X-RAY DETECTORS WITH A BERYLLIUM-WINDOWED IMAGE INTENSIFIER FOR DIFFRACTION STUDIES

Y. Amemiya, K. Ito, PF, KEK, Oho, Tsukuba, Ibaraki 305, Japan,
N. Yagi, Tohoku Univ., Y. Asano, JAERI, K. Wakabayashi, Osaka Univ. T. Ueki, Riken, and T. Endo, Hamamatsu Photonics K.K.

We have developed a large area-sized CCD-based x-ray detector for diffraction studies especially for real-time and time-resolved measurements (Amemiya et al., 1995). The detector consists of i) an x-ray image intensifier, ii) an optical lens, iii) a CCD image sensor, and iv) a data acquisition system. An x-ray image is converted to intensified and de-magnified visible-light image by the x-ray image intensifier. Then the visible-light image is viewed by a cooled CCD (TC-215, 1000 x 1018 pixels) or a TV-rate (30 frames/s) CCD (SONY XC-77) through the optical lens. The signal from the CCD is digitized and stored in the data acquisition system. The x-ray image intensifier uses a 1 mm thick beryllium plate which serves as both an entrance window and a substrate for the phosphor. The CsI:Na phosphor of 150 μm thickness is attached directly on the inner surface of the beryllium window. The CsI:Na crystals are made in a columnar shape along the direction normal to the phosphor surface so that the undesired light scattering within the phosphor in the lateral direction is minimized. A bi-alkali (RbCsSb) photo-cathode is evaporated onto the inner surface of the CsI:Na phosphor. Owing to the photon gain of the image intensifier, as many as 550 visible photons per 8 keV photon are incident to the CCD. This value is large enough to employ a TV-rate CCD with its noise quantum-limited. The image intensifier responds to x-ray intensity range of more than 6 orders of magnitude. The detective quantum efficiency of the detector is 60 %. Because of the convex shape of the beryllium window, the detector has the image distortion and the consequent non-uniformity of response to be corrected by software. Detailed performance of the detector will be described together with its applications to x-ray diffraction experiments with synchrotron radiation.

Amemiya, Y., Ito, K., Yagi, N., Asano, Y., Wakabayashi K., Ueki, T., Endo, T. (1995). *Rev. Sci. Instrum.* 66, 2290-2294.

2C12

THE OPTIMIZATION OF PARAMETERS OF BRAGG-FRESNEL LENSES

L. A. Haroutunyan and K. G. Trouni, Department of Solid State Physics, Yerevan State University, A.Manoukyan 1, Yerevan, 375049, Armenia

One of techniques for hard X-rays focusing is the utilization of zonal plate with incident spherical (or plane) X-ray wave. The phase modulation of X-rays reflected by monocrystal, causing the beam focusing in vacuo, is accomplished by a step-like variation of plate thickness at the Fresnel's zones edges because of the plate exit surface relief. The purpose of our study was to select optimized parameters for experimental set-up. The problem was formulated as follows: what should be a step-like profile of plate thickness for the reflected beam phase shift, associated with the presence of zones, being 180 degree. Both approximate analytical calculations by means of the above-mentioned phase shift series expansion as well as more accurate computer ones are carried out. As a result, in the case of incident spherical wave, for optimized focusing the crystal thickness jump has to be some varying quantity, as a dependence from the zones numbers, and this functional dependence is determined from the concrete experimental conditions.

Aristov V.V., Kuznetsov S.M., Kouyumchyan A.V. & Snigirev A.A. (1991). phys.stat.sol.(a)125, 57-66.

Aristov V.V., Basov Yu.A., Snigirev A.A., Yunkin V.A.

Ishikawa T. & Kikuta S. (1991). Nucl. Instr. and Meth. A308, 413-415.

2C13

THE THEORETICAL AND EXPERIMENTAL STUDY OF X-RAY DIFFRACTION FOCUSING PHENOMENA ON THE TWO-BLOCK CRYSTALLINE SYSTEM WITH MISSORIENTATED BLOCKS

K. G. Trouni and A. H. Grigoryan. Department of Solid State Physics. Yerevan State University. A.Manoukyan 1. Yerevan. 375049. Armenia.

Theoretically and experimentally the problem of the diffraction focusing in LL - interferometer with missorientated plates is investigated. The asymptotic solution for the double reflected beam amplitude is obtained in the approximation of the saddle-point method for the case of small angular missorientations of the blocks. This solution points at the oscillatory behavior of beam intensity in the center of the diffraction pattern depending on small missorientations of the order 0.01 angular seconds. The solution explains as well the phenomenon of the central peak splitting at the same missorientations of plates. The high sensitivity of the diffraction focusing phenomenon to small missorientations is experimentally shown. After preparation of the interferometer it was splitted up into two independent plates orientated on the two goniometric heads. The plates rotation was realized by piezocrystals. There are registered the oscillations and spatial splitting of the peak stimulated by the missorientations of the order 0.01 - 0.1 angular seconds. The correspondence between theory and experiment is fairly well.

Indenbom.V.L., Slobodetski.I.Sh. & Trouni.K.G. (1974). JETP. 66. 1110-1120.

2C14

RECENT DEVELOPMENTS OF X-RAY CRYSTAL STRUCTURE ANALYSIS BY NEW DIFFRACTOMETER AND COOLING EQUIPMENT

Hidehiro UEKUSA and Yuji OHASHI, Department of Chemistry, Tokyo Institute of Technology, Ookayama, Tokyo 152, Japan

Recently we have designed and made a new type of diffractometer for rapid data collection. The purpose of this development is to collect the data of unstable crystals and to determine the structures of reaction intermediates.

The new diffractometer has a Weissenberg camera type mechanism with a feature of a κ-type goniometer, two imaging plates, and spiral motion reading mechanism. It is also equipped with a new type of nitrogen gas stream equipment to adjust the temperature of crystal specimen.

This type of equipment requires no liquid nitrogen, instead, it extracts dry nitrogen gas from the air and cool the gas with a cooling system using closed circle He gas. The cold nitrogen stream is surrounded with dry sheath gas stream to prevent the formation of ice around the specimen. This equipment covers a temperature range of 80 K to room temperature in low temperature mode and up to 420 K in high temperature mode. Successful structure determinations of the crystals that are sensitive to X-ray exposure, loses the solvent molecules easily, and have weak diffraction intensity also demonstrate the ability of this diffractometer. For example, the initial molecular structure of syn-tricyclooctane derivative has been determined by 140 minutes measurement, which has not been analyzed, because the bond cleavage easily occurs under X-ray irradiation.

Although some cobaloxime and cobalt complex with sugar ligands crystals easily decomposed by loss of the solvent molecules, we have successfully determined the structure without sealing the crystal in a capillary.

All the results of the crystal structure analysis indicate that the total accuracy of the new diffractometer is comparable to that of a four circle diffractometer despite a very short measurement time.

2C15

X-ray Wiggler Beamlines at SRRC

Y.-C. Jean , C.-H. Lee, K.-L. Tsang, H.-H. Hung, J.-R. Chen, C.-H. Hsu, L.-Y. Jang, M.-T. Tang, H.-Y. Lee, H.-S.Sheu, T.-E. Dann, J.-F. Lee, J.P. Wang, S.-L. Chang, SRRC & National Tsing Hua University, Hsinchu, Taiwan, R.O.C.

Synchrotron Radiation Research Center (SRRC) is a third generation synchrotron radiation facility being setup in Taiwan for basic science research and advanced technology development. In order to increase the usable X-ray photons up to 15 KeV, a 1.8 T wiggler insertion device has been installed with the 1.3 GeV storage ring. Three X-ray beamlines sharing the 13 mrad horizontal radiation fan from the wiggler have been specially designed to cover various kinds of X-ray experiments including macromolecular crystallography, surface sciences, high resolution powder diffraction, small-angle X-ray scattering, elastic diffuse scattering non-ambient crystallography, and X-ray absorption spectroscopy. The construction of thease three beamlines is nearly completed, however, due to the significant delay in the delivery of mirrors, a temporary back-up beamline has been constructed and under commissioning now. The construction of these three beamlines and the characterization of the back-up beamline will be described in detail.

2C21

HYDROGEN IN METALS: NEUTRON DIFFRACTION STUDIES OF THE CRYSTAL STRUCTURES OF Zr_2NiD_x

M.M. Elcombe and C.J. Howard, Australian Nuclear Science and Technology Organisation, Lucas Heights, NSW 2234, Australia, and S.J. Campbell, Department of Physics, Australian Defence Force Academy, Canberra, ACT 2600, Australia.

Zirconium and zirconium alloys are known to absorb large quantities of hydrogen. This study concerns Zr_2Ni (tetragonal $CuAl_2$ structure, space group I 4/*mcm*) which is found to absorb as much as 5 hydrogen (deuterium) atoms per formula unit. The objectives have been to determine how the hydrogen (deuterium) is accommodated, and what expansion or distortion is associated with the incorporation of hydrogen into the crystal structure.

An advance has been made through the recent unambiguous determination from neutron powder diffraction (Elcombe, Campbell, Howard, Büttner and Aubertin, 1995) of the room temperature crystal structure of Zr_2NiD_4 [monoclinic, space group I2/*c*, a 6.7887(1), b 6.7584(1), c 5.6748(1)Å, β 91.039(1)°]. The deuterium occupies the tetrahedral interstices, subject to the restriction that two tetrahedra sharing a common face cannot both be occupied.

The room temperature structure of Zr_2NiD_5 has been shown to be triclinic, the triclinic distortion being indicated in the high resolution neutron powder diffraction pattern, and confirmed using synchrotron X-rays. The lattice parameters have been determined, and progress towards the solution of the crystal structure from the neutron powder data is encouraging.

Elcombe, M.M., Campbell, S.J., Howard, C.J., Büttner, H.G. and Aubertin, F. (1995). Submitted to *Journal of Alloys and Compounds.*

NUCLEAR DENSITY DISTRIBUTION AND ANHARMONIC THERMAL VIBRATION OF SnO_2 OBTAINED BY THE MAXIMUM ENTROPY METHOD

S.Kumazawa & K.Ishida, Department of Physics, Science University of Tokyo, Japan and M.Takata & M.Sakata, Department of Applied Physics, Nagoya University, Japan and Y.Ishii & Y.Morii, Japan Atomic Energy Research Institute, Japan.

From non-magnetic neutron powder diffraction data, the Maximum Entropy Method (MEM) can provide a high resolution nuclear density distribution. The density distribution describes thermal motion of atoms regardless harmonic or anharmonic. It is, therefore, possible to determine potential parameters of corresponding atoms by the least squares refinement of nuclear density distribution. The purpose of this paper is to calculate the nuclear density distribution of SnO_2 at room temperature by the MEM and to determine the potential parameters from this density distribution

The nuetron powder diffraction experiment was carried out by HRPD (High Resolution Powder Diffractometer) at JAERI-3M. The HRPD has 64 detectors for the efficient collection of a powder pattern. In order to obtain an accurate intensity for the MEM analysis, the measurement was performed by overlapped scanning along 2θ angle with 64 detectors and then the overlapped data were averaged on each step. By comparing the reliability factors of Rietveld Analysis between the new and the conventional measurements, the significant change of accuracy is recognized. The powder pattern is recorded at the wave length 1.823Å and 34 reflections up to $\sin\theta/\lambda=0.538$Å^{-1} are obtained.

The MEM calculation was done by using the super computer, Fujitsu VP2600 at Nagoya University Computation Center. In the calculation, the unit cell was divided into $128\times128\times128$ pixels. The total CPU time took 30 sec for 524 iterations. As shown in the obtained MEM map, the densities of tin and oxygen atoms are deformed into rectangle and triangle shapes, respectively. This is due to an effect of anharmonic thermal vibration of the atoms. The anharmonic potential parameters are analyzed by the least squares refinement using One Particle Potential (OPP) model. For tin atom, 9 OPP parameters are determined with reliability factor R=0.50%. For oxygen atom, 12 OPP parameters are determined with R=5.29%. The comparison with previous study of TiO_2, which have same structure, is now in progress.

2C23

RECENT NEUTRON STUDIES OF HIGH-Tc SUPERCONDUCTORS

A.Sequeira, Rajni Sharma and H.Rajagopal, Solid State Physics Division, B.A.R.C, Trombay, Bombay 400085, India.

Rietveld refinement technique using powder neutron data has been extensively used to characterise the structure and properties of high temperature superconductors (HTSC) in recent years. At Trombay, we have investigated the structural features of a number of HTSC. These include (a) pure and substituted [123]-type compounds, (b) pure and substituted [124]-type compounds, (c) Bismuth cuprates with [2201], [2212] and [2223] structures, (d) Thallium cuprates with [1201], [1212] and [2212] structures.

The recent findings of our studies include (i) observation of interstitial oxygen in Y-layers of [123]-(Ca/Co) substituted compounds, (ii) evidence for direct oxidation of CuO2 layers by Ca in [123]-(Lu/Ca) superconductor, (iii) anomalous excess oxygen and presence of oxygen dimers in [2212]-Bismuth cuprates, (iv) oxygen disorder in [2201]- and [2223]- Bismuth cuprates, and (v) evidence for Redox mechanism of hole generation in [1201]-Tl(Ba/Sr)La cuprate system. Some of the new findings of these studies will be highlighted.

2C24

A NEW ASPECT OF THE REACTION MECHANISM OF COBALOXIME COMPLEXES BY NEUTRON DIFFRACTION

Y. Ohgo[a],Y. Ohashi[a], W. T. Klooster[b] and T. F. Koetzle[b],[a]Department of Chemistry, Tokyo Institute of Technology, Meguro-ku, Tokyo 152, Japan, [b]Chemistry Department, Brookhaven National Laboratory, Upton, New York 11973-5000

It has been found that the chiral alkyl groups bonded to the cobalt atom in some cobaloxime complexes are racemized on exposure to visible light in the solid-state. The reaction process of the crystalline-state reaction have been observed directly from the structures analyzed by X-rays at any intermediate stages. To make it sure of the mechanism of crystalline-state racemization we prepared cobaloxime complexes that α carbon of which in the cyanoethyl group labeled with deuterium. And we attempted neutron diffraction experiment to observe about racemization process. The molecular structure is shown in Fig.1. Although this labeled complex was not racemized because of its large crystal size, some interesting results were obtained. The α deuterium and one of hydrogen atom of the neighboring methyl group, both are hatched in the Fig.1, exchanged with each other. This may suggest quite a new mechanism of the racemization, which will be discussed in detail.

Table 1. Crystal Data.

a/Å	8.686(2)
b/Å	13.516(5)
c/Å	9.618(3)
α/°	–
β/°	96.92(2)
γ/°	–
V/Å^3	1120.9(5)
Z	2
Space Group	$P2_1$

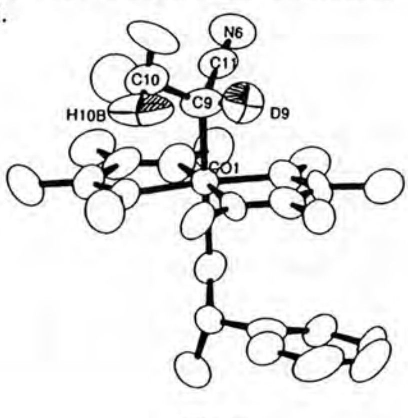

Fig. 1

2C25

NEUTRON DIFFRACTION INVESTIGATION OF PHASE TRANSITION IN $LiNaGe_4O_9$

Y. Iwata, Research Reactor Institute, Kyoto University, Kumatori, Osaka 590-04, Japan, M. Machida, Department of Physics, Kyushu University, Fukuoka 812, Japan, M. Wada, Faculty of Liberal Arts, Shinshu University, Matsumoto 390, Japan, and A. Sawada, Department of Physics, Okayama University, Okayama 700, Japan.

$LiNaGe_4O_9$ crystal (abbrev. as LNG) undergoes ferroelectric phase transition at 112 K.1) Single crystal neutron diffraction was undertaken to investigate the transition. Neutron data collection was made at temperatures above and below the transition point using 4-circle neutron diffractometer at Kyoto University Reactor (KUR). The crystal structure previously determined by X-ray method (corresponding to the paraelectric one) is an orthorhombic system (a=9.31, b=4.68, c=15.88 A, Z=4) with a space group Pcca-D^8_{2h}.2) It is reported that Li atom in the vacant space of the puckered structure is statistically distributed over the two sites with half occupancy. Dielectric dispersion study by Wada *et al.* suggests an order-disorder type phase transition.3) Present structure refinement disclosed that in the paraelectric phase not only the Li atom but also the Na atom is split into two sites. Extinction rules in the ferroelectric phase proved that the space group is $P2_1ca$-C^5_{2v} (Z=4), and the structure was determined based on this symmetry with R-value 0.065 using 870 reflections. A transition mechanism derived is as follows; The disordered Li and Na atoms in the high temperature phase become gradually ordered in one of the two split sites as the temperature goes through the transition point. The *x*- components of displacement of alkali metals at the polarity reversal are estimated as 0.32 A for the Li atom and -0.28 A for the Na atom. These values enable appearance of spontaneous polarization along the a-direction. While atomic shifts in the germanate polyhedra are smaller ones (less than 0.15 A). This implies germanate network in LNG is much rigidly connected compared with that of structurally similar ferroelectrics $Li_2Ge_7O_{15}$ which contains twice of germanate tetrahedra in the structure unit and shows both an order-disorder and softening of the optical phonon at its phase transition.

1) M. Wada *et al.*, J. Phys. Soc. Jpn. 52 (1983) 2981.
2) H. Vollenkle *et al.*, Mh. Chem. 100 (1969) 79.
3) M. Wada *et al.*, J. Phys. Soc. Jpn. 62(1993) 4503.

2C26

SINGLE CRYSTAL NEUTRON STUDY OF STRUCTURAL PHASE TRANSITION IN (Ba/Ca)TiO_3

P.U.M. Sastry, A. Sequeira, B.A. Dasannacharya and H. Rajagopal, Solid State Physics Division, B.A.R.C, Trombay, Bombay 400085 and P. Ramasamy, Crystal Growth Centre, Anna University, Madras 600025, India

Tetragonal to cubic transition in ferroelectric $Ba_{0.92}Ca_{0.08}TiO_3$ (BCT) has been studied using single crystal neutron diffraction technique. The Bragg profiles exhibit anomalous temperature variations of intensities, which initially increase with temperature and then drop sharply before reaching the transition temperature (T_0). The intensity variations as well as T_0 depend on the sample heating rate, with T_0=145°C and the intensities peaking around T=120°C at slow heating rate of 10°C/hr. Structural refinements indicate that the observed intensity variations are essentially due to changes in extinction effects brought about by changes in the domain sizes.
The refined thermal parameters exhibit anomalous changes with temperature, particularly for the Ti-ion, which exhibits significant positional disorder at around 120°C indicating a non-zero value for the soft-mode frequency below T_0. The size of the domains is highly anisotropic with the average equivalent isotropic domain radius decreasing from about 250A° at room temperature to about 100A° just below T_0 in the tetragonal phase and then increasing dramatically to over 1000A° in the cubic phase above T_0. The line widths of the diffraction profiles are influenced by contributions from the anisotropic domain sizes as well as from the internal strains. There is no evidence for the presence of mixed phases upto 120°C. However, the profile widths at 130°C indicate some additional contributions arising from the coexistance of tetragonal and cubic phases. The results suggest that the small domain sizes and the concomitant composition fluctuations may be responsible for the diffuse ferroelectric transition reported for BCT.

3PL1

ADVANCES IN THE USE OF RIETVELD ANALYSIS FOR MATERIALS CHARACTERISATION

Brian H O'Connor, Materials Research Group, Department of Applied Physics, Curtin University of Technology, GPO Box U1987, Perth, W A 6001, Australia.

The advent of the Rietveld method for diffraction analysis of crystalline materials offers exciting prospects for a multiplicity of materials characterisation applications. The author and colleagues now use Rietveld refinement of laboratory x-ray source diffraction data in both research and commercial service work to provide the following information -

- phase composition analysis
- density determinations
- solid solution characterisation
- texture analysis
- residual strain analysis
- crystallite size determination

The paper will examine the capacity and limitations of Rietveld analysis with particular reference to (i) the processing of alumina-matrix ceramics and (ii) gibbsite-corundum transformations including the crystal chemistry of intermediate aluminas.

Bias caused by instrumental factors (optical aberrations, specimen off-set, etc) and specimen-related effects (high backgrounds, micro- and macro-absorption, preferred orientation, extinction, etc) will be reviewed. The value of using synchrotron radiation diffraction and neutron diffraction data, as alternatives to laboratory-source x-ray data, will be discussed.

Questions to be considered will include *What are the strengths and weaknesses of Rietveld analysis? Is it the method of choice for materials characterisation under all circumstances? If not, what are the alternatives?*

3PL2

CHARGE DENSITY STUDIES AND CHEMICAL BOND CHARACTERIZATION

Yu Wang, Department of Chemistry, National Taiwan University, Taipei, Taiwan, R.O.C.

Charge density studies have been investigated both by X-ray diffraction experimentally and by molecular orbital calculation theoretically. The combined study can provide useful information on the characterization of chemical bond. Examples on the bond characterization on a series of compounds, which contain a Cr-L multiple bond, will be given. Cr-nitrido, -imido, -oxo and -carbyne bonds are all isoelectronic, the Cr-L bond (L=N, O, C) is essentially a triple bond with one σ bond and two π-bonds. However the π-density distribution show different polarization along the bond in these compounds. Detail chemical bond characterization is applied to a Ni-complex, Ni(s-disn)$_2$. It is a planar molecule with a fully π-delocalized ligand. All the metal-ligand bonds as well as the π-delocalization of the ligand are expressed in terms of molecular orbital wave functions and in some cases, the localized atomic hybrid orbitals. In addition, the bond characterization is also studied by a topological approach. Atom domain, bond path and bond critical points will be presented.

In all the transition metal complexes, the asphericity on electron density around metal atom are clearly seen and the d orbital populations can be derived from the multipole model. The agreement on the deformation density distribution as well as the topological properties between experiment and theory is very good.

3PL3

CHARGE DENSITY STUDIES REVISITED

Philip Coppens, Department of Chemistry, State University of New York at Buffalo, Buffalo, New York 14260-3000 USA.

Recent developments in hardware and soft ware are increasing the accuracy and the speed with which charge density studies can be performed. This talk will review some of these advances and corresponding results, and discuss the possibilities for future developments with emphasis on transition metal complexes.

3A11

TOPOLOGICAL ANALYSIS OF EXPERIMENTAL ELECTRON DENSITY OF LiF CRYSTAL

Yu. A. Abramov[*], V.E. Zavodnik[#], D. Feil[%] and V.G. Tsirelson[$]

[*] National Institute For Research in Inorganic Materials, Tsukuba, Japan
[#] Karpov Institute of Physical Chemistry, Moscow, Russia
[%] University of Twente, Enschede, the Netherlands
[$] Mendeleev University of Chemical Technology, Moscow, Russia

A parameters of the multipole Hansen & Coppens model of the LiF crystal has been evaluated from an X-ray diffraction experiment (Mo Kα, CAD-4, T=298 K, $(\sin\theta/\lambda)_{max} = 1.291$ A^{-1}, 632 measured and 52 unique reflections, Fm3m, a=4.024(1) A, R=0.0068, wR= 0.0082, S=0.99). The atomic valence shell populations obtained revealed almost pure ionic Li-F bond in crystal. A detailed analysis of the electron density distribution has been performed in terms of Bader's quantum-topological theory using the obtained multipole model parameters. The calculation of the Laplacian and critical points of the electron density has been done using a version of the LSPROP program (Howard & Mallinson). The bond (3,-1) critical point ("saddle") on the Li-F internuclear vector was found and the "sizes" of atoms bonded in the crystal were determined. The corresponding evaluated average radii of F(-1) and Li(+1) ions, 1.24 A and 0.77 A, appear to be rather close to Shannon and Prewitt's ionic radii 1.19 A and 0.90 A, respectively. The Laplacian value at the bond critical point is positive as expected in the case of an ionic bond. At the centre of the (001) plane another (3,-1) critical point was found, reflecting the F-F interaction in the LiF crystal. The (3,+1) critical points ("cycle") are found on the Li-Li vec-tor in the (001) plane at a distance of 0.68 A from each Li ion. This overall picture of the critical points and basins of ions is in good correspondence with theoretical investigations of the bulk LiF crystal (Tsirelson, Zou & Bader. Acta Cryst. A51. 143-153).

Support of this research by the Netherlands Organization for Scientific Research (NWO) is gratefully acknowledged.

3A12

ELECTRON DENSITY IN $YTiO_3$. J. R. Hester, F. P. Okamura (National Institute for Research in Inorganic Materials, Japan), K. Tomimoto, J. Akimitsu (Aoyama Gakuin University, Japan).

Accurate electron density experiments have been performed on the title compound. Three high resolution room temperature experiments were performed, two using AgKα radiation ($\sin\theta/\lambda < 1.5$) and one using W Kα radiation ($\sin\theta/\lambda < 1.3$). The space group, cell dimensions and refinement parameters agree with those reported by MacLean, Ng and Greedan (J. Solid State Chem.,1979, **30**, 35–44).

Despite a noticeable degree of random fluctuation in regions far from the atomic nuclei, the difference density map topographies agree reasonably well for all three data collections, allowing tentative conclusions to be drawn about *d* electron redistribution. Four difference density peaks, perhaps corresponding to Ti t_{2g} d orbitals, are located about 0.6Å from the Ti nucleus (see figure). It appears that electron redistribution around Ti is influenced by the long range symmetry as well as the local octahedral symmetry. There is a fairly complex arrangement of difference density peaks around the Y atom which appear unrelated to the nearest–neighbour symmetry.

Figure 1: Difference electron density around Ti in $YTiO_3$. Contour interval 0.4eÅ^{-3}, borders 3.0Å. Dashed lines–negative, solid lines–positive difference density

3A21

CRYSTAL STRUCTURE OF CHIMERS IN B-FORM SHOW THAT RNA CAN EXIST AS B-RNA

M. Sundaralingam, Xin Chen and B. Ramakrishnan, Laboratory of Macromolecular Structure, Departments of Chemistry & Biochemistry, The Ohio State University, 1060 Carmack Road, Columbus, OH 43210

RNA adopts the A-form and has not been so far observed in the B-form. X-ray fiber diffraction[1], solution CD[2] and NMR spectroscopy[3] have implicated that DNA-RNA chimers could exist in the B-form. Theoretical studies have shown the possible existence of B-RNA with C2'-*endo* sugar puckering[4]. In search of crystal structure of B-form RNA, we undertook the study on the structure of chimeric octamers (IcICICIC) and (IcIcICIC) (lower case letters represent RNA residues) and their complexes with the DNA minor groove binding drug distamycin. This drug was chosen because it is known to bind to only B-form of DNA. The native crystals of these octamers could not be obtained; however, the structures of the complexes with distamycin have been determined at 1.73 and 1.70Å resolution respectively. Crystals of these chimeric octamer drug complexes are isomorphous with their all-deoxy counterpart d(ICICICIC)$_2$ with two drugs bound side-by-side in the minor groove[5]. Surprisingly, the DNA-RNA octamers are in the B-form in contrast to the A-form for all the known free chimer oligomers in crystals. The ribose sugars, like the deoxy sugars, are in the S-type puckering and the 2'-hydroxyl groups are in the major groove and form a direct hydrogen bond to the N7 atom of the succeeding 3'-side inosine residue. Modeling studies indicate that B-form is possible for the all-ribose (ICICICIC) octamer and alternating RNA. In the B-form RNA duplexes, the 2'-hydroxyl groups can be hydrogen bonded to N7 of the 3'-side purines and the backbone phosphates of the 3'-side pyrimidines.

In RNA uracil is present instead of thymine, the 5-methyl group would have steric conflict with the 2'-hydroxyl group in the major groove. This could be the reason why RNA contains "U" instead of "T", enabling it to assume the B-form in stretches when involved in interactions with drugs/protein factors.

1. Zimmerman, S. B. & Pheiffer, B. H. (1981) *Proc. Natl. Acad. Sci. USA* **78**, 78-82.
2. Jayasena, S. D. & Behe, M. J. (1987) *Nucleic Acids Res.* **15(9)**, 3907-3916.
3. Reid, D. G. et al. (1983) *Eur. J. Biochem.* **135**, 307-314.
4. Rao, S. N. & Kollman, P. A. (1986) *J. Am. Chem. Soc.* **108**, 3048-3053.
5. Chen, X., Ramakrishnan, B., Rao, S. T. & Sundaralingam, M. (1994) *Nature Structural Biology* **1**, 169-175.

Supported by NIH grant GM-17378

X-Ray Structure Determination of Abrin-a

Tian-Huey Lu[1], Tahir H. Tahirov[1], Yen-Chywan Liaw[2], Yung-Liang Chen[3] and Jung-Yaw Lin[3].

[1] Department of Physics, National Tsing Hua University, Hsinchu, Taiwan.
[2] Institute of Molecular Biology, Academia Sinica, Nankang, Taipei, Taiwan.
[3] Institute of Biochemistry, College of Medicine, National Taiwan University, Taipei, R. O. C.

The crystal structure of abrin-a, a type II ribosome-inactivating protein from the seeds of *Abrus precatorius* has been determined from a novel crystal form (Tahirov, Lu, Liaw, Chu & Lin, 1994) by molecular replacement method using the coordinates of ricin (Montfort et al., 1987). The cell dimensions determined by area multiwire detector are a=84.58, b=73.07, c=48.23 Å, and ß=96.20° in a monoclinic crystal system with space group $P2_1$.The structure has been refined at 2.14 Å to a R-factor of 18.9% by using X-PLOR program (Brünger, 1990). The r.m.s. deviations of bond lengths and angles from the standard values are 0.013 Å and 1.82° respectively. The overall protein folding is similar to ricin but there are differences in secondary structure, mostly of A-chain. Several parts of the molecule surface differ significantly and some of the differences are quite near the active site cleft and might influence the ribosome recognition. The positions of invariant active site residues are remained except the position of Tyr74, which is more mobile or partially disordered in abrin-a. Three water molecules have been located in active site cleft. B-chain is a glycoprotein and the positions of two sugar chain sites were determined. One of the sugar chains is a bridge between two neighboring molecules since one of its mannose residue have been affiliated by galactose binding site of neighbor molecule. Another sugar chain wraps up the surface of B-chain. Various colourful models of abrin-a will be presented to illustrate the crystal structure of abrin-a.

This work was supported by National Science Council, ROC, under grant NSC84-2311-B007-015.

References:

Brünger, A. T. (1990). Acta Cryst. A46, 46-57.

Montfort, W., Villafranca, J. E., Monjingo, A. F., Ernst, S. R., Katzin, B., Rutenber, E., Xuong, N. H., Hamlin, R. & Robertus, J. D. (1987). J. Biol. Chem. 262, 5398-5403.

Tahirov, T. H., Lu, T. H., Liaw, Y. C., Chu, S. C., & Lin, J. Y. (1994). J. Mol. Biol. 235, 1152-1153.

3A23

THREE–DIMENSIONAL STRUCTURE OF THE PSEUDOMONAS BphC ENZYME HAVING POLYCHLORINATED BIPHENYL (PCB)–DEGRADING ACTIVITY

H.Narita, K.Sugimoto, T.Senda, K.Kimbara, M.Fukuda and Y.Mitsui.
Department of BioEngineering, Nagaoka University of Technology,
Nagaoka, Niigata 940–21, Japan.

Polychlorinated biphenyls (PCBs) are widely distributed environmental pollutants which are recalcitrant to biodegradation. *Pseudomonas* sp. strain KKS102 is one of the PCB–degrading micro–organisms and the " BphC" enzyme (2,3–dihydroxybiphenyl dioxygenase) is a key enzyme in the relevant PCB–degrading pathway. The BphC enzyme is an extradiol type dioxygenase having one ferrous iron in the active site. To gain insight into the catalytic mechanism of the BphC enzyme, we undertook a *de novo* X–ray crystallographic analysis by MIR method. The enzyme (M.W. ca.250 kDa) is made up of eight identical subunits each of 292 amino acid residues.

The BphC enzyme turned out to be a thick–walled cylinder which has a 422 point group symmetry in the molecule. A barrel–shaped central cavity penetrates the molecule. The subunit of the BphC enzyme is composed of four repetitions of a folding motif consisting of ca.55 amino acid residues. The repetitive motif has a " *βαβββ*" topology (Sugiyama et al.,1995). In the active site, we found an Fe ion which was coordinated by side chains of three amino acid residues, His 145, His 209 and Glu 260.

Crystallogrpahic analysis of the BphC enzyme complexed with 2,3–dihydroxybiphenyl (2,3–DHBP) showed that the two hydroxyl groups of 2,3–DHBP are coordinated to the Fe ion resulting in a trigonal bipyramidal form. With the structure of the BphC enzyme–substrate complex at hand, we can identify a putative binding cavity for the oxygen molecule required for the enzymatic reaction.

Sugiyama,K.,Senda,T.,Narita,H.,Yamamoto,T.,Kimbara,K.,Fukuda,M., the late Yano,K. & Mitsui,Y.(1995) Proc.Japan Acad. 71B, 32 – 35.

3A24

CRYSTAL STRUCTURE OF PEA-SEEDLING AMINE OXIDASE

Vinay Kumar, H.C. Freeman, J.M. Guss and V.M. Zubak, School of Chemistry and Department of Biochemistry, University of Sydney, NSW 2006, Australia and D.M. Dooley and M.A. McGuirl, Department of Chemistry and Biochemistry, Montana State University, Bozeman, USA.

Copper-containing amine oxidases (AO) catalyse the oxidative deamination of primary amines to the corresponding aldehyde. An important subcategory found in higher organisms, diamine oxidases, participate in the catabolism of di- and poly- amines which are important agents in many fundamental cellular processes.

Diamine oxidase from pea seedlings is a glycosylated protein consisting of two identical subunits with a total molecular weight ~145 kDa. The protein crystallises in space group $P2_12_12_1$ with one dimer per asymmetric unit. The positions of the individual tungsten atoms in a phosphotungstate $[PW_{12}O_{40}^{3-}]$ derivative were fitted to a difference map which had been obtained by molecular replacement. The molecular replacement calculations used the structure of *E. coli* AO (communicated prior to publication by Professor S.E.V. Phillips) as a search model. An electron density map for the protein was calculated using phases obtained from the phosphotungstate derivative using single isomorphous replacement and optimised anomalous scattering phases. The map, improved by solvent flattening and non-crystallographic symmetry averaging, was readily interpretable.

3B11

THE EFFECT OF COPPER DOPANT ON THE GROWTH AND PROPERTIES OF POTASSIUM SODIUM STRONTIUM BARIUM NIOBATE CRYSTALS

H. C. Chen, Q. Z. Jiang, X. L. Lu and L. Chen. Institute of Crystal Materials, Shandong University, Jinan, 250100. P. R. China

Potassium sodium strontium barium niobate (KNSBN) crystals doped with CuO were grown by pulling method using the MCGS-3 system. The starting materials we used are 4N K_2CO_3, Na_2CO_3, $SrCO_3$, $BaCO_3$, Nb_2O_5, and CuO. They were mixed according to the formula of $(K_xNa_{1-x})_{0.2}$ $(Sr_yBa_{1-y})_{0.9}$ $Nb_2)_6$,where $0.3< X < 0.7$, $0.25 < Y < 0.75$. A very small amount of CuO ,0.03%-0.07%, was added to the mixture. The growth conditions are pulling rate 3-5 mm/h and rotation rate 15 r.p.m. The as-grown KNSBN:Cu crystals were annealed at 1050 °C for 24 h and then cut into samples with size of $5 \times 6 \times 6$ mm^3 along the *a, b* and *c* axes. The samples were polished and poled at 100 °C under a 6 kv/cm of C.D. electrical field

From the transmission curves we can see that the Cu ions have caused two absorption peaks at 475 and 495 nm. Because the positions of the peaks are not affected by the doping level of CuO, it means that these two peaks correspond to the intrinsic energy levels of Cu ions , 2.61 ev and 2.50 ev in KNSBN. These two deep energy levels in the band gap can increase the effective charge-combination-center concentration

The two-wave coupling gain and the response time of KNSBN crystals are increased while the photoconductivity and the effects of a dc field on the photorefractive properties are reduced. Self-pumped phase conjugation experiments have revealed that the effect of Cu ions on the photorefractive properties have a wavelength dependence. The SPPC response time can be shortened to 200 ms.

3B12

SINGLE CRYSTAL GROWTH AND GROWTH MECHANISM OF YNi_2B_2C SUPERCONDUCTORS BY FLOATING ZONE TECHNIQUE

H. Takeya, K. Kadowaki, K. Hirata, T. Hirano and K. Togano
National Research Institute for Metals, 1-2-1 Sengen, Tsukuba, Ibaraki 305, Japan

Since the discovery of a new family of borocarbide intermetallic superconductors, a great deal of studies have been performed on the arc-melted polycrystalline samples which contain many micro cracks and a trace of the second phase. In this study, we have succeeded in growing the single crystals of YNi_2B_2C by floating zone technique.

Czochralski method using a tetra-arc furnace or a skull melting furnace was preliminarily applied, but the grown crystals contained dense lamellar structure which consisted of YNi_2B_2C, YB_2C_2 and Ni-rich phase. Metallurgical studies and composition analyses on the grown crystals suggest that YNi_2B_2C is an incongruent material and decomposes to YB_2C_2 and Ni-rich phase. In such a case, YNi_2B_2C is precipitated from the solution of the Ni-rich phase. However, no improvement was observed in the crystals grown out of a Ni_2B flux by the Czochralski method.

On the contrary, the considerable improvement has been performed by the floating zone technique without any solvent. No second phase was observed in the grown single crystal. The as-grown crystal showed the superconductivity at 15.6 K (onset) with the transition width of 0.7 K by the SQUID magnetometer, which is compared to 14.8 K (onset) with the transition width of 2.3 K for the arc-melted polycrystalline samples. de Haas-van Alphen effect was also successfully observed on the single crystal. These results suggest the high quality of the grown crystal.

Since the successful result by the floating zone technique without solvent is inconsistent with the preliminary study that YNi_2B_2C is an incongruent material, the further investigation on the growth mechanism has been made by the back-scattered electron micro-analysis and X-ray diffraction. According to the analyses, a considerable amount of YB_2C_2 was seen at the tip of a feed rod just above the molten zone and the molten zone was rich in Ni. This suggests that YNi_2B_2C decomposes to YB_2C_2 and the Ni-rich solution at the tip of the feed rod. Though any solvent is not prepared at the beginning, the Ni-rich solution forms the molten zone and the single crystal of YNi_2B_2C is precipitated from the solution.

3B13

ANOMALOUS DENSITY VARIATION OF SILICON MELT AND MELT FLOW IN CZ PROCESS

K. Terashima, Department of Materials Science and Ceramic Technology, Shonan Institute of Technology, 1-1-25 Tsujido-Nishikaigan, Fujisawa, kanagawa251, Japan, and H. Sasaki, S. Togawa, S. Kawanishi, K. Izunome and S. Kimura, Kimura Metamelt Project, ERATO, JRDC, Tukuba Research Consortium, Satelite-2, 5-5-9Tokodai, Tukuba, Ibaraki 300-26, Japan

The temperature dependence of silicon melt density was determined accurately in the range from about 1420℃ to 1650℃ using a technique for improved Archimedian density measurement. The temperature range was found to be divided into three regions in terms of the temperature coefficient of the density. An anomalous value in the thermal volume expansion coefficiet of about 7.6×10^{-4}℃$^{-1}$ was observed just above the melting point. A thermal volume expansion coefficient of about 1.0×10^{-4}℃$^{-1}$ was obtained for the range from about 1430℃ to 1540℃. This anomaly widely varid depending on impurity species. We next studied the silicon melt flow during the Czochralski growth in a crucible depending on the anomalous density variation.
At first, the temperature fluctuations under the growth interface region were measured. The flow structure of this region was basicaly random and it was clarified the "soft turbulence" of Rayleigh-Benard. The flow structure changed by the species of impurity in the melt. These phenomena above mentioned suggest the density anomaly strongly changes the melt flow structures in a crucible during pulling process. Melt properties (density, viscosity and surface tension) variation, melt flow structures and crystal uniformity will be discussed.

3B14

ETCHING STUDIES OF SOLUTION-GROWN CRYSTALS : (100) FACES OF MIXED KDP:ADP ($K_{1-x}NH_{4x}H_2PO_4$) CRYSTALS.

Suparna Sen Gupta and S. P. Sen Gupta,* Department of Materials Science, Indian Association for the Cultivation of Science, Jadavpur, Calcutta - 700 032, INDIA.

The study of mixed crystals of KDP:ADP ($K_{1-x}NH_{4x}H_2PO_4$) has attracted considerable attention in recent years as they present a new class of materials with intrinsic interests due to their potential applications in opto-electronics. However, in the past very few work have been reported on this system. Mixed crystals of KDP-ADP have been grown by the method of slow evaporation over the entire range of composition. The growth conditions to obtain transparent and moderate single crystals have been critically examined by several tests. In order to understand their defect configurations, we have undertaken chemical etch technique with greater details. Different etchants including acids and alcohols with varying etch time have been employed to reveal dislocation sites in these crystals. Growth hillocks, pits of different inclination, low angle tilt boundary and many other features were observed on the etched surface. It is also observed that KDP-rich and ADP-rich mixed crystals exhibit few similar features like pure KDP and pure ADP respectively. An interesting pattern e.g. a trisection of boundaries and branching of closely spaced etch pits (Fig. 1(a,b)) were clearly seen on the etched surface of mixed crystals. These etch patterns have been observed and photographed under an optical microscope and also in SEM. The details will be presented through optical and electron micrographs.

Fig. 1(a) trisection of boundaries.

Fig. 1(b) branching of dislocations

3B21, 3P22

THE ATTEMPT TO DESIGN SOLID STATE REACTION BY REACTION CAVITY

D. Hashizume and Y. Ohashi, Department of Chemistry, Tokyo Institute of Technology, Meguro-ku, Tokyo 152, Japan

The 2-cyanoethyl group bonded to the cobalt atom in cobaloxime complexes is isomerized to 1-cyanoethyl group on exposure to visible light in the solid state. The reaction cavity for the cyanoethyl group is an important factor determining the rate and selectivity of the reaction. We report the attempted to control the reaction rate and the reactivity.

The (2-cyanoethyl)(3-hydroxypyridine)cobaloxime complex crystallizes into a triclinic system from a methanol solution. There are two crystallographically independent molecules in the asymmetric unit and the structures of these two molecules are almost the same and one of them is shown in Fig. 1. The cyanoethyl group are well packed with neighboring molecules.

The monoclinic system crystal was obtained from a chloroform solution , contains chloroform molecules which are placed around the cyanoethyl group. As a result, the reaction cavity around the cyanoethyl group is expanded, and therefore the rate of the isomerization of cyanoethyl group different from triclinic one.

Table 1. Crystal Data.

a/Å	12.367(2)	9.230(2)
b/Å	15.207(3)	23.985(3)
c/Å	11.356(1)	11.450(2)
α/°	104.45(1)	–
β/°	93.69(1)	93.15(2)
γ/°	73.77(2)	–
V/Å^3	1985.6(6)	2531.0(8)
Z	4	4
Space Group	$P\bar{1}$	$P2_1/n$

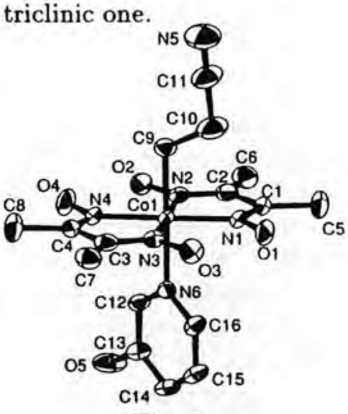

Fig. 1

3B22, 3P23

STUDY ON COMPLEXES OF ALKYLAMMONIUM SALTS-AROMATIC ADDITIVE

Kulthida Vongbupnimit, Keiichi Noguchi and Kenji Okuyama, Faculty of Technology, Tokyo University of Agriculture and Technology, Koganei, Tokyo 184, Japan

Recently, some amphiphiles such as ammonium salts, phosphonium salts and other onium salts without any intramolecular cavities have been found to form complexes with organic guest molecules. In some cases, formation of complexes can also be prepared simply by mixing both powders of host amphiphiles and small guest molecules. In the present work, we will present the complex crystal structures of the host amphiphilic molecule; dodecyltrimethylammonium chloride (DTAC) with various kinds of guest aromatic molecules, i.e., hydroquinone (HQN), catechol (CTC) and p-iodophenol (p-IoPh).

Crystal data :
DTAC/HQN; $CH_3(CH_2)_{11}N^+(CH_3)_3Cl^-/p\text{-}C_6H_6O_2 \cdot 2H_2O$, monoclinic $P2_1/n$, $a = 7.212(2)$, $b = 45.099(5)$, $c = 8.208(2)$ Å, $\beta = 108.96(2)°$.
DTAC/CTC; $CH_3(CH_2)_{11}N^+(CH_3)_3Cl^-/o\text{-}C_6H_6O_2 \cdot 2H_2O$, monoclinic $P2_1/n$, $a = 7.084(4)$, $b = 44.271(6)$, $c = 8.415(2)$ Å, $\beta = 108.98(3)°$.
DTAC/p-IoPh; $CH_3(CH_2)_{11}N^+(CH_3)_3Cl^-/p\text{-}C_6H_5IO$, monoclinic $P2_1/n$, $a = 9.840(7)$, $b = 9.976(3)$, $c = 26.357(10)$ Å, $\beta = 100.43(4)°$.

The complex crystal structures and the amphiphile aggregation system depended on the kinds of guest molecules have been discovered. The packing structures of complexes, DTAC/HQN and DTAC/CTC are similar to each other, but they are quite different from that of DTAC/p-IoPh. In addition to the complex crystal structures, to get better understanding about behaviors of these complexes, the phase transitions and thermal behaviors of host molecule and complex molecules will be discussed by differential thermal analysis (DTA) and X-ray powder diffraction patterns too.

3B23, 3P24

Diverse Mode of Crystal Structures in the Host-Guest Complexes of Diols

Yasushi Kai, Hiroshi Suzuki, Nobuko Kanehisa, Koichi Tanaka,† and Fumio Toda†
Department of Applied Chemistry, Faculty of Engineering, Osaka University, Suita, Osaka 565, Japan
†Department of Chemistry, Faculty of Engineering, Ehime University, Matsuyama, Ehime 790, Japan

cis-1,4-Diphenylcyclohexane-1,4-diol forms the crystalline Host-Guest complexes with methanol (1:1) (complex **1**), cis-2-butene-1,4-diol (1:1) (complex **2**), and trans-2-butene-1,4-diol together with water (1:1:1) (complex **3**). The crystal structures were determined by X-Ray diffraction method. Crystal data and final R values are; for complex **1**, monoclinic, $P2_1$, a=7.589(2), b=10.057(2), c=11.033(2)Å, β=93.81(1)°, V=840.2(3)Å^3, D_C=1.187gcm^{-3}, Z=2, and R=0.039 for 1341 observed reflections, for complex **2**, monoclinic, $P2_1/n$, a=9.565(1), b=9.371(1), c=21.633(1)Å, β=98.27(1)°, V=1918.8(2)Å^3, D_C=1.234gcm^{-3}, Z=4, and R=0.055 for 3059 observed reflections, and for complex **3**, monoclinic, $P2_1/a$, a=7.479(2), b=35.328(2), c=7.801(1)Å, β=100.58(1)°, V=2026.0(5)Å^3, D_C=1.228gcm^{-3}, Z=4, and R=0.045 for 3087 observed reflections. In spite of the common mode stacking of 2_1 symmetry for host molecules in all the crystals, the packing structures are quite different from each other. Guest molecules are arranged separately in the channel of host molecules in **1**, while guest molecules form strings through the hydrogen bonds with host molecules in **2**. In complex **3**, guest molecules arrange in layer sandwiched by the hydrophilic part of the host molecules.

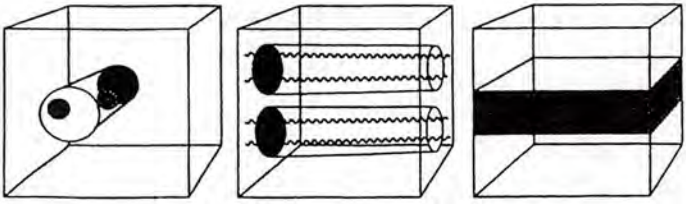

1 **2** **3**

Scheme 1. Schematic presentation of the crystal packing of complexes **1** to **3**.

3B24, 3P25

EXTENDED MOLECULAR NETWORKS INCORPORATING THE 1,4-BIS(IMIDAZOL-2-YL)BUT-2-YNE LIGAND

Damian A. Slizys, Bernard F. Hoskins and Richard Robson

School of Chemistry, University of Melbourne, Parkville, Victoria 3052,
AUSTRALIA

Extended molecular networks can be constructed from metal centres linked by bridging ligands. Examples of ligands used to construct such networks include cyanide, 4,4'-bipyridine and pyrazine.

Our research has focused on using bridging ligands incorporating nitrogen-based heterocycles as the binding functions. In particular the imidazole moiety has been the preferred binding function because of its relatively high affinity for metal ions and its small size when compared to other nitrogen-based heterocycles such as pyridines. One novel ligand of this type that we have developed is 1,4-bis(imidazol-1-yl)but-2-yne.

Molecular networks incorporating this ligand have been prepared from $CdSiF_6$ and $ZnSiF_6$. In both cases crystals separated from an aqueous solution of 1,4-bis(imidazol-1-yl)but-2-yne and the appropriate metal salt. The crystals were insensitive to solvent loss.

The two structures are very closely related. X-ray diffraction studies show them to be composed of sheets of metal atoms each linked by four molecules of 1,4-bis(imidazol-1-yl)but-2-yne to four other metal atoms. These sheets in turn were linked vertically by SiF_6 anions coordinating to the metal atoms above and below. Overall the topology was equivalent to α-polonium.

The crystal structure of these networks will be presented.

3B25, 3P26

DYNAMIC BEHAVIOR OF *N*-(2,4-DINITROPHENYL)-*o*-ANISIDINE CRYSTALS

M. Yasui, K. Taguchi and F. Iwasaki, Dept. of Applied Physics and Chemistry, The Univ. of Electro-Communications, Chofu, Tokyo 182, Japan.

N-(2,4-Dinitrophenyl)-*o*-anisidine crystallizes in two modifications, orange and red forms. The condition to crystallize each form is very subtle, so that it is by chance which form can be obtained. The coexistence of these forms is often observed. In the wide temperature range from 110 to 158°C depending on specimen, orange crystals begin to transform to red crystals in the solid state, which have been found to be identical to the red form recrystallized from the solution by mean of the powder diffraction. This transformation is irreversible since the red crystals do not return to the orange form by the cooling. However some orange crystals directly melt without this transformation. The molecular structure of the red form is a rotational isomer of the orange form. In the red form, the NH group is hydrogen-bonded to nitro and methoxy groups bifurcately, while in the orange form the hydrogen-bond between NH and OMe groups is not formed. Oscillation photographs of the partially transformed orange crystal were taken on a rapid X-ray measurement system using the Imaging Plate. At the orange form the crystallographic b axis is parallel to the needle axis of the crystal. The diffraction patterns from the transformed region, a red form, are concentric circles with many sharp spots. These spots show that the single crystal of a red form coexists in the polycrystalline and that the crystallographic b axis of a red form is coincident with that of the unchanged orange crystal. The relationship of b axis between the orange and the transformed red crystals was kept in the several specimens. From these results, we conclude the mechanism of the transformation from an orange to a red form as follows. The conversion may be performed by twisting of the molecule as well as the intra-molecular rotation. As a result of twisting, the crystal structure may be changed to the red form. However, such motion needs a large space, so that this rearrangement may occur at defects in a crystal and destroy the orientation of whole molecule to be a polycrystalline.

3B26, 3P27

MODELLING AND REFINEMENT OF DISORDERED MOLECULAR STRUCTURES FROM SINGLE CRYSTAL X-RAY DATA

Fun Hoong Kun, K. Sivakumar and Yip Boon Chuan, X-Ray Crystallography Unit, School of Physics, Universiti Sains Malaysia, 11800 USM, Penang, Malaysia.

Crystal structure refinement becomes a routine work with the high speed computers and software packages available to us. Even then it is not a routine work in the scientific sense that, many problems are faced in individual cases particularly when the structure has any form of disorder. Hence one has to be careful in analysing the intermediate results of the refinement procedure and carry out the next step with reasoning. Analysis of the mode of disorder and suitably carrying out the refinement with constrains and restraints comes with experience. In our laboratory, we have come across many such occasions with different types of disorder present in the molecular structures. There are examples of rotation of a group of atoms with respect to a bond, disorders due to the conformational flexibility of certain rings, mixture of two isomorphous structures and many more. A detailed survey of all such disordered cases and how the structures were refined to give a good model will be discussed. The presentation will also include how to identify the minor conformational components present in the structure and model them to get better structural informations.

Poster Presentation

1P01

NORMAL MODE ANALYSIS OF INCOMMENSURATE MODULATIONS AND ITS RELATION TO THE ATOMIC DEBYE- WALLER FACTORS OF THE NORMAL PHASE

By N.Achiwa*, M. Machida and Y.Yamauchi, Department of Physics, Kyushu University, Fukuoka 812, Japan.

We have developed a geometrical method to analyse molecular modulation modes in incommensurate crystal structures. From the three dimensional locus of each modulated atom which is pulled back to the original unit cell, that of a special mode, for example translational or rotational external molecular displacement is subtracted. Then, the remainder figure suggests the next main mode, for example, internal molecular mode. So we can find successively miner modes orthogonal to the subtracted modes by the trial and error method. The atomic Debye-Waller factors(ADWF) in a normal phase is tightly related to the mode amplitude of the incommensurate phase, because the lowest frequency normal mode contributes most strongly to the ADWF in the normal phase. Then, we have estimated contributions of the external and the internal modes to the ADWF in the normal phase. The family compounds $(C_3H_7NH_3)_2MCl_4$ (M=Cu, Mn, Cd) shows the following phase sequence: $\alpha \rightarrow \beta \rightarrow \gamma \rightarrow \delta \rightarrow \epsilon \rightarrow \zeta$, with the two incommensurate ϵ and γ-phases. These incommensurate structures were extensively studied using superspace symmetry. We have applied the new geometrical method to find the displacive modulation modes in the γ and ϵ phases and its application to analyse the ADWF in the normal δ phase by the external and internal modes. The main normal modes of modulated γ (superspace group, *Pbca:(α00)ss0,* Doudin Chapuis, 1990 B46 180.) and ϵ (superspace group, $BP2_1/b11{:}(0,0.5,\xi)1\bar{1}$, Ikeda and Achiwa) phases of $(C_3H_7NH_3)_2CuCl_4$ are a translational modulation along the c-axis and a twisted intra-molecule mode of propyl ammonium base, respectively, though in both phases each orbit of atomic modulation consists of multi-molecular modes.

1P02

ATOMIC ANISOTROPIC DISPLACEMENT PARAMETERS FOR SILICATES AND OXIDES: A LATTICE-DYNAMICAL DERIVATION FROM EMPIRICAL POTENTIALS

Tullio Pilati, Centro del C.N.R. per lo Studio delle Relazioni, fra Struttura e Reattività Chimica, Via Golgi 19, I-20133 Milano, Italy, Francesco Demartin, Dipartimento di Chimica Strutturale e Stereochimica Inorganica, Università degli Studi di Milano, Via Venezian, 21, I-20133 Milano, Italy, and Carlo Maria Gramaccioli, Dipartimento di Scienze della Terra, Università degli Studi di Milano, Via Botticelli 23, I-20133 Milano, Italy.

Using empirical potentials derived from fitting the vibrational frequencies of a group of neso-silicates and oxides, a Born-von Karman rigid ion lattice-dynamical model extended to the whole Brillouin zone has been applied to a series of oxides and silicates, such as quartz, bromellite (BeO), corundum (α-Al_2O_3), chrysoberyl (Al_2BeO_4), forsterite (α-Mg_2SiO_4), fayalite (Fe_2SiO_4), tephroite (Mn_2SiO_4), monticellite ($CaMgSiO_4$), andalusite (Al_2OSiO_4), grossular ($Ca_3Al_2Si_3O_{12}$), andradite ($Ca_3Fe_2Si_3O_{12}$), almandine ($Fe_3Al_2Si_3O_{12}$), pyrope ($Mg_3Al_2Si_3O_{12}$), and diopside ($CaMgSi_2O_6$) to obtain estimates of anisotropic atomic displacement parameters (A.D.P.'s); as by-products, a consistent interpretation of the vibrational spectra of all these minerals and of their thermodynamic behaviour at different temperatures have also been derived. The agreement with the corresponding experimental data is quite satisfactory, even for substances such as diopside and grossular, whose spectra and physical properties in general were not included in the process of fitting the potentials. For garnets, in particular, the problem of the anomalous behaviour of thermodynamic properties of pyrope and almandine (especially with respect to the specific heat Cp and entropy S as a function of temperature) can be very reasonably explained on grounds of an order-disorder transition occurring at low temperature, involving the Mg or the Fe atom, respectively: such an anomalous behaviour is reflected very well also in the atomic displacement parameters, especially when the observed values are compared with the corresponding lattice-dynamical estimates.

1P03

THE ANOMALOUS SCATTERING FACTOR OBTAINED FROM ROCKING CURVE MEASUREMENTS OF Ge SINGLE CRYSTAL

M. Kuribayashi, T. Kanamaru, A. Inoue, H. Katoh and K. Ishida, Dept. of Phys.
Science Univ. of Tokyo, Noda, Chiba 278, Japan

We derived a new formula 1) based on the Takagi equation 2) for a rocking curve of a perfect single crystal. It is well known that the traditional formula 3) for a rocking curve is not applied when the real part of the structure factor is very small . To avoid the difficulty, Fukamachi and Kawamura proposed an improved formula 4) which can be applied for the case. However, they used the anomalous scattering factors to define the "W" parameter, so that the formula is not suitable to obtain the anomalous scattering factor. On the other hand, the present formula does not use the anomalous scattering factors to define the "W" parameter. Therefore, the formula is suitable to determine the real and imaginary parts of the anomalous scattering factor, f' and f", from rocking curve measurements near the absorption edge. The SR measurement was carried out at BL-14B of the KEK Photon Factory in Tukuba. Radiations at BL-14B were well monochromatized with a series of three monochromators, Si(111) double crystals, a Si(440) grooved crystal and a Si(660) grooved crystal. The wavelength was selected by a little rocking of the third monochromator and the energy resolution was about 0.1eV. Ge(111) rocking curves with a symmetrical Bragg case were measured at 124 energy points below and above the absorption edge. The total range of the measurement was 220eV. The f' and f" were obtained by fitting the measurement rocking curve to the present formula. The obtained values below the edge are in good agreement with the calculated ones for a free atom. But, above the edge, the XANES effect is clearly observed for both f' and f".

1) to be published in J.Phys.Soc.Japan
2) S.Takagi, (1969) J. Phys. Soc. Jpn. **26**, 1239-1253.
3)W.H.Zachariasen, (1945) Theory of X-ray Diffraction in crystals (Dover,New York)
4)T.Fukamachi and T.Kawamura, (1993) Acta Cryst. **A49**, 384-388.

1P04

X-RAY STUDY OF DEFECTS PRODUCED BY MeV ION IMPLANTATION INTO Si PERFECT CRYSTALS

M. Kuribayashi, A. Inoue, T. Kanamaru, H. Katoh and K. Ishida, Dept. of Phys. Science Univ. of Tokyo, Noda, Chiba 278, Japan, H. Tomimitu , K. Aizawa and Y. Kazumata, Japan Atomic Energy Research Institute, Tokai, Ibaraki 305, Japan

Ion implantation in the energy range of several 10-100KeV into Si crystals is a well established technique for fabrication of semiconductors. The damage produced by the implantation is also well studied. In the present work, the defects caused by MeV ion implantation is investigated by X-ray measurements using the diffraction theory in distorted crystals 1). Implantations of Ni,Cu and Au ions into Si(111) wafers were carried out using the tandem Van de Graff accelerator at JAERI in Tokai with the energy range of 80-230MeV. X-ray rocking curves were measured with multi-crystal diffractometer at BL-14B in Photon Factory at KEK in Tukuba. The monochromator system used was Si(111) double crystals and a Si(220) grooved crystal with (+, -, -, +) setting. A sample wafer was mounted on a precise diffractometer.The measured rocking curves had a typical profile which consist of a main peak and many subsidiary maxima. The strain distribution could be determined by fitting the measured rocking curves to calculate ones. The strain profiles obtained by the simulations were compared with distributions of loss energy and stopping-atoms calculated with Aruga's program2) which is an expanded code of EDEP-1 for high energy region. It was found that the main profiles of strain distribution were nearly equal to those of the distributions of stopping ions regardless of the ion species. In the region near the crystal surface, the magnitude of strain, $\Delta d/d$, has a negative sign. The decrease of lattice spacing near the surface can be interpreted that crystal atoms are scattered by the collision of implanted ions. The magnitude and the range of the decreased layer depend on ion species.The annealing effect is also studied.

1) S.Takagi, (1969) J.Phys.Soc. Jpn..26, 1239-1253.

2) T.Aruga, K.Nakata and S.Takamura, (1988) Nuch.Instr. and Meth. B33,748

1P05

MEASUREMENTS OF X-RAY DIFFRACTION INTENSITIES FROM UNIFORMLY BENT SINGLE CRYSTALS

T. Takama and K. Itoh, Department of Applied Physics, Faculty of Engineering, Hokkaido University, Sapporo 060, Japan.

Diffraction phenomena in uniformly bent single crystals were studied by measuring the integrated intensities as a function of X-ray wavelength. Two kinds of isosceles triangular specimens with different orientation were cut from Fz silicon wafers of about 0.55 mm in thickness. One specimen has the (111) surface orientation with [01-1] direction parallel to the base and the other has the (001) with [1-10] parallel to the base. Bending was introduced by keeping the base of the triangle fixed and using a differential micrometer screw to push the apex. The integrated intensities were measured for the X-ray wavelength range from 0.2 to 0.6-0.9Å by the energy-dispersive diffraction method.

As the curvature increases, the following changes were observed in most cases. The diffracted intensities increased especially for the short wavelength side. The positions of the Pendellösung beats shifted to the short wavelength side. In addition, the amplitude of the beat decreased and finally smeared out. The magnitude of the changes was dependent not only on the induced curvature but also on the index and the sign of the reflection plane, and the geometrical arrangement of the plane. The following phenomena were noticed as exceptions. The (220) and the reverse reflections in the symmetrical Laue case for the latter specimen did not show any change in the profiles. On the other hand, when the (2-20) reflection for the former specimen showed stronger intensities in comparison with those from a perfect crystal, the reverse reflection showed weaker intensities for the wavelengths longer than about 0.6Å.

The diffracted powers obtained were compared with the Kato theory (1976) for distorted crystals. A fairly good agreement was drawn between the experiment and the theory if the elastic anisotropy is taken into account for the calculation of displacement fields due to the bending.

Kato, N. (1964). J. Phys. Soc. Japan, 19, 971-985.

1P06

Observation of Defects Without Directly Reflected Wave in Bragg Case

T.S. Uragami, H. Kobayashi and D. Orii, Faculty of Engineering, Okayama University of Science, Okayama, 700 Japan.

By using X-ray diffraction with an incident wave of finite width, the defects in a Silicon single crystal was oberved in Bragg case. At the point where X-ray enters on the surface of the crystal, the strong diffracted wave is created at that entrance point in the Bragg case. This directly reflected wave contains information at the vicinity of the surface in the X-ray fan, since the wave has not penetrated so deep inside of the crystal to create the direct reflection. When the transmitted wave encounters a defect in the X-ray fan on the other hand, the Pendelloesung fringes are disturbed and the disturbed diffracted wave propagates in the direction parallel to the diffracted wave vector toward the entrance surface again. This diffracted wave, which may be said to be proportionally as strong as the diffracted wave at the location of defect, can be oberved without disturbance of the directly reflected wave when the width of the entrance wave is adjusted as to eliminate the overlapping of the directly reflected and the image carring diffracted waves at the exit point because the directly reflected wave, which does not contain information inside of the crystal gives rise to the background to the really requested wave from the inside. Silicon (220) net plane was used for diffraction with the entrance slit of 0.01mm wide to observe defects just outside of the direct reflection. There could be seen defects in the range of 3 extincion distances if expressed in terms of thickness of crystal. The receiving slit was arranged as it stopped the direct reflection falling on the photographic plate.

1P07

THE GRAZING INCIDENCE DIFFRACTION OF X-RAYS WITH WAVE FRONT AMPLITUDE PERIODICALLY VARYING ALONG THE CRYSTAL ENTRANCE SURFACE (SYMMETRICAL LAUE CASE)

A.P.Bezirganyan and S.E.Bezirganyan, Dep. of Solid State Physics, Faculty of Physics, Yerevan State University, 375049 Yerevan-49, Armenia.

The modern technology based on use of thin-layered materials with layer thicknesses in nanometre ranges, e.g. in integrated circuits, X-ray mirrors etc. Interfacial regions extending over a few monolayers can strongly degrade device performance (see Forster et al.), especially as the thicknesses of performing elements become rather thin with further miniaturization of devices. If the device performing elements are deposited periodically on the substrate, such layer is like a diffraction grating (DG). The reflection (or transmission) function of DG may be used for the control and monitoring of device surface elements quality.

With that end in view the following scheme is investigated: reflected from DG X-ray wave field falls at grazing angles onto a single crystal (SC). The reflecting net planes of SC are normal to entrance surface (symmetrical Laue case).

DG has the following reflection (or transmission) function:

$$g(x) = t(x) * u(x),$$

where $t(x)$ is rectangle unit impulse function with length L same as for DG; $u(x)$ is an arbitrary periodic normalized function with the period D; $L=ND$; N is an integer; $1 \ll KD$; K is the wave number of incident X-ray plane wave. The description of reflected from DG wave field is given by the quasi-optics approximation. The incident wave field may be presented by the plane wave with wave front amplitude periodically varying along the SC surface. The surface waves' origin conditions are also obtained for this problem.

Forster, A., Lange, J., Gerthsen, D., Dieker, C. & Luth, H. (1994). J. Phys. D27, 175-180.

1P08

DENSITY OF THE p3 CLOSE PACKING OF IDENTICAL ELLIPSES

Takeo Matsumoto, Dept. of Earth Sciences, Faculty of Science, Kanazawa University, Kakuma-machi, Kanazawa 920-11, Japan and Masaharu Tanemura, The Institute of Statistical Mathematics, 4-6-7 Minami-Azabu, Minato-ku, Tokyo 106, Japan

Concerning the systems of the densest packing of ellipses, Nowacki (1948) considered four plane groups: p2, c2mm, p2gg and p31m. In all of these packings, every ellipse is in contact with 6 neighbour ellipses. Matsumoto (1968) and Matsumoto and Nowacki (1966) have shown that the first two of the above densest packings of ellipses, p2 and c2mm, always attain the maximum density, $\rho=\pi/2\sqrt{3}$, which are derived from the densest packing of circles, p6mm, by affine transformation. That of third, p2gg, cannot exceed this maximum density. Tanemura and Matsumoto (1992) have shown that the density of p31m packing of ellipses, the fourth one of the above list, never exceeds the above maximum density ρ. Grünbaum and Shephard (1987) showed four new types of periodic patterns of ellipses, three of them, p3 and two p2gg, have 6 contacting neighbours. We investigate the density of p3 packings of ellipses $\rho(k, \theta)$, through numerical calculations and series expansions depending on k (axial ratio of ellipses) and θ(tilt angle of ellipses). We obtain the following equation as expanding form in terms of $\varepsilon=k-1$ and θ:

$$\rho(k, \theta) = \pi/2\sqrt{3}\ \{1-3/32\varepsilon^2+ 1/128(17-90\sin^2\theta+240\sin^4\theta -160\sin^6\theta)\varepsilon^3 \\ -3/4096(411-1440\sin^2\theta+3840\sin^4\theta-2560\sin^6\theta)\varepsilon^4\} + O(\varepsilon^5).$$

The following relations are obtained:

$\rho(k, \theta) =\rho(k, -\theta) =\rho(k, \theta+n\pi/3)$ [n: an integer] and

$\rho(k, \theta) =\rho(1/k, \theta+\pi/6)$.

For the tilt angle $\theta=n\pi/3$, the p3 packing coincides with the p31m packing, and if $k=1$, this corresponds to the densest p6mm packing of circles. For values of k not equal to 1, the density of p3 packing of ellipses is always smaller than $\rho=\pi/2\sqrt{3}$.

Reference:

Matsumoto, T. & Tanemura, M. (1995) Z. Krist., 210, (in print).

1P09

THE USE OF THE DIFFRACTOMETER AT THE AUSTRALIAN NATIONAL BEAMLINE AT THE PHOTON FACTORY FOR UNUSUAL EXPERIMENTS

D.C. Creagh, Department of Physics, University College UNSW, Northcott Drive, Canberra ACT 2600, Australia

The Australian National Beamline at the Photon Factory was designed (Creagh (1992)) for operation on a bending magnet port, and can be used either with a Hart-type channel-cut monochromator with harmonic rejection, or a Matsushita-type monochromator in which the first crystal is of the Hart type and the second is capable of being bent sagittally to provide typically, a gain of 20 in flux. Its range of operation is 5.5 to 20 keV.

The diffractometer (BIGDIFF) was designed (Creagh and Wilkins (1989)) to be a versatile diffractometer capable of vacuum or helium operation, with a choice of mode of operation ranging from powder diffraction using imaging plates (camera mode) to triple axis counting geometry. In its camera mode a Weissenberg screen can be fitted, and the IP cassette can be moved in synchronism with the θ-motion of the diffractometer. Because the Weissenberg motion exists a number of unusual experiments, not possible in conventional diffractometer systems, can be performed.

Experiments performed so far include a Diffraction Anomalous Fine Structure (DAFS) (Creagh and Cookson (1995)) and the dynamical tensile stressing of polymer fibres. In its DAFS mode the motion of the IP cassette is synchronized to the monochromator as it is scanned through the absorption edge of a particular element. The entire range of diffraction from the crystal, are recorded at the same time. As well the fluorescent background can be analysed to give Fluorescent XAFS information to complement the DAFS data. *In situ* electrochemistry experiments, synchronizing the applied cell potential to the motion of the IP cassette, are also planned in 1995.

This paper will describe progress made in the development of these new techniques.

Cookson, D.J., Garrett, R.F., Foran, G.J., Creagh, D.C., and Wilkins, S.W.(1992) *Japanese Journal of Synchrotron Radiation*, 6,1, 127-130.

Barnea, Z., Clapp, R., Creagh, D.C., Harada, J., Hashizume, H., Stephenson, A. and Wilkins, S.W. (1989): *Rev.Sci.Instrum.* 60, 2537-2540.

Creagh, D.C. and Cookson, D.J. (1995) Photon Factory Activity Report, submitted.

1P10

IN - SITU STUDY OF STRUCTURAL DEFECTS IN MATERIALS USING SYNCHROTRON RADIATION

G.N.Yeritsian, A.A.Sahakian, S.K.Nickogosian, Yerevan Physics Institute,
2 Alikhanian Brothers St., 375036, Yerevan, Armenia

The possibility of direct measurements is suggested by use of synchrotron radiation with related experiments to study the atom displacement phenomena in materials.

The displacement of an atom plays important role in the defect formation of materials. That's why several mechanisms of defect production are discussed. The classic one is the elastic collision when energy of an atom is greater than threshold for adiabatic displacement of the lattice host or impurity atom.

Under certain conditions, the electronic excitation mechanism is more efficient during subthreshold and even superthreshold processes. The subthreshold defect formation probably is analyzed on the basis of Klinger's impurity ionization theory.

This mechanism may be efficient:

1. when energy of Coulumb repulsion between the host and impurity atoms is greater than threshold for adiabatic displacement
2. the time of the positive charge localization is greater than the atom displacement time.

Some experimental results in this field were fairly optimistic. The estimations showed high probability of this effect when using synchrotron radiation: high intensity; sufficient time of positive charge localization of ionized host atoms; required energy for inner shell ionization of host material atom.

To our opinion the most sensitive experiment shall be applied to measure in - situ with high accuracy the displacement of an atom and thus point out simple defects and clusters of desordered regions.

In other words the synchrotron radiation should be used as defect production source and measurement beam at the same time.

1P11

INVESTIGATIONS ON SOLID STATE PHYSICS AND CRYSTALLOGRAPHY USING SYNCHROTRON RADIATION AT YEREVAN PHYSICS INSTITUTE

D.L. Egikian, Yerevan Physics Institute, Yerevan 375036, Armenia

At Yerevan Physics Institute the investigations on solid state physics and crystallography using synchrotron radiation (SR) beams from the 6 GeV electron accelerator are carried out. For these investigations Si, Ge, GaP, InP and other single crystals are used as the samples. The following important results were obtained. The integral coefficient of reflection and other parameters for Si, Ge, GaP single crystals were measured in wide range of wave-length including K-edge of Ge and Ga. The main diffractometrical parameters of "forbidden" (222) reflex for Si, Ge and their dependence on structural perfection of the samples were investigated. The method of the single crystal structural defect investigation with the depth variation of the layer from several up to few tens micrometers by monochromatic topography in different orders of reflection was developed. The method for determination of surface and volume perfection degree of crystalline samples by means of measuring the widenning of collimeting slit image in SR beams diffracted by (n'+n) spectrometer was developed and studied in experiment. Several investigations were carried out to develop the apparatus and measurement technique of the SR beams. All these results are observed in the paper.

1P12

RIKEN CONTRACT BEAMLINES FOR STRUCTURAL BIOLOGY AT SPring-8

H. Iwasaki and RIKEN SR Structural Biology Research Group, The Institute of Physical and Chemical Research (RIKEN), Wako-shi, Saitama 351-01, JAPAN

SPring-8 (Super Photon ring-8GeV) is one of the largest high-brilliance synchrotron radiation source placed at Harima in Hyogo Prefecture, about 100km west of Osaka. The construction is in progress by JAERI-RIKEN SPring-8 Project Team, and the first beam is foreseen in 1997. It has 61 beamlines in all, of which more than 30 will be "public" open to all domestic and foreign scientists. At our Institute RIKEN, structural biology is considered as one of the most important research fields, and two contract beamlines for structural biology are now being designed and developed. The first one is for protein crystallography (PX) and small-angle solution scattering (SAXS). The X-ray sources are two undulators arranged serially. The dichromatic SR, with energy from 6 to 14 keV, is branched by a diamond beam splitter. It acts also as a first monochromator for the SAXS experimental station, and the beam which goes through the beamsplitter is guided to the PX station. The optical system for PX has been optimized for multiwavelength anomalous diffraction (MAD) method and includes a newly developed "trichromator" which enables us to collect three kinds of data sets at three wavelengths quasisimultaneously for the same protein crystal without changing the setting. The second one is for time-resolved PX using Laue methods and for XAFS. The X-ray source is a bending magnet, and both white and monochromatic beam will be used. The operation of these RIKEN contract beamlines will be started at the initial stage of SPring-8.

THE BIO-CRYSTALLOGRAPHY (MIR-OAS) BEAMLINE AT THE SPRING-8

N. Kamiya, T. Ueki, H. Iwasaki, The Institute of Physical and Chemical Research (RIKEN), Hirosawa 2-1, Wako 351-01, Japan, N. Tanaka, Faculty of Bioscience and Biotechnology, Tokyo Institute of Technology, Nagatsuda, Midori-ku, Yokohama 226, Japan, and K. Miki, Department of Chemistry, Faculty of Science, Kyoto University, Sakyo-ku, Kyoto 606-01, Japan.

SPring-8 (Super Photon ring-8GeV) is a third-generation synchrotron radiation facility of Japan, which is under construction by the JAERI-RIKEN SPring-8 Project Team. The storage ring commissioning will be started early at 1997. The Bio-Crystallography beamline1) is constructed for routine analyses of macromolecular crystallography by the multiple isomorphous replacement method with optimized anomalous scattering (MIR-OAS). The beamline also focuses on data collections for small crystals less than 100 μm or those for very large macromolecules such as ribosomal particles and viruses. The light source of this beamline is an in-vacuum type undulator of magnetic periodicity of 3.2 cm, which emits highly brilliant X-rays in an energy range between 9 and 38 keV. The highest power and power density of the undulator are 5 kW and 300 $kW/mrad^2$, respectively. To handle the tremendous power density, a rotated-inclined double-crystal monochromator will be used. To focus the high energy X-rays up to 38 keV, two super mirrors (Ovonic Synthetic Materials Co.) will be installed to get quasi-isotropic and small beam profile of about 100 μm at focal position. For recording the diffraction patterns of sample crystals, a κ-type goniostat and an imaging plate on-line detector will be used in the experimental station. The station further includes an XAFS apparatus, which determines suitable values of X-ray energy for the data collections with the heavy atom derivatives near its L_3 absorption edges, a cooling system for specimen and a software system dedicated to the MIR-OAS routine analysis.

1) N. Kamiya *et al.* (1995), *Rev. Sci. Instrum.* **66**, 1703-1705.

1P14

ELECTRON DENSITY DISTRIBUTION IN PYRITE-TYPE MnS$_2$ USING SR

M. Ueki, N. Ishizawa, Research Laboratory of Engineering Materials, Tokyo Institute of Technology, Nagatsuta Yokohama 227, Japan, and F. Marumo, Department of Earth Sciences, Nihon University, Setagaya Tokyo 156, Japan

Pyrite-type structure consists of octahedrally coordinated M atoms and X$_2$ dumbbell molecules. Stevens et al. (1979) carried out the population analysis of low-spin Fe^{2+} in pyrite-type FeS$_2$, stating that the calculated excess electrons in dγ orbital were possibly due to the interaction between Fe and S. The low-spin transition elements such as Fe^{2+} show an anisotropic electron density distribution due to the enriched electrons in dε orbital, which obscures the observation of the weak metal-ligand interaction along the bond by the conventional Fourier method. The present study has been carried out to detect such interaction on MnS$_2$ containing Mn^{2+} cations of d^5 electron configuration in the high-spin state. The three-dimensional X-ray diffraction data of natural MnS$_2$ were obtained using the horizontal-type four-circle diffractometer at KEK BL14A with SR of the 0.75 Å wavelength. The least-squares refinement employing atomic scattering factors of neutral atoms yielded the final R/Rw value of 0.0119/0.0122 for 539 independent reflections in the range $2\theta<138°$. The difference Fourier map on the section including Mn and S-S dumbbell is shown in the figure with contour intervals of 0.1 eÅ^{-3}. The positive residual peaks with heights of 0.49 eÅ^{-3} around Mn is supposed to be due to the bonding interaction between dγ orbital of Mn and π_g^* orbital of S$_2$$^{2-}$, which has been predicted from the band calculation in previous studies.

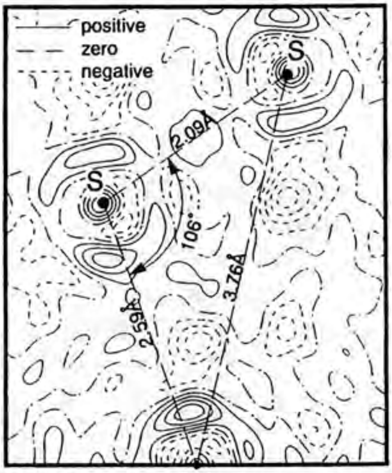

Stevens, E. D., Delucia, M. L. & Coppens, P. (1980) Inorg. Chem. **19** 813-820.

1P15

SIZE DEPENDENCY OF THE c/a RATIO OF TETRAGONAL BARIUM TITANATE MICRO-CRYSTALS USING SR

K. Suda, M. Kataoka, N. Ishizawa, Research Laboratory of Engineering Materials, Tokyo Institute of Technology, 4259, Nagatsuta, Midori-Ku, Yokohama 226, and F. Marumo, Department of Earth Sciences, Nihon University, 3-25-40 Sakurajosui, Setagaya-Ku, Tokyo 156, and K. Ohsumi, National Laboratory for High Energy Physics (KEK), 1-1 Oho, Tsukuba 305, Japan

The tetragonality of submicrometer-sized crystals of barium titanate, $BaTiO_3$, has been investigated by the ultra-micro single-crystal X-ray diffraction technique using synchrotron radiation at the beam line 4B of the Photon Factory, KEK. Laue photographs were taken using the Imaging Plate and processed on the DIP310SOR system. Size of the crystal was measured using a scanning electron microscope after the SR experiment. Conversion diameter of the crystal with anisotropic shape was calculated assuming a sphere with the same volume. The c/a ratios have been determined using the splitting of Laue spots due to the presence of 90° domains of tetragonal form. They are 1.0072(2), 1.0098(3) and 1.0106(6) for crystals with conversion diameters of 0.56, 1.32 and 10 μm, respectively. The c/a ratios of the 1.32 and 10 μm crystals are approximately the same as that of the bulk crystal, while it is significantly small for the 0.56 μm crystal. The rapid decrease of the c/a ratio can be explained based on the effect of depolarization. No clear splitting was observed for the crystal with conversion diameters of 0.32 and 0.25 μm. The disappearance of splitting can be interpreted in several ways; one is that the crystal becomes mono-domain with cubic or tetragonal symmetry, and the other is that the crystal is still composed of 180° domains of tetragonal form. The structure analysis using the integral intensities measured for the 0.32 μm crystal will contribute to solve this problem.

STRUCTURE ANALYSIS OF $CaYAlO_4$ SMALL CRYSTAL USING SR

K. Morita, K. Suda, N. Ishizawa, Research Laboratory of Engineering Materials, Tokyo Institute of Technology, Nagatsuta Yokohama 227, Japan, and N. Kodama, Tosoh Cooperation, Hayakawa, Ayase 252, and M. Yamaga, Department of Physics, Gifu University, Gifu 501-11, Japan

Chromium-doped $CaYAlO_4$ is expected to exhibit a spectral hole-burning at low temperatures. The present study has been undertaken to obtain a detailed knowledge about the host structure of the K_2NiF_4-type $CaYAlO_4$. Single crystals were grown by the Czochralski technique in an inert atmosphere. Three dimensional diffraction data were collected from a crystal with dimensions of 12x12x6 μm^3 using a vertical-type four-circle diffractometer at the beam line 14A of the Photon Factory, KEK. The wavelength of 0.75 Å, which is 508 eV below the Y K edge, was selected to avoid the contamination due to the fluorescence of Yttrium in the compound and to reduce the absorption effect. X-rays were focused using a toroidal mirror. Crystal data are; tetragonal I4/mmm, a=3.6437(1) Å, c=11.8682(3) Å, Z=2, μ=53.6 cm^{-1}. In all 426 independent reflections with $|F| \geq 3\sigma(|F|)$ were obtained from 2648 measured reflections in the range $2\theta \leq 138°$. The least-squares refinement gave a final R value of 0.011 employing anisotropic temperature factors for all atoms. No improvement in the R factor, nor any significant alteration in the residual electron density distribution was observed when the secondary extinction correction was applied in the least-squares procedure. The minimum y value was 0.994 for the 200 strongest reflection when the correction was included. It was concluded that the secondary extinction was negligibly reduced in this experiment. Presence of excess Ca and deficient Y atoms from the nominal composition were detected, generating a small amount of oxygen vacancies at the apical O(2) site of the AlO_6 octahedron. The Al and Ca atoms adjacent to the O(2) vacancy are supposed to be displaced along the c axis from their ideal positions. A strong anisotropy of the thermal parameters of oxygen atoms indicated a conspicuous librational vibration of AlO_6 octahedra around axes in the basal plane, or a kind of disordering accompanying the presence of oxygen vacancy. All these features provide a clue for understanding the unusual behavior of Cr^{3+} in $CaYAlO_4$ observed by the electron paramagnetic resonance study.

1P17

SINGLE CRYSTAL X-RAY DIFFRACTION AND EXAFS ANALYSIS OF $(Y_{0.2}Zr_{0.8})O_{1.9}$ FLUORITE-TYPE COMPOUND

Y. Matsushima, M. Hayashi, K. Suda, N. Ishizawa, Research Laboratory of Engineering Materials, Tokyo Institute of Technology, Nagatsuta, Midori, Yokohama 226, Japan, and H. Oyanagi, Electrotechnical Laboratory, Umezono, Tsukuba 305, Japan

Determination of the local structure around a solute atom in a host structure provides important information on the understanding of the physical properties of the solid solution. Positional disorder of constituent atoms in $(Y_{0.2}Zr_{0.8})O_{1.9}$, a member of the fluorite-type ZrO_2-Y_2O_3 solid solution, has been investigated by the single crystal X-ray diffraction technique and by the EXAFS analysis. Crystals were grown by melting a calcined rod made of Y_2O_3 and ZrO_2 powders, using the focused YAG laser beam. A transparent part of the melt-quench product was ground into a sphere of 35 μm in diameter for the diffraction experiment using SR. Intensity data were measured with the four-circle diffractometer at the beam line 14A, KEK-PF. The wavelengths employed were 0.75 and 0.7281 Å (10 eV below the Y K edge). EXAFS spectra of the powdered sample were measured near the Y K and Zr K edges employing the transmission mode at 14A. A provisional refinement using 83 independent reflections out of 2278 measured reflections for the 0.75 Å data set converged with R/Rw factors of 0.0277/0.0263 assuming the ideal fluorite model which consists of Y and Zr atoms at origin and oxygens at 1/4,1/4,1/4. The R/Rw factors became 0.0137/0.0172 assuming a more complicated structural model similar to that adopted for Y_3TaO_7 fluorite-type compound by Tanaka et al (1995). This model consists of Zr atoms at origin and Y atoms at x,x,x with x=0.030(1) and half of the O atoms at 1/4,1/4,1/4, and the rest at 1/4,1/4,z with z=0.320(2). The mean Y-O and Zr-O distances calculated from this model agreed well with the EXAFS results.

Tanaka, T., Ishizawa, N., Yoshimura, M., Marumo, F. & Oyanagi, F. (1995) *J. Solid State Chem.*, **114**, 79-87.

STRUCTURAL STUDY ON THE DEFECT-PEROVSKITE-TYPE COMPOUNDS $La_{1/3}MO_3$ (M=Ta,Nb)

K. Tanabe, K. Suda, N. Ishizawa, J-H. Sohn and M. Itoh, Reseach Laboratory of Engineering Materials, Tokyo Institute of Technology, 4259, Nagatsuta, Midori-ku, Yokohama 226, Japan

Double-layered defect-perovskite-type compounds $La_{1/3}MO_3$ (M=Ta,Nb) have ordered vacancies at every other A sites along the c axis of ABO_3 perovskite. From the view of material science, they are promising host crystals for the Li ion intercalation. Single crystal diffraction study has been carried out to verify the structural details relating to their physical properties. Crystals were grown by the floating zone method. Crystal data of $La_{1/3}TaO_3$ are a=b=3.9163(1) Å, c=7.9138(4) Å, Z=2, SG=P4/mmm. Three dimensional diffraction data were collected using the horizontal-type four-circle diffractometer at the beam line 14A of KEK PF with λ=0.7 Å. The specimen has a spherical shape with diameter of 45 μm. The SR data were compared with those taken by the rotating anode four-circle diffractometer using Ag$K\alpha$. The specimen used for the Ag experiment was also spherical with diameter of 93 μm. The conventional least-squares refinement gave a converged R value for the SR data of 0.026 using 800 independent reflections in the range $\sin\theta/\lambda < 1.35$ while 0.015 for the Ag data set using 249 reflections in the range $\sin\theta/\lambda < 0.90$. The split atom models for O(2) and O(3) were employed after Iyer et al (1967). No evidence was found for the presence of La atoms at the vacant sites at z=0.5, which might take place at higher temperatures. A superstructure with doubled a and b dimensions was observed for $La_{1/3}NbO_3$ from the SR experiment. The superstructure was hardly detectable from the Ag experiment. The cell dimensions are a=7.8199(3), b=7.8394(3) and c=7.9119(3) Å. The deviation from the tetragonal symmetry was obvious.

Iyer, P. N. & Smith, A. J. (1967). *Acta Cryst.* **23**, 740-746.

X-RAY DIFFUSE SCATTERING STUDY OF MAGNETITE BY THE VALENCE-DIFFERENCE CONTRAST METHOD

Takeshi Toyoda and Satoshi Sasaki, Research Laboratory of Engineering Materials, Tokyo Institute of Technology, Nagatsuta, Midori-ku Yokohama, 226, Japan, and Masahiko Tanaka, Photon Factory, National Laboratory for High Energy Physics, Oho, Tsukuba 305, Japan.

Magnetite is a mixed valence compound of an inverse-spinel type, $[Fe^{3+}]^A[Fe^{2+}Fe^{3+}]^BO_4$. The high electronic conductivity suggests the continuous interchange of the electrons between Fe^{2+} and Fe^{3+} at the B sites above the Verwey transition ($T_v \cong 125$ K), while the hopping is frozen as charge ordering below T_V. Even above T_V, anomalous diffuse streaks were observed in electron and neutron scattering [1,2].

It is recognized that a chemical shift of XANES spectrum occurs among different valence states. The anomalous scattering effect related to the chemical shift promises the possibility of distinguishing different ions of the same elements in a mixed valence crystal by selecting a wavelength to give the different f' values [3]. In this study to use synchrotron X-rays, valence fluctuations of ferrous and ferric ions in the B site are examined in terms of diffuse scattering just above T_V.

X-ray experiments were performed on synthetic, and partly natural, single crystals with vertical-type four-circle diffractometer at PF-BL-10A. The synthetic crystals were kindly provided by H. Kawata and S. Todo. Intensity measurements in various 2-D reciprocal planes were made around the 400, 800, 440, 221, and 444-type reflections at 130, 200, and 300 K. The wavelength $\lambda = 1.7421$ Å was chosen with the f' difference of 1.6 between Fe^{2+} and Fe^{3+}. Weak diffuse streaks were observed in the disk-like or cross-like shape except 221, having some difference from the neutron scattering results at 130K. The diffuse streaks are possibly occurred by local charge ordering or local lattice distortion. Modeling and further experiments are in progress.

[1] Chiba, K., Suzuki, K. & Chikazumi, S. (1975) J. Phys. Soc. Jpn 39, 839-840.

[2] Shapiro, S.M., Iizumi, M. & Shirane, G. (1976) Phys. Rev. B 14, 200-207.

[3] Sasaki, S. (1995) Rev. Sci. Instrum. 66, 1573-1576.

Structural changes of (Pb,Cu)SrLaCuO$_{5+\delta}$ on oxygen introduction into block layers

N.R. Khasanova[a], F. Izumi[a], M. Shida[b], B. Chakoumakos[c], E. Ohshima[b], M. Kikuchi[b] and Y. Syono[b]

[a] National Institute for Research in Inorganic Materials, 1-1 Namiki, Tsukuba 305, Japan

[b] Institute for Materials Research, Tohoku University, Katahira, Aoba-ku, Sendai 980-77, Japan

[c] Solid State Division, Oak Ridge National Laboratory, Oak, Ridge, TN 378311-6393, USA

The crystal structures of superconducting (Pb,Cu)SrLaCuO$_{5+\delta}$ with different oxygen contents ($\delta = 0.03$ and 0.13) have been studied by neutron powder diffraction. The fully oxidized sample with $\delta = 0.13$ was prepared by calcinating a starting mixture at 800°C in air, cooling slowly and heating at 1010°C in O_2. Removing extra oxygen in an atmosphere of N_2 and subsequent quenching raised the superconducting transition temperature from 27 K ($\delta = 0.03$) to 36 K ($\delta = 0.13$). The neutron diffraction data of the two samples were measured on the HB-4 powder diffractometer at HFIR and analyzed by the Rietveld method using space group P4/mmm (Kwei et al., 1991). Oxygen atoms in the (Pb,Cu)O layer at $z = 0$ were split into four pieces at a 4n site (x, 1/2, 0; $x = 0.31$). In the fully oxidized sample, the 2f site (0, 1/2, 0) in the (Pb,Cu)O layer was slightly occupied by excess oxygen. On the other hand, this site proved to be vacant in the deoxidized sample. Possible models of atomic arrangements in the (Pb,Cu)O layer were considered in our structure refinements. The resulting values of isotropic thermal parameters, B, indicate that atoms in the (Pb,Cu)O layer and apical oxygen are disordered to a greater extent in the fully oxidized sample than in the deoxidized sample. The oxidation-reduction behavior of Pb and Cu in this system and its effect on T_c will be discussed on the basis of crystal data obtained in this study.

Kwei, G.H., Canfield, P.C., Fisk, Z, Thompson, J.D, & Von Dreele, R.B. (1991). *Physica C* 176, 57–63.

1P21

NEUTRON DIFFRACTION STUDY OF THE IMPROVED CHEMICAL STABILITY OF CATION SUBSTITUTED '123' SUPERCONDUCTOR $Y_{0.6}Ca_{0.4}Ba_{1.6}La_{0.4}Cu_3O_{7-d}$

A. Sequeira and H. Rajagopal, Solid State Physics Division, and R. Ganguly and J.V. Yakhmi, Chemistry Division, Bhabha Atomic Research Centre, BOMBAY - 400085, India

It has been shown recently that appropriate cation substitutions such as $Y_{1-y}Ca_yBa_{2-y}La_yCu_3O_{7-d}$ not only help to keep the T_c above 80K, but also relieve the tensile stresses which exist in the parent $YBa_2Cu_3O_7$ compound in the Ba-O and $Cu(2)O_2$ layers due to bond-length mismatch. In fact, an othorhombic to tetragonal transition occurs at $y \approx 0.4$ and this particular composition (title compound) has been demonstrated to be remarkably corrosion resistant and stable against reaction with water for upto 150 days as against decomposition of the unsubstituted sample within 2 days of soaking in water (Zhou et al, 1994). We have, therefore, carried out a comparative structure analyses of the tetragonal (P4/mmm) $Y_{0.6}Ca_{0.4}$ $Ba_{1.6}La_{0.4}Cu_3O_{7-d}$ (T_c=79K) and orthorhombic $YBa_2Cu_3O_{7-d}$ (T_c=93K) by Rietveld analyses of powder neutron data recorded at room temperature (λ= 1.216 A). The composition of the title compound estimated after refinement is $Y_{0.59}Ca_{0.41}Ba_{1.68}La_{0.32}Cu_3O_{6.95}$. Major differences observed between the two samples are: a slightly shortened apical Cu(1)-O(4) bond(1.898A) and an elongated Cu(2)-O(4) bond(2.258A) plus a slightly reduced puckering of the Cu(2)-O(2) planes for the title compound, indicating a reduced stress in the perovskite lattice which is likely to make the cation-substituted compound more stable chemically. The results will be discussed in detail.

Zhou et al (1994) Jour.Am.Chem.Soc. 116, preprint.

1P22

THE INVERSE PROBLEM IN MULTIPLE SMALL-ANGLE SCATTERING

S. Mazumder and A. Sequeira, Solid State Physics Division, Bhabha Atomic Research Centre, Trombay, Bombay-400085

Small Angle Scattering data from many materials are affected by multiple scattering more often than it is normally conceived. The presence of multiple scattering is indicated by the invalidity of the functional invariance property of the observed scattering profile with variation of any of the experimental parameters like thickness of the sample, wave length of the probing radiation and contrast of the inhomogeneities in the sample. The inverse problem in multiple scattering involves extraction of single scattering profile from scattering data affected by multiple scattering. The inverse problem in conventional small-angle scattering deals with extraction of real space structural information like particle size distribution (PSD) of the inhomogeneities from scattering profiles.

Recently, we have developed an algorithm to extract single scattering profile from scattering data affected by multiple scattering. The algorithm is based on the theory on multiple small angle scattering as outlined in the review article (Mazumder & Sequeira, 1992).

It uses the findings that functionality of multiple scattering profile depends on thickness, wave length, contrast etc., while the functionality of single scattering profile is independent of all these factors. The algorithm is based on the extraction of scattering mean free path from at least two sets of scattering data recorded either by varying the sample thickness or by changing the wavelength.

The input data sets can be used both in the absolute as well as in relative scale but the output single scattering profile can be obtained in absolute scale.

In the limiting case when the thickness of the sample is very large in comparison to the scattering mean free path, it is possible to extract information like PSD from multiple scattering profile itself, without going for extraction of single scattering profile, either by invoking variational technique like maximum entropy or assuming that particle size distribution has some well-defined functionality like log-normal, Gaussian etc.

The algorithm has been applied for analysis of scattering data from some alumina based system and some cements.

Mazumder, S. & Sequeira, A.(1992). Pramana, J.Phys. 38, 95-159.

1P23

SANS from SDS Micellar Solutions in Presence of Amines and Ammonium Salts

Sanjeev Kumar[+], V.K.Aswal[*], P.S.Goyal[*] and Kabir-ud-Din[+]
+ Department of Chemistry, AMU, Aligarh 202 002, India
* Solid State Physics Division, BARC, Bombay 400 085, India

This paper reports the effect of addition of amines ($(CH_3CH_2)_m-NH_2$; m = 5, 6, 7) and ammonium halides (NH_4X; x = Cl, Br, I) on the growth of sodium dodecyl sulphate (SDS) micelles as studied using small angle neutron scattering (SANS) and viscosity measurements. The surfactant concentration was kept fixed (= 0.3M) and the additive concentration was varied (x = 0.0 to 0.1M for amines and x = 0.0 to 1.6M for amonium halides). The SANS experiments were carried out using SANS spectrometer at Cirus reactor, Trombay and the viscosity measurements were made using a Brookfield cone/plate viscometer.

SANS experiments on SDS/Amines solutions show that micellar sizes are quite sensitive to addition of n-amines. For example, we find that the c/a for ellipsoidal micelles (a = b~ 18A, c~ 35A) in pure SDS solution increases from 2.0 to 5.0 as the n-octylamine (m = 7) concentration is increased from 0.0 to 0.065M [1]. We further find that the structures of isoviscous SDS/Amines solutions, as obtained by adding different amounts of the three amines are not identical.

The viscosity of SDS solutions is less sensitive to addition of ammonium halides as compared to that for addition of amines. SANS experiments on (0.3M SDS + 0.1M NH_4X) solution show that there is only a small increase in micellar size on addition of ammonium halide. It is seen that the SANS distribution for the above solutions are independent of the halide ion.

[1]. Sanjeev Kumar, V.K.Aswal, H.N.Singh, P.S.Goyal and Kabir-ud-Din, Langmuir 1994, 10, 4069

MICROPHASE SEPARATION IN ADSORBED PARAFFIN MIXTURES

E.P. Gilbert, P.A. Reynolds and J.W. White

Research School of Chemistry
The Australian National University
Canberra. ACT 0200. AUSTRALIA.

When equimolar mixtures of normal C_{30} and C_{36} paraffin hydrocarbons are quenched from the melt to room temperature, the mixed system undergoes solid state phase separation into lamellar phases. In this 'bulk' system the microphase separation is essentially longitudinal, the molecules slipping along their long axes to separate into lamellar components which neutron scattering can easily detect when isotopic substitution of one of the components is employed.

Our STM studies have shown that when the same unlabelled hydrocarbons are spread onto a clean graphite surface from a non-polar solvent, only the longer chain is imaged. This indicates a strong demixing enthalpy in the two-dimensional layer.

We have investigated the microphase separation process in which the two-component protonated/deuterated melt is quenched inside the gallery structures present in exfoliated graphite. In this system, it is possible for phase separation not only to occur in the longitudinal direction, as in the 'bulk', but also in a transverse direction due to the graphite surface forces. We report here results for the modified system.

VANADIUM AND VANADIUM-BEARING MICAS

G.K.Bekenova, Institute of Geological Sciences NAS RK, Almaty, 480100, Kazakhstan

The all-round mineralogical study of vanadium-bearing di-octahedral micas from the Cambrian carbonaceous-cherty formation of the Bolshoi Karatau Range (South Kazakhstan) allows to establish 4 basic groups: chernykhite (V_2O_3+V_2O_4 - 23-26%), Ba-roscoelite (V_2O_3+V_2O_5 - 12-25%), vanadium-bearing muscovite and phengite (V_2O_3 to 5%) and secondary mica-V^{4+}-Ba-phengite ($V_2O_3 << V_2O_4$ - 6-8%). In the last-mentioned group the tetravalent vanadium locates within tetrahedral positions in the crystal structure. The mineralogical description, physical properties, chemical compositions and structural data of studied micas are presented. The comparison of the chemical compositions, optical properties and structural data of the micas from South Kazakhstan and also ones of other V-micas from different regions throughout the world is given. The diagram of the dependence of the unit cell parameter b (Å) from vanadium content is shown. The value of b (Å) increases with increasing vanadium content in the structure.

1P26

THE CRYSTAL STRUCTURES OF DEHYDRATED FULLY Cd^{2+}-EXCHANGED ZEOLITE X AND OF ITS CARBON MONOXIDE SORPTION COMPLEX

Se Bok Jang, Jeong Hwa Kwon, Un Sik Kim, and Yang Kim, Department of Chemistry, Pusan National University, Pusan 609-735, Korea, and Karl Seff, Department of Chemistry, University of Hawaii, Honolulu, Hawaii 96822, U. S. A.

Large single crystals (stoichiometry $Na_{92}Si_{100}Al_{92}O_{384}$) of sodium zeolite X used in this work were prepared in St. Petersburg, Russia.[1] Each of two single crystals, a colorless octahedron about 0.2 mm in cross-section was lodged in a fine Pyrex capillary and exchanged by flow methods using an exchange solution of $Cd(NO_3)_2$ and $Cd(O_2CCH_3)_2$ in the mole ratio of 1 : 1 with total concentration of 0.05 M. Each crystal was dehydrated at 450 ℃ under a constant pressure of 2 x 10^{-6} Torr for 48 h. To prepare the carbon monoxide complex, one crystal (crystal 2) was treated with 100 Torr of zeolitically dried carbon monoxide gas for 1 h at 21(1) ℃. Diffraction data were collected with an automated Enraf-Nonius four-circle computer controlled CAD-4 diffractometer using Mo $K\alpha$ radiation. Their structures were refined to the final error indiecs, R_1 = 0.055 and R_w = 0.077 with 546 reflections and R_1 = 0.063 and R_w = 0.065 with 523 reflections, respectively, for which $I > 3\sigma(I)$.

Crystal Data: (1) $Cd_{46}Si_{100}Al_{92}O_{384}$, cubic, space group $Fd\,\bar{3}$ (No. 221)
a 24.935(1) Å.
(2) $Cd_{46}Si_{100}Al_{92}O_{384}28CO$, cubic, space group $Fd\,\bar{3}$ (No. 221)
a 24.905(1) Å.

In the crystal structure of dehydrated Cd_{46}-X, Cd^{2+} ions are located at the two different sites of high occupancy. The Cd^{2+} ions at Cd(1) lie at site I, the center of the double six-oxygen ring.[2] This sixteen-fold position is fully occupied (Cd(1)-O(3) = 2.35(1) Å, O(3)-Cd(2)-O(3) = 90.4(4)°). The Cd(2) position is at site II in the supercage. Thirty Cd^{2+} ions at Cd(2) nearly fill the thirty-twofold site II. The Cd(2)-O(2) distance, 2.16(1) Å, is shorter than the sum of the radii of Cd^{2+} and O^{2-}, 0.97 Å + 1.32 Å = 2.29 Å[3], a consequence of the low coordination number, three, at this site. In the structure of a carbon monoxide sorption complex of dehydrated Cd_{46}-X, twenty-eight carbon monoxide molecules are found per unit cell. Cd^{2+} ions are found at three different crystallographic sites. Thirteen Cd^{2+} ions at Cd(1) occupy the sixteenfold site I in the centers of a double six-oxygen rings and each coordinates to three framework oxygens at 2.37(1) Å. The Cd(2) position is on a threefold axis in the sodalite unit opposite the double six-ring at site I′. This thirty-twofold position is occupied by only five Cd^{2+} ions. Each coordinates at 2.50(1) Å to three O(3) framework oxygens, and is recessed ca. 1.60(1) Å into the sodalite cavity from their plane. To coordinate to carbon monoxide, each of twenty-eight Cd^{2+} ions at Cd(3) has moved 0.14 Å along its threefold axis toward the center of the supercage and away from their triads of three O(2) oxygen to a more tetrahedral coordination environment. Each Cd^{2+} ion coordinates to three framework O(2) oxygens at 2.16(1) Å. The O(2)-Cd^{2+}-O(2) bond angle changed from the near trigonal planar value of 119.2(5)° in dehydrated Cd_{46}-X to 117.7(4)° in the carbon monoxide complex. The C-O distance is 1.36(4) Å and the Cd-C-O angle is 180(3)°.

1. Bogomolov, V. N., Petranovski, V. P. (1986). *Zeolites*, 6, 418-419.
2. Kim, Y.; Han, Y. W., Seff, K. (1993). *J. Phys. Chem.* 97, 12663-12664.
3. *Handbook of Chemistry and Physics*, 70th ed. The Chemical Rubber Co.
Cleveland, Ohio, 1989/1990, p. F-187.

1P27

Structural investigation of high- and low-symmetry vesuvianite

Makio Ohkawa and Setsuo Takeno, Department of Earth and Planetary Systems Science, Faculty of Science, Hiroshima University, Higashi-Hiroshima 724, Japan, and Akira Yoshiasa, Department of Earth and Space Science, Faculty of Science, Osaka University, 1-16 Machikaneyama, Toyonaka, Osaka 560, Japan

Vesuvianite (idocrase) is a well-known rock-forming mineral with complex crystal chemistry and structure. The crystal structure of vesuvianite is related to that of grossular garnet. In fact, the two minerals often coexist intimately in nature. High-symmetry (*P4/nnc*) vesuvianite occurs in metamorphic calc-silicate rocks mostly in skarn, and formed at high temperatures. Low-symmetry (non-*P4/nnc*) vesuvianite occurs in rodingites, in veins found in mafic rocks and serpentinites and rarely in metamorphic calc-silicate rocks in which it formed at relatively low temperatures during retrogressive metamorphism.

The crystal structures of six high- and four low-symmetry vesuvianites were determined by single-crystal X-ray diffraction method. The structure refinements were carried out in the space group *P4/nnc*, *P4/n* and *P4nc*, respectively. 3.1-8.2% of *R* indices were obtained.

Two types of possible ordered arrangements (*P4/n* and *P4nc*) are determined. The satisfaction of the local charge balance on O(10) anions requires alternate occupancy of oxygen and hydroxyl with an associated hydrogen bond and ordering sequences of cations.

The high-symmetry vesuvianite can contain Cl^- ions preferentially occupying the O(10) site that is split into two sites; one is occupied by Cl^- and the other by F^-.

Non Cl-bearing high-symmetry one indicate an additional tetrahedrally coordinated cation site probably be occupied by Al^{3+}.

1P28

SYNTHESIS AND CHARACTERIZATION OF ALKALI-METAL TIN(IV) ARSENATES: $ASnOAsO_4$ (A = K and Rb), $Cs_2Sn_3As_6O_{22}$ and $CsSn_2As_3O_{12}$

Kuan-Jiuh Lin and **Kwang-Hwa Lii**, **Institute of Chemistry, Academia Sinica, Taipei, Taiwan, R.O.C.**

Materials containing octahedral $M^{IV}O_6$ and tetrahedral X^VO_4 groups are of interest because of their potentially useful physical properties. For examples, $KTiOPO_4$ has been recognized as an outstanding nonlinear optical crystal for frequency conversion; $NaTi_2(PO_4)_3$ belongs to the NASICON family of compounds which exhibit fast ion conduction and low thermal expansion. In view of the technological interest in these compounds, we are currently making efforts to synthesize other new phases in the A^I-M^{IV}-X^V-O (X = P, As) systems. To our knowledge, very few compounds are known in the ternary tin arsenate phase space. This poster reports the results of our exploratory synthesis using a flux method and single-crystal X-ray structures of four arsenates, $KSnOAsO_4$, $RbSnOAsO_4$, $Cs_2Sn_3As_6O_{22}$ and $CsSn_2As_3O_{12}$.

Both $KSnOAsO_4$ and $RbSnOAsO_4$ are isostructural with $KTiOPO_4$. The oxygen framework for both tin compounds approximate very closely to a centrosymmetric arrangement, as indicated from the analysis of atomic coordinates. $RbSnOAsO_4$ has a powder SHG signal about the same magnitude as that of quartz. $Cs_2Sn_3As_6O_{22}$ adopts a new structure. Its three-dimensional framework consists of corner-sharing SnO_6 octahedra, AsO_4 terahedra and As_2O_7 groups, forming 12-sided tunnels in which the Cs^+ cations are located. $CsSn_2As_3O_{12}$ has a monoclinically distorted NASICON-type structure.

Crystal data: $KSnOAsO_4$, $Pna2_1$, a = 13.406(3) Å, b = 6.678(1) Å, c = 10.921(2) Å, Z = 8, R = 0.034; $RbSnOAsO_4$, $Pna2_1$, a = 13.567(3) Å, b = 6.791(1) Å c = 10.891(2) Å, Z = 8, R = 0.035; $Cs_2Sn_3As_6O_{22}$, $P2_1/n$, a = 10.465(1) Å, b = 13.198(2) Å, c = 15.623(2) Å, β = 94.80(1)°, Z = 8, R = 0.028; $CsSn_2As_3O_{12}$, $P2_1/c$, a = 10.733(4) Å, b = 10.275(3) Å, c = 9.267(4) Å, β = 93.09(4)°, Z = 4, R = 0.031.

CRYSTAL STRUCTURE STUDIES OF $CeAlO_3$ BY SYNCHROTRON RADIATION

Masahiko TANAKA[1], Hiroyuki HORIUCHI[2], Toetsu SHISHIDO[3] and Tsuguo FUKUDA[3]
1) Photon Factory, National Laboratory for High Energy Physics. Oho, Tsukuba, Ibaraki 305, Japan. 2) Mineralogical Institute, Graduate School of Science, University of Tokyo, 7-3-1 Hongo, Bunkyo-ku, Tokyo 113, Japan. 3) Institute for Materials Research, Tohoku University, Katahira, Aoba-ku, Sendai, Miyagi 980, Japan.

$CeAlO_3$ crystallizes in perovskite-type structure, and its crystal system has been reported to be tetragonal or trigonal. Tanaka et al.[1] recently reported the crystal structure with tetragonal lattice of **ato1=ato2**=3.7669(9) and **cto**=3.7967(7)A. The electron distribution of oxygen atoms in its structure was remarkably deviated from spherical distribution, and they discussed that it would be the result of an averaged electron distribution over multiplied unit cells. Since the superlattice reflections have not been observed by means of single-crystal and powder X-ray diffractometers with shield tube X-ray sources, diffraction intensities caused by the multiplied unit cell should be very weak if they exist. So we performed single crystal X-ray diffraction experiments applying synchrotron radiation X-ray sources using crystals which are the same samples as those used by Tanaka et al.[1]. Experiments were done using a vertical type 4-circle diffractometer at BL-10A, Photon Factory, National Laboratory for High Energy Physics. Since we could observe superlattice reflections corresponding to the unit cell with 2 × **ato1**, 2 × **ato2** and 2 × **cto** by peak hunting on a single crystal diffractometer, we assumed a new lattice with the above unit cell and measured all reflection intensities in the range of $-7<h, k, l<7$, $0< 2\theta <26$. Where **ato1, ato2** and **cto** are lattice vectors for original tetragonal lattice vectors by Tanaka et al.. As a result, the crystal was found to be tetragonal with lattice of **at1=ato1-ato2**, **at2=ato1+ato2** and **ct**=2 × **cto**. Where, **at1=at2**=5.3757 and **ct**=7.6672A. Laue symmetry is tetragonal, 4/mmm, with systematic absences of $h+k+l=2n+1$. By assuming the space group I4/mcm, the magnitude of the structure factors for weak reflections with $l=2n+1$ could successfully explain by the displacement of oxygen atoms. However, on the difference-Fourier map, weak but residual electron distributions which were caused by the deviation from the ideal positions of Ce were observed around the Ce atoms. As a conclusion, the actual unit cell of $CeAlO_3$ is a multiplied lattice of original tetragonal lattice, and it might have still some problems for the structure analysis due to twinning in which reciprocal lattice points corresponding to each domain are superposed each other.

[1] Tanaka et al.,Jour.Alloys and Compounds, 192, 87-89(1993)

SODIUM MAGNESIOSILICATES WITH THE CARNEGIEITE, OR "STUFFED CRISTOBALITE", STRUCTURE

C. J. Lobo, S. Schmid, J. G. Thompson and R. L. Withers, Research School of Chemistry, The Australian National University, Canberra ACT 0200, Australia, and R. Stranger, Department of Chemistry, The Faculties, The Australian National University, Canberra ACT 0200, Australia.

Alkali aluminosilicates and alkali magnesiosilicates with structures related to the mineral carnegieite, which has the "stuffed cristobalite" structure (Buerger, 1954), are of interest because of their property of ionic conductivity at elevated temperatures. Previous studies on sodium magnesiosilicates with this structure-type reported various and contradictory compositions, unit cells and space group symmetries for the phases they produced.

A systematic study of the pseudo-binary system SiO_2-$NaMg_{0.5}Si_{0.5}O_2$ using various reactive reagents as starting materials, including magnesiosilicate minerals, has identified two crystalline phases with the "stuffed cristobalite" structure type. At high temperatures, *i.e.* ≥ 800°C, the stable phase has a stoichiometry close to $Na_{0.9}Mg_{0.45}Si_{0.55}O_2$ with an orthorhombic unit cell, $a = 7.067(3)$, $b = 10.855(6)$, $c = 5.286(3)$ Å. At lower temperatures, *i.e.* between about 500 and 800°C, a higher symmetry disordered phase occurs as a narrow solid solution with a tetragonal unit cell of typical dimensions $a = 10.497(2)$, $c = 14.334(5)$ Å.

The crystal structures of these two phases have been refined from X-ray powder diffraction data using the Rietveld method. The number of degrees of freedom required in each case was minimised by using a modulated structure approach to the structural model refinement (see Withers and Thompson, 1993).

Buerger, M.J. (1954) *Amer. Mineral.* **39**, 600-614.
Withers, R.L. & Thompson, J.G. (1993) *Acta Cryst.* **B49**, 614-626.

1P32

CATION DISTRIBUTION AND CRYSTAL CHEMISTRY IN $Y_3Al_{5-x}Ga_xO_{12}$ ($0 \leq x \leq 5$) GARNET SOLID-SOLUTIONS

A.Nakatsuka, A.Yoshiasa and T.Yamanaka, Faculty of Science,
Osaka University, Toyonaka, Osaka 560, Japan

The large single crystals of garnet solid-solutions (x=0.0, 1.0, 2.0, 3.0, 4.0 and 5.0) were grown using PbF_2 flux. These crystal structures were refined by single-crystal X-ray diffraction analyses using high power X-ray source. Cation distributions and anisotropic thermal parameters in the crystal structure were examined in detail. The larger Ga^{3+} ions occupy preferentially the 4-coordinated site in the all composition range, whereas the smaller Al^{3+} ions occupy 6-coordinated site. The tendency of site preference of Ga^{3+} ions is most probably caused by the covalency of the ions and geometric restriction. The precise examination of polyhedral distribution and atomic thermal motion also revealed the enhancement of the cation-cation interaction is caused by both the geometric restriction due to the symmetry and the properties of chemical bonding. Moreover, the lattice constants are smaller than those calculated based on Vegard's law. The deviation from the Vegard's law is also reported in the system of Grosular and Hydro-grosular.

Obtained crystal data: cubic, space group $Ia\bar{3}d$ (No.230)

at x=0.0	a=12.0062(5)A
at x=2.0	a=12.0926(9)A
at x=3.0	a=12.1552(6)A
at x=4.0	a=12.2123(8)A
at x=5.0	a=12.2730(10)A

THE CRYSTAL STRUCTURE OF VESUVIANITES FROM TAIWAN

S. C. Yu, J. S. Lee and C. P. Wang, Department of Earth Sciences, National Cheng Kung University, Tainan, Taiwan 70101, R.O.C.

The crystal structure of two vesuvianites in rodingite from the Chinshuichi area, Yuli, Taiwan, were determined from data collected on a Nonius CAD-4 four-circle diffractometer. Two samples are brown and green in color, respectively. Electron-microprobe analysis of vesuvianites used in this study were carried out on a Jeol instrument equipped with EDS and WDS attachments.

The results indicate that the brown vesuvianites have high Ti content and that the increase in Ti is fairly well correlated with the decrease in Al. In contrast, the green ones are characterized by very low Ti concentration. Very low fluorine and boron content in these two samples were also found.

The two samples belong to the space group of P4/nnc and have similar chemistry and cell parameters (a=15.548, 15.508; c=11.833, 11.815 Å). Full-matrix least squares refinement of the structure, including anisotropic temperature factors, gave conventional and weighted R values of 6.73, 4.47 and 6.67, 4.59 %, respectively for these two specimens. The structures are virtually identical, and very similar to that proposed by Coda el al. (1970). The refinement results show the position for the H atom at the distance of about 0.6 Å from O11. According to the analysis of a difference Fourier synthesis, the bond-valence calculations and relationship between B-O10 and O10-O10 distance, it demonstrates that another H atom should bond to O10.

Cations in vesuvianites are mainly confined to the 6-fold AlFe-sites (Al, Fe, Mg, Ti) and 5-fold B-sites (Fe, Al, Mg). The 4-fold sites are filled with Si, the 8-fold sites with Ca (minor Na), and the 6-fold A-sites with Al. Furthermore, along the 4-fold axis of the structure, adjacent B-sites (tetrahedral pyramid) and C-sites (square antiprism) are half occupied because of the close cation-cation distance of about 1.4 Å.

Charge Density Study of Nonlinear Optical Crystals of LBO and KB5

Hwo-shuenn Sheu and Yu Wang

Department of Chemistry, National Taiwan University, Taipei, Taiwan &
Synchrotron Radiation Research Center, Hsinchu, Taiwan, R. O. C.

Borate compounds have attracted great attention recently because of its excellent UV NLO(nonlinear optical) property. KB5($KB_5O_{10}H_4 \cdot 2H_2O$) is the first developed borate NLO crystal and LBO(LiB_3O_5) is the best one so far. LBO crystallized in a noncentric orthorhombic space group $Pna2_1$, with cell parameters a = 8.450(2), b = 7.380(2), c = 5.1381(9) Å, Z = 4, R = 0.017, wR = 0.023 for 5902 observed reflections ($I > 2.0\ \sigma(I)$). KB5 crystallized in a noncentric orthorhombic space group Aba2, with cell parameters a = 11.034(2), b = 11.179(2), c = 8.961(2) Å, Z = 4, R = 0.032, wR = 0.034 for 6230 observed reflections ($I > 2.0\ \sigma(I)$). Accurate single crystal X-ray diffraction data were measured at room temperature and 125K using Mo Kα radiation for LBO and KB5 respectively. The data resolution is up to $\sin(\theta) / \lambda$ = 1.32 and 1.22 $Å^{-1}$ for LBO and KB5 respectively. Charge density distribution studies were made in order to investigate the correlation between the electron density distribution and the NLO property.

The NLO property of LBO and KB5 are believed to be mainly contributed from their anionic group, $(B_3O_7)^{5-}$ & $[B_5O_6(OH)_4]^{1-}$. The former one is a six membered ring with three alternate B and O atoms. Two B atoms are coordinated by three O atoms in a sp^2 fashion but the other B atom is coordinated by four O atoms with sp^3 hybridization. The anionic group is also connected to four other anion groups through oxygen bridges forming an infinite polymeric anionic chain. The latter one can be taken as a dimer of the six member ring with four OH group on the side chain; the anionic groups are connected by hydrogen bonds. Deformation density maps of LBO & KB5 are derived using the multipole model. They appear that asymmetric and symetric charge distribution of the six membered ring for LBO and KB5 respectively. Certainly, there is difference between the 4-coordinated and 3-coordinated B-atoms. A slight difference between the two 3-coordinated B is detected, however, a pseudo mirror symmetry through the 4-coordinated B and the oxygen atom at para-position is possible from the geometric data. Such model is also tried, the comparison of two models will be given.

1P35

STRUCTURAL CHANGE OF $Ca_2(Mg,Fe)Si_2O_7$ BY HEAT TREATMENT.

K.Hagiya, K.Kusaka, N.Haga and M.Ohmasa, Department of Life Science, Himeji Institute of Technology, Kanaji 1479-1, Kamigori, Akogun, Hyogo 678-12, Japan, and K.Iishi, Department of Mineralogical Science and Geology, Yamaguchi University, Yoshida, Yamaguchi 753, Japan.

Incommensurate phases of synthetic åkermanite solid solution were found by Hemingway *et al.*[1] and Seifert *et al.*[2] independently. They found that åkermanite undergoes a reversible phase transition from the high-temperature normal phase to the low-temperature incommensurate phase. The modulated structures of the Co end member [3] and $Ca_2(Mg,Fe)Si_2O_7$ were determined by us based on the five-dimensional description. Since a comparison of the structure of the incommensurate phase to that of the normal phase was expected to be informative to elucidate causes of the modulation, the present studies on effects of heat treatment of the material have been carried out.

The specimen of the single crystal $Ca_2(Mg,Fe)Si_2O_7$ was synthesized by one of the authors (K.I.). On the precession photograph taken at room temperature, the satellite reflections caused by two-dimensional modulation were observed. The diffraction pattern at 200°C was taken by a high temperature precession camera, and the satellite reflections were disappeared. After this heat treatment, however, no satellites were reappeared in the diffraction pattern at room temperature. Since this phenomenon was not reversible, a new structure different from the normal phase should be formed and the structure was analyzed to detect the structure change. The cell parameters and the intensities were determined on an Enref-Nonius CAD-4 diffractometer with Mo$K\alpha$ radiation monochromatized by graphite. The cell parameters a=7.8304(5)Å, c=5.0009(2)Å with a tetragonal symmetry are shorter than those of the basic structure of the incommensurate phase (a=7.8668(7)Å, c=5.0138(4)Å). The positional and thermal parameters were refined to R=0.096 for 710 unique reflections.

[1] Hemingway *et al.* (1986). Can. Mineral. **24**, 425-434.
[2] Seifert *et al.* (1987). Phys. Chem. Minerals **14**, 26-35.
[3] Hagiya *et al.* (1993). Acta Cryst. **B49**, 172-179.

1P36

STRUCTURE AND RESIDUAL DENSITY OF $CaFeO_3$ WITH Fe^{4+}

S.Morimoto, Faculty of Engineering Science, Osaka University, Toyonaka, 560, Japan., T.Yamanaka, Faculty of Science, Osaka University, Toyonaka, 560, Japan., M.Tanaka, Photon Factory, National Laboratory for High Energy Physics, Tsukuba, 305, Japan.

Fe^{4+} in $CaFeO_3$ shows "charge disproportionation reaction" into two valence states of Fe^{3+} and Fe^{5+} at low temperature (Takano et al. (1977), Nasu et al. (1992)) and the structure analysis on $CaFeO_3$ is of great interst.
The crystal structures of $CaFeO_3$ at 293K and 113K are investigated by means of single crystal diffractometry.
Data collections were performed at BL-10A in the Photon Factory with a radiaton of λ=0.69848(3)Å.

Crystal data:$CaFeO_3$ (at 293K), Pbnm, Z=4, a=5.3480(3), c=7.5730(5)Å: (at 113K), Pbnm, Z=4, a=5.3409(3), c=7.5585(13)Å.

$CaFeO_3$ was revealed to have an "orthorombic perovskite structure" even at 113K at which "chrage disproportionation" has been confirmed. The smaller angle (ca. 160° of Fe-O-Fe in $CaFeO_3$ than that in $SrFeO_3$ with no "disproportionation" leads the weaker 180° interaction, which causes "disproportionation". The very small elongation of the FeO_6 octahedron in $CaFeO_3$ observed at 293K is comparable to that in $GdFeO_3$ (Marezio et al. (1970)) and suggests little contribution of the Jahn-Teller effect.
Residual charge density of $CaFeO_3$ was revealed by difference Fourier map at 293K and 113K. Large residual density peaks with 1.2e/Å^3 as a maxima are confirmed clearly at the center of Fe-O bond. These are from a covalent contribution on the account of a overlapping of Fe^{4+} 3d level and O 2p.

1P37

STRUCTURE AND TWINNING OF A SMALL CRYSTAL OF MAWBYITE, $PbFe_{1-x}Zn_x(AsO_4)_2(OH)_{1-x}$, $x = 0.06$.

Kharisun, Max R. Taylor, School of Physical Sciences, Flinders University, GPO Box 2100, Adelaide, 5001, Allan Pring, South Australian Museum, Adelaide, 5000, A. David Rae, Research School of Chemistry, Australian National University, Canberra, ACT 0200, Australia.

Reflection data were collected from a very small crystal of Mawbyite, *a* 9.066(4), *b* 6.286(3), *c* 7.564(3) Å, β 114.86(3) °, *C2/m*, Z = 2, using a sealed tube Mo X-ray source and a SIEMENS SMART CCD detector system, courtesy of Dr C. F. Campana, Siemens Industrial Automation Inc. Reflections indexed according to a primitive unit cell with extra weak reflections for $h+k$ odd, l odd but not $h+k$ odd, l even. An initial structure solution and refinement was obtained in *C2/m* using only $h+k$ even reflections. The angle between **c** and 2**a** + **c** is 89.98(1)° and allows the use of a twin rule to create a second unit cell orientation with $\mathbf{a'} = -(\mathbf{a} + \mathbf{c})$, $\mathbf{b'} = -\mathbf{b}$, $\mathbf{c'} = \mathbf{c}$, $[2\mathbf{a'} + \mathbf{c'} = -(2\mathbf{a} + \mathbf{c})]$ and observations $(1 - \alpha)\,|F(hkl)|^2 + \alpha\,|F(h'k'l')|^2$ where $h' = -h-l$, $k' = -k$, $l' = l$. Only the twin components of reflections with l even overlap. A value of $\alpha = 0.109(2)$ was obtained using 361 reflections with $I > 3\sigma(I)$. Values for $R_1 = \Sigma\,|\Delta F|/\Sigma|F\mathrm{obs}|$ were 0.035 (127 $h+k$ even, l even), 0.037 (132 $h+k$ even, l odd), 0.091 (103 $h+k$ odd, l odd), 0.043 (overall). A twin plane at $x = 1/4$ may be constructed using a 2 fold rotation axis parallel to **c**, *i.e.* $1/2-x$, $1/2-y$, $1/4-x+z$ relative to the cell **a**, **b**, **c**. On the twin plane, the octahedrally coordinated Fe(III) atoms at 1/4, $N\pm1/4$, 1/2 (usually $\bar{1}$ sites) and the coordinated OH are replaced by 4 coordinated Zn(II) atoms on local rotation axes. Apparent valence and tetrahedral coordination requirements of the Zn can be met by moving the twin plane to $x = 1/4+\delta$ with the 2 fold rotation axis, now described by the operation $1/2+2\delta-x$, $1/2-y$, $1/4+\delta-x+z$, passing through a Zn atom at $1/4+\delta, 1/4, 1/2+\varepsilon$.

1P38

COMPARISON OF CRYSTAL STRUCTURES BETWEEN Li-DOPED AND UNDOPED SUPERCONDUCTORS OF THE TYPE $Bi_2Sr_2CaCu_2O_8$

K. Kitahama, T. Horiuchi and T. Kawai, The Institute of Scientific and Industrial Research, Osaka University, 8-1 Mihogaoka Ibaraki 567 Japan.

To survey high T_c superconductors and to study the transport mechanism, substitution of metal ions for Cu position in $Bi_2Sr_2CaCu_2O_{8+\delta}$ (Bi2212) has extensively attempted. Significant elevation of T_c ($\Delta T_c < 4$ K) was noted in Li addition to the starting material, which fact stimulated us to determine the location of Li in the crystal. Since the substance include quite heavy atoms like Bi, we cannot locate the Li atom without ambiguity. Therefore, this study was intended to detect small change in atom positions and thermal parameters associated with the Li incorporation. Single crystals of $Bi_{2.2}Sr_{1.8}CaCu_2O_x$ and $Bi_{2.2}Sr_{1.8}CaCu_{1.74}Li_{0.26}O_x$ were prepared by the traveling solvent FZ method. Their chemical compositions were found from an ICP method. Three dimensional X-ray analysis has been performed on both crystals. Both crystals easily cleave along the ab-plane. These crystals were cut into square plates in dimensions $0.2 \times 0.2 \times 0.02$ mm^3. Each crystal was installed with the c axis along the ϕ axis of the goniostat of a four-circle diffractometer. Both crystal lattices are expressed by an approximate space group Pbmb with a=5.416(2) b=5.411(3) c=30.858(11) for the undoped crystal and a=5.411(4), b=5.408(3), c=30.914(13) A for the doped crystal, respectively. In addition, precession photographs of both crystals exhibit incommensurate super spots along the b* axis with the separation 4.8 b*. To avoid heavy absorption effects, *hkL* reflections with $L<10$ were withdrawn from the succeeding least-squares refinement. Refinements were initiated with the atom positions reported by Imai, et al. [1], which converged to $R \sim 10\%$ for both crystals. However, only inter atomic distances concerning metal atoms are meaningful and precision of oxygen position is not enough due to presence of quite heavy atoms. Significant change is noted in Sr···Ca distance which extends from 3.360(5) to 3.374(5) A by Li incorporation. Location of Li will be conjectured based on the present X-ray analysis and non-diffraction data like ^{7}Li-nmr and Raman spectra.

[1] K. Imai, I. Nakai, T. Kawashima, S. Sueno and Ono, A. (1988) Jpn. J. Appl. Phys. 27, L1661-L1664.

SYNTHESES AND CRYSTAL STRUCTURES OF ZIRCONOLITE POLYTYPES

Y. Ono, The University of Tokyo, Hongo 7-3-1, Tokyo 113, Japan.*

Zirconolite($CaZrTi_2O_7$) has a layer structure which consists of TiO_6 layers related to that of hexagonal tungsten bronze-type(HTB) compounds and inter layer cations. Different stacking sequences of the HTB layers yield some kinds of polytypes as seen in mica. According to the description generally used in mica, these polytypes are described as zirconolite(2M), zirkelite($3T_1$), polymignite(2O) and pyrochlore($3T_2$).

In this work, the syntheses of these polytypes with two systems of chemical composition were investigated to know what factor affect the different polytype structures formation. Crystal structures were analyzed by X-ray diffraction methods.

1. Substitution of Ca for REE and part of Ti for Mg or Al in $CaZrTiO_7$
   (REE=Nd,Sm,Dy,Y, REE Al : $REEZrTiAlO_7$,
   REE Mg : $REEZrTi_{1.5}Mg_{0.5}O_7$)

As the substituted REE^{3-} ion radius become larger from Y to Nd, a series of polytypes formation was obteined that theree polytypes appered in the order of zirconolite(2M) ⇒ zikelite($3T_1$) ⇒ polymignite(2O), in both Mg and Al system.

2. Substitution of Ca for Nd and 0.5Ti for Mg in $CaZrTiO_7$ with different NdMg %.

In this solid solution system, the compositions are described by percentage of NdMg($NdZrTi_{1.5}Mg_{0.5}O_7$) for NdMg + CaTi($CaZrTiO_7$). There seems to be same series of polytypes formation, zirconolite ⇒ zikerite ⇒ polymignite, as the NdMg percentage increased. Zirkelite was obtained in the range of NdMg=40～80%.

This order of polytypes formation series is consistent with the order of a localization degree of their five-coordinated cation sites occupied by Ti, Mg or Al. The localization degree was estimated by frequency of their apperance along one cations column, which extends to the direction of stacking. These five-coordinated cation sites are situated in every twelve HTB layers along one cations column for zirconolite, but in every six layers for zirkelite. Polymignite contains them in every layer.

One factor of different polytypes formation is suggested that it is the different circumstances of these five-coodinated cation sites, including correlations with neighbor eight-coordinated cation sites which occupied by Ca or REE.

---

* present adress: Sibaura Engineering Works co.,ltd. Sagamigaoka 6-25-22, Kanagawa 228, Japan.

1P40

SUPERSTRUCTURE OF $Ba_{6-3x}Sm_{8+2x}Ti_{18}O_{54}(x=0.71)$

H.Ohsato, H.Kato, M.Mizuta & T.Okuda, Nagoya Institute of Technology
Gokiso-cho, Showa-ku, Nagoya 466, Japan.

$Ba_{6-3x}Sm_{8+2x}Ti_{18}O_{54}$ solid solutions have high dielectric constant (ε_r=70-80), high quality factor (Q·f>=9000) and low temperature coefficient (Ohsato et al. 1993, 1995). Recently, this dielectric ceramics have been used for microwave resonator. Ohsato et al. (1992) investigated the crystal structure of $Ba_{3.87}Sm_{9.42}Ti_{18}O_{54}$ (x=0.71) and found a superlattice with doubled c-axis lattice parameter.

Crystal data of true cell: Orthrombic system, $Pbn2_1$ (No.33) or Pbnm (No.62), Z=2, a=12.131(3), b=22.271(5), c=7.639(5)Å.

In this work, the superstructure of the $Ba_{3.87}Sm_{9.42}Ti_{18}O_{54}$ solid solution was analyzed based on the fundamental structure reported by Ohsato et al. (1993). Refinement of the structure was performed on Pbnm (No.62).

The solid solution has tungsten bronze type structure with 2x2 perovskite blocks and pentagonal sites. The TiO_6-octahedra tilts alternately along the c-axis. The tilting causes a doubling of the fundamental cell along the c-axis. And the two-fold rotation axis of fundamental cell (Pbam (No.55)) changes to the two-fold screw axis of true cell (Pbnm (No.62)). Split of O-atom found in fourier map of the fundamental cell can be explained by the tilting of TiO_6-octahedra.

Superstructure of this solid solution consists of repeat of two fundamental cell along the c-axis, and is caused by the tilting of TiO_6-octahedra.

Ohsato H., Ohhashi T. and Okuda T. : Ext. Abstr. AsCA'93 Conf., Singapore, November, 14U-50.

Ohsato H., Nishigaki S. & Okuda T. (1992). Jpn. J. Appl. Phys. 31, 3136-3138

Ohsato H., Ohhashi T., Nishigaki S. & Okuda T. (1993). Jpn. J. Appl. Phys. 32, 4323-4326

Ohsato H., Ohhashi T., Kato H., Nishigaki S. & Okuda T. (1995). Jpn. J.

1P41

INTRAMOLECULAR INTERACTIONS OBSERVED IN FOUR BIS(PHTHALOCYANINATE)-LANTHANOID(III) COMPLEXES

N. Koike, H. Uekusa, and Y. Ohashi, Faculty of Science, Tokyo Institute of Technology, O-okayama, Meguro-ku, Tokyo 152, Japan, and C. Harnoode, F. Kitamura, T. Ohsaka, and K. Tokuda, Interdisciplinary Graduate School of Science and Engineering, Tokyo Institute of Technology, Nagatsuta, Midori-ku, Yokohama 227,Japan.

The bis(phthalocyaninato)lanthanide(III) complexes have stimulated a great deal of interest because of their electrical conductivity and electrochromic properties. In order to investigate the above properties, a series of structures of bis(phthalocyaninato)lanthanoid(III), $[LnPc_2]^-$, have been determined by X-ray diffraction analysis [Ln = Nd(III), Gd(III), Ho(III), Lu(III)].

Each lanthanoid ion is eight-coordinated by two phthalocyanine ligands ,which rotate to each other from the eclipsed conformation by 6.2, 26.2, 43.2, and 45.0° for $[NdPc_2]^-$, $[GdPc_2]^-$, $[HoPc_2]^-$ and $[LuPc_2]^-$, respectively. Each crystal contains tetrabutylammonium, $[NBu_4]^+$. The $[LnPc_2]^-$ anion and the $[NBu_4]^+$ cation stacks alternatively as a column along a four-fold axis. Figure 1 shows the crystal structure of $[NBu_4][HoPc_2]$.

The difference in rotation angle among the four compounds seems to be attributed to the ionic radii of the central lanthanoid ions, i.e. the smaller ionic radius is, the larger rotation angle is. This indicates a fairly strong intramolecular π-π interaction of $[LnPc_2]^-$. Further detail will be discussed on the basis of the analyzed structures.

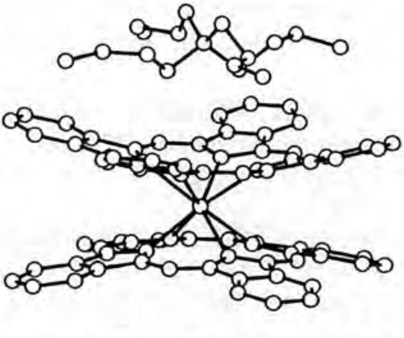

Figure 1. Structure of $[NBu_4][HoPc_2]$

STRUCTURE ANALYSIS OF $(NH_4)_3H(SO_4)_2$ AT 150K

Y. Noda, S.Fukuchi and I.Tamura , Faculty of Science, Chiba University,
Yayoi, Chiba 263, Japan

Triammonium hydrogen disulfate $(NH_4)_3H(SO_4)_2$ abbreviated as A3HS shows successive phase transitions from phase I to VII. Not only that, deuteration of sample gives a large isotope effect upon the phase transition temperature, and an extra phase appears in d-A3HS. Concerning the structures at low temperature phases, almost no information was reported except the structure of phase III given by M.Tanaka and Y.Shiozaki(1986). Proposed space group was *P2*. However, our recent work with low temperature Weissenberg photograph by using an Image-plate revealed that the space group was *P2/n*, and the transition was characterized by the appearance of superlattice reflections at Z-point in the *A2/a* space group. We performed the structure analysis of the phase III(150K) by the off-center-type four-circle diffractometer with a closed-type refrigerator cryostat. The structure analysis at room temperature (phase II) was consistent with the reported data, with *A2/a* and R_F=0.0345.

Crystal data: 150K, $(NH_4)_3H(SO_4)_2$ monoclinic, space group *P2/n* (No.13)
a 15.582(7) , b 5.821(3), c 10.064(7)Å, β 101.57(9).

Here, the lattice is chosen so that the compatible room temperature phase is expressed by *C2/c*. Intensity of superlattice reflection and lattice parameters are measured as a function of temperature. At the transition temperature 263.5K, the lattice parameter a starts to deviate as a continuos transition. Characteristics of the phase transition from the phase II to the phase III was analyzed based on the obtained structural parameters. The remarkable change of positional parameters deviated from the room temperature phase was seen for oxygen atoms, whose displacement pattern was expressed by an anti-phase rotation of the SO_4 molecules. On the other hand, N and S atoms are staying at the original position.

Tanaka ,M. and Shiozaki,Y. (1986). *Acta Cryst.* C42, 776-780.

INCOMMENSURATE-COMMENSURATE PHASE TRANSITION OF INTRAMOLECULAR HYDROGEN-BONDED MATERIAL d-BrHPLN

I. Tamura, Y. Noda and Y. Kuroiwa, Faculty of Science, Chiba University, Yayoi, Chiba 263, Japan, and T. Mochida, Institute for Molecular Science, Okazaki, Aichi 444, Japan ad T. Sugawara, Department of Pure and Applied Sciences, College of Arts and Science, The University of Tokyo, Komaba, Tokyo 153, Japan.

The hydrogen-bonded materials are well-known to show a large isotope effect. In order to investigate the origin of isotope effect, the simplest hydrogen bonded system was studied recent years. Since intramolecular hydrogen-bonded materials have no hydrogen network and a hydrogen-bond is fixed by a molecular frame, such materials prevent us the simplest system which is not bothered by the 'geometrical model'. In order to investigate the structure change associated with the phase transition, X-ray scattering experiment was performed on the deuterated 5-bromo-9-hydroxyphenalenone (abbreviated d-BrHPLN). The d-BrHPLN undergoes the phase transition at 34K and at 22K studied by dielectric measurements by Mochida et al. (1994) and Moritomo et al. (1995). The temperature dependence of lattice constants showed anomalous behavior at the points of T_C(=22.8K) and of T_I(=34.5K). The superlattice reflections are found at $(h\ k+0.5\ 0)$ below 14.4K by an X-ray Weissenberg photograph using the image plate by Noda et al (1994). The phase transition at T_C is characterized by a commensurate-incommensurate transition, and the phase transition at T_I is characterized by an incommensurate-normal transition. The peak shift δ shows a thermal hysteresis and is pinned on the position deviated from the exact commensurate position after the thermal cycles. It was found that the pinning effect was caused by X-ray radiation damage. The detailed structure analyses of H - and D - compounds at room temperature were performed, and the results will be given.

Mochida, T. et al. (1994). J. Chem. Phys. **101**, 7971-7974.
Moritomo, Y. et al. (1995). J. Phys. Soc. Jpn. **64**, 1892-1895.
Noda, Y. et al. (1994). J. Phys. Soc. Jpn. **63**, 4286-4289.

OBSERVATION OF ANOMALOUS DIFFUSE ROD BELOW 200K IN $Ba_2NaNb_5O_{15}$

T. Shobu, Y. Noda, Faculty of Science, Chiba University, Yayoi, Chiba 263, Japan, and K. Fujishiro and Y. Uesu, School of Science and Engineering, Waseda University, Ohkubo, Tokyo 169, Japan.

Barium sodium niobate $Ba_2NaNb_5O_{15}$ (abbreviated BSN) has been reported that the crystal undergoes transitions to an incommensurate phase at 573K and that to a commensurate phase at 533K studied by J. M. Kiat et al (1994). It has been also reported that the crystal has reentrant phase transition to the point-group symmetry of the high temperature phase below 110K studied by W. F. Oliver et al (1990). In addition, anomalous changes of birefringence Δn_{ab} and strain χ_{12} were observed at about 200K. We have performed X-ray studies to clarify the nature of BSN at low temperature region. At first we took a Weissenberg photograph using Imaging Plate at low temperature. Diffuse rod connecting to superlattice reflections were found below 200K. We also measured temperature dependence of this diffuse scattering using a scintillation counter. Shown in Fig.1 is the intensity of diffuse scattering at (6.25 -8.5 0.5) as a function of temperature. The diffuse scattering starts to increase at about 200K. We could not find any other characteristic scattering relevant to the anomalous behavior of Δn_{ab} and χ_{12}. Therefore, only short range order establishes below 200K. This result indicates that the nature below 200K is glass state. In this sample, the so-called reentrant transition was not observed. The authors would like to thank Dr. J.M.Kiat to provide a single crystal of BSN.

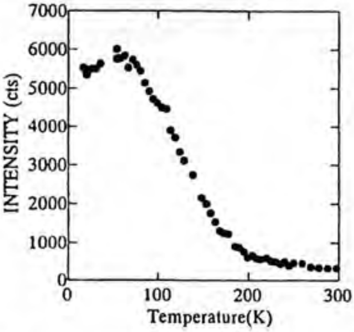

Fig.1 Temperature dependence of the intensity of diffuse scattering at (6.25 -8.5 0.5).

Kiat.J.M. *et al*, (1994). *Phys. Rev. B* **49,** 776-785.
Oliver W. F. *et al*, (1990). Ferroelectrics , **112**,3-25

1P45

Structure change investigation of perovskite-type $(Nd,Sm)AlO_3$ by X-ray powder diffraction.

Akira Yoshikawa[1)], Hiroyuki Horiuchi[1)], Masahiko Tanaka[2)], Toetsu Shishido[3)] and Tsuguo Fukuda[3)]

1) Mineralogical Institute, Faculty of Science, University of Tokyo, Hongo 7-3-1,Bunkyo-ku, Tokyo 113, Japan
2) Photon Factory, National Laboratory for High Energy Physics, Oho,Tsukuba, Ibaragi 305, Japan
3) Institute for Materials Research, Tohoku University, Katahira,Aoba-ku,Sendai 980, Japan.

Structure change of solid solution phases of $(Sm_{1-x},Nd_x)AlO_3$ was investigated by the analyses of powder X-ray diffraction profiles using samples obtained by a solid state reaction. They are based on a perovskite-type structure with slightly deformed lattices from an ideal cubic structure. By substituting Sm^{3+} for Nd^{3+}, the atomic position of (Sm,Nd) becomes close to an ideal position, and the structure of solid solution phase finally changes from orthorhombic to trigonal system at around x=0.7 [Fig.1], while the lattice distortion is the smallest in the phase with around x=0.0 [Fig.2]. The partial substitute of Sm^{3+} for Nd^{3+} play a role to control the size of ions in the structure, as a result, an apparent first order phase transition takes place in the structure, and the structure change does not pass through an ideal cubic structure.It is interesting that the phase transition of $SmAlO_3$ from orthorhombic to trigonal structure at high temperatures (O'Bryan et al.,1990) showed the similar structure change as observed by substituting Sm^{3+} for Nd^{3+} in this investigation.

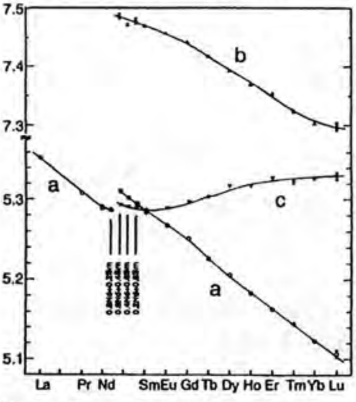

[Fig.1] Change of lattice constants depending on the rare earth elements. The structure changes from orthorhombic to trigonal at around x=0.7

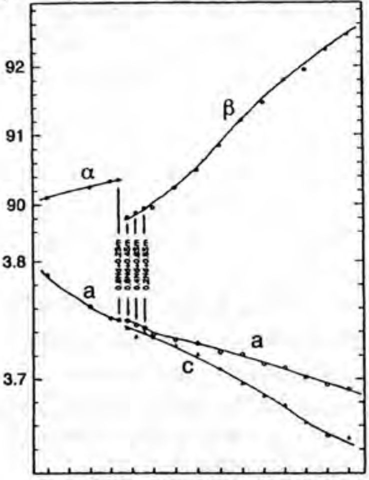

[Fig.2] Change of lattice parameters corresponding to basic lattices. The lattice distortion is the smallest in the phase with around x=0.0

H.M.O'Bryan, P.K.Gallaher, G.W.Berkstresser and C.D.Brandle, (1990). J.Mater.Res.,5,183-189

1P46

STRUCTURAL PHASE TRANSITIONS AMONG COMPLEX METAL OXIDES WITH PEROVSKITE- TYPE STRUCTURE : STUDIES BY PRECISE X-RAY POWDER DIFFRACTOMETRY.

Sergey Ivanov, Vladimir Zhurov, X-ray laboratory, Karpov' Institute of Physical, Chemistry, Ul.Vorontsovo pole,10 103064, Moscow K-64, Russia.

The application of temperature resolved precise X-ray powder diffractometry for the detailed investigation of atomic structure and phase transitions of ferroelectric and superconductive materials with perovskite-type structure is described. X-ray diffraction patterns were collected in the temperature range 20 - 1100K on the following complex metal oxides: $SrTiO_3$, Li doped $KTaO_3$ and $BaPbO_3$. Full-profile analysis was carried out in order to obtain the high-precision estimates of slight lattice distortions. Accurate values of profile parameters for sensitive reflections were calculated after separating and fitting of overlapping peaks which were carried out using our special software package for IBM PC computer. From the temperature evalution of splitting of diffraction reflections the temperatures of structural phase transformations were determined. The components of thermal expansion tensor of different phases and the volume changes during the phase transitions were obtained. The crystal structures for different phases were refined with the Rietveld method and the results were presented. An interpretation of physical properties of tested oxide materials as well as possible mechanisms of structural phase transformations were discussed also in detail using the obtained experimental results.

1P47

A SINGLE CRYSTAL X-RAY DIFFRACTION STUDY OF THE LOW TEMPERATURE PHASE OF RbCN

Y.Yoshimura, S.Shinohara, N. Tsuda and H. Iwasaki, Department of Physics, Ritsumeikan University, Noji, Kusatsu, Shiga 525 Japan.

At room temperature RbCN has the NaCl type cubic structure, with a disorder of linear CN ion orientations. As the temperature is decreased, the crystal undergoes an order-disorder phase transition associated mainly with the change in the orientation of the CN ions. Recent neutron powder diffraction study confirmed that the structure of the low temperature phase is monoclinic with the space group Cc. The space group Cc lacks a center of symmetry and can accommodate either ferroelectric or antiferroelectric ordering or anything in between. However, no ordering of the dipoles is observed in dielectric and optical measurements. In order to clarify some of the uncertainties in the crystal structure of the low temperature phase, the present authors took several precession photos at low temperatures. A structural change was observed from the cubic phase to a low temperature phase at about 125K. A variety of diffraction photos were obtained which indicate a coexistence of various forms. Paying attention to the presence of new reflections and splitting reflections, a monoclinic and a triclinic form were found in the low temperature phase. The lattice constants of the monoclinic form are a_M=4.81(1), b_M=4.87(1), c_M=7.92(1)Å, β=122.7(1)° at 85K, and the structure is A-base-centered with the space group A2/m. The lattice constants of the triclinic form are a_T=9.84(1), b_T=4.665(1), c_T=4.90(1)Å, α=121.3(1)°, β=119.1(1)°, γ =90.0(1)° at 85K.

1P48

SINGLE-CRYSTAL X-RAY DIFFRACTION STUDY OF $AgGaS_2$ UNDER HIGH PRESSURES

H. Kitahara, N. Ishizawa, Research Laboratory of Engineering Materials, Tokyo Institute of Technology, 4259 nagatsuta, Midori-ku, Yokohama 226, F. Marumo, Department of Earth Sciences, Nihon University, 3-25-40 Sakurajosui, Setagaya-ku, Tokyo 156 and Y. Noda, Department of Materials Science, Faculty of Engineering, Tohoku University, Aramaki, Aoba-ku, Sendai 980-77, Japan

The crystal of $AgGaS_2$ has been reported by Carlone et al.(1980) to undergo the first phase transition at about 4.2 GPa and the second at 11.6 GPa. The present study was undertaken to obtain crystallographic information of the intermediate high-pressure phase between 4.2 and 11.6 GPa employing a single crystal X-ray diffraction technique with a diamond-anvil cell. Single-crystals of $AgGaS_2$ were grown with the Bridgman method. A mixture of Ag_2S and Ga_2S_3 in the 1:1 molar ratio was sealed in an evacuated silica ampoule, kept at 1050°C for 12h, and then cooled at a lowering rate of 10 mm/day. The crystal is tetragonal, $I\bar{4}2d$, a=5.7626(5) and c=10.3128(9) Å at ambient pressure. The precession photographs taken under pressures between 4.7 and 5.4 GPa indicated that the systematic condition of 2h+l=4n for hhl reflections was broken, suggesting that the diamond glide planes parallel to {110} have been disappeared in the high-pressure phase. In addition, several diffraction spots became split in the high-pressure phase and again became unified when the pressure was released. These results indicate that (1) the unit cell of the high-pressure phase is close to the body-centred tetragonal one at ambient pressure, but (2) the diamond glide planes are lost and a twinning seems to take place above 4.2 GPa, and (3) the transition is essentially reversible. The high-pressure study phase is thought to possess a symmetry of $I2_12_12_1$, one of the maximal non-isomorphic subgroup for $I\bar{4}2d$.

C.Carlone, D.Olego, A.Jayaraman, and M.Cardona (1980). *Phys. Rev.* B **22**, 3877-3885

1P49

STRUCTURE OF PYRIDINIUM TETRAFLUOROBORATE AND ITS PHASE TRANSITIONS OBSERVED BY A NEW DIFFRACTOMETER

T. Nemoto, Y. Ohashi, M. Hanaya and M. Oguni, Department of Chemistry, Tokyo Institute of Technology, O-okayama, Meguro-ku, Tokyo 152, Japan.

The crystal of title compound belongs to the trigonal system $R\bar{3}$ at room temperature (Phase I). On cooling this crystal, first order phase transition occurred at 239K, and the permitivity was significantly changed(Phase II). But the cell dimensions are almost the same as those at room temperature. Below 205K, another low temperature phase (Phase III) is observed. The crystal system becomes to monoclinic system by this phase transition.

To examine the difference of crystal structure, the X-ray diffraction data sets are collected at 297K(Phase I), 223K(Phase II) and 173K(Phase III) using IP-weissenberg camera.

Crystal structures at room temperature is shown in Fig. 1. Both of the PyH^+ and BF_4^- ions are disordered around $\bar{3}$ symmetry.

Because of increase of the mosaicity, the diffraction spots are enlarged and precise cell dimensions of low temperature phases are not yet determined. Data reductions at two low temperature phases are now in progress.

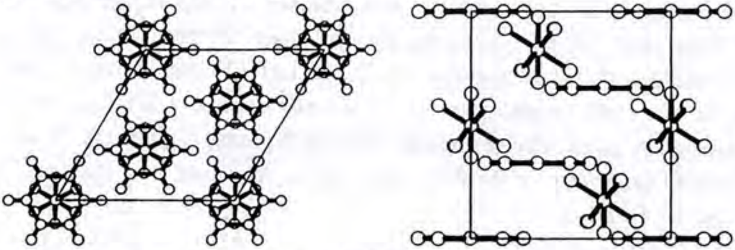

Fig 1. Crystal Structure at 297K.

(a) viewed along c axis. (b) viewed along b axis.

1P50

BUNYIP: A NEW APPROACH TO DETECTING ERRANT SYMMETRY

James Hester, NIRIM, Namiki 1-1, Tsukuba, Ibaraki 305, Japan *[jrh@nirim.go.jp]* and Syd Hall, Crystallography Centre, University of Western Australia, Nedlands *[syd@crystal.uwa.edu.au]*

The incorrect assignment of space group symmetry to crystal structures appears to be on the increase[1]. The reasons are several fold. Automatic alignment and space group assignment software is more widely used on diffractometers and these tend to assign lower symmetry space groups because of spurious systematic absence data. That is, the presence of intensities due to multiple Bragg scattering complicates automatic symmetry identification. Expert intervention is then needed. Additionally, structure analysts often lack adequate crystallographic training in symmetry identification. After all, *"its not the symmetry that counts; its the molecular conformation"* [if you agree with this statement, please come and argue this point with us at the poster!].

BUNYIP is a new approach to identifying extra symmetry in a solved structure. It complements the program MISSYM[2] which can fail if the symmetry relationships are badly distorted by refinement in the wrong space group.

The BUNYIP algorithm scans a structure for mid-points between any two sites which coincide within a common centre (indicating the presence of an inversion), axis (indicating a 2-fold rotation or screw) or plane (indicating a mirror or a glide). If a large proportion of midpoints coincide within a specified tolerance, the centre, the rotation/screw, or the mirror/glide, are identified.
The mid-point search is performed in Cartesian coordinates (orthogonal angstroms) and makes no assumptions about existing symmetry or cell, apart, that is, in aligning different molecules in the asymmetric unit into the optimally packed cluster.

BUNYIP is a new addition to the Xtal System[3] and has a direct link to the interactive molecular display routine PIG[4]. This enables the symmetry element detected by BUNYIP to be displayed and manipulated as part of the structure. This visualisation link is important to understanding the nature of the additional symmetry detected.

[1] Submission statistics to *Acta Crystallographica (personal communication).*

[2] Page, Y Le (1987) *J. Appl. Cryst., 20.* 264-269.

[3] Hall, S R, Flack & H D Stewart, J M(1992) Editors. Xtal *System of Crystallographic Programs.*

[4] Bartsch, U and Hall, S R (1992) *PIG: Display and Manipulate Atom Sites.* Xtal System of Crystallographic Programs.

1P51

A FLEXIBLE FOUR-CIRCLE DIFFRACTOMETER CONTROL SYSTEM FOR BEAM LINE 14A AT THE PHOTON FACTORY

T. P. Vaalsta Crystallography Centre, University of Western Australia, Nedlands, WA 6709, Australia, N. Ishizawa, Research Laboratory of Engineering Materials, Tokyo Institute of Technology, 4259 Nagatsuta, Midori-Ku, Yokohama 227, Japan.

Abstract

An operating system independent user friendly single-crystal four-circle diffractometer control system that is user friendly is under development. The objective is to provide greater flexibility of use for a number of applications of the powerful imaging capabilities of the vertical wiggler beam line. The system can operate across a diverse range of computers from UNIX workstations to 80x86 PCs. The control system allows the same software to be used on other diffractometers, helping to prepare specimens for the beam line diffractometer. The orientation matrix and other crystallographic related information thus obtained could be transfered electronically when the specimen is mounted for study at the beam line. Ease of use is enhanced by the on-line help available and the program's ability to run operating system commands from within it. The Crystallographer is not required to understand intricacies in operating the computer, and is free to concentrate on the task at hand. The initial version has been tested on DEC and Silicon SGI-Iris workstations, as well as 80486-based PCs running high-quality freely available UNIX and X systems such as Linux. The tests were conducted with four-circle diffractometers at the Crystallography Centre as well as on Beam-Line 14A at the Photon Factory at Tsukuba.

The new control system software conforms to the POSIX standard. That maximises the portability of the code between different computing systems. In todays environment of rapidly changing computer hardware and operating systems such portability of software is essential. The program's modular nature enhances its portability by separating hardware specific and generic elements of four-circle diffractometer control. The generic elements includes the user interface, crystallographic related computing, and storing-receiving data. Diffractometer specific elements include software that is unique to the control of a diffractometer—such as device driver modules and its related code.

The trend towards networking computing and network transparent windowing systems is recognised in the software design. The program also offers the possibility of monitoring the diffractometer from a remote location during data collection and intervention if necessary.

1P52

ANALYSIS OF METALLIC AND RELATED COMPOUNDS USING ICDD METALS AND ALLOYS INDEXES. J. N. Dann, T. C. Huang, W. F. McClune, M. H. Mueller, A. C. Roberts, and P. L. Wallace, Metals and Alloys Subcommittee of the Technical Committee, International Centre for Diffraction Data, 12 Campus Boulevard, Newtown Square, PA 19073, USA.

The interest in metals and alloys, as well as related nonmetallic and corrosive phases have continuously increased in recent years. The properties of these materials strongly depend on their crystalline structures, and a detailed study of the structures is important for the research and development in materials science and technology. The powder diffraction method is one of the techniques commonly used for the structural characterization of these compounds. Information on crystalline phases and their unit cell data such as lattice parameters, space groups, etc. can be obtained from the Powder Diffraction File (PDF) of the International Centre for Diffraction Data (ICDD). Another useful tool for the analysis of metallic and related phases is the Metal and Alloys (M&A) Indexes recently published by the ICDD. The M&A Indexes make the identification of these materials easier and more accurate by providing a chemical formula index; namely, the Alphabetical Formula Index (AFI). The AFI allows systematic searches of chemical analogs and a greater use of partial chemical knowledge. Other M&A indexes are the Pearson Symbol Code Index which gives all the materials in a given structure and allows for the comparison of atomic contents and lattice parameters; the Common Names Index which cross-references common metallurgical names; and the Strukturbericht Symbol Index which cross-references the Strukturbericht Symbols and the equivalent Pearson Symbols and structure prototypes. The organization, selection of materials, and the use of alphabetical formulas in the M&A Indexes are similar to those of standard metallurgical references such as Pearson, Villars and Calvert. The Indexes contain direct references to the PDF, and thus, distinguishes them from other metallurgical references. Additionally, it permits material characterization by comparison of the diffraction data for an unknown with PDF data. Applications of the M&A indexes for the determination of Pearson Symbols, prototype structures and so forth from indexed powder diffraction patterns and for the indexing of new diffraction patterns will be presented.

1P54

ORGANO-TEMPLATE CONTROL OF INORGANIC STRUCTURES : A SHEET ALUMINOPHOSPHATE OF LOW SYMMETRY 3[$NH_3CHMeCH_2NH_3$][$Al_6P_8O_{32}$][H_2O]

Ian D. Williams and Zhenyang Lin, Department of Chemistry, Hong Kong University of Science & Technology, Clear Water Bay, Kowloon, Hong Kong and Qiuming Gao, Jiesheng Chen and Ruren Xu, Key Laboratory of Inorganic Hydrothermal Synthesis, Jilin University, Changchun, China.

The 2-D ALPO family with [$Al_3P_4O_{16}$]$^{3-}$ anionic sheets are known with two network types, (4.6.8 or 4.6.12) dependant on counter cation size, Gao et al (1995). Use of (+/-)1,2-diaminopropane as template results in the formation of crystals of the title compound with a new low symmetry *(pg)* network.

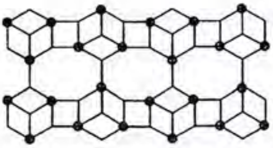

a) 4.6.8 Network, templated by [$NH_3CH_2CH_2NH_3$]$^{2+}$

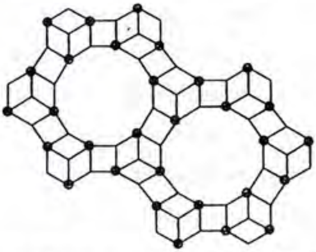

b) 4.6.12 Network, templated by [$NH_3CH_2CH_2CH_2CH_2NH_3$]$^{2+}$

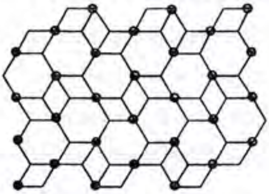

c) 4.6 Network templated by [$NH_3CHMeCH_2NH_3$]$^{2+}$

d) Al_3P_4 Building Blocks

Crystal Data: [$C_9H_{36}N_6$][$Al_6P_8O_{32}$].[H_2O], monoclinic, space group Ia (No 9), a = 18.119(2), b = 16.236(2), c = 14.736(2)Å, β = 91.35(1)°, V = 4333.8(1.0)Å^3. For 4451 data R = 0.040. Ave. lengths: Al-O 1.73, P-O 1.52, P=O 1.49Å esd .0005Å

The templating action of the organic base and alternate 2-D networks are discussed. The results are encouraging for the idea of creating surfaces with highly specific recognition properties via an organic-inorganic interface.

Gao, Q., Li, S., Chen,J., Xu, R., Williams, I.D. ,Zheng, J. & Barber, D. J. (1995) *J. Solid State Chem.*, submitted

1P55

STRUCTURAL CHANGES IN MODIFIED SMECTITES: Li-DIFFUSED MONTMORILLONITE CASE

A.Mulaba-Bafubiandi[1], J.Helsen[2], A.Maes[3], G.Langouche[4] and R.Prost[5]

1: *Faculty of Metallurgy and Materials Engineering, Ghulam Ishaq Khan Institute of Engineering Sciences and Technology, Topi, district Swabi, NWFP, PAKISTAN* 2: *Departement Metaalkunde en Toegepaste Materiaalkunde, K.U.Leuven, De Croylaan 2, B-3001 Heverlee, Belgium* 3: *Laboratorium voor Colloidchemie, Kardinaal Mercierlaan 200D, B-3001 Heverlee, Belgium* 4: *Institute voor Kern-en Stralingsfystoa, K.U.Leuven, Celestijmenlaan 200D, B-3001 Heverlee, Belgium.* 5: *Institut National de la Recherche Agronomique, route de St-Cyr F-78026 Versailles, France.*

Abstract

Montmorillonite is defined as 2:1 dioctahedral smectite with a cationic exchange capacity due to isomorphic substitutions. Li migration in this clay mineral perturbs the physico-chemistry within the lattice. The irreversible diffusion of this small cation ($r < 0.70$ Å) due to a heat treatment (between 200-300 °C) first observed by Hofmann and Klemen (1950) has been confirmed. The possible location of the migrating Li is assessed. The changes in the "microstructure" of this fine divided material and the influence of the migration of this small ion into the montmorillonite lattice have been studied. The kinetics of the migration could be followed. These observations are backed by XRD, FTIR, SEM and Mössbauer measurements. By Mossbauer spectroscopy the perturbation of the iron ions, located in Montmorillonite of Camp-Berteaux mainly in the octahedral layer, is studied. As the Fe(III) substitution is not at the origin of the cation exchange capacity, only a second order effect can be expected. As it will be shown, the effect is indeed small but visible.When modifications are int introduced in a crystal lattice, the whole vibrational situation of the crystal will be affected. Consequently, the vibrational spectra will be subject of change. The OH-stretching domain has been thoroughly explored by Prost et al.(1969). In this context a spectral study in the region below 2000cm^{-1} will be presented. At first, it was tried to perform this by advanced decomposition of spectra. The spectra are, however, far too complex in order to obtain reliable results. Finally a technique was developed that enabled us to record difference spectra of self-supporting films. It allowed us to record spectra of Li/Na-montmorillonites at given temperatures as a function of time and to study the kinetics of the Li migration process. XRD and SEM observations have confirmed the above results.

References

1. U.HOFMANN and R.KLEMEN, Zeitschrift fur anorganische chemie band 262 (1950) 95-99
2. R.PROST and R.CALVET, note dans C.R. Acad.Sc.Paris t.269 (1969) 539-541

2P01

THE EFFECT OF ENDING ANGLE ON THE STRUCTURAL PARAMETERS AND PROFILE AGREEMENT INDICES IN RIETVELD REFINEMENT

Changlin KUO and Hongchao LIU, Shanghai institute of Ceramics, Chinese Academy of Sciences , Shanghai 200050, P. R. China

The diffraction pattern of $Ca_3(PO_4)_3F$ was taken as sample data.

The parameters determined by Rietveld refinement showed different sensitive to the ending angle in the calculation. The coordinates of light atoms were influenced more than the heavy ones. When the ending angle was great than 70°, the results of these parameters almost kept constant. The values of this region were plausible. The determinations of these values were insensitive to the discrete position of ending angle, even if the stop two theta angle was in the region of a reflection. The test of weighted mean values and its two values of estimated standard deviation showed that no visible systematic errors appeared in the varying ending angle determination, except for cell parameters. Although the spread of O-atom coordinates was large due to its lower scattering cross section, the weighted mean value determined was more agreement than other methods. The determination of cell parameters appeared including systematic errors. This may be attributed to the incompleteness of Rietveld method.

Most of the agreement indices was not sensitive to the fitting quality in the Rietveld refinement. When the parameters were refined, the R agreement indices increased slowly with the increase of ending angle. The high angle data should not be included as many as possible according to the calculation results.

In fact, there is an inherent danger in.relying too heavily on the numerical values of criteria of the fit when these values are affected by factors unrelated to the fit of the crystal structure and peak profile models, as shown above. It is urgent to introduce a new set of agreement indices to access the fitting quality of Rietveld analysis of powder diffraction data.

CRYSTAL STRUCTURE AND DATA ON $Bi_4(SiO_4)_3$ BY X-RAY RIETVELD ANALYSIS

Changlin KUO and Hongchao LIU, Shanghai Institute of Ceramics, Chinese Academy of Sciences, Shanghai 200050, P. R. China

The sample for diffraction analysis was prepared by grinding the powder manually and passing the resultant powder through a 400 mesh sieve. Diffracion data were recorded on a conventional diffractometer. Various counting time strategy was applied to reduce the statistical error in the high angular due to low counts.

F_{30} was calculated based on the results of Rietveld analysis and observed data set. F_{30} is 158.90 with 30 observed reflections out of 32 possible lines and 0.0059° average difference of 2Θ.

Initial values of parameters taken from the Model II proposed by Menzer gave acceptable values. The final results showed that the cubic unit cell($a=10.2867$Å) contains four molecules in the following positions of space group I-43d (No. 220): Bi in 16c uuu with $u=0.0849$; Si in 12a 3/8 0 1/4; and O in 48e xyz with $x=0.0581$, $y=0.1319$, $z=0.2899$; $R_{wp}=11.8$; $R_{Bragg}=4.65$.

In this crystal structure, the distance of Si-O in one SiO_4 tetrahedra is 1.613Å; such a length corresponds to the equilibrium distance of Si-O bond. The Si atom is surrounded by four O atoms, four Bi atoms at distance of 3.543Å, four other O atoms at 3.554Å and four other Bi atoms at 3.578Å. Each O atom is coordinated with one Si, two Bi atoms at distances of 2.181Å and 2.590Å, respectively, two O atoms with a distance of 2.595Å and one O of 2.709Å in the same tetrahedra, other six atoms with distances ranging from 2.835Å to 3.186Å. The varied distances of O-O leads to the change of Si-O-Si angle from 107.13° to 114.26°; the large angle corresponds to long distance of O-O bond.

2P03

CRYSTAL STRUCTURE ANALYSIS OF ALKALINE PROTEASE (M-PROTEASE) FORM1 CRYSTAL.

T. Shirai, A. Suzuki, T. Yamane and T. Ashida, Nagoya university, Chikusa-ku, Nagoya 464-01, Japan. T. Kobayashi and S. Ito, Research Laboratories of Kao Corporation, 2606 Akabane, Ichikai, Haga, Tochigi 231-34, Japan.

M-protease is an subtilisin-family serine protease produced by alkalophilic bacteria *Bacillus sp.*. strain KMS-K16. A character of the enzyme is its high alkali resistance. The optimum pH of the M-protease is 12.3. The X-ray crystal structure analysis of the M-protease was carried out to study the mechanisms of high alkali resistance. Two morphologically different crystal forms 1 and 2 of the enzyme were obtained under a crystallization condition. The form1 crystals belong to ortholombic crystal system, space group $P2_12_12_1$, a=62.3, b=75.5 and c=47.2 Å.

The form1 crystal reflects beyond 1.Å, which is much better than previously analyzed form2 crystal (T. Yamane *et al.* 1995). The reflection data were collected using synchrotron radiation light source at the Photon Factory, National Laboratory of High Energy Physics, Japan.

The crystal structure of form1 was solved by the molecular replacement method, using the structure of form2. The model has been refined to the crystallographic R-factor of 0.175, using 9433 unique reflections between 8.0 and 1.7 Å resolutions. The high-alkali adaptation mechanisms were studied on the basis of the refined structure. From a comparison of primary structures of high- alkali proteases (M-portease, PB92, Savinase, etc.) and other homologous proteins (Subtilisin *bpn'*, Carlsberg, Protease K, etc.), 32 residue sites which side chains were replaced between two groups, were selected. The spatial arrangements and interactions of these sites were tested on the refined structure. These replaced sites are mainly localized upon the C-terminal region of the protein. Some positively charged amino acid residues on the C-terminal region are suggested to contribute in stabilizing the conformation in high pH range. The salt bridges, Arg19 - Glu271 - Arg275 is formed to connect the N- and C-terminals. Two basic amino acid residues Arg170 and Lys251 which occured at the entrance of the C-terminal calcium ion binding site, are possibly regulating the calcium ion binding.

2P04

CRYSTAL STRUCTURE OF AN ACYL-ENZYME INTERMEDIATE OF GUANIDINOHEXANOYL-TRYPSIN

Yasushi Nitanai, Shuji Noguchi, and Yoshinori Satow, Faculty of Pharmaceutical Sciences, University of Tokyo, Hongo, Bunkyo, Tokyo 113, and Chizuko Sasaki and Takao Matsuzaki, Research Center, Mitsubishi Kagaku Corporation, Midori-ku, Yokohama, Kanagawa 227, Japan.

The crystal structure of an acyl-enzyme intermediate of bovine trypsin has been determined at 2.2 resolution. Ethyl *p*-(6-guanidinohexanoyloxy) benzoate is a substrate analog that is slowly hydrolyzed by serine proteases. In order to clearly elucidate hydrolysis mechanisms of serine proteases by the X-ray diffraction method, substrate-complexed crystals were prepared with the soaking technique. First, the orthorhombic crystals of the low-packing-density form inhibited by benzamidine were obtained from an ammonium sulfate solution. They belong to space group $P2_12_12_1$, with cell dimensions of $a = 63.64$, $b = 63.48$, and $c = 68.89$. These crystals were back-soaked in a benzamidine-free solution, and finally were soaked into a substrate-analog solution containing acetonitrile as co-solvent. The diffraction data were collected from 8 crystals of the acylated enzyme, by use of a specially designed Imaging Plate camera. From each crystal, reflections measured in the first 6 hours were merged into a complete data set. The structure was refined to a crystallographic R-factor of 0.167.

A clear electron density corresponding to a guanidinohexanoyl moiety is extending from the O_γ atom of Ser 195 to the side chain of Asp 189 of trypsin. The guanidinohexanoyl group covalently bound to Ser 195 O_γ, forming an acyl intermediate, and is also involved in 7 van der Waals interactions with trypsin. A water molecule hydrogen-bonded to His 57 $N_{\varepsilon 2}$ is located on the imidazole plane of His 57. The oxygen atom of this water is located right above the carbon atom in the plane of the acylated carbonyl moiety, and is in a close contact with the carbon atom, at a distance of 2.95 . This geometrical arrangement of the water oxygen and the catalytic residues indicates that this water would act as a catalytic nucleophile in the subsequent deacylation step.

2P05

VISUALIZATION OF THE 3D-STRUCTURE OF CALOTROPIN DII A PLANT THIOL PROTEASE AT 3Å RESOLUTION

Sreya Ghosh, Bishnu P. Mukhopadhyay, A. Pal, A. Seal, A. Bera, I. Dey, N. K. Sinha and Asok Banerjee, Biophysics Department, Bose Institute, Calcutta-54, India.

The structure of a novel thiol protease, Calotropin DII, having two independent molecules in the $P2_1$ space group (Banerjee et al. 16T-45, AsCA92) each containing 215 amino acid residues has been solved at 3Å resolution by molecular replacement methods (X-PLOR) using the phases of Papain(Pickersgill et al. Acta Cryst., B48, 59-67, 1992). The successive refinement (X-PLOR) of the positional and isotropic thermal parameters reduced the R index to 0.25. The molecules are related through a noncrystallographic pseudo diad. The electron density map is well defined for the two independent molecules. The general Cα-backbone conformations, geometries and the disposition of the characteristic α-helix and the β-sheets around the catalytic active site of Cys 25, within the cleft of two domains, seem nearly similar in both the molecules in the asymmetric unit. The presence of the catalytic triad and their involvement in the thiol-protease activity are visualized from this structural investigation. Attempts for high resolutions studies are underway.

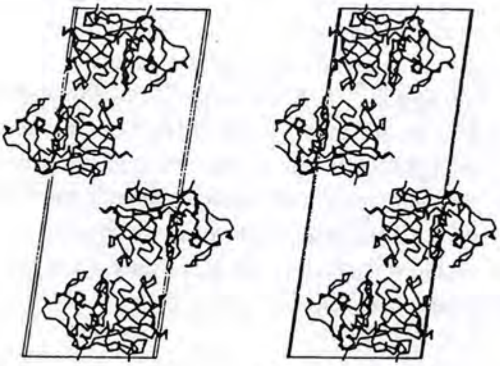

2P06

CRYSTAL STRUCTURE OF A COMPLEX OF WHEAT GERM TRYPSIN INHIBITOR II-5 WITH BOVINE TRYPSIN.

E. Kibushi, A. Suzuki, T. Shirai, T. Yamane, T. Ashida, Department of Biotechnology, School of Engineering, Nagoya University, Nagoya 464-01, Japan, and S. Odani, Department of Biology, Faculty of Science, Niigata University, Niigata 951, Japan.

A trypsin inhibitor II-5 from wheat germ contains 61 amino acid residues and five disulfide bridges, its molecular weight being 6,500. We determined the crystal structure of the complex between inhibitor II-5 and bovine β-trypsin. The crystals were obtained using polyethylene glycol mono-ethylether (Mw 5,000) as a precipitant at pH 6.5. The crystals belong to space group $P2_12_12_1$ with a=63.5, b=70.4 c=61.0Å. An asymmetric unit contains one complex molecule. All diffraction data up to 2.2Å were collected on a Weissenberg camera installed at BL-$6A_2$ station of Photon Factory. The structure analysis was proceeded with the molecular replacement method using a trypsin as a search model. Rotation search was performed using the modified Crowther fast rotation function(Tanaka, N. (1977) *Acta Crystallogr.* **A33**, 191-193). In the search, 6.0 to 3.5 Å resolution data and a 20.4Å integration radius were used. Translation search was carried out using Crowther & Blow method(Crowther R.A. & Blow, D.M. (1967) *Acta Crystallogr.* **23**, 544-548) at 3.5 Å resolution. Each of the search gave a significant unique solution. The structure of truly positioned trypsin in the unit cell was refined to an R-factor of 0.230 at 3.0Å resolution by the program *X-PLOR*. Then the structure of II-5 was constructed on a 3Å-resolution difference-Fourier map using the graphics program *TURBO-FRODO*. Currently 46 residues of II-5 were built. The R-factor of the model is 0.220 for 11,631 reflections between 10.0 and 2.2Å resolution. The polypeptide folding of II-5 is similar to that of Bowman-Birk type Protease inhibitors, especially near the reactive site. The interaction manner of II-5 with trypsin is essentially the same as that observed in the other trypsin inhibitor proteins.

2P07

Structure of a Kunitz-type chymotrypsin inhibitor protein from winged bean seeds at 2.95 Å resolution

J.K.Dattagupta, A.Podder, C.Chakrabarti and U.Sen, Crystallography and Molecular Biology Division, Saha Institute of Nuclear Physics,1/AF Bidhan Nagar, Calcutta 700 064, India, and S.K.Dutta and M.Singh, Indian Institute of Chemical Biology, Calcutta 700 032, India.

An α-chymotrypsin inhibitor protein(WCI) has been isolated from winged bean (*Psophocarpus tetragonolobus*) seeds which is a single polypeptide chain having a molecular weight of 20,244 Da with 183 amino acids. This inhibitor belongs to the Kunitz(STI) family which is characterized by the presence of two disulfide bridges and a molecular weight of around 20 K Da. Structural information about the members of this family is limited only to a few structures and none of them is a chymotrypsin inhibitor. This protein also has the unique property of inhibiting bovine α-chymotrypsin in the molar ratio 1:2 at higher concentrations of the enzyme. The crystal structure of this inhibitor protein has been solved at 2.95Å resolution using x-ray diffraction methods. Crystals of the molecule belong to the hexagonal space group $P6_122$ with cell dimensions a=b=61.4Å and c=210.9Å. The structure has been obtained by molecular replacement method using the 2.6Å coordinates of Erythrina trypsin inhibitor as a starting model and it has been refined to a R-factor of 19.1% with 58 water molecules incorporated. The three-dimensional structure displayed by the protein molecule consist of 12 antiparallel β-strands with connecting loops arranged in a characteristic folding common to other homologous serine protease inhibitors in the Kunitz(STI) family. The crystallographic and structural details and a comparison with related inhibitor structures emphasizing the differences in the reactive site loop region will be presented.

2P08

CRYSTAL STRUCTURE OF MACROCYCLIC INHIBITOR FOR ELASTASE AND STRUCTURAL COMPARISON BETWEEN NON-BINDING AND BINDING STATES

T.Kinoshita, T.Tada, T.Yasuda, H.Fujita, and H.Hatanaka, Fujisawa Pharmaceutical Co., Ltd., Osaka, Japan

The title compound(I) was isolated from *Streptomyces resistomicificus.* (I) has a unique macrocyclic structure and exhibits potent inhibitory activity for elastase. Elastase belongs to the serine protease family of enzymes which are capable of cleaving connective tissue components. Uncontrolled proteolysis by the elastase can cause some inflammatory diseases. For the rational drug design, it is one of the most significant information to look into the difference between non-binding and binding states. Three different crystal forms of (I) were obtained from methanol / water (a), ethanol / water (b), ethyleneglycol / water (c), respectively. Each reflection data measured on the graphite-monochromated diffractometer using a MoK α radiation. Only using data of (c), the partial structure was obtained by direct method. Then the procedure of the weighted fourier and the assignment some atoms were repeated. As a result, the whole structure was obtained and eight water molecules were found out. The final refinement converged to R=0.092. The final structure of (I) is shown as figure 1. The binding structure in the complex with porcine pancreatic elastase was reported previously. The difference of the both structures is slight(rmsd =0.58 Å) , especially, the binding portion of the both is almost identical. The details of the comparison will be reported.

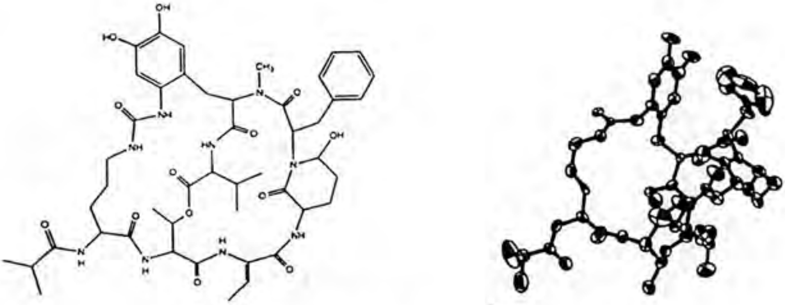

figure 1. structure of the compound (I)

2P09

Ligand-induced conformational changes of 3-isopropylmalate dehydrogenase from Thermus thermophilus

H. Moriyama, S. Kadono, M. Sakurai, T. Oshima, and N. Tanaka, Faculty of Bioscience and Biotechnology, Tokyo Institute of Technology, Nagatsuta 4259, Midori-ku, Yokohama 226 Japan, and M. Sato, Institute for Protein Research, Osaka University, 3-2 Yamada-oka, Suita, Osaka 565, Japan

The structures of 3-isopropylmalate dehydrogenase (IPMDH; Imada et al, 1991; Moriyama et al, 1995) from Thermus thermophilus in complexes with its substrate, cofactor, and a cofactor analog were investigated by X-ray diffraction in a crystalline state and by small-angle X-ray scattering (SAXS) in solution (Sato et al, 1982). The structures at 2.8 Å resolution of the complexes with the substrate, 3-isopropylmalate (IPM), and with a cofactor analog of NAD, ADP-ribose, were both very close to the structure of the ligand-free enzyme with an open conformation. However, the binding of a ligand induced a small conformational change near the binding site. This result contrasts with that for NADP$^+$-bound or isocitrate-bound isocitrate dehydrogenase (ICDH) from Escherichia coli, which takes a closed conformation. The SAXS analysis in solution clearly showed that the ligand-free IPMDH adopts two distinct intermediate conformations between the open and closed states upon binding of NADH and IPM respectively, and does a fully closed conformation in a ternary complex with NADH and IPM.

Imada, K., Sato, M., Tanaka, N., Katsube, Y., & Oshima, T. (1991) J. Mol. Biol. **222**, 725-738.
Moriyama, H., Onodera, K., Sakurai, M., Tanaka, N., Kirino-Kagawa, H., Oshima, T., & Katsube, Y. (1995) J. Biochem. **117**, 408-413.
Sato, M., Kasai, N., Hata, Y., Ii, Y., Miki, K., Tanaka, N., Kakudo, M., Tanaka, M., & Ozawa, T. (1982). Biochemistry International **5**, 595-602.

2P10

CRYSTALLIZATION AND PRELIMINARY X-RAY CRYSTALLOGRAPHIC STUDY OF STREPTOMYCES OLIVACEOVIRIDIS E-86 β-XYLANASE

Z. Fujimoto and H. Mizuno, National Institute of Agrobiological Resources, Tsukuba, Japan., A. Kuno, S. Yoshida and I. Kusakabe, Institute of Applied Biochemistry, University of Tsukuba, Japan., and H. Kobayashi, National Food Reserch Institute, Tsukuba, Japan.

β-Xylanase (EC 3.2.1.8) is a key enzyme for the degradation of xylan, a major hemicellulose in plant cell wall, since it hydrolyzes β-1,4-xylopyranosyl linkages of the backbone. β-Xylanases fall into two of families, denoted F and G, on the basis of amino acid sequence. However, a few information of the structures of F family b\-xylanases has been reported. The present study, therefore, is an attempt to determine the crystal structure of Streptmyces olivaceoviridis E-86 β-xylanase, a member of the F family.

Crystallization was done by the hanging-drop method in tissue culture plates. The droplets, consisted of 5 μl of protein solution (20 mg/ml) in distilled water and 5 μl of reservoir solution, were equilibrated against 1 ml of reservoir solution at room temperature (25°C). Crystals appered in the droplets within 1 week when the reservior solution of 25% saturated ammonium sulfate in 50-fold dilution of McIlvaine buffer (pH 5.7) was used.

Diffraction experiments were carried out at the PF synchrotron facility, Tsukuba. Cristals were orthorhombic with unit cell parameters, a = 79.6 Å, b = 95.2Å, c = 140.3 Å. The value of Vm is 2.95 $Å^3$/Da, assuming two molecules (MW = 45 K) in the asymmetric unit. Crystals diffract beyond 2.0 Å.

Native data set was collected, and its processing is in progress. A search for heavy atom derivatives is also in progress.

2P11

ABILITY OF SOME SPECIFIC NATURAL STRUCTURES TO INTERACT CONCURENTLY CONTRARY TO DIOXIN. ESR STUDY.

Nguyen Van Tri, Pham The Vung, Dinh Pham Thai
Hanoi National University of Technology
Ha Van Mao, Dinh Ngoc Lam - Cancer Research Center.
Hanoi, Vietnam

On the basis of the ESR experimental results, some new active natural complexes (symbolized XD*) present in special vegetable produces have been revealed. The nucleus structure of these complexes can show a electron Spin combination almost similar to the one of Dioxin (2, 3, 7, 8 - TCDD). However, it is especially remarkable that the Spin combination of XD* occupies a quintuplet ground state with a deeply negative exchange energy $J < 0$. This behaviour opposes entirely to the one of Dioxin possessing a combination of four π electron Spins with a singlet ground state ($S = 0$) and a positive exchange energy $J > 0$.

Special binding complexes of Dioxin to XD* structures have been also observed with a negative exchange energy $J < 0$. These [XD* - Dioxin] complexes appear with a very high probability, about 10^3 times of the one of the [Hemoglobin - Dioxin] complex in human blood and of the [Mn - Porphyrinoprotein - Dioxin] complex in human liver. The properties of these interaction complexes corresponding with the results achieved in some respective experimental clinical studies over a long period of time suggest that the specific natural XD* structures are able to conquer and arrest potently Dioxin molecules, i.e. to interact concurently contrary to the toxicity of Dioxin, namely to its carcinogenous activity. This ability depends on many factors such as the concentration and the lifetime of the XD* state, the kinetic conditions of the surrounding and the interaction.

2P12

X-RAY CRYSTALLOGRAPHY OF METHIONYL-tRNA SYNTHETASE FROM *THERMUS THERMOPHILUS* HB8

I. Sugiura, Y. Ugaji, S. Maeda and M. Konno, Department of Chemistry, Faculty of Science, Ochanomizu University, Bunkyo-ku, Tokyo, 112, Japan, O. Nureki and S. Yokoyama, Department of Biophysics and Biochemistry, School of Science, Tokyo University, Bunkyo-ku, Tokyo, 113, Japan

Aminoacyl-tRNA synthetases (aaRS) are a class of enzymes that catalyze the reaction of an ester linkage formed between the amino acid (aa) and a hydroxyl group of the 3'-terminal adenosine of tRNA.

aa + ATP + tRNA → aa-tRNA + AMP + PPi

Methionyl-tRNA synthetase (MetRS) was reported to recognize strictly anticodon of tRNA. In order to know the mechanism of the anticodon recognition and delineate the role of Mg^{2+} ion required for this aminoacylation reaction, dimerization-domain-truncated MetRS from *Thermus thermophilus* HB8 of molecular weight 58,000 have been analyzed by X-ray crystallography. This truncated MetRS has been expressed in *E. coli*. Crystals have been grown by the hanging drop vapor diffusion method. A 10µl drop containing 15mg/ml protein, 5% PEG6,000 and 100mM HEPES was equilibrated against 25% PEG6,000 in the same buffer at pH7.5, 20°C. Small crystals was obtained after 2-4days. Small crystal was inserted as a seed into a protein drop with the same condition except 10mg/ml protein. The crystal belongs to space group $P2_12_12_1$, Z=4, with unit cell dimensions of a=83.1, b=117.4, c=56.7Å. Intensity data for native and three $CH_3CO_2HgC_6H_4NH_2$, K_2PtCl_4 and $Sm(OAc)_3$ derivatives were collected using Weissenberg camera at wavelength of 1.00Å by synchrotron radiation source at KEK. A data set for native crystals with 25611 independet reflections, R-merge of 5.95% and the completeness of 88.7% to 2.2Å resolution was obtained. After refinement of metal parameters for derivative crystals, the overall figure of merit was 0.65 by PROTEIN to 3.5Å resolution. The electron density maps calculated from this phase gave obvious molecular boundary against solvent region. Moreover, the phase was improved by solvent flattening method using the program DM.

2P13

CRYSTALLOGRAPHIC STUDIES OF HAMMERHEAD RIBOZYMES. II.

T. Chatake, O. Matsumoto*, Y. Chen, M. Tsunoda, N. Imaizumi and A. Takenaka, Faculty of Bioscience and Biotechnology, Tokyo Institute of Technology, Nagatsuta, Midori-ku, Yokohama 226, Japan, A. Ohta, Y. Komatsu, M. Koizumi and E. Ohtsuka, Faculty of Pharmaceutical Sciences, Hokkaido University, Sapporo, Hokkaido 060, Japan

It has been postulated that hammerhead ribozymes have a common structure which is basically composed of three RNA segments. In order to reveal the structure of ribozymes and their reaction mechanism, we have been engaged in X-ray analysis. Crystals obtained from a mixture of three RNA components were found to be composed of the two RNAs(1). In the present study we have investigated the structural composition of the hammerhead ribozymes, and re-examined the crystallization conditions.

Electrophoresis was carried out in poly-acrylamide gel with different combinations of the RNAs. Crystallization conditions were surveyed by the hanging- and the sitting-drop vapor diffusion methods. Eleven kinds of hammerhead ribozymes were examined. For the enzymatic part of the ribozyme, the binary complex of the two chains, CL-2 and CL-4, was crystallized. For the full complex formation with its substrate, CL-3m, the ternary mixture was crystallized.

CL-2 5'-**GCCUAGCUGAUGAAGGGUGAU**-3'
CL-4 5'-**ACCCUGAAACCA**-3'
CL-3m 5'-**GGUCmCUAGGA**-3'

To ensure the complex formation, the ternary mixture was annealed after heating for 2min at 80 °C. X-ray experiments were done using synchrotron radiation source (λ=1.0 Å) at the Photon Factory in Tsukuba. Diffraction patterns of crystals obtained from the binary mixture were recorded on imaging plates by a Weissenberg camera.

Electrophoresis patterns indicated that the two chains except for the substrate one form a binary complex and that they form a ternary complex when mixed with the substrate chain. Crystals of the binary complex between CL-2 and CL-4 were grown up to 0.05 × 0.05 × 0.12mm, but those from the ternary mixture were too small for x-ray experiment. The newly obtained crystal had a good quality and gave reflections up to 4.5 Å resolution. From diffraction patterns, it was determined that the unit cell had a Laue symmetry of 32 with a space group of $P321$, $P3_121$ or $P3_221$, and that the lattice constants were $a = b = 53.4$ and $c = 59.4$Å. The number of the binary complexes in the asymmetric unit was estimated to be one from the volume per nucleotide. 3016 reflections with $Fo > 3\sigma$ were collected, 519 of which were the independent reflections. R_{sym} and R_{merge} were 0.046 and 0.049, respectively. Parallel to preparation of the heavy-atom derivatives, we are trying to solve the structure with the molecular replacement method.

(1) O. Matsumoto, Y. Chen, S. Hasegawa, A. Takenaka, A. Ohta, M. Koizumi and E. Ohtsuka. 16th Congress and general assembly, International union of crystallography MS-04.02.07, Beijing, China 1993.

---

* Present address : Faculty of Pharmaceutical Sciences, Kyoto University, Kyoto, Japan.

2P14

ON REFINEMENT OF PROTEIN STRUCTURES BY MEANS OF SHELXL-93

Geoffrey B. Jameson and Ross A. Edwards, Department of Chemistry and Biochemistry, Massey University, Palmerston North, New Zealand

The least-squares refinement program SHELXL93 (G.M. Sheldrick) is increasingly being used for the refinement of protein structures when reasonably high resolution data (better than 2.0 Å) are available. We report our experiences with SHELXL93 for the refinement of apo- and holo-azurin, both of which crystallize isomorphously with two molecules in the asymmetric unit, features which facilitate analysis of refinements. Both of these structures have been refined earlier to R ~ 0.16, by means of PROLSQ. We have paid particular attention to the solvent water molecules, which often have an artefactual existence. Comparison of the refinement of these proteins with SHELXL93 and other commonly used programs for the refinement of macromolecules will be made.

2P15

MEASUREMENTS OF THE FARADAY EFFECTS AND X-RAY BIREFRINGENCE AT COBALT K-EDGE WITH THE X-RAY POLARIMETER

Y. Amemiya, T. Oguchi, K. Okitsu, PF, KEK, Oho, Tsukuba, Ibaraki 305, Japan, and H. Maruyama, Okayama Univ.

We have developed a tunable x-ray polarimeter in order to measure x-ray optical activities such as circular birefringence (Faraday effect), circular dichroism, linear birefringence, and linear dichroism. The x-ray polarimeter consists of an x-ray polarizer and an x-ray analyzer which are placed orthogonal with each other around an x-ray beam direction (Hart et al., 1991). It also includes two sets of ionization chambers to measure an absorption spectroscopy of a specimen. Both x-ray polarizer and x-ray analyzer are made of a channel-cut silicon 422 crystal of four-bound reflections with its offset angle adjustable. The two reflection planes of the channel-cut silicon crystal is set to be slightly offset from parallel so that only the σ polarization is reflected while the π polarization is diminished near $\theta_B=45°$. The state of the polarization of an x-ray beam which transmits a specimen is obtained by measuring x-ray intensities from the analyzer with a SSD while the analyzer is rotated around the x-ray beam direction. The accuracy of measured rotation angles of the x-ray polarization is 30 μrad and the minimum measurable ellipticity of the polarization $(I(\pi)/I(\sigma))$ is $\sim 10^{-7}$. The Faraday rotation spectra of Co and CoFe were measured near K-absorption edge by applying magnetic field to the specimen with its direction parallel and anti-parallel to the x-ray beam direction. The results were compared with those of magnetic circular dichroism which were obtained by using a circular polarized x-ray beam from an x-ray undulator. It has been found that the results of Faraday effect and those of magnetic circular dichroism relates quantitatively with each other by Kramers-Kronig equation. Linear birefringence and linear dichroism of a single crystal Cobalt (hcp) has also been observed near K-absorption edge without applying magnetic field to the specimen. It is found that linear birefringence and linear dichroism also relates quantitatively with each other by Kramers-Kronig equation.

Hart, M., Siddons, D. P., Amemiya, Y., Stojanoff, V. (1991). *Rev. Sci. Instrum.* **62**, 2540-2544.

2P16

CRYSTAL AND MOLECULAR STRUCTURE OF A 1:1 COMPLEX OF PHATHYLYL SULPHATHIAZOLE AND SALICYLIC ACID

Ashok. K. Verma and R. K. Tiwari, School of Studies in
Physics, Jiwaji University, Gwalior 474011, India.

The crystal and molecular structure of a 1:1 complex of phathylyl sulphathiazole and salicylic acid [$C_{25}H_{18}O_8N_2S_2$] has been solved using "SHELX-76" from CAD-4 diffractometer data. The complex crystallizes in the orthorhombic space group with two molecules in the unit cell of dimensions a=5.555(3)Å, b=7.506(1)Å, c=24.539Å and d_m=1.48 gm/cc in all 1217 observed unique reflections were used for the refinement and final R value is 0.035. The geometry obtained is compatible as observed in similar structures. The structure is stabilized by The network of Hydrogen bonds. The structural geometry around sulphonamide group deviates as usual from the tetrahedral. The structural features compared with other sulpha drugs will be discussed and the geometry and packing details will be highlighted in the presentation.

2P17

STRUCTURE CHARACTERIZATION OF CONSTITUENTS FROM *BRIDELIA OVATA* DECNE AND FROM *DAVALLIA SOLIDA* SW.

Kenneth J. Haller, Metallurgy and Materials Science Research Institute, Chulalongkorn University, Bangkok 10330 Thailand; Amorn Petsom, Sophon Roengsumran, Preecha Lertpratchya, Suparb Boonyaratavej, Nisakorn Thongkon, Jatuporn Phaopongthai, Chemistry Department, Chulalongkorn University, Bangkok 10330 Thailand.

Single crystal x-ray structural studies were undertaken on two crystalline constituents isolated from the title plants in quantities too minute to characterize by conventional chemical and spectroscopic techniques.

From the rhizome of *Davallia solida* Sw, (**1**) 19-Hydroxyneohopane. Crystal data: $C_{30}H_{48}O$, colorless, monoclinic $P2_1$ (No. 4), $a = 12.587(3)$, $b = 7.558(2)$, $c = 13.620(3)$, $\beta = 102.68(3)°$, $Z = 2$, $d_{calc} = 1.112\ \mathrm{Mg/m^3}$.

From the leaves of *Bridelia ovata* Decne, (**2**) the 2,4-diethyl-1,3,5,8-Tetramethylporphine-6-formic acid ethyl ester-7-propionic acid ethyl ester. Crystal data: $C_{36}H_{42}N_4O_4$, purple, triclinic $P\bar{1}$ (No. 2), $a=9.409(2)$, $b=12.589(2)$, $c=14.683(2)$, $\alpha=103.19(2)$, $\beta=107.49(2)$, $\gamma=103.40(2)°$, $Z=2$, $d_{calc}=1.292\ \mathrm{Mg/m^3}$.

The x-ray structure of the previously identified Filicene (**3**), a constituent available in larger quantity from *Davallia solida* Sw, was also determined. Crystal data: $C_{30}H_{50}$, colorless, monoclinic $P2_1$ (No. 4), $a = 11.037(2)$, $b = 7.669(1)$, $c = 30.106(2)$, $\beta = 99.08(1)°$, $Z = 4$, $d_{calc} = 1.084\ \mathrm{Mg/m^3}$.

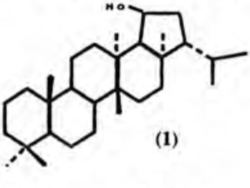

(1)

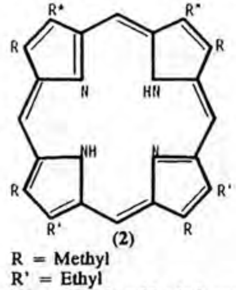

(2)

R = Methyl
R' = Ethyl
R" = Formic acid ethyl ester
R* = Propionic acid ethyl ester

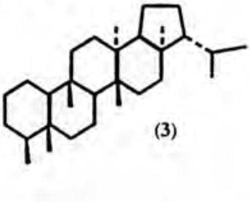

(3)

2P18

SYNTHESES AND CRYSTAL STRUCTURES OF GROUP 6 METAL CARBONYLS CONTAINING POLYPHOSPHINE LIGANDS

Chuen-Her Ueng, Den-Nan Horng, Tzuoo-Tsair Luo and May-Hwai Shieh, Department of Chemistry, National Taiwan Normal University, Taipei 11718, TAIWAN

Eight types of group 6 metal carbonyl complexes were synthesized from $[M(CO)_6]$ (M= Cr, Mo or W) and the corresponding polyphosphine ligands ($PhP((CH_2)_2PPh_2)_2$ (Pf-Pf-Pf), $CH_3C(CH_2PPh_2)_3$ (MeC-Pf_3), $P((CH_2)_2PPh_2)_3$ (P-Pf_3) or $(Ph_2P(CH_2)_2PPhCH_2)_2$ (Pf-Pf-PF-Pf)): 1) Mononuclear biligate complex- $[Mo(CO)_4(MeC\text{-}Pf_3)]$ have a dangling phosphine group; 2) Mononuclear triligate complex- The geometry of the coordination sphere of $[W(CO)_3(Pf\text{-}Pf\text{-}Pf)]$ is a facial octahedron; 3) Homo-binuclear triligate complex- Two isomers for $[Cr(CO)_4(Pf\text{-}Pf\text{-}Pf)Cr(CO)_5]$, one having a 5-membered chelating ring and the other having a 8-membered ring, are successfully isolated and characterized; 4) Hetero-binuclear triligate complex- Each complex of $[M(CO)_4(Pf\text{-}Pf\text{-}Pf)M'(CO)_5]$ and $[Mo(CO)_4(MeC\text{-}Pf_3)Mo(CO)_5]$ contains two different group 6 metals; 5) Homo-binuclear tetraligate complex- $[W(CO)_4(P\text{-}Pf_3)W(CO)_4]$ have a 5-membered and a 8-membered chelating ring; 6) Hetero-binuclear tetraligate complex- Each complex of $[M(CO)_3(P\text{-}Pf_3)M'(CO)_5]$ contains two different metals with the metal M are trisubstituted; 7) Trinuclear triligate complex- Each phosphorus atom of the ligands of $[\{M(CO)_5\}_3(L_3)]$ is coordinated to the $M(CO)_5$ moiety; 8) tetranuclear tetraligate complex- The geometry of the four metals for the complex containing tripodal ligand is a distorted tetrahedron, but the four metals for the linear ligand are mutually opposite and are almost located in the same plane.

2P19

APERIODIC CRYSTAL STRUCTURE IN VEGETABLE FIBRES

Nguyen Van Tri, Nguyen Van Thang, Pham The Vung - Institute of Technical Physics, **Tran Nhat Chuong** and **Hoang Thi Linh** - Department of Textiles. ***Hanoi University of Technology, Hanoi Vietnam***

The particular molecular - electronic microstructure and related properties of many different genera of vegetable fibers (such as cotton, jute, pineapple, sisal) have been studied with ESR in combination with other methods. The partner radicals $C^{\bullet}$ and $O^{\bullet}$, and especially a new (2Fe-2S) exchange complex in the fibred structure were revealed. This physical local structure coupled by fivefold (2Fe-2S) rhombic combinations diagonally bonding a macromolecule chain with five neighbouring ones is based on a pentagon created by five sulfur atoms whose plane is perpendicular to the axis of the fibre. The important roles of this structure in the formation of the elementary fibres and in specific features of the material (such as the strength, the tensility, the torsional module) have been partly discovered. Some technological treatments to improving fibre properties have been also efficiently examined.

This publication is completed with financial support from the National Basic Research Program in Natural Sciences and the Textile Research Institute

2P20

Outer-sphere coordination of phenanthroline in aquachlorotri(*p*-chlorophenyl)tin·1,10-phenanthroline dimer

Ng Seik Weng[1] and **V.G. Kumar Das**[2]

[1]Institute of Advanced Studies and [2]Department of Chemistry, University of Malaya, 59100 Kuala Lumpur, Malaysia

Abstract

Dimeric aquachlorotri(*p*-chlorophenyl)tin·1,10-phenanthroline $[(p\text{-}ClC_6H_4)_3SnCl \cdot H_2O \cdot 1,10\text{-phen}]_2$ crystallizes in the triclinic $P1$- space group, with $a = 11.878(5)$, $b = 12.747(4)$, $c = 20.515(6)$ Å, $\alpha = 84.37(1)$, $\beta = 80.74(3)$, $\gamma = 69.39(2)°$, $V = 2867(2)$ Å^3; $Z = 2$. In the crystal structure, the two heterocyclic bases interact with the *trans*-C_3SnClO trigonal-bipyramidal tin atoms through the coordinated water molecules, each of which forms a hydrogen bond to its phenanthroline and another to the phenanthroline belonging to the other moeity. The location of the hydrogen atoms in this structure from the diffraction measurements at -105°C has enabled the role of water in the unsubstituted chlorotriphenyltin complex (Gabe, Lee & Smith, *Inorg. Chim. Acta*, 90, L11, 1984) to be clarified.

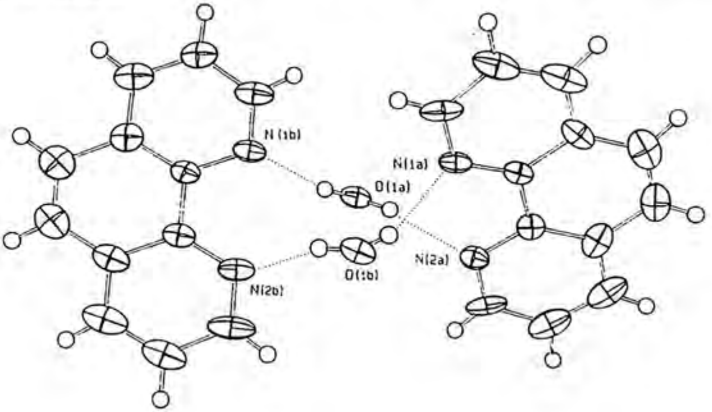

Fig. 1. Hydrogen bonds involving the water and 1,10-phenanthroline molecules. O(1a)···N(1b) = 2.873(7), O(1b)···N(1a) = 2.864(8), O(1a)···N(2a) = 3.083(8), O(1b)···N(2b) = 3.000(8) Å; N(1b)···O(1a)···N(2a) = 130.9(2), N(1a)···O(1b)···N(2b) = 124.2(2)°.

2P21

NOVEL POLYCHALCOGEN-PNICOGEN COMPLEXES OF CHROMIUM

W. Chen, L. Y. Goh and R. C. S. Wong, Department of Chemistry, University of Malaya, Lembah Pantai, 59100 Kuala Lumpur, Malaysia.

Structural features of novel tetrachromium complexes obtained from reactions of $[CpCr(CO)_3]_2$ with P_4S_3 (E = S, Se) where P_4E_3 undergoes multiple bond cleavage without fragmentation (not observed as yet in other transition metals) (Goh, Chen & Wong (1993); Goh et al. (1995)) will be described.

Goh, L.Y., Chen, W. & Wong, R.C.S. (1993). Angew. Chem. 105, Nr.12, 1838-1840; Int. Ed. Engl. 32, No.12, 1728-1729.

Goh, L.Y., Chen, W., Wong, R.C.S., Zhou, Z.Y. & Fun, H.K. (1995). Mendeleev Commun., 60-61

2P22

STRUCTURE ANALYSIS OF UNSTABLE CRYSTALS USING RAPID X-RAY MEASUREMENT SYSTEM

T. Watanabe, N. Manabe, H. Nishiyama, M. Yasui, F. Iwasaki,
Department. of Applied Physics and Chemistry, The University of Electro-Communications, Chofu-shi, Tokyo 182, Japan

Recently a rapid X-ray measurement system with the imaging plates has been developed by Kamiya & Iwasaki (1995). A performance test of this equipment indicated that the accuracy of the intensity data are reliable and the system can work as a tool of the structure analysis for typical organic crystals.(Iwasaki, et al., 1995) This equipment, however, had some retrictions of 2θ range and an alignment of a specimen. We have developed a new machine which will overcome the above problems. In this system; 1) 2θ range is widened from 45° to 60°, 2) a three-circle goniometer with κ axis is equipped to align specimens in the wide range and 3) the equi-inclination μ axis is equipped to rotate the Weissenberg-type IP camera in the horizontal plane. Using this system with MoKα radiation (50kV, 200mA), we have determined the structures of unstable crystals, **1**, **2** and **3**, for which intensity measurements by a four-circle diffractometer were failed. The total time of intensity measurement was 7 ~ 14 hours for each crystal. Stable crystals of **4** were so tiny to measure intensities by a four-circle diffractometer. The crystal size using intensity measurement was 0.08x0.03x0.15 mm. In this paper a performance test of this system including the inclination axis (μ axis) will be also reported.

	1	**2**	**3**	**4**
FW	1166.56	1327.07	988.20	439.41
Sp. gr.	$P2_1/n$	$P2_1/n$	Pn	$P\bar{1}$
a/Å	14.179	28.127	15.984	8.753
b/Å	26.447	16.797	9.949	11.173
c/Å	28.245	14.103	14.854	11.194
α/°	90.0	90.0	90.0	110.1
β/°	118.0	101.2	100.9	103.8
γ/°	90.0	90.0	90.0	106.0
V	9351	6536	2319	918.4
Z	8	4	2	2
Meas. time/h	7	7	7	14
No.meas.	46719	37227	14890	8213
No.unique	15298	12100	4688	3394
No.obs	11013	8552	4294	2084
R	0.076	0.106	0.067	0.102

1 $(C_{10}H_{16}N_4S_2Pd)_3\cdot C_6H_6$ **2** $C_{54}H_{44}Cl_3N_4P_2S_2Rh\cdot 2CHCl_3$
3 $C_{46}H_{46}ClN_4OP_2SRh\cdot CH_2Cl_2$ **4** $C_{17}H_{12}N_4S_3Cl_2$

Iwasaki, F., Sakuratani, M., Kaneko, H., Yasui, M., Kamiya, N. & Iwasaki, H. (1995). *Acta Cryst.*, B51, in press.
Kamiya, N. & Iwasaki, H. (1995). *J. Appl. Cryst.*, in press.

STRUCTURE OF $\{[(Ph_2NCH_2PPh_2)Au]_3S\}Cl \cdot H_2O$

Ju-Chun Wang & Lin-Shu Liou
Department of Chemistry, Soochow University,
Taipei, Taiwan 11102, REP OF CHINA

The title compound has been isolated as a minor product when $Au(Ph_2NCH_2PPh_2)Cl$ was reacted with DMSO in the presence of base. The pale yellow crystals suitable for X-ray analysis were grown by slow diffusion of Et_2O into the DMSO solution of the compound. The crystal structure has been determined at room temperature using Cu Kα radiation. The S atom locates on a crystallographic C3 axis and is bonded to three $Au(Ph_2NCH_2PPh_2)$ unit. Thus each asymmetric unit contains only 1/3 of the molecules. Three Au-atoms and one S-atom form a perfect pyramidal geometry with S atom on the apex. The coordination environmental of Au is as expected linear. The Au-S and Au-P bond distances are 2.320(3) and 2.234(6) Å, respectively. Short Au-Au contacts have been observed. This contact distance 3.174(2) Å is comparable to those found in other Au dimers and trimers suggested that the so-called "relativistic bonding interaction" may exit in this system. Small Au-S-Au angle, 86.3(2)°, also supports existing this type of interaction.

Crystal Data: $\{[(Ph_2NCH_2PPh_2)Au]_3S\}Cl \cdot H_2O$ is cubic, a=23.967(2), V=13767(2)Å^3, Z=8, space group Pa-3 (NO 205). Final R values are R=0.0460, R_w=0.0501 and S=1.49 for 1067 observed reflections [$I > 3\sigma(I)$] and 95 parameters.

2P24

CRYSTAL STRUCTURE OF BINUCLEAR 1:1 SILVER(I) 2-HYDROXY-3,5-DINITROBENZOATE:TRIPHENYLPHOSPHINE COMPLEX

A. Hamid Othman, Jabatan Kimia, Universiti Kebangsaan Malaysia, 43600 Bangi, Malaysia, and Effendi and Allan H. White, Department of Chemistry, The University of Western Australia, Nedlands W.A. 6907.

A binuclear complex $[(Ph_3P)(Ag(\mu\text{-}O\text{-}OAc)_2\text{-}Ag(PPh_3)]$ was obtained by addition of molar excess of triphenylphosphine to silver acetate in boiling toulene. Reaction of this complex in methanol with 2-hydroxy-3,5-dinitrobenzoic acid gave yellow crystals that retain the binuclear structure of the parent complex. The single crystal X-ray structure determination of the 1:1 adduct of silver(I) 2-hydroxy-3,5-dinitrobenzoate:triphenylphosphine ($AgL{:}PPh_3$) shows it to be a centrosymmetric system with the silver atoms bridged by one of the carboxylate oxygen atoms of each ligand, $[(Ph_3P)Ag(\mu\text{-}O\text{-}L)_2Ag(PPh_3)]$ as in the acetate (Othman & Ng, 1995).

Crystal data : $[(Ph_3P)Ag(\mu\text{-}O\text{-}L)_2Ag(PPh_3)]$ triclinic, spacegroup $P\bar{1}$, a 15.846(5), b 9.444(3), c 9.084(3) Å, α 62.73(2), β 77.25(2), γ 73.62 °, Z 1 (dimer), R was 0.051 for 3176 'observed' ($I>3\sigma(I)$) reflections.

The Ag...Ag' distances are identical, as are O...O' to those of the parent acetate complex. The central $Ag(\mu\text{-}O)_2Ag$ ring is exactly planar, and very precisely so in the acetate despite the lack of inversion centre. The phenolic oxygen is disordered over two possible sites.

Othman, A.H. & Ng Seik Weng (1995). Z. Krist. (submitted for publication)

2P25

CRYSTAL STRUCTURE OF [4-[ω-(cholesteryloxycarbonyl)-hexyloxycarbonyl] phenyl] ferrocene

N.Nakamura and T.Takayama, Department of Chemistry, Faculty of Science and Engineering, Ritsumeikan University, 1916, Noji, Kusatsu, Shiga 525, Japan

A selected orange needle crystal of $C_{51}H_{71}O_4Fe$ having approximate dimensions of 0.2 x 0.4 x 0.05 mm was mounted on a glass fiber. All measurements were made on a Rigaku AFC5R diffractometer with graphite monochromated Cu-Kα radiation and a 18kW rotating anode generator. Unit cell dimensions obtained from a least-squares refinement using the setting angles of 25 carefully centered reflections in the range $46.4° < 2\theta < 57.0°$.

The data were collected at a room temperature of 296K using the ω-2θ scan technique to a maximum 2θ value of 120.4°. Scans of $(1.1+0.3\tan\theta)°$ were made at a speed of $4° \mathrm{min}^{-1}$ (in ω). Of the 7524 reflections which were collected, 7021 were unique. The intensities of three representative reflection were measured after every 150 reflections. An empirical absorption correction based on azimuthal scans of several reflections was applied. The data were corrected for Lorentz and polarization effects. The structure was solved by direct methods with SHELX86 (Sheldrick, G.M., 1985) and expanded using Fourier with DIRDIF92 (Beurskens, P.T. et al, 1992). The non-hydrogen atoms were refined anisotropically. Hydrogen atoms were included but not refined. The final cycle of full-matrix least-squares refinement was based on 3198 observed reflections ($I > 3\sigma(I)$) and 1009 variable parameters, $\Sigma w(|Fo|-|Fc|)^2$ minimized, R=0.060, wR=0.082.

2P26

SOLVANT INFLUENCE ON CRYSTALLIZATION OF PHENYL CARBAMIDONITRILE

Qing-chuan Yang, Dan-mei Huang, Hui-ying Chen and You-qi Tang,
Department of Chemistry, Peking University, Beijing 100871, China.

The polymer of phenyl carbamidonitrile(I) has noticeable electric bistability properties. During the study on the crystal structure of the monomer I, it was found that the selection of solvant was important. The crystals of compound I were obtained from the tetrahydrofuran solution, but other crystals of adduct of phenyl-carbamidonitrile: w,w'-diphenyl-biuret (1:1) were obtained from the ethanol or ethyl acetate solution of compound I. The formation mechanism for the adduct product was estimated.

The project was supported by the National Natural Science Foundation of China.

CRYSTAL STRUCTURE OF cis [-5-(2-Dimethylaminoethyl)-3-hydroxy-2- (4-methoxyphenyl)-2,3-dihydro-1,5-benzothiazepine](±)

P.Kumaradhas and K.A.Nirmala, Department of Physics, Bangalore University, Bangalore-560 056, India, and M.A.Sridhar, Department of studies in Physics, Mysore University, Mysore-570 006, India.

The title compound is a drug intermediate of Diltiazem. Diltiazem is an enantiomerically pure drug with calcium antagonist activity (Kojic - Prodic et al., 1984). This compound was obtained by (2R,2S)-3-(4-methoxyphenyl)methyl glycidate was treated with 2-amino thiophenol in presence of triethyl amine the resulting product was hydrolysed and treated with acetic anhydride and pyridine. Recrystallization was from ethonal.

Crystal data: $C_{20}H_{22}N_2O_3S$, Orthorhombic, space group Pbcn, a=11.447(1), b=12.978(1), c=24.881(1)Å. R=0.048, wR=0.108.

The seven membered ring is distorted showing twist boat conformation. Methoxyphenyl and hyroxy groups are cis oriented.

The methoxyphenyl group adopts axial and carbonyl oxygen atom and aminoethyl groups are psuedo-axial. The molecule is stabilized by covalent bonding and weak hyrogen bonding, but the crystal packing is stabilized by van der Waals interactions.

Programs used to solve and refine the structure: SHELXS-86 and SHELXL-93.

Kojic-Prodic, B., Ruzic-Toros, Z. & Sunjic, V. (1984).
Helv.Chim. Acta. 67, 916-926.

CRYSTAL STRUCTURE OF cis[1,5-Benzothiazepine-4(5H)-one- 1-oxide-3-(acetoxy) - 2,3-dihydro-2-(4-methoxyphenyl)](+)

K.A.Nirmala and P.Kumaradhas, Department of Physics, Bangalore University, Bangalore-560 056, India.

The title compound is a drug intermediate of Diltiazem (Kojic-Prodic et al., 1984). Diltiazem belongs to the family of drugs commonly named calcium channel blockers or calcium antagonists and is useful for the treatment of cordiac and coronary diseases. The crystals were grown from ethonal- acetone mixture at room temperature.

Crystal data: $C_{18}H_{17}NO_5S$, Orthorhombic, space group Pbca, a=8.200(8), b=13.326(9), c=32.093(6)Å, R=0.045, wR=0.13.

The molecular packing is stabilized by weak hyrogen bonding between the polar atoms and van der Waals interactions between the non-polar atoms. The seven membered ring is distorted showing twist boat conformation. Methoxyphenyl and acetoxy groups are cis oriented. The methoxyphenyl group adopts axial position in the molecule but sulphoxide oxygen in equitorial.

Programs used to solve and refine the structure: SHELXS-86 and SHELXL-93.

Kojic-Prodic, B., Ruzic-Toros, Z. & Sunjic, V. (1984).
Helv. Chim. Acta. 67, 916-926.

2P29

CRYSTAL STRUCTURE OF TIN XANTHATES.

M. I. Mohamed-Ibrahim[a], Omar bin Shawkataly[a], Hoong-Kun Fun[b] and K.Sivakumar[b], [a]Chemical Sciences Programme, Centre for Distance Education and [b]X-Ray Crystallography Unit, School of Physics, Universiti Sains Malaysia, 11800 USM, Penang, Malaysia.

The crystal structures of $Me_2Sn(S_2CO\text{-}c\text{-}C_6H_{11})_2$ and $Ph_3Sn(S_2CO\text{-}CH_2C_6H_5)$ have been determined by X-ray diffraction methods. The former crystallises in orthorhombic Pnma, with cell dimensions a = 10.224(1), b = 21.514(2), c = 10.230(1) Å, Z = 4 and Dx = 1.474 Mgm^{-3} while the latter crystallises in monoclinic P21/n with a = 12.636(1), b = 14.367(2), c = 13.415(1) Å, β = 93.09(1)°, Z = 4 and Dx = 1.456 Mgm^{-3}. Both structures were solved by direct methods and refined by a full matrix least-squares technique to final R = 0.067 and 0.030 respectively. The environment about each tin atom in both compounds is a distorted tetrahedron with the xanthate ligands being essentially unidentate. However in the first compound, the xanthate is in a 'S,S' mode of orientation whereas in the second compound, an 'O,S' mode was found. Details of the structure analysis will be presented in the conference.

2P30

CARBON NANOTUBES ON THE TOP SURFACE OF CATHODE DEPOSIT AT DC ARC-DISCHARGE

Y. Ando, X. Zhao and M. Ohkohchi, Department of Physics, Meijo University, Tenpaku-ku, Nagoya 468, Japan, and M. Wang, Department of Physics, Nagoya University, Chikusa-ku, Nagoya 464, Japan

Carbon nanotubes were first found by Iijima (1991) in the carbon deposit on the cathode, although the original specimens were prepared by one of the present authors (Y. A.) as byproduct for fullerene formation by dc arc-discharge evaporation of graphite rods. The nanotubes can be prepared in the atmospheric gas of He and CH_4 (Ando and Iijima, 1993). Such carbon nanotubes could be observed by high resolution scanning electron microscopy (SEM) in the top surface of cathode deposit also (Ando, 1993), which is the part just finished arc-discharge.

The apparatus used for the preparation of carbon nanotubes was the same with that used for the preparation of ultrafine particles of SiC by gas evaporation method. In the case of fullerene formation, the Si-block of anode was replaced by graphite rod installed vertically. After the evaporation of graphite rod of anode, a part of evaporated carbon deposits on the cathode. The section and the top surface of the cathode deposits were observed by a high resolution SEM.

On the top surface of cathode deposit prepared in He gas, the co-existence of carbon nanotubes and carbon nanoparticles were usually found. When the evaporation has been carried out in CH_4 gas, the top surface of cathode deposit shows various morphology depending on the pressure of CH_4 gas and on current density of dc arc-discharge. In the case of high pressure CH_4 gas and high current density, first prepared carbon nanotubes are embelished by carbon nanoparticles as seen in Fig. 1. It means the activity of the surface of carbon nanotubes prepared in CH_4 gas.

Ando, Y. (1993), *Jpn. J. Appl. Phys.* **32**, L1342-L1345.
Ando, Y. & Iijima (1993), *Jpn. J. Appl. Phys.* **32**, L107-L109.
Iijima, S. (1991), *Nature*, **354**, 56-58.

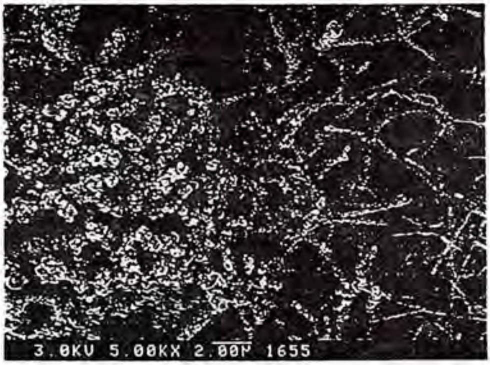

Fig. 1 SEM image of carbon nanotubes embellished by carbon nanoparticles.

CRYSTAL STRUCTURES OF GROUP 15 MIXED LIGAND DERIVATIVES OF $Ru_3(CO)_{12}$.

Omar bin Shawkataly[a], Sok-Tin Lee[a], M.Parameswari[a], Hoong-Kun Fun[b] and K.Sivakumar[b], [a]Chemical Sciences Programme, Centre for Distance Education and [b]X-Ray Crystallography Unit, School of Physics, Universiti Sains Malaysia, 11800, Minden, Penang, Malaysia.

The X-ray structural studies of group 15 ligand derivatives of $Ru_3(CO)_{12}$ have been widely studied[1]. The M.I.Bruce-A.H.White research group has undertaken the study of X-ray structures of numerous complexes of this type. However, crystal structure studies of group 15 mixed ligand derivatives of $Ru_3(CO)_{12}$ have not been reported so far. As a part of our study of mixed ligand substitutions on $Ru_3(CO)_{12}$ with group 15 ligands, we have undertaken the synthesis and structural characterisation of a series of such compounds. Several mixed ligand derivatives were prepared using the radical anion Ph_2CO method[2]. $Ru_3(CO)_8$(dpam)(dppm) and $Ru_3(CO)_9$(dpam)(PCy_2Ph) were prepared by ligand substitution on $Ru_3(CO)_{10}$(dpam) and were purified by preparative TLC and characterised by spectroscopic methods (IR, ^1H, ^{13}C and ^{31}P NMR) and X-ray crystallography. Single crystals of $Ru_3(CO)_8$(dpam)(dppm) and $Ru_3(CO)_9$(dpam)(PCy_2Ph) were grown from dichloromethane/methanol by solvent/solvent diffusion method. The former crystallises in orthorhombic space group $Pca2_1$ with a = 21.586(2), b = 15.839(1), c = 18.383(1) Å, Z = 4 and Dx = 1.459 Mgm^{-3} while the latter crystallises in the triclinic system, space group P-1, a = 12.575(1), b = 12.902(1), c = 16.959(2) Å, α = 92.07(1), β = 110.50(1), γ = 98.14(1)°, Z = 2, Dx = 1.704 Mgm^{-3} . This paper will describe and discuss the results derived from the crystal structure analyses of these two compounds.

References:

1. M.I.Bruce, M.J.Liddell, O.b.Shawkataly, I. Bytheway, B.W.Skelton & A.H.White. (1989). J. Organomet. Chem., **369**, 217.
2. M.I.Bruce, J.G.Matisons & B.K.Nicholson. (1983). J. Organomet. Chem., **247**, 321.

2P32

STRUCTURE OF 1-[4,5-DIHYDRO-1*H*-IMIDAZOL-2-YL]-IMIDAZOLIDIN-2-THIONE HYDROBROMIDE

Y. Wattanakanjana and C. Pakawatchai, Department of Chemistry, Prince of Songkla University, Hat Yai 90112, Thailand, and B. W. Skelton and A. H. White, Department of Chemistry, University of Western Australia, Nedlands, W.A. 6907, Australia.

The reaction of copper(I) or copper(II) halides with substituted thioureas(L) yields a variety of complexes or compounds such as CuLX, CuL_2X, $Cu_2L_3SO_4$, L_2 or LL' (where L' is a deprotonated or desulfurated ligand) depending on the nature of L, solvent and the mole ratio of halides and ligands. The title compound was obtained from the reaction between copper(I) bromide and ethylenethiourea(L) in the mole ratio 1:2.5 using water as reaction medium. Qualitative elementary analysis was performed using X-ray fluorescence spectrometry. The crystal structure of this compound determined by single X-ray diffraction methods revealed the compound to consist of discrete desulfurated diethylnethiourea cations, $[C_6H_{11}N_4S]$ and bromide anions. All non hydrogen atoms including the bromide ion, and the N-hydrogen atoms, lie in the same plane. The C - S distance 1.647(4) Å, is short compared with the parent ethylenethiourea molecule{1.688(2) Å} due to the resonance effect.

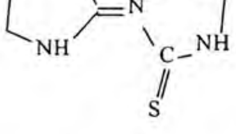

Fig. 1 Desulfurated diethylenethiourea cation.

Crystal data : $C_6H_{11}BrN_4S$, orthorhombic, space group *Pnam*(No. 62)
a 15.295(3), *b* 9.063(2), *c* 6.895(7) Å

2P33

STRUCTURAL AND CONFORMATIONAL STUDIES OF TRITERPENOIDS: 19-EPIMERS OF LUPENES

Tamiko Kiyotani, Kazuo Masuda and Hiroyuki Ageta
Showa College of Pharmaceutical Sciences, Machida, Tokyo 194, Japan

Ferns are known to produce various skeletal triterpenoids. We have isolated many triterpenoids from ferns and elucidated their structures. Triterpenoids are biosynthesized from squalene which consists of six isoprene (C_5H_8) units. The titled compounds, lup-20(29)-ene (**I**) and isolup-20(29)-ene (**II**) were isolated from the same fern: *Lemmaphyllum microphyllum* (Polypodiaceae). Their structures were elucidated by spectroscopic methods. In order to determine their conformations, especially an isopropenyl moiety, we investigated X-ray crystallographic analysis. As a result, **I** seems to have two conformations (**Ia** and **Ib**) at the side chain (isopropenyl group) as a stable conformation, but **II** showed only one stable conformation (**II**) as shown in Figure. The above result was also explained in $CDCl_3$ solution by the NMR NOE experiments. Further, molecular mechanics calculations by Chem3D plus for several kinds of the conformations considered at the side chains of C-19 of **I** and **II** respectively. The conformations of **I** and **II** at the side chain will be discussed.

Crystal data: **Ia**, $C_{30}H_{50}$, Mr=410.73, orthorhombic, space group $P2_12_12_1$, a=10.664(1), b=14.054(1), c=17.157(1) Å, V=2571.4(2) Å^3, Z=4, Dx=1.06 g cm^{-3}, R=0.052, wR=0.061 for 1890 reflections. **II**, $C_{30}H_{50}$, Mr=410.73, monoclinic, space group $P2_1$, a=7.654(1), b=16.521(2), c=10.109(1) Å, β=97.85(1) °, V=1266.3(2) Å^3, Z=2, Dx=1.08 g cm^{-3}, R=0.042, wR=0.048 for 1598 reflections. Data collections were performed on an Enraf-Nonius CAD4 express diffractometer with monochromated-graphite Mo Kα radiation (λ=0.71073 Å). Both were solved by direct method using SIR88 and refined by full-matrix least-squares. Non-hydrogen atoms were refined anisotropically and all hydrogen atoms were refined isotropically using riding model.

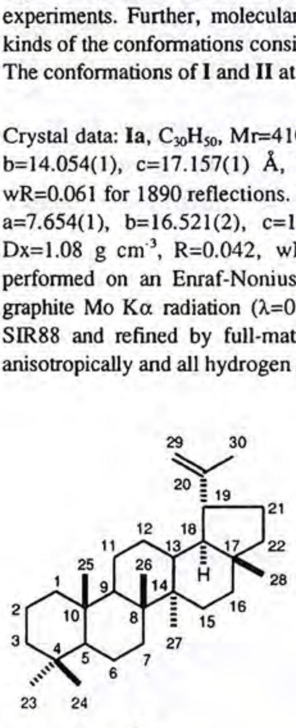

Ia

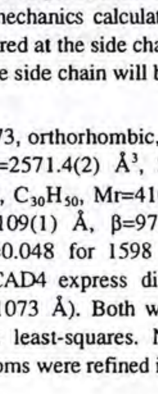

Ib

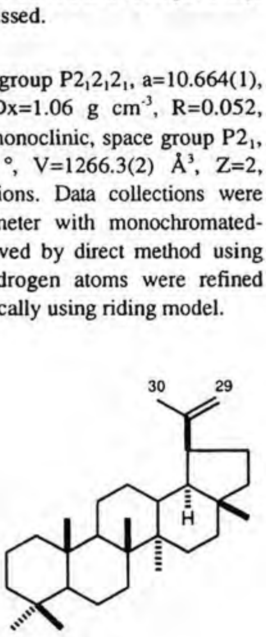

II

2P34

SYNTHESES, CHARACTERISATION AND CRYSTAL STRUCTURE OF TRIOSMIUM ALKYLIDYNE CARBONYL CLUSTER CONTAINING CHIRAL AUXILIARIES

WAI-YEUNG WONG and WING-TAK WONG*

Department of Chemistry, The University of Hong Kong, Pokfulam Road, Hong Kong.

Treatment of $[Os_3(\mu\text{-}H)_3(CO)_9(\mu_3\text{-}CCl)]$ with a large excess of (-)-(*R*)-N,N-dimethyl-1-[(*S*)-1',2-bis(diphenylphosphino)ferrocenyl]ethylamine [(*R*,*S*)-bppfa] in the presence of DBU leads to the air-stable chiral complex (*R*,*S*)-$[Os_3(\mu\text{-}H)_2(CO)_9\{\mu_3\text{-}CPPh_2(\eta^5\text{-}C_5H_4)Fe(\eta^5\text{-}C_5H_3(PPh_2)CH(Me)NMe_2)\}]$ **1** in moderate yield. Yellow crystals of **1** were obtained from slow evaporation of a dichloromethane solution at room temperature. Complex **1** consists of a triosmium alkylidyne metal core with the chiral ligand (*R*,*S*)-bppfa co-ordinated directly through the PPh_2 group on the C_5H_4 ring to the apical carbon atom. The other PPh_2 moiety on the disubstituted cyclopentadienyl ring remains pendant, see Figure 1.

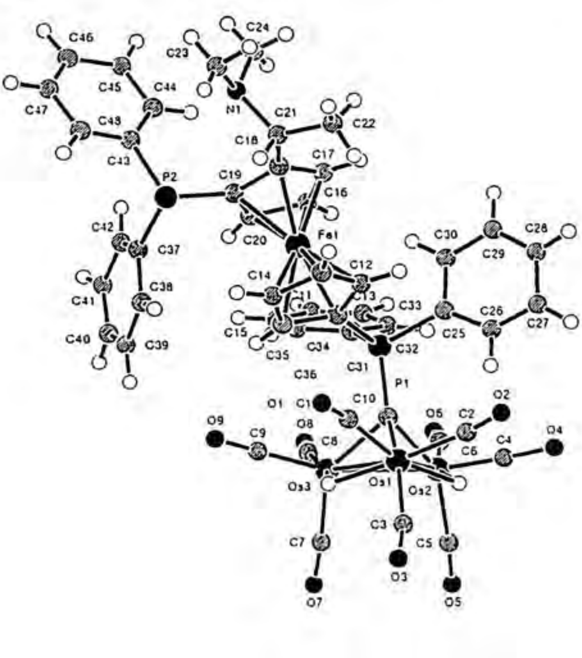

Figure 1

MOLECULAR STRUCTURES OF ORGANIC LANTHANIDE COMPLEXES HAVING ETHYLENE POLYMERIZATION ACTIVITY

N. Kanehisa, H. Hashimoto, M. Yamagashira. and Y. Kai, Department of Applied Chemistry, Faculty of Engineering, Osaka University, Suita, Osaka 565, Japan
M. Nodono, E. Ihara, and H. Yasuda
Department of Applied Chemistry, Faculty of Engineering, Hiroshima University, Higashihiroshima, Hiroshima 724, Japan

We have proceeded the X-ray structure analyses of a series of organic lanthanide complexes to elucidate the correlation between the molecular structure and the activity for ethylene polymerization. Recently, we obtained the single crystals of an organic lanthanide complex of this series without the activity for ethylene polymerization. We have carried out the X-ray structure analysis for this complex and compared the structure with the ones having the polymerization activities.

Crystal data: $SiMe_2[\eta^5\text{-}C_5H_2SiMe_3SiMe_2({}^tBu)]_2Sm(THF)_2$ (THF) (**1**),$C_{42}H_{82}O_3SmSi_5$, $F.W.$=925.94, monoclinic, $P2_1/c$, a=12.147(3), b=20.780(3), c=21.718(2)Å, β=103.55(1)°, V=5329(1)$Å^3$, Z=4,

X-ray intensity data were collected on a Rigaku AFC-5R diffractometer with graphite monochromatized Mo$K\alpha$ radiation. A total number of observed reflections $[|F_o| > 3\sigma(F_o)]$ are 3540. Structure analysis was carried out by using the TEXSAN program system. The crystal structure was solved by the heavy atom method and refined by the full-matrix least-squares. At the present stage of the refinement, the discrepancy factors; R (R_w) is 0.070(0.089).

Fig.1 shows the molecular structure of **1**. The complex **1** has a slightly distorted tetrahedral geometry around the Sm atom formed by two THF ligands and two Cp ligands. This complex has a non-crystallographic C_2 symmetry with pseudo 2-fold rotation axis passing through the Sm and the bridged Si atoms. For ethylene polymerization activity, it may be considerable that one of the important factors is a non-symmetrical geometry around the central metal atom in the catalyst monomer.

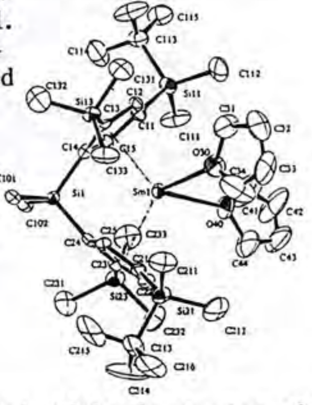

Fig.1. Molecular structure of **1**

2P36

CRYSTAL STRUCTURE OF 2,10-DICHLORO -6- (2,4 DIMETHYL PHENOXY)- DIBENZO [*d,g*] [1,3,6,2] DIOXATHIAPHOSPHOCIN -6- SULFIDE.

N.Jagadeesh Kumar[§], M.Krishnaiah[§], B.Sankara Reddy[¶] & C.D.Reddy[¶],
Department of Physics[§]/Chemistry[¶], Sri Venkateswara University,
Tirupati-517 502, INDIA.

Considerable interest has been shown to study the X-ray crystallographic studies on dibenzo [*d,g*] [1,3,6,2] dioxathiaphosphocins because of their potential use as antioxidants and stabilizers in polymers and oils. We present the crystal structure of the title compound, to understand the effect of the substituents on the molecular geometry and conformation of hetero cyclic ring.

The colourless transparent crystals of the title compound ($C_{20}H_{15}O_3Cl_2PS_2$) obtained from 2-propanol are monoclinic, $P2_1/n$ with cell parameters $a=13.272(2)$, $b=9.225(1)$, $c=17.251(1)$Å, $\beta=90.39(1)°$, $V=2112.8(4)$Å^3, $Z=4$, $D_c=1.475$Mg/m^3, F(000)= 960, λ(MoKα)=0.7107Å. The structure has been solved by direct methods (SHELXS-86) using 3153 reflections, collected at room temperature by Enraf- Nonious CAD-4 diffractometer with monochromated radiation using ω-2θ scan. The structure was refined by full-matrix least-squares method using SHELXL-93 to the final value of $R=0.0359$ for 3,011 significant reflections $I>2\sigma(I)$. The eight membered dioxathiaphosphocin ring has boat-chair conformation. The sulfur substituent is axial and the dimethyl phenoxy group is equatorial to the hetero ring. There is no short contacts between the molecules and the structure was stabilised by van der Waals interaction.

2P37

X-RAY STRUCTURAL STUDIES ON SUBSTITUTED THIOUREA DERIVATIVES

K. Sivakumar[a], R. Akilan[b], K.Subramanian[b] and Fun Hoong-Kun[a], [a]X-Ray Crystallography Unit, School of Physics, Universiti Sains Malaysia, 11800 USM, Penang, Malaysia and [b]Department of Physics, Anna University, Madras - 600 025, India.

Crystal structure analyses of many metal complexes of thiourea and only a few of those with substituted thioureas have been reported in the past. There is no structural report exclusively on the substituted thiourea derivatives; this may be due the difficulty in getting good crystals suitable for X-ray diffraction studies. These thioureas find applications as rubber accelerator and intermediates for dye preparation; they are also very useful agrochemical intermediates. We are interested in the molecular conformations and N-H...S hydrogen bond formation details of these molecules in the solid state. We were able to crystallise more than fifteen thiourea derivatives and determined their molecular structure by X-ray diffraction methods. We have classified them as symmetrically substituted and unsymmetrically substituted thioureas. The structural information we observed are highly interesting with respect to various substitutions. The packing of the molecules in the crystal lattice are governed mainly by N-H...S hydrogen bonds and leads to one dimensional chains of molecules, dimer formation and two dimensional nets as the case may be. A detailed analysis of individual structures and a comparison of all of them will be presented.

2P38

'Sheet with Holes' Structure of Lead(II) Iodide—N-methylethylenediamine(3/2), $(PbI_2)_3(Me\text{-}en)_2$

H. Miyamae, T. Ito, G. Hihara. Department of Chemistry, Josai University, Keyakidai 1-1, Sakado-shi, Saitama 350-02, Japan

Ethylenediamine sometimes forms nonstoichiometric addition compounds with lead(II) halides.[1] 0.1 ml of N-methylethylenediamine (Me-en) are added to 5 ml of saturated solution of PbI_2 in DMF. After allowing the solution for absorbing MeOH in a sealed container, we have obtained crystals of the title compound. Structure determination of the compound at 298K by single-crytal X-ray diffraction method showed that 2/3 of the Pb atom were coordinated by a Me-en in a form of distorted octahedral PbI_4N_2 coordination [Pb(2)], while the other were surrounded by six I atoms almost octahedrally [Pb(1)]. Thus the [(Me-en)PbI_3-PbI_3Pb(Me-en)] moieties are connected through I atoms to form a sheet in **ac** plane as shown in Fig. 1. All of the Pb-I bond distances around the Pb(1) are ca. 3.21 Å, but those around the Pb(2) are scattered between 3.14 to 3.58 Å.

Crystal data: [Pb_3I_6-(Me-en)$_2$]
orthorhombic, space group Pbca (No. 61)
a 12.440(5) Å
b 16.879(6)
c 12.106(6)
V 2541.9(16) Å^3.

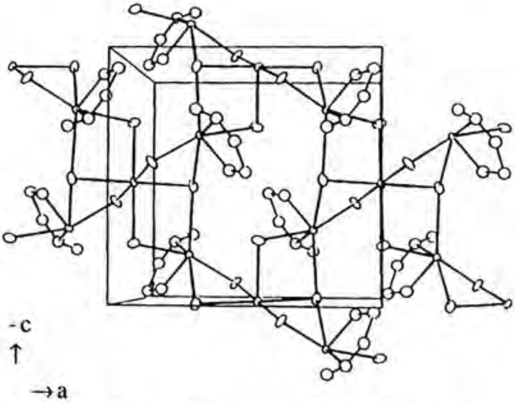

Fig.1. Perspective view of a sheet of the title compound.

1) G.Hihara, H.Miyamae, and M.Nagata, Chem.Lett., 647-650 (1982).

2P39

STRUCTURES OF FURO AND THIENO DERIVATIVES OF 5-AMINO-8-METHYL-1,2-DIHYDRO[2,3-h] [1,6] NAPHTHYRIDINES

R. Kingsford-Adaboh and S. Kashino, Department of Chemistry, Faculty of Science, Okayama University, Tsushima, Okayama 700, Japan, and K. Sasaki, R.A.S. Shamsur and T. Hirota, Faculty of Pharmaceutical Sciences, Okayama University, Tsushima, Okayama 700, Japan

The crystal structures of pharmacological agents having tracheal relaxation activity, 5-amino-8-methyl-1,2-dihydrofuro[2,3-h] [1,6] naphthyridine, $C_{11}H_{11}N_3O$ (I) and 5-amino-8-methyl-1,2-dihydrothieno[2,3-h] [1,6] naphthridine, $C_{11}H_{11}N_3S$ (II) have been determined. The crystals of I and II are isomorphous: monoclinic, space group $P2_1/n$ (No.14), Z=4; a=9.975(5), b=9.695(5), c=10.145(9) Å, β=97.92(6)° for I, and a=10.04(1), b=9.572(4), c=10.680(5) Å, β=98.16(6)° for II. For both molecules, N(9)-C(8), C(6)-C(7), C(5)-N(4), and C(10)- C(11) bonds show a double bond character. Widening of the bond angles C(1)-C(10)-C(13) and N(4)-C(11)-C(10) are remarkable, and is more pronounced in I [133.2(2) and 129.0(2)° for I, 127.4(2) and 126.9(2) for II]. The molecules related by a center of symmetry are linked through an N-H...N hydrogen bond with N...N 3.060(3) Å for I (Fig. 1) and 3.135(4) Å for II. The crystal and molecular structures are compared with those of related compounds.

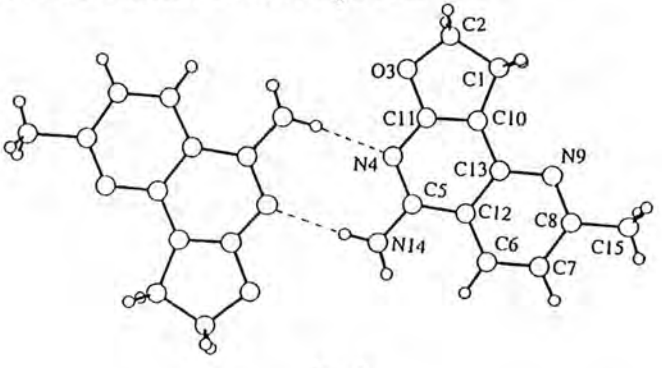

Fig. 1

2P40

X-RAY INVESTIGATION ON STRUCTURAL PHASE TRANSITION IN HOOC$(CH_2)_4$COOH

M. Machida and S. Nishimoto, Department of Physics, Kyushu University, Hakozaki, Higashi-ku, Fukuoka 812, T. Kobayashi, Department of Physics, Hokuriku University, Kanagawa-machi, Kanazawa 920-11

Adipic acid ($HOOC(CH_2)_4COOH$) is known to be monoclinic at room temperature and its symmetry is described by $P2_1/c$ with two formula units in the unit cell$^{1)}$. The adipic molecules are linked by two hydrogen bonds one another and resultant hydrogen bond systems run along the a-axis. An occurrence of the phase transition has been indicated by differential thermal analysis and Raman scattering$^{2)}$. New bands appear at T_c in the Raman spectra and behave like an order-parameter; the critical exponent β is determined to be 0.33 which corresponds to that of the three-dimensionally interacted system. However no investigation on the structure and symmetry of the low temperature phase has been performed so far. We have investigated the phase transition in this crystal by X-ray diffraction in order to elucidate the above interesting behavior.

It was found that additional reflections defined by the modulation wave-vector $\mathbf{q} \sim \mathbf{a}^*/3$ appear at T_c associated with the phase transition; the intensities of these reflections increase with decreasing temperature in the low temperature phase. The modulation of the structure will be discussed in connection with the phase transition.

1) P.J.Housty and M.Hospital, Acta Cryst., **18**,639(1965).

2) H.Ohki, N.Nakamura and H.Chihara, J. Phys. Soc. Jpn., **57**,382(1988).

2P41

VERY RAPID PHOTOISOMERIZATION OF 1-CYANOETHYL GROUP IN COBALOXIME CRYSTALS

P. Inthapanya,[a] Y. Ohgo,[b] D. Hashizume [b] and Y. Ohashi,[b]
[a]Department of Biology and Chemistry, Pedagogy Institute, Dongdok, Vientiane, Laos
[b]Department of Chemistry, Tokyo Institute of Technology, Meguro-ku, Tokyo 152, Japan

It has been found that the chiral 1-cyanoethyl groups bonded to the cobalt atom in some cobaloxime complexes are racemized on exposure to visible light with retention of the single crystal form. The reaction rate was well explained by the size of the reaction cavity. Recently we prepared the 1-cyanoethyl complexes with 2-mercaptobenzimidazole **1** and 4-chloropyridine **2** as axial base ligands. Crystal data is shown in Table 1 and crystal structure of 4-chloropyridine derivative is shown in Fig. 1. On exposure to a xenon lamp the reaction rates of the two crystals were too fast that the crystals were easily decomposed, although the reaction cavity calculated from the analyzed structures, however, are smaller than those showing the crystalline-state reaction.

Table 1. Crystal Data.

	1	**2**
a/Å	11.334(2)	8.621(5)
b/Å	11.647(2)	28.645(3)
c/Å	8.565(1)	8.891(4)
α/°	95.10(1)	–
β/°	101.14(1)	115.60(4)
γ/°	78.08(2)	–
V/Å^3	1084.0(3)	1980.0(2)
Z	2	4
Space Group	$P1$	$P2_1$

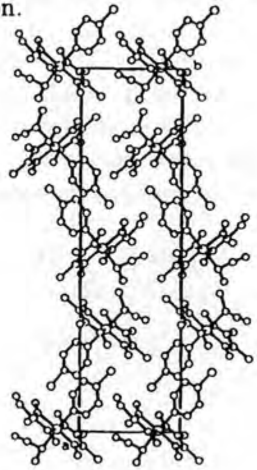

Fig. 1

2P42

CRYSTALLINE-STATE RACEMIZATION OF CHIRAL METHOXYCARBONYLETHYL GROUP IN COBALOXIME COMPLEXES

Masaru Saito, Daisuke Hashizume, Hidehiro Uekusa, and Yuji Ohashi
Department of Chemistry, Tokyo Institute of Technology,
O-okayama, Meguro-ku, Tokyo 152, Japan.

It was reported that crystalline-state racemization of 1-methoxycarbonylethyl (mce) group bonded to the cobalt atom occurs only at high temperatures in a few cobaloxime complexes. In order to investigate more details of this reaction we have synthesized three cobaloxime complexes with (a)cyclohexylamine, (b)cyclopentylamine and (c)benzylamine (Fig. 1) and examined their reactivities.

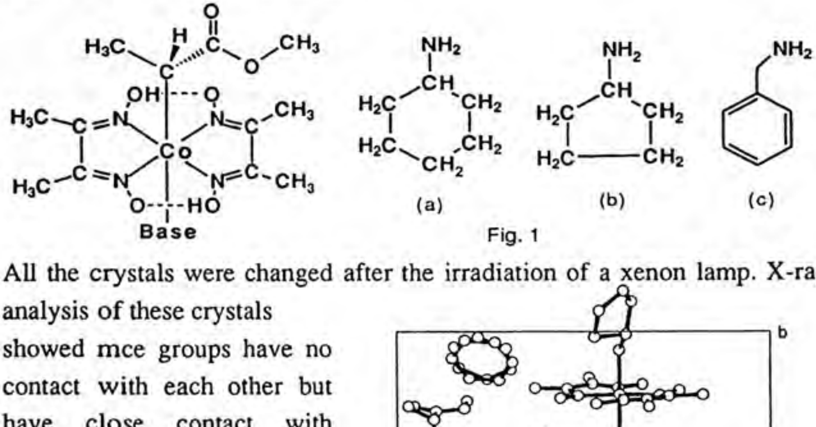

(a) (b) (c)

Fig. 1

All the crystals were changed after the irradiation of a xenon lamp. X-ray analysis of these crystals showed mce groups have no contact with each other but have close contact with crystal solvents (Fig. 2). The solvent molecules appear to play an important role in the crystalline-photoracemization. Further discussion will be done comparing with the racemization reported so far.

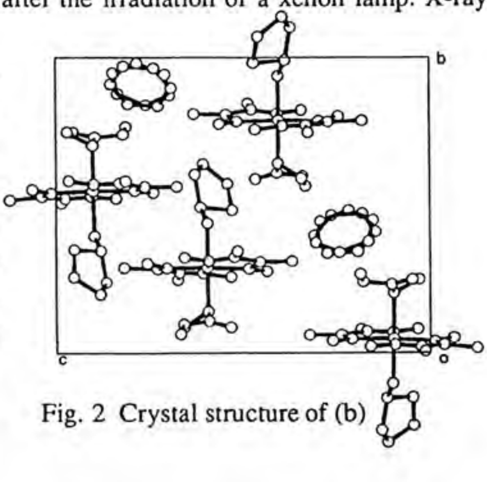

Fig. 2 Crystal structure of (b)

2P43

A CHIRAL *N*-METHYLBENZAMIDE

K. Yamaguchi, Chemical Analysis Center, Chiba University, 1-33 Yayoi-cho, Inage-ku, Chiba, 263, Japan, and I. Azumaya, I. Okamoto, H. Kagechika and K. Shudo, Faculty of Pharmaceutical Sciences, University of Tokyo, 7-3-1 Hongo, Bunkyo-ku, Tokyo, 113 Japan.

We found an interesting compound, 1,2-bis(*N*-benzoyl-*N*-methylamino)benzene (1), which exists in an optically active form in solution and in the crystal. Recrystallization of 1 from distilled ethyl acetate yielded beautiful crystals, each of which is optically active. Sometimes all the crystals belong to the same chiral group, or one large crystal spontaneously forms a solution in good yield. The optically active crystals are orthorhombic and are classified into the space group $P2_12_12_1$. The absolute configuration of 1 was determined using cocrystallization with (R)-1,1'-bi(2-naphtol). The structure of the mixed crystal contains one molecule of 1 and one molecule of 1,1'-bi(2-naphtol) in an asymmetric unit. This may be regarded as an example of the chirality induction from the racemic solution of 1. Detailed crystallographic study will be shown.

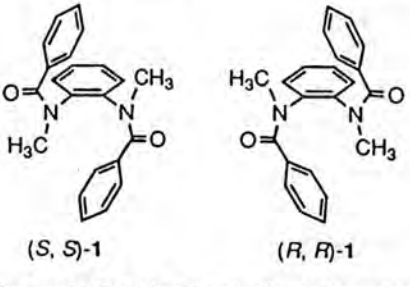

(*S*, *S*)-1　　(*R*, *R*)-1

Two enantiomeric *anti-cis*/*cis* conformations of 1

2P44

ASYMMETRIC PHOTOISOMERIZATION OF (2-CYANOETHYL) (2-BUTYLAMINE) COBALOXIME COMPLEXES IN THE SOLID STATE

T.Koura , H.Kogo and Y.Ohashi , Department of Chemistry , Tokyo Institute of Technology , O-okayama , Meguro-ku , Tokyo 152 , Japan .

It is known that 2-cyanoethyl group bonded to cobaloxime complexes is isomerized to 1-cyanoethyl group with a chiral carbon atom on exposure to visible light in the solid state . The configuration of the chiral carbon atom in the produced complex is seemed to depend on the chirality of the crystalline field around cyanoethyl group . In order to examine above result 2-cyanoethyl cobaloxime complexes with [*R*]- or [*S*]-2-butylamine were prepared and were exposed to visible light under the same conditions .

The specific rotation of the irradiated sample was measured by a polarimeter in a chloroform solution and the crystal structures of [*R*]- and [*S*]-2-butylamine complexes were analyzed by X-ray diffraction method .

The specific rotations increased by +1.63° for [*R*]-2-butylamine complex and decreased by 1.51° for [*S*]-2-butylamine complex . This result indicates that [*S*]-1-cyanoethyl group were produced from [*R*]-2-butylamine complex and [*R*]-1-cyanoethyl group were produced from [*S*]-2-butylamine complex . Such asymmetric induction is well-explained by the reaction cavity around cyanoethyl group , as shown in Figure 1 .

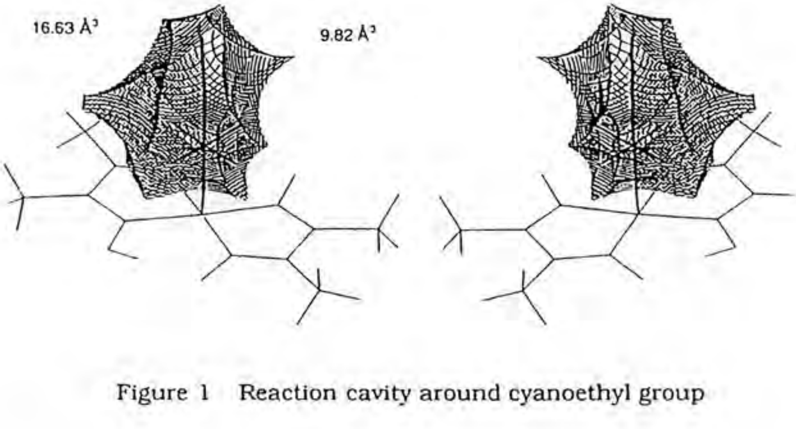

Figure 1 Reaction cavity around cyanoethyl group

2P45

Structure of A Briarein Diterpenoid : (1S*, 2S*, 5Z, 7S*, 8R*, 9S*, 10S*, 11Z, 14S*, 17R*)-2,14-diacetoxy-8,17-epoxy-9-hydroxy-briara-5,11-dien-18-one[++]

Tsong-Jen Lee and Arlohun Wang, Department of Physics, National Tsing Hua University, Hsinchu, Taiwan 300 and Jyh-Horng Sheu & Ping-Jyun Sung, Department of Marine Resources, National Sun Yat-Sen University, Kaohsiung, Taiwan 804, ROC & Fun Hoong Kun, School of Physics, Universitti Sains Malaysia, 11800 Minden, Penang, Malaysia

Diterpenoids of the briarein class, are commonly found in the Gorgonacean genus Briareum and the Alcyonacaean genus Minabea as well as in sea pancy and sea pens. Several briareins have been found to show interesting biological activities, such as antifouling activity, cytotoxicity and antiinflammatory activity. As part of our studies directed in searching bioactive compounds from marine organisms of southern Taiwan, an investigation of the secondary metabolites from Taiwan soft coral Briareum sp. has been carried out. In this work, we report the isolation and relative stereo-chemistry of a briarein diterpene, (1S*, 2S*, 5Z, 7S*, 8R*, 9S*, 10S*, 11Z, 14S*, 17R*)-2,14-diacetoxy-8,17-epoxy-9-hydroxy-briara-5,11-dien-18-one (1) from Briareum sp. The ethyl acetate extract of the soft coral, collected at Kengting, Taiwan, in 1991 by **SCUBA** diving, was chromatographed on a silica gel column (hexane/ ethyl acetate, $1/3 \rightarrow 1/2$) yielding (1) as colorless prisms (from slow evaporation of ethyl acetate solution): mp 238-240 °C; $[\alpha]_D$ 12.2° (C 0.23, $CHCl_3$). ^1H-NMR and ^{13}C-NMR spectra of (1) are in full agreement with those reported previously. Structure determination of the title compound at 300 K by single crystal X-ray diffraction methods reveals that five and six membered rings are in plannar form and the ten membered ring are in a chair form. Absolute configuration of the molecule will be determined by use of anomalous dispersion effects of 25 reflections, selected in that the absorption effect of I(hkl) is nearly equal to that of I(-h,-k,-l) (private communication with Dr.Mamoru Sato, Institute for Protein Research, Osaka University, March 24,1995).*Crystal data*: Orthorhombic $P2_12_12_1$ a= 9.729(2), b=13.794(3), c=20.014(4) Å.

[++] Work supported by National Council of Taiwan under contract number NSC82-0212-M007-118, NSC81-0418-B110-511-BR.

2P46

GRAZING-INCIDENCE DIFFRACTION OF X-RAYS ON SINGLE CRYSTAL WITH NEAR-SURFACE LATTICE DISTORTION

V. S. Haroutyunyan, Dept. of Solid State Physics, Yerevan State University, A. Manoukian 1, 375049 Yerevan, Armenia

The original and sensitive X-ray diffraction scheme under conditions of radiation specular reflection with noncoplanar geometry of the scattering has been considered in [1 to 3]. This scheme enables to carry out structural investigations of thin subsurface layers of crystals.In [3] the equations of diffraction are solved in the kinematical limit for crystal with depth-dependent arbitrary variation of its lattice distortion.

In present paper the diffraction of plane monochromatic X-ray wave on single crystal for above-mentioned geometry of scattering is considered provided that there is a small distortion of crystal lattice in thin surface layer. It is supposed that this distortion varies along the entrance surface with weak constant gradient directed parallel to reciprocal lattice vector of active reflection (in present scheme reflecting atomic planes are perpendicular to the entrance surface, i.e Laue reflection scheme is used). The solution of diffraction equations is found with use of perturbation theory. The angular dependence as well as the integrated intensity dependence of a specular reflected diffraction beam on the parameter of incidence and the value of gradient of lattice distortion are obtained. These results are compared with data corresponding to case of grazing-incidence diffraction on a perfect crystal.

Theoretical approach developed in the present paper can be useful for investigations of lattice distortions caused in a crystal by near-surface impurities, vacancies and other defects with inhomogeneous distribution along the entrance surface.

1. Marra, W.C., Eisenberger, P. & Cho,A.Y. (1979).J.Appl. Phys. 50, 6927-6931.
2. Afanasèv, A.M. & Melkonyan, M.K.(1983).Acta Cryst.A39, 207-211.
3. Melikian, O.G.(1991). Kristallografia 36, 549-553.

2P47

MODEL-INDEPENDENT DETERMINATION OF ELECTRON DENSITY PROFILES FOR Al-C MULTILAYERS USING ANOMALOUS-DISPERSION X-RAY REFLECTOMETRY DATA

T. Ohkawa, Y. Yamaguchi, O. Sakata and H. Hashizume, Res. Lab. of Eng. Mater., Tokyo Inst. of Tech., Nagatsuta, Midori, Yokohama 226, Japan, and A. Datta and M. K. Sanyal, Saha Inst. of Nuclear Physics, 1/AF Bidhan Nagar, Calcutta 700 064, India

A method of obtaining a model-independent electron density profile for a thin film deposited on a substrate using anomalous X-ray reflectivity measurements has been applied to single and triple bilayers of 30 Å aluminum and 70 Å carbon on germanium substrate, prepared with the magnetron sputtering technique. Specular reflection data were collected at a synchrotron source in Photon Factory using X-ray wavelengths 1.3 Å away from and 1.117 Å close to the Ge*K* absorption edge. The measurements covered intensity ranges of 1 : 10^{-8} by the use of attenuators. For each sample the obtained profiles are different at the two X-ray wavelengths, demonstrating changed amplitudes and phases of the reflectance at the film-substrate interface. The profiles involve features similar to those in specular-reflectance coefficients calculated assuming $f' = -8.0, f'' = 0.496$ for the anomalous scattering factors of Ge at 1.117 Å. The data are used to solve Eq.(3) of Sanyal, Sinha et al. [1] to obtain the real and imaginary parts of the Fourier transform of $\Delta\varrho(z)$, the deviation of film electron density from the mean value as a function of depth z. The equation uses a distorted-wave Born approximation to calculate specular reflectivities over a wide scattering-angle range and recovers the lost phase information. The results are inversely Fourier transformed to reconstruct real-space electron density profiles for the Al-C multilayers. The density profile obtained for the single bilayer Al-C shows a density step height which is smaller by 0.02 e/Å^3 than the calculated value. Deviations of the obtained profiles from the model structures are discussed in terms of the finite q_z range ($q_z < 0.6$ Å^{-1}) used for the Fourier transform. The specular data are also least-squares fit to Parratt's formula to evaluate the layer thickness, surface/interface roughness and density variation, which are compared with the information available from the reconstructed electron density profiles.

[1] Sanyal, M. K., Sinha, S. K., Gibaud, A., Huang, K. G., Carvalho, B. L., Rafailovich, M., Sokolov, J., Zhao, X. & Zhao, W., (1993). *Europhys. Lett.* **21**, 691-696.

2P48

IN-PLANE STRUCTURE OF ARSENIC-DEPOSITED SILICON SURFACES STUDIED USING GRAZING-ANGLE X-RAY STANDING WAVES.

O. Sakata, S. Kumano, A. M. Nikolaenko and H. Hashizume, Res. Lab. Eng. Mater., Tokyo Institute of Technology, Nagatsuta, Midori, Yokohama 226, Japan.

Grazing-angle diffraction of X-rays by crystal planes normal to a surface produces dynamical standing waves with intensity modulates along the surface. The X-ray field outside the surface has two components, $B(x)$ and A, with and without lattice-position dependence in the direction of the reciprocal-lattice vector parallel to the surface. The profile of A and $B(x)$ as a function of $\Delta\theta$ behave distinctly when the glancing incidence angle ϕ_0 is varied near the critical angle for total external reflection (Sakata, Hashizume & Kurashina (1993)). This property has been exploited to accurately determine the position x and disorder of As atoms on an Si(111): As 1×1 surface. As K emission profiles, observed from a sample in ultra-high vacuum environment at a synchrotron source, showed As atoms located in the threefold coordinated sites of the bulklike Si(111) surface with little disorder. The displacement is smaller than 2% of the d spacing of the $(2\bar{2}0)$ planes and the coherent fraction is higher than 80% (Sakata & Hashizume (1995)). The same technique was applied to an As-deposited Si(100) surface with mixed 1 × 2 and 2 × 1 domains. The substrate surface was cut at 4 ° to the (100) plane towards the [011] axis, on which As was deposited in an MBE facility. A LEED picture showed strong 2 × 1 spots and weak 1 × 2 spots, indicating predominant As dimers parallel to the double-layer-height step edges along the $[0\bar{1}1]$ direction. We collected As emission data in the vicinity of the 022 and $0\bar{2}2$ Bragg peaks, which were used to evaluate the h parameter defined by $\eta = f_i + f_j\cos(2\pi l)$ $(i,j=1,2)$, where f_i and f_j are the fractions of the As atoms forming 1 × 2 and 2 × 1 dimers and l is one half the dimer bond length normalized to the (022) d spacing. The indeterminate equations can be solved using an assumed value for the fraction of the ordered As atoms to evaluate f_1, f_2 and l.

Sakata, O. , Hashizume, H. & Kurashina, H. (1993) *Phys. Rev.* **B48**, 11408-11411.

Sakata, O. & Hashizume, H, (1995) Acta Cryst. **A51**, 375-384.

2P49

MICROMORPHOLOGY OF POLISHED SILICON SURFACES STUDIED BY X-RAY REFLECTOMETRY

Y. Yamaguchi, M. Nakanishi, O. Sakata and H. Hashizume, Res. Lab. of Eng. Mater., Tokyo Inst. of Tech., Nagatsuta, Yokohama 226, Japan, and M. Nakano, Shin-Etsu Handoutai Co. Ltd., Shirakawa, Japan, and J.M Bennett, Naval Air Warfare Center, China Lake CA, USA

Micromorphology of polished silicon surfaces has been studied using X-ray reflectometry at a synchrotron source, in conjunction with classical profilometry techniques using optical (WYKO) and mechanical (Talystep) probes. The samples studied are Si (100) wafers polished with a standard mechanochemical technique to four distinct roughness levels A, B, C and D. X-ray experiments at a Photon Factory source measured specular reflectivity profiles of the samples using 1.38 Å X-rays, which were fit to Parratt's formula. The fits determined the r.m.s. values of the vertical roughness at 14.8, 7.4, 3.9, 4.1 Å for surfaces A, B, C and D respectively, which compare with those from WYKO (11.3, 3.7, 2.5, 2.5 Å) and Talystep (19.5, 6.1, 2.9, 2.6 Å). The lateral resolutions of these methods are quite different, 10 Å for X-rays, 1 μm for WYKO, and about 0.5 μm for Talystep. The similar roughness values obtained with the three methods for each surface indicate that the statistical fluctuation of the polished silicon surfaces includes structures of quite wide spatial wavelength ranges in the lateral direction. To give information on correlated structures, we measured diffuse X-ray intensity profiles at non-specular scattering angles and analyzed the data using the theory developed by Sinha et al. [1]. The height-height correlation lengths thus determined are 1.8, 1.7, 0.02, 0.03 μm for surfaces A, B, C and D respectively. These values are quite different from 3.6~6.0, 1.5~6.7, 10.2~30.0, 14.7~45.4 μm determined from the Talystep traces over surface lengths of 0.2 to 1 mm. The data show that surfaces C and D include short-wavelength fluctuations superposed on long-range waviness which is detected by Talystep, but not X-rays.

[1] Sinha, S. K., Sirota, E. B., Garoff, S. & Stanley, H. B., (1988). Phys. Rev. B38, 2297-2311

2P50

DISLOCATION STRUCTURE OF SOME INDUSTRIAL ALUMINUM ALLOYS AFTER ROLLING.

Tran Quoc Thang, Materials Science Center, Hanoi University of Technology, Dai Co Viet Road, Hanoi, Vietnam, F. Louchet, L. T. P. C. M., E. N. S. E. E. G., I. N. P. Grenoble, France.

Al, Al-Mg, Al-Mn-Si alloys heavily strained by rolling are submitted to examine in transmission electron microscopy.

The results of observation show that dislocation cells are formed during rolling, which are elongated along the rolling direction.

Dislocation cell's formation is retarded in Al-Mg solid solution and in Al-Mn-Si with dense incoherent precipitation.

The cell's thickness, D, depends on rolling deformation, ε, by 2 steps:

For $\varepsilon \leq \varepsilon_{cr}$, D vs. ε corresponding to modification of macro-size in rolling, agrees with a dislocation walls multiplication. For $\varepsilon \geq \varepsilon_{cr}$, D decrease towards constant, that could be explained by walls annihilation. Some energetic model has been proposed to account for observations.

2P51

STRUCTURE OF MICROCRYSTALLINE Ag-BASED AMALGAM ALLOYS

Do Minh Nghiep, Materials Science Center, Hanoi University of Technology, Vietnam, Cao The Ha, Department of Chemistry, National University of Hanoi, Vietnam, Nguyen Van Dzan, Center for New Materials, Technical University of Ho Chi Minh City, Vietnam, and Lecong Dzuong, Materials Science Center, Hanoi University of Technology, Vietnam

The influence of Cu content (6-32 weight %) of Ag-based amalgam alloys prepared from microcrystalline melt - spun ribbon powders on their phase structure has been studied by XRD, EMPA and optical microscopy. For these alloys the Cu atoms either existed in Cu - Sn phases or dissolved in γ and / β phases as "activated" atoms. The quantity of the last atoms plays an important role in the phases formation depending on the Cu content and the solidification rate. In comparison with conventional amalgam alloys of the same composition the rapidly solidificated alloys are characterized by:

1. a very fine and homogeneous microcrystalline structure,
2. a decrease of the Cu_3Sn phase and at higher Cu content the δ phase ($Cu_{31}Sn_8$) may be present,
3. a supersaturation of the "activated" Cu atoms in γ and / β phases, which may lead to clustering of Cu atoms or to formation of the Cu_6Sn_5 phase during a proper aging and
4. a decreased amount of γ_2 phase (Sn_8Hg) in consequence of decreasing Cu_3Sn phase and increasing "activated" Cu atoms with Cu content.

Such variations of the alloy structure improved markedly the amalgam properties.

2P52

COMMON FEATURES OF P-TYPE AND N-TYPE POROUS SILICON LAYERS WITH VISIBLE PHOTOLUMINESCENCE

Osamu NITTONO and **Kuniko TAKEMOTO**, Department of Metallurgical Engineering,Tokyo Institute of Technology, Meguro-ku, Tokyo 152, Japan

Porous silicon (PS) is a kind of silicon having a pore structure. Recently, Canham demonstrated strong visible photoluminescence from p-type PS, and stated that the visible light emission is attributed to a quantum size effect. Our previous studies have revealed that the microstructure of PS layer formed on p-type silicon (Si) wafer including pore size and morphology is strongly dependent on doping quantity and wafer resistivity as well as anodization conditions such as formming current density and electrolyte concentration. In this study, PS layers, formed on heavily doped p-type and n-type silicon wafers of low resistivity less than 0.02 Ωcm, have been investigated by mainly X-ray multi-crystal diffractometry, supplemented with electron diffraction and electron microscopy including scanning electron microscopy and transmission electron microscopy. Observed X-ray diffraction profiles give directly the lattice mismatch between PS layer and Si substrate. Broad diffuse scattering is always seen under a coherent peak for PS layer in a large angular range as shown in Fig. 1, indicating some modification of the nanostructure of PS layer. It is also shown that PS layers which exhibit intensive photoluminescence under He-Cd laser illumination at room temperature are not amorphous, but crystalline, and their crystallinity is still preserved in the residue until they are heavily distorted and finally divided into small crystallites when anodized with higher forming current densities. The experimental results reveal that the visible photoluminescence was strongly related to the microstructure of PS layer near the surface that shows a spongelike structure consisting of a large number of silicon crystalline parts of few nm's in size.

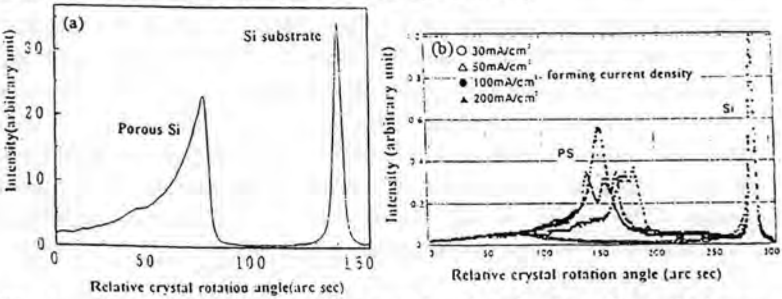

Fig. 1 X-ray rocking curves of p-type in (a) and n-type PS in (b) layers

3P01

On Cross-sectional Transmission Electron Microscopy Study of Carbon Nanotubules

G. Hu, X.F. Zhang and Z. Zhang
Beijing Laboratory of Electron Microscopy, Chinese Academy of Sciences,
P.O. Box 2724, Beijing 100080, China

Both coil-shaped and straight carbon nanotubules have been investigated by cross-sectional transmission electron microscopy (XTEM), especially by cross-sectional high resolution electron microscopy (XHREM). These tubules are hallow and consist of concentric graphene sheets but with different shapes in the cross-sectional view. The XTEM images of the coiled-shaped tubules exhibiting a polyhedral shape, while the XHREM images show that the cross-section of strait tubules are normally with elliptical shape.

A coil-shaped coaxial carbon nanotubules is imaged along the coil-axis direction. It has been demonstrated that one pitch of the coiled tubule contains twelve straight segments with a joint angle of 30o between each other. Each straight segment is composed of coaxial graphite multilayer tubules with turbostratic stacking between neighbouring layers as confirmed by nanomicro electron diffraction (μμ-ED). These experimental results strongly support the models for tubule joints relevant to pentagon-heptagon pairs. A comparison of μμ-ED patterns obtained from adjacent straight segments allows to determine the joint rules even for helical tubules. Primary evidence for toroidal form of carbon cage is also presented.

Bundles of strait carbon nanotubules were collected from the cathodic graphitic deposits, embedded in an epoxy mould, and then cut into slices of thickness of 20-30 nm by aultramicrotomy with diamond knife. XHREM images reveal that the strait tubules consist of concentric cylindrical graphene sheets, but normally with elliptical shapes, rather then circulars, in cross-section. This may corresponding to the observation of non-symmetrical lattice spacing of tubules view along the longitudinal projection in a certain direction. Dislocation walls have also been observed in the cross-section view. The crystallographic structure of the carbon nanotubules are discussed based on a comparison of the theoretical consideration with the number of the dislocation walls observed in the complete circumference of each successive concentric graphene sheets of tubule.

3P02

LOCAL STRUCTURE AROUND MAGNESIUM IN $CaMgSi_2O_6$ GLASS BY OXYGEN K-EDGE EXELFS ANALYSIS

Y. Tabira, Research and Development Center, RICOH, Co. Ltd., Shin'ei-cho, Tsuzuki, Yokohama 224, N. Ishizawa, Research Laboratory of Engineering Materials, Tokyo Institute of Technology, Nagatsuta, Midori, Yokohama 226, and F. Marumo, Department of Earth Sciences, Nihon University, Setagaya, Tokyo 156, Japan

An electron energy-loss spectroscopic study was performed using a transmission electron microscope (TEM). Previous study on the glass and the high-temperature melt with the title composition by the X-ray diffraction technique showed that Mg atoms in both compounds have co-ordination numbers less than six as found in the diopside crystal with the same chemical composition. In order to confirm the local structure around Mg in the glass, the extended energy-loss fine structure (EXELFS) around the oxygen K-edge of the powdered glass was investigated. The Mg K-edge was unsuitable for quantitative analysis because of its low peak-to-background ratio. The EXELFS spectra up to over 1400 eV (loss-energy) were collected by the parallel-type detector with the TEM operated at 200 kV. Diameter of the selected area of a fragment was 200 nm and the maximum scattering angle collected in a spectrometer aperture was 16 mrad. The interatomic distance obtained from the radial distribution function around the oxygen atom was longer by 0.006 nm than that in a synthetic $MgAl_2O_4$ spinel crystal in which Mg atoms are surrounded regularly by four nearest-neighbor oxygen atoms. The difference of 0.006 nm is significantly small compared with the difference of 0.017 nm observed between the O-Mg distances of diopside and spinel. This result is concordant with the implication from the X-ray diffraction experiment.

3P03

Optimization of Prolyl endopeptidase Crystal Growth

Y. Kagawa, Y.Kawauchi and T.Sato, Faculty of engineering, University of Tokushima, Tokushima 770, Japan, and E.Yamashita and T. Tsukihara, Institute for Protein Research, Osaka University, Suita 565, Japan and G. Sazaki and H.Komastu, Institute for Materials Research, Tohoku University, Sendai 980, Japan

Protein crystal growth often depends on the combination of many different factors. Some affect protein solubility and aggregation state directly; others may act indirectly by causing conformational changes. Systematic characterization of these factors can be important for yielding good crystals. It can also give the useful indication into the biochemical behavior of the protein being crystallized. Here we focus on biochemical technique and statistical method to achieve two directions as followed. (1) Characterization of the protein conformation under different levels of biochemical parameters, such as pH. Tests of the reproducibility of crystal growth experiments indicate the quantitative scales of crystal quality can be statistically significant. Analysis of variance for a replicated, incomplete factorial design in which four factors which are [pH], [Protein concentration], [Precipitant concentration] and [temperature] were tested, has been used to demonstrate highly significant, biochemically relevant, two-factor interactions strongly implicating pH and conformational changes, corresponding to a result of the isoelectric titration curve used the zymogram analysis. (2) Optimization of crystal growth for response-surface experiments. 'Minimum predicted variance' designs provide for efficient response-surface experiments aimed at constructing quadratic models in several parameters. We have used such models to improve crystal size and quality significantly of Flavobacterium meningosepticum prolyl endopeptidase. Recently advances in this recombinant DNA and the protein expression technologies permit such a systematic search of potential crystallization conditions with large quantities of highly purified starting sample. The two-dimensional level surfaces have a number of 'ridges', where the same result is obteined for many combinations of the factors usually varied when trying to improve crystals. An important inference is drawn from the surface that it may be better to sample simultaneously for the interaction effects of protein concentration and molecule aggerate. For a system involving only one crystallizing agent (PEG1500), supersaturation can be approximated as the product of [Protein concentaration] and [Precipitant concentration]. Use of this search method will significantly improve the performance of response-surface experiments. Growing crystals at stationary points of their response surfaces generate better crystals and high reproducibility, since crystal growth at stationary points is not influenced by any harmful effects of experimental errors. This arises because the derivatives of the model function are by definition zero with respect to the experimental variables. Quantitative analysis of appropriate design for crystal growth experiments can thus be a powerful tool to characterize complex and interacting biochemical dependencies in macromolecular systems and to optimize parameters important to the crystallization.
OptimaizedCrystallizationCondition:
[Buffer] = 50mM NaPi + 0.2M NaCl, [Final pH] = pH6.9, [Temperature] = 25℃, [Protein concentration]=25mg/ml, [Precipitant concentaration]= 18～20%w/v PEG1500

3P04

Use of Dynamic Light Scattering to Compare Crystallinities of the Single Stranded DNA Binding Protein (SSB) and Ribosome

A. Nakagawa, Y.Kawauchi, T.Sato, Faculty of engineering, University of Tokushima, Tokushima 770, Japan, and T. Tsukihara, Institute for Protein Research, Osaka University, Suita 565, Japan and G. Sazaki and H.Komastu, Institute for Materials Research, Tohoku University, Sendai 980, Japan

Crystallization frequently represents the main rate limiting step in X-ray crystallographic studies of the structure of biological macromolecules and organelle. Recently introduced incomplete factorial and/or sparse matrix strategies and advances in reconbinant DNA and protein expression technologies have had a dramatic effect on the area of protein crystallization. Certein criteria may be set before crystallizationtrials are started, such as solubility, purity and aggregation tendencies. Crystallization trials depend on varying many different parameters, searching for supersaturation conditions where homogeneous preparations will first nucleate and then support crystal growth. Unfortunately, inpurity (commonly assayed by SDS-PAGE electrophoresis or ion-spray mass spectrometry) or macroheterogeniety coupled with wide screening offers no insulant of success. The protein sample is then examined using laser light-scattering techniques. This method allows us to detect the presence of aggregates in the protein and organelle solution by which may be disturbed to crystal nucleation or growth. Empiricalobservations suggest that mocromolecules and organelle that are monodisperse, which are all the same size, under 'normal' solvent conditions crystallize readily, on the other hand randomly aggregating or polydisperse systems rarely, if ever, produce crystals. Monodispersity which lead to crystal was found by the single staranded DNA binding protein (SSB) and polydispersity to form aggregates which lead to precipitateswas detected with Ribosome, early in the evolution of a supersaturated solution of macromolecules and organelle. We hereinafter refer to the former as pre-crystalline aggregates and the latter as pre-precipitating aggregates. Dynamic light scattering (DLS) can be employed to detect monodispersity as candidates for crystallization. A measure of the translational diffusion coefficient, 'D', of SSB and Ribosome molecules in various precipitating agent solutions as a founction of salt and protein concentration using DLS. Assuming a spherical model for the protein, its hydrodynamic diameter, 'd', can then be calculated. Variationof 'd' as a function of certain biochemical solution properties such as [Protein concentration], [pH], [Precipitant concentration], or [Temperature] can be estimated. The protein concentrationdependence of 'd' has been suggested as a way to differentiate between pre-crystalline aggregates and pre-precipitating aggregates in solution. The protein concentrationdependence of 'd' has been the two types of aggregates

Crystallization efforts may be limited to monodisperse preparations, saving valuable time-loss on trials with samples which are not enough to be transferred to the crystallization procedure. Application of this technique to find unknown crystallization conditions of other proteins or Ribosome is discussed on the basis of a quantitative experimentalmeasurement of SSB.

3P05

SINGLE CRYSTAL GROWTH OF VACANCY DEFECT TYPE SULFIDE SPINEL COMPOUNDS USING BRIDGMAN TECHNIQUE

T. Ohachi, Y. Ohmuro, K. Asahi and I. Taniguchi

Department of Electrical Engineering, DOSHISHA UNIVERSITY, Tanabe, KYOTO 610-03, Japan

Single crystals of vacancy type sulfide spinel (M=Cu,Ag), MIn_7S_{11}, MIn_9S_{14}, $MIn_{11}S_{17}$, $MIn_{21}S_{32}$, $CoIn_8S_{13}$ and $CoIn_{18}S_{28}$ were grown by a horizontal Bridgeman method with successive annealing at high temperature. The crystal structures were analyzed by a X-ray diffraction method. Lattice constants of crystals are calculated by the diffraction pattern using silicon powder as a standard material. X-ray photoelectron spectroscopy (XPS) is used to analyze the valence of metallic ions. The single crystallinity was checked by Laue photographs.

Spinel structure is known as one of structures of ferrite and is expected to show electronic and ionic mixed conduction. Studying sulfide spinels is more advantage than that of oxide in order to invent a large ionic conductor because lattice constants of sulfides are larger than those of oxide ones.

From phase diagrams of In_2S_3-Cu_2S[1], In_2S_3-Ag_2S[2] and In_2S_3-CoS[3] each vacancy type sulfide spinel is a solid solution between normal sulfide spinel, MIn_5S_8 (M=Cu,Ag) or $CoIn_2S_4$ and a defect spinel, In_2S_3. These ternary compounds dose not decompose before melting, large single crystals are possible to grow by a melt technique. The amount of vacancy defects are able to be controlled by the amount of indium content[4]. Because of spinel structure, in which chemical diffusion coefficients of metallic atom are large, and large amount of vacancy defects,the uniform composition of the vacancy defect spinels are obtained.

Stoichiometric amounts of high purity copper or silver and indium of about 2 g and a proper quantity of sulfur are sealed into a transparent quartz tube. The tube was evacuated, sealed, and heated in an electric furnace at the temperature 1150～1200℃ which is over melting point(1075, 1085, or 1110 ℃ for Cu, Ag, or Co system), and are melted 1～3 hours. To make single crystals by horizontal Bridgeman method of single directional solidification, one end of this quartz tube was kept at 100℃ lower than the other part. It is cooled down to 900℃ at the cooling rate of 10～100℃ /h, and annealed 30～40 hours at 900～1000℃ to make an uniform crystal of vacancy distribution.

Specimen made by this method are used for measurement of electrical characteristics. Ionic conductivity has been studied by a vector network analyzer in the range of 26.5GHz～60GHz for Cu and Ag systems.[5]

References:

[1] J.J. M. Binsma, L. J. Giling and J. Bloem, J. Crystal Growth 50 (1980) 429.

[2] G. Petzow, G. Effenberg, " Ternally Alloys: A Comprehensive Compendium of Evaluated Constitutional Data and Phase Diagrams", VCH vo;.1.

[3] R. E. Johnson, J. Electrochem. Soc. 110 (1963) 593.

[4] T. Ohachi and B.R. Pamplin, J. Crystal Growth 42 (1977) 598.

[5] Y. Ohmuro, T. Ohachi and I. Taniguchi, Solid State Ionics in press (1995).

3P06

CRYSTAL STRUCTURE OF THE C-TERMINAL DOMAIN OF RABBIT SERUM HAEMOPEXIN AT 1.8 Å RESOLUTION

E.N. Baker, H.M. Baker, H.R. Faber and C.R. Groom, Department of Chemistry and Biochemistry, Massey University, Palmerston North, New Zealand and W.T. Morgan and A. Smith, School of Biological Sciences, University of Missouri-Kansas City, MO 64110, USA.

Haemopexin is a serum protein that binds and transports haem as part of the body's mechanism for iron conservation and protection against free radical damage. Haemopexin is a glycoprotein (60 kDa) that consists of two homologous domains; the N-terminal domain binds haem through two His residues, while the C-terminal domain modulates haem binding and is involved in receptor interactions. Both domains are related to similar domains that occur in proteins of quite unrelated function, for example collagenases and the serum adhesion protein vitronectin.

We have crystallized the C-terminal domain of rabbit haemopexin, after first removing its attached carbohydrate. The three-dimensional structure has been determined by multiple isomorphous replacement (3 heavy atom derivatives) and has been refined at 1.8 Å resolution; the final R-factor is 0.176 for a model comprising 1630 protein atoms (209 residues), 2 Na^+, 1 Cl^-, 1 phosphate and 100 water molecules.

The structure of the haemopexin domain shows a remarkable pseudo-fourfold symmetry. The molecule is folded into four modules of 40-50 residues each, which are arranged successively round a central tunnel, to create a disc-shaped structure. Each module is based on a four-stranded β-sheet, of W topology. A striking feature of the structure is a row of bound ions that fills the central tunnel, comprising two cations (Na^+ or Mg^{2+}) and two anions (Cl^- and phosphate). The end of the tunnel where the phosphate is bound widens into a funnel shape and a shallow surface cleft; we propose that it is a similar feature in the N-terminal domain that enables haem to be bound. The relationship of this domain to the similar domain in human collagenase will be discussed, as will the relationship with other β-propellor proteins.

3P07

CRYSTAL STRUCTURE OF L-2-HALOACID DEHALOGENASE FROM *Pseudomonas* sp. YL AT 2.5 Å RESOLUTION

T. Hisano, Y. Hata, T. Fujii, T. Kurihara, N. Esaki and K. Soda, Institute for Chemical Research, Kyoto University, Uji, Kyoto 611, Japan.

L-2-haloacid dehalogenase from *Pseudomonas* sp. YL is a thermostable dimeric enzyme formed by two identical subunits consisting of 232 amino acid residues. It catalyses the hydrolysis of carbon-halogen bond of L-2-haloalkanoic acids with various carbon-chain lengths to produce D-2-hydroxyalkanoic acids. The catalytic mechanism of the enzyme is still unclear. In order to elucidate the catalytic mechanism from structural viewpoints, we have analyzed the crystal structure of L-2-haloacid dehalogenase from *Pseudomonas* sp. YL by X-ray diffraction method.

Crystals were obtained at 4°C by vapor diffusion against 50 mM potassium dihydrogenphosphate solution (pH 4.5) containing 15% (w/v) PEG 8000 and 1% (v/v) *n*-propanol. They belong to the space group *C*2 with unit cell dimensions $a = 92.21$ Å, $b = 62.78$ Å, $c = 50.84$ Å and $\beta = 122.38°$, and contain one subunit per asymmetric unit. The structure was solved by a multiple isomorphous replacement method using Au- and U-derivatives, and refined at 2.5 Å resolution with X-PLOR to the R-value of 0.198 for 7,848 intensity data ($I \geq 2\sigma(I)$) collected on a R-AXIS IIC.

The structure of the enzyme consists of two structural domains. The core domain which occupies about 70% of the total residues has an α/β structure where a six-stranded parallel β-sheet is flanked with five α-helices as often observed in nucleotide-binding domains. The subdomain inserted between the first β-strand and α-helix of the core domain is connected to the core domain by two antiparallel β-strands. The two domains compass the cleft having the active site in its inside. Mutagenesis studies have suggested that Asp10, Lys151, Tyr157, Ser175, Asn 177 and Asp180 may be involved in the activity. These residues are found to be clusterd at the bottom of the cleft, implying that they are positioned in the active site and may include catalytic residues. Two subunits of the dimeric molecule are related to each other by the intramolecular two-fold axis equivalent to the crystallographic symmetry axis. The contact surface between the subunits is mainly formed by hydrophobic residues.

3P08

CRYSTAL STRUCTURE OF 3-ISOPROPYLMALATE DEHYDROGENASE FROM FACULTATIVE THERMOPHILE, *BACILLUS COAGULANS*

D. Tsuchiya, O. Matsumoto* and A. Takenaka, Department of Life Science, Tokyo Institute of Technology, Yokohama, Japan, and T. Murakami, T. Sekiguchi and Y. Nosoh, Department of Fundamental Science, Iwaki Meisei University, Fukushima, Japan

3-Isopropylmalate dehydrogenase (IPMDH ; EC1.1.1.85) catalyzes the oxidative decarboxylation of 3-isopropylmalate using NAD as cofactor. IPMDH from facultative thermophile *Bacillus coagulans* (BcIPMDH) is composed of two identical subunits (M_w=39,808 ; 366 amino acid residues). To reveal the reaction mechanism and the thermostability, we have engaged in the x-ray analysis.

Several crystalline forms were obtained by surveying various conditions using hanging drop vapor diffusion method. One of them, which belongs to a space group of P3$_1$21 with cell dimensions of a=b=114.4 and c=194.9 Å, was found to be suitable for x-ray analysis because the asymmetric unit contains one dimeric molecule. The x-ray diffraction data were collected on imaging plates using the weissemberg camera at the Photon Factory in Japan. 86,904 reflections were processed, of which 27,274 independent reflections were obtained within 2.8 Å resolution (R-merge = 0.069, completeness = 73.62 %). Their primary phases were estimated by the molecular replacement method using IPMDH from extreme thermophile *Thermus thermophilus* (TtIPMDH) as a probe molecule. The molecular model was constructed on electron density maps, modified using solvent flattening, NCS averaging and histogram matching technique. Almost all amino acid side chains except for 12 C-terminal residues were assigned and the atomic parameters were refined to be R-factor of 0.204 using the data within 10-3.0 Å resolution.

BcIPMDH takes an open α/β structure similar to that of TtIPMDH. As seen in the figure, remarkable differences are observed around the inserted residues in the loop region. The 12 C-terminal residues could not be identified in electron density maps, suggesting some disorder by extruding into solvent region.

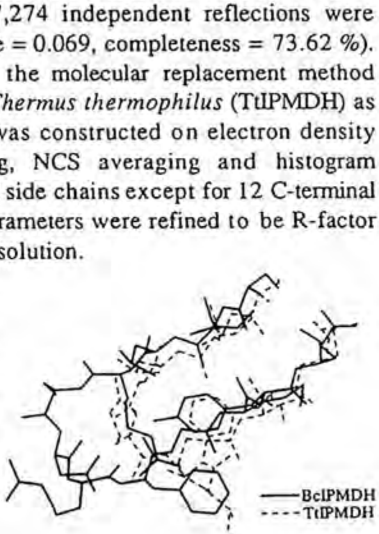

---

* Present address : Faculty of Pharmaceutical Sciences, Kyoto University, Kyoto, Japan

3P09

Structures of Substrate-Complexed G4-Amylase Inactivated by Mutation of Catalytic Residues

K. Hasegawa, H. Yamaguchi, Y. Yoshioka, Y. Matsuura, Institute for Protein Research, Osaka University, Suita, Osaka 565, Japan, and M. Kubota, Hayashibara Biochemical Lab. Inc., Amase-minami, Okayama 700, Japan

Maltotetraose forming α-amylase (G4-amylase) consisting of 429 amino acid residues from *Pseudomonas stutzeri* is an *exo*-type α-amylase which degrades starch from its nonreducing end. We previously determined the structure of wild-type enzyme and that of E219Q mutant complexed with maltotetraose (G4). Although we cocrystallized inactivated mutant enzyme (E219Q) with maltopentaose, structure analysis revealed that maltopentaose was hydrolyzed to give maltotetraose and also showed that the fourth glucose unit from the nonreducing end was deformed adopting half-chair conformation. For the purpose of revealing the structure of this enzyme complexed with non-hydrolyzed substrate and of determining the residue that is crucial to deformation of the sugar ring , we analyzed the structure of E219G and D193G mutants complexed with the substrate by X-ray crystallography.

The complexed mutant crystals were obtained by cocrystallization with maltopentaose. Intensity data to 2.0 Å resolution were collected on the imaging plate diffractometer RAXIS-IIC. In the case of E219G, the crystal form was same as that of E219Q/G4 complex and we used the coordinates of E219Q/G4 complex structure as a starting model for the refinement. The cell dimensions of D193G complex crystal were slightly different from those of E219Q/G4 complex, and the structure was solved by the molecular replacement method with the program AUTOMR by using E219Q/G4 complex as the search model.

In both structures, maltopentaose was hydrolyzed to maltotetraose and the fourth glucose unit was still deformed. In E219G/G4 complex structure, two water molecules that were not observed in E219Q/G4 complex were found near the catalytic site structure. One of these water molecules was located at the position that was occupied by the atom Gln219CD in E219Q/G4 complex. The position of the sugar rings was almost same as that of E219Q/G4 complex. In D193G/G4 structure the fourth glucose unit moved toward the Cα atom of Gly193 and the side chain of Glu219 took different conformation from that of Gln219 in the E219Q/G4 complex. The position that was occupied by the atom Asp193OD in E219Q/G4 complex was replaced by a water molecule.

3P10

X-RAY STRUCTURAL ANALYSIS OF THE FIVE ISOLEUCINE TO VALINE MUTANTS OF HUMAN LYSOZYME: CONTRIBUTION OF HYDROPHOBIC RESIDUES TO THE STABILITY

Yuriko Yamagata, Hidetomo Kaneda, and Satoshi Fujii, Faculty of Pharmaceutical Sciences, Osaka University, Yamadaoka, Suita, Osaka 565, Japan. and Kazufumi Takano, Kyoko Ogasahara and Katsuhide Yutani, Institute for Protein Research, Osaka University, Yamadaoka, Suita 565, Japan.

In order to understand the contribution of hydrophobic residues to the conformational stability of human lysozyme, five Ile mutants (Ile->Val; I23V, I56V, I59V, I89V and I106V) in the interior parts were constructed. The thermodynamic parameters characterizing the denaturation of theses mutant proteins were obtained by scanning calorimetry. X-ray analyses (resolution=1.8Å; R-factor=0.154-0.160; completeness of data=86.3- 95.4%) showed that the overall structures of all the mutant proteins examined were identical to that of the wild-type protein, but small structural arrangements were observed locally around some of the mutation sites. The most striking change among the mutant proteins was found in the I59V protein, which contains a new water molecule in the cavity created by the methylene deleted mutation. This water is fixed by two hydrogen bonds with the carbonyl oxygen of Ala92 and one of the internal waters found in the wild-type and mutant crystal structures. The B-factor of the newly bound water is 24.0Å^2, which is smaller than the averaged value (36.5Å^2) of the solvent molecules. In the case of I23V, the movements were observed in the loop region (residues 99 to 105) facing position 23, rather than in the vicinity of residue 23. The largest backbone shift, 1.0Å, is in the oxygen atom of Pro103. We observed the better correlation between changes in the thermodynamic parameters of denaturation and the accumulation of subtle structural changes, such as in ASA(solvent accessible surface area) values and cavity volumes. The total structural rearrangements involved in the overall structure partially compensated for the destabilization due to the removal of the methylene group by the mutation.

3P11

CRYSTAL STRUCTURE OF ACIDIC PHOSPHOLIPASE A2 FROM THE VENOM OF AGKISTRODON HALYS PALLAS AT HIGH RESOLUTION

X. Q. Wang, J. Yang, L. L. Gui, Z. J. Lin, National Laboratory of Biomacromolecules, Institute of Biophysics, Academia Sinica, Beijing, China, and Y. C. Zhou, Shanghai Institute of Biochemistry, Academia Silica, Shanghai, China.

The venom of Agkistrodon halys pallas contains three highly homologous phospholipase A2 (PLA2), which are quite different from each other in enzymatic activity, toxicity and pharmacological activity. The structural analysis and comparison of these three PLA2 will be beneficial to understanding of the relationship between the structure and function of this enzyme. The acidic PLA2 showing weak toxicity has a function of inhibiting platelet aggregation.

Single crystals were grown by vapour diffusion technique. The space group is $P6_1$, with a=b=83.57Å and c=32.72Å,and one molecule per asymmetric unit. Diffraction data to 2.0Å (Rmerge=4.18%) were collected on a Siemens multiwire X200-B area detector. The structure was solved by molecular replacement with Crowther's fast rotation and translation function, and the search molecule constructed from one subunit (L) of C. atrox PLA2. The structure was refined using programs PROLSQ and X-PLOR and model building techniques. The current model containing 133 water molecules gives a crystallographic R-factor of 0.157 and stereochemistry with root-mean-square deviation from ideality of 0.013Å or bond lengths and 2.7 degree for bond angles. The overall structure of the molecule is very similar to those of other phospholipase A2 of known structure. The catalytic site, hydrophobic channel as well as the N-terminal region show greatest structural conservation. The calcium-binding region has a conformation that resembles closely to that of bovine PLA2 , but not C. atrox PLA2. Compared with other PLA2, the conformation of C-terminal ridge shows significant difference due to the insertion of two residues. The putative site for platelet function was proposed.

Calcium ion is an essential cofactor for the catalysis. In order to study calcium ion induced conformational changes, calcium- free and calcium-containing PLA2 were crystallized and their diffraction data were collected to 2.0 and 1.6Å resolution respectively. The crystal structure analysis and comparison of the both PLA2 forms are in progress. The results will be presented.

Acknowledgments: This work was supported by grants from Academia Sinica and national natural science foundation.

3P12

CRYSTALLIZATION AND PRELIMINARY X-RAY STUDIES OF PHOSPHOENOLPYRUVATE CARBOXYLASE FROM *Escherichia coli*

Y. Nagara, T. Inoue, Y. Suzuki, R. Ohtsuka, K. Fukuhara, S. Nishiura, R. Kitagawa, H. Nakanishi, M. Hayashi, M. Inoue, S. Sugimoto and Y. Kai, Department of Applied Chemistry, Faculty of Engineering, Osaka University, Suita, Osaka 565, Japan
K. Izui, Department of Applied Botany, Faculty of Agriculture, Kyoto University, Sakyou-ku, Kyoto 606, Japan

Phosphoenolpyruvate carboxylase (PEPCase†; EC4.1.1.31) from *Escherichia coli* catalyzes CO_2-fixation to form oxaloacetate and inorganic phosphate. It is composed of four identical subunits with molecular weight of *ca.* 100,000 dalton. Although the primary structure was determined in 1984,[1] the molecular of PEPCase has not been determined. In order to study its biological function based on the three dimensional structure, we have crystallized PEPCase by using PEG4000 as precipitant,[2] however, the quality of the diffraction patterns was rather low. To get crystals suitable for X-ray crystallographic studies, hanging drop vapor diffusion method were examined in many conditions with variety of pH, molecular weight of PEG, and additives as control parameters. The crystals under the best conditions appeared in tetragonal bypyramidal shape with orthorhombic crystal lattice, space group *I*222. The unit cell parameters were determined to be a=117.9, b=250.0, and c=81.8Å (1Å= 0.1 nm). A set of intensity data for native PEPCase was obtained up to 3.4Å resolution using an imaging plate detector operated in the Rigaku RAXIS-IIc system with graphite monochromated CuKα radiation from a 12kW rotating anode generator. Among 93,327 accepted observations up to 3.4Å resolution, 29,756 independent reflections were obtained, the completeness of which was 87.6% with an R-merge of 7.4%. Another set of diffraction data was collected with synchrotron radiation in the Photon Factory, the National Laboratory for High Energy Physics (KEK), Tsukuba, Japan. Now, many data sets of heavy-atom derivatives are collecting to get the low resolution map of the enzyme.

1) Fujita, N., Miwa, T., Ishijima, S., Izui, K. & Katsuki, H. (1984) *J. biochem*, **95**, 909-916
2) Inoue, M., Hayashi, M., Sugimoto, S., Harada, S., Kai, Y. & Kasai, N. (1989) *J. Mol. Biol.*, **208**, 509-510

---

†Abbreviations used: PEPCase, phosphoenolpyruvate carboxylase

3P13

CRYSTAL STRUCTURE OF FERREDOXIN FROM A THERMOACIDOPHILIC ARCHAEON

T. Fujii and Y. Hata, Institute for Chemical Research, Kyoto University, Uji, Kyoto 611, Japan, and M. Oozeki, H. Moriyama, T. Wakagi, N. Tanaka and T. Oshima, Department of Life Science, Faculty of Bioscience and Biotechnology, Tokyo Institute of Technology, Nagatsuta, Yokohama, Kanagawa 226, Japan.

Archaea are classified into a third kingdom of biological world different from Bacteria and Eukarya. Many studies on the evolution of archaeon have been performed from the biochemical and biophysical aspects. In order to elucidate the molecular evolution of thermoacidophilic archaeal ferredoxin, we have determined the crystal structure of the ferredoxin from a thermoacidophilic archaeon, *Sulfolobus* sp. strain 7 .

Crystals belong to the space group $P4_32_12$ with unit cell dimensions $a = b = 50.12$ Å and $c = 69.52$ Å. Intensity data of the native and two heavy-atom derivative crystals were collected on an R-AXIS IIC using Cu-Kα radiation. Phase angles were determined at 2.0 Å resolution by a MIR method supplemented with anomalous effects from iron atoms of the iron-sulfur clusters. An electron density map calculated with these phase angles were improved by a solvent-flattening method. The density map enabled us to build the model. In spite of the entire interpletation, one high peak remained in the density map. The peak was identified to a zinc atom by anomalous Fourier techniques using data collected with X-rays of wavelengths 1.275 Å and 1.290 Å produced by the synchrotron radiation source of Photon Factory, KEK, Japan. The model was refined with X-PLOR to the present R-value of 19.1 % at 2.0 Å resolution.

The molecule consists of two parts: a core and an N-terminal extended parts. The folding of the core part is similar to the common folding among bacterial dicluster type ferredoxins, and has the [3Fe-4S] and [4Fe-4S] clusters. The N-terminal extended part is mainly constructed from three β-strands. The zinc atom is tetrahedrally liganded by four amino acid residues, and is placed at the interface between the core part and the N-terminal extended part. The analysis of the present ferredoxin is the first example for the presence of structural zinc in ferredoxin.

3P14

THE REFINED CRYSTAL STRUCTIRE OF BENCE JONES PROTEIN PAV AT 2.4Å AND ITS DOMAIN-DOMAIN ASSOCIATIONS

Chwan-Deng Hsiao[1], John Rose[2], S. Swaminathan[3], W. Furey[3], and Bi-Cheng Wang[2], [1]Crystallographic Laboratory, Institute of Molecular Biology Academia Sinica, Taipei, Taiwan, 11529, [2]Departments of Crystallography and Biological Sciences, University of Pittsburgh, Pittsburgh, PA 15260, Biocrystallography Laboratory, VA Medical center, Pittsburgh, PA 15240

The crystal structure of the protein Pav, a lambda type light-chain dimers, has been determined at 2.4Å resolution by Iterative Single Isomorphous Replacement (ISIR) with phase extension and crystallographic refinement. The final model consists of 3220 non-hydrogen atoms (no solvent atom) from 436 residues (two monomers) with a crystallographic R-factor of 0.234 for 15,570 reflections between 8-2.4Å resolution. The structure has root-mean-square deviations of 0.015Å from "ideal" bond length and 1.706^{o} from "ideal" bond angles. The angle formed by the local two-fold axes of the "variable" (V) and "constant" (C) domains, the "elbow bend" is 132.5^{o}, similar to Mcg light-chain dimer crystallized in deionized water. Whereas, the hapten-binding site formed by the two V domains of Pav light-chain dimer is similar to Loc light-chain dimer crystallized in ammonium sulfate in which the two variable domains formed a protrusion instead of the concave hapten binding cavity in other light-chain dimer and Fabs. The large side chains of residue Trp-92 from both V-domain in Pav are located in the middle of the entrance of the binding pocket when compare to concave hapten binding cavity. Therefore, the three-dimensional structure of Pav in the antigen-binding site may be considered as two independent concave binding pocket on opposite sides divided by two Trp-92 residues.

3P15

STRUCTURE OF BOVINE CYTOCHROME C OXIDASE AT 2.8Å RESOLUTION.

Hiroshi Aoyama[1], Eiki Yamashita[1], Takashi Tomizaki[1], Hiroshi Yamaguchi[1], Tomitake Tsukihara[1], Kyoko Shinzawa-Itoh[2], Ryosuke Nakajima[2], Rieko Yaono[2] and Shinya Yoshikawa[2]

[1]Institute for Protein Research, Osaka University, 3-2 Yamada-oka, Suita 565, Japan, Department of Life Science, [2]Himeji Institute of Technology, Kamigohri Akoh, Hyogo 678-12, Japan.

Bovine heart cytochrome *c* oxidase is a membrane protein complex with molecular weight of 200 KDa containing 13 different polypeptide subunits, 2 hemes A, two redox active copper sites, one zinc, one magnesium and possibly some phospholipids as the intrinsic constituents. This enzyme is one of the most intriguing biological macromolecules in the cell, since it reduces O_2 to H_2O at the active site with the four redox active transition metals coupling with proton pumping across the mitochondrial inner membrane. This enzyme have been explored most extensively among the enzymes involved in biological oxidation, ever since this enzyme was discovered. However, in spite of these extensive efforts, lack of the crystal structure at atomic resolution limits seriously understanding of the reaction mechanism of this enzyme.

Electron density distribution of oxidized bovine cytochrome *c* oxidase at 2.8 Å resolution indicated a dinuclear copper center with a novel structure similar to [2Fe-2S] type iron-sulfur center and the O_2 binding site containing heme a_3 iron and copper atoms (Cu_B) with an inter-atomic distance of 4.5 Å without any detectable bridging ligand between iron and copper atoms, in spite of a strong antiferromagnetic coupling between them. A hydrogen bond between a hydroxyl group of the long alkyl side chain of heme a_3 and a phenol OH of a tyrosine located near an imidazole group bonded to Cu_B and a phenyl alanine sandwiched between the heme a_3 and an imidazole liganded to the other heme (heme *a*) could either provide intra-molecular electron transfer pathways or induce the redox coupled conformational change.

3P16

PII: The Structure of a Signal Transducing Protein

D.L.Ollis, E. Cheah, P. Carr, P. Suffolk

Research School of Chemistry,
ANU, Canberra, ACT 0200, Australia

The balance of nitrogen in organisms is a key growth determinant and studies of the machinery that regulate this balance are of fundamental importance. PII is a signal transducing protein involved in the regulation of nitrogen metabolism in bacteria. It participates in the regulation of glutamine synthetase at the level of transcription and enzymatic activity and in so doing, interacts with a number of other proteins.

The protein is a trimer and at low resolution, could be described as a barrel with a loop projecting from the top surface. The protein fits into the alpha + beta category with three internal beta sheets packed against one another around a three fold axis. Each sheet consists of 8 strands which emanate from the three subunits. Each subunit also has two alpha helices which form the side of the barrel.

The loop of PII contains an exposed tyrosine that is uridylylated as part of the signalling process. Sequence comparison and other evidence suggest that the top of the barrel is important for interacting with other molecules. PII interacts with a number of effector molecules and these may bind in a cleft on the side of the molecule.

3P17

THE UTILITY OF 4-AMINOBENZOIC ACID IN THE PROMOTION OF HYDROGEN BONDING IN CRYSTALLIZATION PROCESSES

G. Smith, Centre for Instrumental and Developmental Chemistry, Queensland University of Technology, GPO Box 2434, Brisbane, 4001, Australia.

4-Aminobenzoic acid (4-ABA) is one of the most versatile of the carboxylic acids for cocrystal formation, promoting molecular self-assembly via hydrogen bonding through both the carboxylic acid group and the ring-substituted amino group. Since the first crystallographic characterization of a 1:1 adduct with 4-nitropyridine-*N*-oxide (Lechat, 1984), only two other complexes having potential as non-linear optical materials have been described [with 1,3-dimethyl-1-imidazolidinone (1:1) (Ueda *et al.*, 1986) and 3,5-dinitrobenzoic acid (1:1) (Etter & Frankenbach, 1989)], until the work completed by our group, summarized in this report. This includes five adducts with carboxylic acids, three with Lewis bases and one with a neutral organic species, while an unusual (3:1:1) 4-aminobenzoic acid : 2,4,6-trinitrobenzoic acid : 1,3,5-trinitrobenzene triheteromolecular adduct has also been found, being one of the three components associated with the 4-ABA : TNBA cocrystal product (Lynch *et al.*, 1992). While most of the adducts described are (1:1), both (1:2) and (2:1) cocrystals have been found [with 3,5-dinitrosalicylic acid (2:1) and 4-(4-nitrobenzyl)pyridine (1:2) (Smith *et al.*, 1995)]. Hydrogen bonding patterns are analyzed and the enhancement of the stability of these sytems noted particularly in those examples where protonation of the amino group of 4-ABA occurs {with 3,5-dinitrosalicylic acid [$(4\text{-ABA})^+(\text{DNSA})^-(\text{DNSA})$] and with pyrazine-2,6-dicarboxylic acid [$(4\text{-ABA})^+(\text{PDCA})^-$]}. In each case, the protonated group is subsequently involved in up to five interactive hydrogen bonding associations.

Etter, M.C. & Frankenbach, G.M. (1990). *Chem. Mater.* **1** ,10-12.

Lechat, J. (1984). *Acta Cryst.* **A40**, C-264.

Lynch, D.E., Smith, G., Byriel, K.A. & Kennard, C.H.L. (1992). *J. Chem. Soc. Chem. Commun.*, 300-301.

Smith, G., Lynch, D.E., Byriel, K.A. & Kennard, C.H.L. (1995). (unpublished work).

Ueda, M., Onishi, H. & Nagu, T. (1986). *Acta Cryst.* **C42**, 462-464.

3P18

MAD Analysis of Rat Liver Macrophage Migration Inhibitory Factor

Mamoru Suzuki[1]*, Hiroshi Sugimoto[1], Atsushi Nakagawa[1], Isao Tanaka[1], Mami Fujinaga[2], and Jun Nishihira[2]

[1]Division of Biological Sciences, Graduate School of Science, Hokkaido University, Sapporo 060, Japan
*Present address : Photon Factory, National Laboratory for High Energy Physics, Tsukuba 305, Japan
[2]Central Research Institutes, School of Medicine, Hokkaido University, Sapporo 060, Japan

Lymphocytes secrete a large number of soluble protein mediators, known as lymphokines, in response to antigenic or mitogenic stimulation. The first lymphokine discovered was macrophage migration inhibitory factor (MIF), which was originally identified by its ability to prevent the migration of guinea pig macrophage out of capillary tubes *in vitro*. It was speculated that MIF concentrates macrophages at the infection site and make them function in antigen processing and phagocytosis.

The recombinant macrophage migration inhibitory factor (MIF) of a rat liver was crystallized using the hanging-drop vapor diffusion method. We also crystallized a selenomethionyl rat MIF under similar conditions for X-ray structure analysis using multiwavelength anomalous diffraction (MAD) method. Furthermore, two kinds of selenomethionyl rat MIF mutants, in which one or two of three methionine residues were replaced by alanine were constructed and crystallized. These crystals belong to two different forms of the hexagonal space group $P6_3$. The first form(large cell) has cell dimensions of $a = b = 95.7Å$ and $c = 87.9Å$ and contains 2 dimers in an asymmetric unit. The second form(small cell) has cell dimensions of $a = b = 61.8Å$ and $c = 53.4Å$ with one monomer in an asymmetric unit. Intensity data sets of small cell were collected with synchrotron radiation at the BL18B beam line of Photon Factory, National Laboratory for High Energy Physics, Tsukuba, Japan.

We will report MAD analysis by selenomethionine anomalous scattering.

3P19

CRYSTAL STRUCTURE OF VHR, A DUAL-SPECIFIC PHOSPHATASE.

J. Yuvaniyama, M. A. Saper, Biophysics Research Division, The University of Michigan, 930 North University, Ann Arbor, MI 48109-1055, USA, J. M. Denu, and J. E. Dixon, Department of Biological Chemistry, The University of Michigan, Medical Science I Bldg., Ann Arbor, MI 48109-0606, USA.

The human VHR (VH1-related) phosphatase is a member of the class of phosphatases that possess an in vitro dual specificity towards both phosphoseryl or phosphothreonyl (alkyl phosphates) and phosphotyrosyl (aryl phosphate) substrates (1). Examples of other members of this group of proteins include cdc25, and the mitogen-activated protein (MAP) kinase phosphatases 3CH134, CL100, and PAC1. Thus, these dualspecific phosphatases are believed to be important regulators of cell cycle control and mitogenic signal transduction. Despite a limited sequence similarity between these dual-specific phosphatases and the protein tyrosine phosphatases (PTPases), they share the PTPase signature motif, HCxxGxxR. Biochemical studies have also shown similar trends in kinetic behavior between the two groups of enzymes.

We have recently determined the crystal structure of VHR to 2.4 resolution by the method of multiple isomorphous replacement (MIR) using three heavy-atom derivatives. This first structure of the dual-specific phosphatase shows structural similarity to the known structures of PTPases: human PTP1B and Yersinia YOP51, suggesting that the dual-specific phosphatases are indeed PTPases but with less specificity towards aryl phosphates. The comparison of these phosphatase structures reveals the substrate recognition loop present in PTP1B and YOP51, but absentin VHR. This missing loop responsible for phosphotyrosine recognition explains the basis of dual specificity in VHR. We show VHR can be used as a "core" structure to model structures of other dualspecific phosphatases such as 3CH134, CL100, and PAC1.

1) Denu, J. M., Zhou, G., Wu, L., Zhao, R., Yuvaniyama, J., Saper, M. A. & Dixon, J. E. (1995) J. Biol. Chem. 270(8), 3796-3803.

3P20

CRYSTAL STRUCTURES OF THE ACTIVE-SITE MUTANTS OF *ESCHERICHIA COLI* ASPARTATE AMINOTRANSFERASE

I. Miyahara, K. Okada, K.Hosomi and K.Hirotsu, Faculty of Science, Osaka City University, Sumiyoshi-ku, Osaka 558, Japan, and H. Kagamiyama, Department of Medical Chemistry, Osaka Medical College, Takatsuki, Osaka 569, Japan.

Aspartate aminotransferase (AspAT), which has a coenzyme, pyrydoxal 5'-phosphate (PLP) , catalyzes a reversible transamination reaction. On the basis of the X-ray structures of wild-type AspAT, a detailed reaction mechanism has been proposed. In order to understand the role of each active-site residue on the reaction, X-ray crystallographic study of single or multiple replacement mutants by site-directed mutagenesis have been undertaken.

The transamination reaction consists of many elementary steps in which the electron distribution within coenzyme or coenzyme-substrate conjugate must be changed. Some polar active-site residues, which have direct or indirect interactions with PLP, delicately control the pK_a of the PLP-Lys258 or PLP-substrate aldimine for the reversible proton transfer reaction. These active-site residues were replaced by non-polar amino acids and crystal structures of their mutants were determined. (N194A, N194A/ Y225F, N194A/R386L, etc.)

The replacement of polar side chains by non-polar ones has large effects on the enzyme activity, nevertheless, the active-site structures of the mutants are very similar to those of wild-type enzyme. The reason for this is that a water molecule occupies the position of the polar side chain or main chain to keep the hydrogen bonds previously formed. W140G belongs to an unusual case. In wild-type AspAT, the role of Trp140 is not only to make hydrogen bond with a substrate but also to make a parallel stacking to the pyridine ring of PLP. In the case of W140G, Trp is replaced by Gly and a water molecule which are too small to take the place of Trp, therefore, the distal residue, Pro141 stacks to the pyridine ring of PLP instead of Trp140.

3P21

UNIQUE POLYMORPHISM AND INCLUSION COMPLEX FORMATION OF DIANILINEGOSSYPOL

B.T.Ibragimov, K.M.Beketov and S.A.Talipov., Institute of Bioorganic Chemistry, H.Abdullaev, Str.,83, Tashkent, 700143, Uzbekistan

It is well known that gossypol, physiologically active compound of cottonseeds, is a versatile host giving clath rates with practically all small and medium size molecules.

In order to explain the universality of gossypol as host we have gradually changed its chemical structure and investi gated including properties of the obtained derivatives. Di aniline derivative of gossypol, a product of the condensa tion of gossypol with anyline, is one of them.

Dianilinegossypol has a good including ability too, but it cannot form clathrates with first members of the carbon acids and alcohols. The single crystals of 34 host-guest complexes are obtained and their crystallograp hic parameters are determined. The structure of 10 of them is solved. The peculiarities of dianilinegossypol clathra teformation are discussed in comparision with gossypol ones.

By changing the crystallization conditions 7 dianili negossypol polymorphs is obtained and identified by X-ray method. Another 3 polymorphic modifications of dianiline gossypol are obtained by decomposition its unstable host-guest complexes. The structure of 3 polymorphs is de termined. It is shown that no solid state thermotropic transitions between these polymorphs. Other a lot of inte resting peculiarities of dianilinegossypol polymorphism and clathrateformation will be discussed.

3P29

STRUCTURE ANALYSIS OF *N*-(2,4-DINITROPHENYL)-*o*-ANISIDINE AT HIGH TEMPERATURE USING IP-DIFFRACTOMETER

K. Takada, T. Watanabe, K. Taguchi, M. Yasui and F. Iwasaki, Dept. of Applied Physics and Chemistry, The Univ. of Electro-Communications, Chofu, Tokyo 182, Japan.

The structure analyses at several temperatures of *N*-(2,4-dinitrophenyl)-*o*-anisidine were performed. The diffraction data were measured by the Imaging-Plate-diffractometer equipped with the N_2-gas-stream high-temperature apparatus. This crystal has two modifications, orange and red forms, and exhibits a phase transition at the wide temperature range from 110 to 158°C depending on the specimen. We expected to catch some intermediate state of this phase transition from the diffraction data of the single crystal. Each data set was measured within 2 hours using same specimen. In order to study the time-dependent variation, 3 and 2 sets of data were measured every 3 hours at 120 and 130°C, respectively.

Crystal Data: $C_{13}H_{11}N_3O_5$, monoclinic, *P*2/a

Temp.(°C)	24	50	75	100	120	130
a /Å	21.538	21.555	21.514	21.592	21.554	21.594
b /Å	4.228	4.253	4.272	4.310	4.328	4.344
c /Å	16.743	16.736	16.655	16.714	16.694	16.716
β /°	122.29	122.28	122.22	122.21	122.12	122.08
No. observed	1612	1652	1601	1517	1370	1289
R	0.084	0.090	0.091	0.092	0.090	0.089

The crystal structures were successfully refined using each data set. The structure was revealed to be an orange form at the 130°C. Thus the phase transition did not occur in this case. However the cell parameters changed anisotropically during the heating. The b axis simply elongated while the a and c axes did not show significant changes. This lengthening corresponds to the widening of the distance between molecular planes which arrange vertically to the b axis. These results may partially support our plausible mechanism of the phase transition (Yasui, *et al.*, 1995). The data collections at higher temperature will be carried out.

Yasui, M., Taguchi, K. and Iwasaki, F. a paper in AsCA95.

3P30

CRYSTAL STRUCTURES OF TEMPO RADICALS SHOWING FERROMAGNETIC INTERACTION

H. Yamamoto, H. Yoshikawa, H. Mitsuda, K. Takada, M. Yasui, T. Ishida, T. Nogami and F. Iwasaki, Department of Applied Physics and Chemistry, The University of Electro-Communications, Chofu, Tokyo 182, Japan

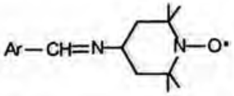

Recently some 4-arylmethyleneamino-TEMPO radicals (TEMPO = 2,2,6,6-tetramethyl-piperidin-1-oxyl) were revealed to show an intermolecular ferromagnetic interaction, of which **1** ~ **4** exhibit a ferromagnetic transition (Tc) at an extremely low temperature (Ishida, et al., 1994; Nogami, et al., 1994). **5** ~ **8** showed only a ferromagnetic interaction ($\theta > 0$), while **9** showed an anti-ferromagnetic interaction ($\theta < 0$). The X-ray structure analyses were performed on these crystals at room temperature to investigate whether any systematic intermolecular interactions were demonstrated among these crystals.

Crystal Data

	Ar	Tc/K	θ/K	Sp. gr.	a/Å	b/Å	c/Å	β/°	V/Å^3	Z
1	Ph	0.18	0.7	$P2_1/c$	12.684	11.740	11.024	111.40	1528	4
2	p-Cl-Ph	0.4	0.7	$P2_1/c$	5.909	24.475	11.421	103.84	1604	4
3	p-bi-Ph	0.4	0.6	$P2_1/c$	5.955	28.486	11.795	106.72	1916	4
4	p-phenoxy-Ph	0.2	0.4	$Pbc2_1$	5.993	30.565	22.032	90.0	4035	8
5	p-Br-Ph		0.5	$P2_1/c$	7.541	20.847	10.590	91.56	1664	4
6	3,5-di-Cl-Ph		0.7	Pbca	14.035	22.964	10.710	90.0	3452	8
7	3-pyridyl		0.4	$P2_1/c$	12.426	11.598	11.038	109.52	1499	4
8	naphthyl		0.3	$Pna2_1$	20.084	5.697	15.107	90.0	1728	4
9	p-F-Ph		-2.6	Pbca	20.010	15.249	10.417	90.0	3178	8

The molecular structures of these compounds are very similar. The arylmethyleneamino moieties are planar and almost perpendicular to the piperidine rings of which conformation is a chair form. For all crystals, **1** ~ **9**, two-dimensional O···O networks are constructed, although of which forms are various. The O···O distances are 5.47~8.75 Å. Between sheets the aryl groups of each sheet arrange alternately. The intersheet O···O distances are 8.96~13.40 Å. The sheet-like arrangement of the N-O radicals is considered to be essentially important for the magnetic interactions.

Ishida, T., Tsuboi, H., Nogami, T., Yoshikawa, H., Yasui, M., Iwasaki, F., Iwamura, H., Takeda, N. & Ishikawa, M. (1994). *Chem. Letters*, 919-922.

Nogami, T., Tomioka, K., Ishida, T., Yoshikawa, H., Yasui, M., Iwasaki, F., Iwamura, H., Takeda, N. & Ishikawa, M. (1994). *Chem. Letters*, 29 - 32.

3P31

THE CENTRAL C-C BOND LENGTH IN THE BI(ANTHRACENE-9,10-DIMETHYLENE) PHOTOISOMER: UNUSUAL ELONGATION AND CRYSTALLINE STATE REACTION

Jun Harada, Keiichiro Ogawa, and Shuji Tomoda, Department of Chemistry, College of Arts and Sciences, The University of Tokyo, Komaba, Meguro, Tokyo 153, Japan

The central bond length in the title compound (**1**) has been a subject of considerable interest because of the anomalously long C–C bond (1.77 Å) obtained from X-ray analysis by Ehrenberg (1966). This has been widely accepted as one of the longest C–C single bonds and several attempts to rationalize it have been made. Allinger and his co-workers estimated the bond length to be 1.64 Å from the molecular mechanics and the *ab initio* calculations (1993). They state "it seems clear that the X-ray results are unreliable." Very recently Siegel and his co-workers redetermined the X-ray structure of **1** and showed that the C–C bond length is 1.648(3) Å (1995). This value closely agrees with the structures obtained from HF and DFT calculations. This paper shows that the anomalous elongation of C9–C10' bond of **1** in the previously reported X-ray structure is ascribed to an unresolved disorder caused by the partial cycloreversion of **1** to **2** in the crystalline state and that the true bond length of C9–C10' is 1.66 Å.

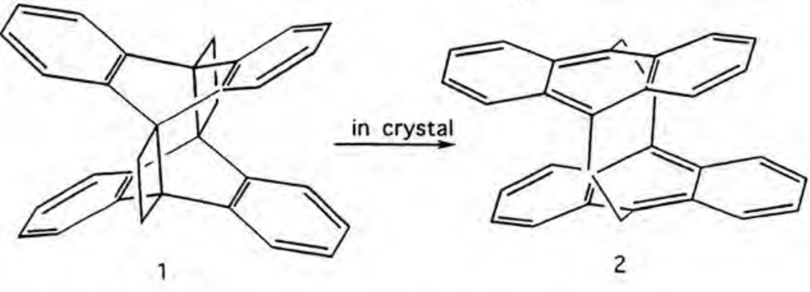

1 2

Battersby, T. R., Gantzel, P., Baldrigde, K. K. & Siegel, J. S. (1995) *Tetrahedron Lett.*, **36**, 845-848.

Ehrenberg, M. (1966). *Acta Cryst.*, **20**, 183-186.

Zhou, X., Liu, R. & Allinger, N. L. (1993). *J. Am. Chem. Soc.*, **115**, 7525-7526.

3P32

CRYSTAL STRUCTURES OF COPPER COMPLEXES SHOWING FERROMAGNETIC INTERACTION

Y. Ishikawa, M. Yasui, F. Iwasaki, T. Ishida and T. Nogami, Dept. of Applied Physics and Chemistry, The Univ. of Electro-Communications, Chofu, Tokyo 182, Japan.

We have determined the crystal structures of complexes of copper(II) bis(1,1,1,5,5,5-hexafluoropentane-2,4-dionate), Cu(hfac)$_2$, with a quinazoline (**I**) and a pyrimidine (**II**). Both complexes were revealed to exhibit a ferromagnetic interaction. The ferromagnetic transition of **I** was observed at about 0.12K (Ishida *et al.*, 1994). However **II** does not show a ferromagnetic transition at a low temperature.

Crystal Data:

	Sp. Gr.	*a* /Å	*b* /Å	*c* /Å	β /°	Observed	R
I	$P2_1/n$	12.300(2)	12.123(2)	15.155(2)	102.46(1)	2704	0.044
II	$I4_1cd$	18.598(1)	18.598(1)	22.331(3)	90.0	1559	0.060

In each crystal, Cu atoms have the distorted octahedral structures. For **I**, two quinazoline moieties coordinate to a Cu atom on both axial positions and bridge the complexes to form a one-dimensional chain. There are two types of crystallographically independent Cu atoms which are located on the center of symmetry. The Cu···Cu distance within a chain is 6.06Å. In **II**, one pyrimidine coordinates on the axial and another one on the equatorial position. **II** also has a structure of a one-dimensional chain. The Cu···Cu distance within a chain is 6.01Å. The first and second shortest Cu···Cu distances between chains are 8.68 and 10.59Å for **I**, and 9.30 and 9.82Å for **II**. We presume that some critical differences may exist in the inter-chain interaction between **I** and **II**.

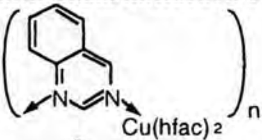

I

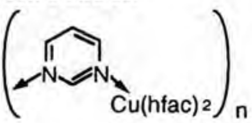

II

Ishida, T., Mitsubori, S., Nogami, T., Ishikawa, Y., Yasui, M., Iwasaki, F., Iwamura, H., Takeda, N., and Ishikawa, M. (1995). *Synthetic Metals*, **71**, 1791–1792

3P33

CRYSTALLINE-STATE RACEMIZATION OF BULKY GROUPS ON EXPOSURE TO VISIBLE LIGHT

Yuji Ohashi and Hiroyuki Sato, Department of Chemistry, Tokyo Institute of Technology, Ookayama, Meguro-ku, Tokyo 152, Japan, and Yoshifusa Arai and Yoshiaki Ohgo, Niigata College of Pharmacy, Kamishineicho, Niigata 950-21, Japan

we found that the chiral cyanoethyl group bonded to the cobalt atom in some cobaloxime complex crystals was racemized by X-ray or visible light with retention of the single crystal form. The rate of the racemization was so slow that we can see the structural change directly by X-ray analysis. Recently the chiral group was replaced with bulkier groups, bis(ethoxycarbonyl)ethyl (bece) and bis(allyoxycarbonyl)ethyl (bace) groups. Several cobaloxime complexes were prepared with different axial base ligands. Among the complex crystals, the bace complex with pyridine as an axial base ligand (bece-py) and the bace complex with water as an axial base ligand (bace-aqua) showed the gradual cell changes on exposure to a Xe lamp and the racemization occurred with retention of the single crystal form.

The bece-py crystal has the space group $P2_12_12_1$ and has one molecule in the asymmetric unit. When the crystal was exposed to the Xe lamp, the chiral bece group was transformed to the disordered racemates. On the other hand, the bace-aqua crystal has the space group $P2_1$ and has two crystallographically independent molecules in the asymmetric unit. One of the two bace groups was fully inverted to the opposite configuration on exposure to the Xe lamp and the space group was changed to $P2_1/n$.

In order to explain why only these two crystals were converted to racemic crystals without degradation of the crystallinity, the reaction cavity was drawn for each crystals. From the size and shape of the reaction cavity, the inversion mechanism of the chiral group was made clear.

3P34

CYCLIC O-H···N/C-H···O H-BOND COUPLING IN THE DESIGN OF SUPRAMOLECULAR ASSEMBLIES

V. R. Pedireddi and W. Jones, Department of Chemistry, University of Cambridge, Lensfield Road, Cambridge CB2 1EW, U. K. and A. P. Chorlton and R. Docherty, Zeneca Specialities, PO Box 42, Hexagon House, Blackley, Manchester, M9 3DA, U.K.

The exploitation of both strong (O-H···O, N-H···O etc.) and weak (C-H···O) H-bonds in the design of supramolecular assemblies is currently of interest. In many cases, individual H-bonds are arranged as rings - the well-known case of carboxylic acid pairs is a good example, Scheme 1(a). To date, however, no cyclic couplings which have been identified as being important in building assemblies consist of both a strong and a weak H-bond, Scheme 1(b).

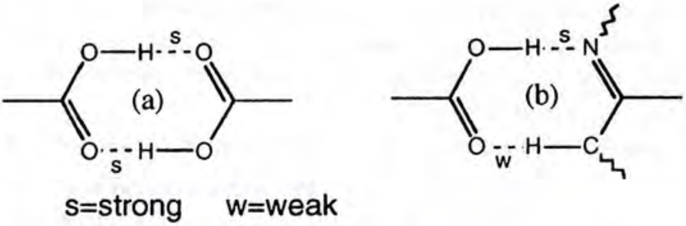

Scheme 1

To illustrate the use of this particular coupling in building supramolecular arrays we have studied the co-crystal formation of phenazine with various carboxylic acids. We have also investigated the extent to which this particular coupling exists within structures in the Cambridge Structural Database (CSD). Whilst structures containing this motif have been deposited, its role in influencing crystal packing does not seem to have been appreciated.

3P35

LAYERED STRUCTURES OF ANTIFERROELECTRIC MESOGENS

K. Okuyama, N. Kawano, S. Uehori and K. Noguchi, Faculty of Technology, Tokyo University of Agriculture and Technology, Koganei, Tokyo 184, Japan, and N. Okabe, Y. Suzuki and I. Kawamura, Central Research and Development Laboratory, Showa Shell Sekiyu Co. Ltd., 123-1 Shimokawairi, Atsugi 243-02, Japan

Recently, antiferroelectric mesogens attract much attention not only from their application to flat-panel displays but also from relationships between physical properties and their unique bilayered superstructures. Based on the physicochemical observations, the structure of antiferroelectric liquid crystal phase was proposed to be one of the smectic C phases and termed the antiferroelectric chiral smectic liquid crystal (SCA*) phase. According to the proposed structure for this phase, all the mesogen molecules in one smectic layer tilt in one direction and those in the neighboring layers tilt in the opposite direction (herringbone structure). Because of this alternate tilting from layer to layer, the total spontaneous polarization in one layer is canceled by that in the adjacent layer. By applying external electric field, the spontaneous polarization were aligned in the same direction, which induced a ferroelectric state. In this study, the crystal structures of several antiferroelectric mesogens were investigated by an X-ray diffraction method.

In spite of the chemical similarities of mesogen compounds, they showed different characteristics. Three of them ((1), (2) and (4) in Fig.1) have their SCA* phases just above their crystal phases. Structure analyses showed that the layer structures of (1) and (4) were a herringbone structure similar to the proposed structure of SCA* phase mentioned above. The packing structure of (2), however, was rather similar to that of (3) which had the intermediate phase between SCA* and crystal phases. No close relation was found between these structures and the proposed structure for SCA* phase. The direction of dipole moments calculated from the obtained conformations of (1) and (4) in one layer coincided with one of the axes parallel to the layer plane. However, since the dipole moment in the next layer had the same magnitude and the opposite direction, the over-all dipole moment became zero as proposed for the SCA* phase.

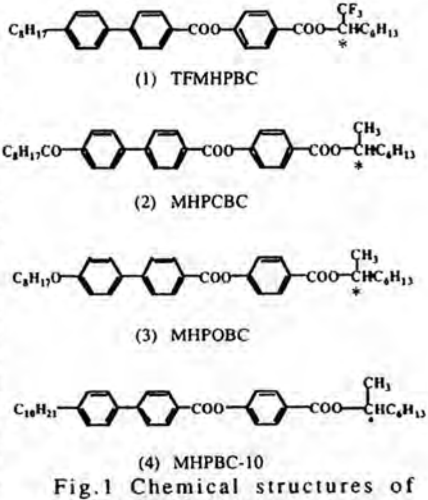

Fig.1 Chemical structures of antiferroelectric mesogens

3P36

COMPLEX FORMATION OF SURFACTANT MOLECULES WITH AROMATIC COMPOUNDS IN A MORTAR

Keiju Sawada and Yuji Ohashi, Department of Chemistry, Tokyo Institute of Technology, 2-12-1, O-okayama, Meguro-ku, Tokyo 152, Japan, and Nahoko Iimura and Hirotaka Hirata, Niigata College of Pharmacy, 2-13-5 Kamishin'eicho, Niigata, 950-21, Japan

Various complexes were recrystallized from an aqueous solution with cationic surfactants and aromatic compounds; i.e. Cetyltrimethylammoniumbromide ($C_{16}H_{33}N(CH_3)_3$, CTAB) and o-iodophenol ($I\text{-}C_6H_4\text{-}OH$). Their structures were analyzed using X-ray diffraction analysis. The mixture of the two compounds in a mortar were also analyzed using powder X-ray diffraction analysis, which revealed that the complexes were formed only by mixing surfactant molecules with aromatic compounds in a mortar. There are hydrogen bonds between these molecules. It was expected that the hydrogen bond is a driving force to form these complexes.

In this study, we succeeded to obtain complex of CTAB and biphenyl ($C_{10}H_8$) in aqueous-methanol solution (Fig.1). But these molecules have no interaction as hydrogen bonds. CTAB and biphenyl were mixed in a mortar, then the mixture were also analyzed by X-ray powder diffract meter. The same pattern as that of the complex crystals was obtained. This means that there should be an interaction between the alkyl group and the aromatic rings and that the driving force of these formation must be the interaction.

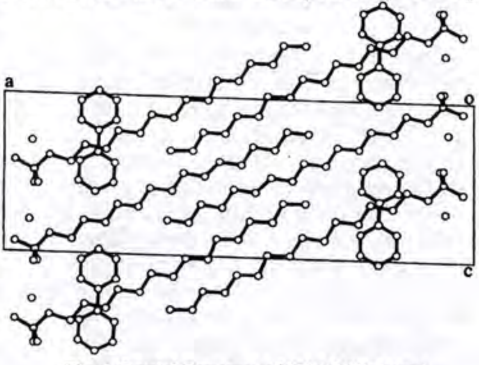

Fig. 1 Crystal Structure of CTAB/Biphenyl

3P37

GENERATION OF ASYMMETRY IN THE CRYSTALLINE STATE PHOTOISOMERIZATION OF COBALOXIME COMPLEX

T. Yoshimiya, A. Sekine and Y. Ohashi, Department of Chemistry,
Tokyo Institute of Technology, O-okayama, Meguro-ku, Tokyo 152.

It has been found that the 2-cyanoethyl group bonded to the cobalt atom in some cobaloxime complex crystals is isomerized to the 1-cyanoethyl group on exposure to visible light in the solid state. Recently the 2-cyanoethyl group of the complexes with 3-methylpyridine, 4-methylpyridine as axial base ligands was found to be isomerized with retention of the single crystal form. The generation of the asymmetry of the produced 1-cyanoethyl group was clearly observed by the crystal structure analysis after the isomerization. In order to obtain the quantitative relation between the chirality of the produced group and the asymmetry around the reactive group, the isomerization of the complex with 4-ethylpyridine as an axial base ligand has been analyzed.

The title complex was synthesized in the same way as reported previously and the crystal structure before the irradiation was analyzed by X-rays. The crystal is triclinic, the space group being $P\bar{1}$ and Z=2.; a=11.218(3), b=11.265(3), c=9.390(2)Å, and, α=93.30(2), β=114.05(2), γ=98.68(2)° and V=1061.8(5) $Å^3$. The crystal was exposed to a 500W Xe lamp for 168 hours. The crystal was not decomposed, but the cell dimensions were significantly changed; a=11.162(3), b=11.309(2), c=9.347(2)Å, and, α=93.38(2), β=113.78(2), γ=97.66(2) ° and V=1061.8(5) $Å^3$. The produced 1-cyanoethyl group does not take a disordered racemate but an ordered chiral one. This clearly indicates that the asymmetry is generated in the chiral crystal environment.

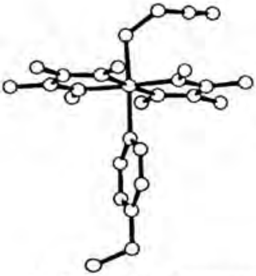

Molecular Structure
before the irradiation

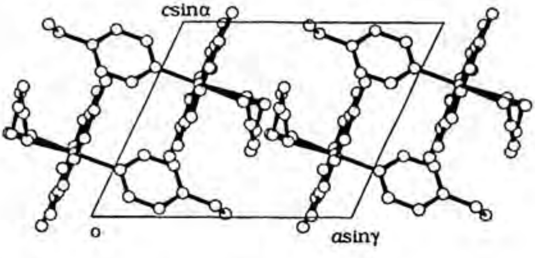

Crystal Structure
after the irradiation

3P38

CHEMICAL BOND AND ATOMIC DISPLACEMENTS IN $Ba_{0.87}K_{0.13}BiO_3$ CRYSTAL

Yu. A. Abramov*, I.M. Reznik# and V.G. Tsirelson$

* National Institute For Research in Inorganic Materials, Tsukuba, Japan
# Physical Technical Institute, Donetsk, Ukraine
$ Mendeleev University of Chemical Technology, Moscow, Russia

The electron density distribution and Bi atom displacements in $Ba_{0.87}K_{0.13}BiO_3$ perovskite single crystal are studied using both X-ray diffraction data (Wignacourt J.P. et al. (1980). Appl.Phys.Lett. 53. 1753-1756) and modified statistical method calculations. A noticeable covalent component in the Bi bond with neighbouring oxygens is revealed. The nature of the Bi atom anharmonic displacements reflect either dynamic or static instability in its ideal crystallographic position. The results obtained indirectly support the interpretation of the nature of incommensurate modulation in $Ba_{1-x}K_xBiO_3$ crystals under electron-irradiation (Verweft M. et al. (1991). Phys. Rev. B44. 9547-9555)

Support of this research by the International Scientific Foundation (Grant U1G000) is gratefully acknowledged.

3P39

HRTEM CHARACTERIZATION OF HOMOLOGOUS SERIES OF SUPERCONDUCTORS $GaSr_2Ca_{n-1}Cu_nO_{2n+3}$ (n=3 AND 4)

J. Ramirez-Castellanos*, Y. Matsui and E. Takayama-Muromachi, National Institute for Research in Inorganic Materials, Tsukuba, Ibaraki 305, Japan, and M. Isobe, Sony Co. Research Center, Yokohama 240, Japan. (*Also at, Department of Applied Physics, Tsukuba University, Tsukuba 305, Japan)

Recently, Isobe et al. [1] reported that a new homologous series of superconductors, $GaSr_2Ca_{n-1}Cu_nO_{2n+3}$; or *Ga-12(n-1)n*, are obtained under high-pressure (6GPa, 1250°C), and that superconductivity apper at T_C=70 K (for n=2 and 3) and at Tc=107 K (for n=4). Powder X-ray and neutron diffraction data suggested that they have pseudo-tetragonal orthorhombic structures (*Ic2m*), with lattice parameters $a \approx b \approx \sqrt{2}a_p$ & $c \approx (2n+2)a_p$, where a_p is the parameter for the cubic perovskite. The electron diffraction patterns, however, shows weak extra-reflections in some diffraction networks and this indicates that a double periodicity along *b*-axis ($b = 2\sqrt{2}a_p$) are formed, due to "intra-layer" ordering of two types of GaO_4 chains (*R* and *L*). It is also found that these extra reflection spots have strong streaking along the c*-direction, as seen in Fig.1 [2]. This indicates that "inter-layer" disordering of the *R* and *L*-types of GaO_4 chains is formed, as previously suggested for *Ga-1212* structures [3]. The corresponding HRTEM image, in Fig.2, shows such disordering clearly [2].

References
[1] M. Isobe et al. (1994) Physica C222, 310.
[2] J. Ramirez-Castellanos et al. (1995) Physica C, in the press.
[3] T. Krekels et al. (1993) J. Solid State. Chem. 105, 313.

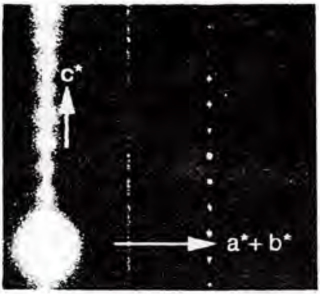

Fig. 1. Electron diffraction pattern of Ga-1223 projected on [1$\bar{1}$0], showing streaking along the c*-direction.

Fig. 2. HRTEM image of Ga-1223 projected along [1$\bar{1}$0], showing "inter-layer" disordering of GaO_4 chains.

3P40

ANALYSIS OF QUASICRYSTAL STRUCTURES BY USE OF POWDER NEUTRON AND SINGLE CRYSTAL X-RAY DATA

Akiji Yamamoto, National Inst. Res. Inorg. Mat. Namiki 1, Tsukuba, 305 Japan, Tsuyoshi Kajitani, Dept. Appl. Phys. Tohoku University, Aramaki, Sendai, 980, Japan, Yukio Morii, Japan Atomic Energy Research Institute, Tohkai-Mura, Ibaraki, 319-11, Japan

There exist many difficulties in the structure analysis of quasicrystals, which are usually ternary alloys. One of them is the determination of partial occupancies of a site. It is known that one site is occupied by Al and Cu statistically in icosahedral Al-Cu-Li quasicrystals. In order to determine the partial occupancy of a site, it is efficient to refine it in binary alloys. On the other hand, there are two partial occupancies for a site in ternary alloys and there exists the correlation between them when only one data set is used. The combined use of X-ray and neutron diffraction data will reduce the correlation because these two have independent information for the partial occupancies. For this purpose, we developed a program in which the Rietveld method and the single crystal method are used. In the program, the sum of the weighted R factors of two data sets are minimized by the least-squares method. It was applied to the analysis of face-centered icosahedral Al-Pd-Mn with the 6-dimensional superspace group $Fm\overline{35}$, where single crystal X-ray and powder neutron data were used. The X-ray data include 1137 independent reflections (Yamamoto, et al. 1993) while 249 reflections are used in the Rietveld method. The correlation between two partial occupancies seems to be large but the divergence of the least-squares method could be restrained by using a large Marquardt parameter in the normal matrix and the partial occupancies were refined. The final R_w factors were 0.103 for X-ray and 0.107 for neutron data.

Yamamoto A., Sato A., Kato K. Tsai A. P. and Masumoto T. (1993) *Mat. Sci. Forum* **150-151**, 211-221.

3P41

A NEW BARIUM COPPER OXYCHLORIDE, $Ba_2Cu_3O_4Cl_2$; ITS SYNTHESIS AND CRYSTALLOGRAPHIC CHARACTERIZATION

Zhigang. Zou, O. Tachikawa and H. Horiuchi
Mineralogical Institute, Graduate School of Science,
University of Tokyo, 7-3-1 Hongo, Bunkyo-ku, Tokyo 113, Japan.

A new crystalline phase of oxychloride, $Ba_2Cu_3O_4Cl_2$, was synthesized by a reaction of the mixture of CuO, $BaCl_2$, $Ba(OH)_2$ and KCl, and by a heat treatment of the hold for 6 hours at 800°C and gradual decrease of the temperature to 650°C by 48 hours. $Ba(OH)_2$ and KCl apparently play a role of flux. The atomic ratio of the product was analyzed by EPMA, and the result of Ba:Cu:Cl=2:3:2 was obtained. In order to examine the oxygen content of the product, it was heated up to 850°C by the rate of 5°C/min in air, and the weight loss by this heat treatment was 9.17%. The final phase obtained by this process was identified as $Ba_2Cu_3O_5$[1] by X-ray powder diffraction. As a result, the chemical composition of the initial phase was confirmed as $Ba_2Cu_3O_4Cl_2$. By these experiments, the valency of Cu was concluded to be +2 in this crystal structure. The product was cystallographically examined by precession camera, X-ray powder and single crystal diffraction methods. As a result, the crystal structure was found to belong to a tetragonal system with lattice constants of a=5.519(1)Å and c=13.834(2)Å. Diffraction symmetry is *4/mmm* with a body-centered lattice. Detailed crystal structure of the product is now under investigation.

[1] Kubel, F. and Janner, A.-M.(1993). Acta Cryst. C49, 657.

3P42

SYNCHROTRON RADIATION IMAGING OF THE DEFORMATION ELECTRON DENSITY IN $LiNbO_3$ and $LiTaO_3$

R Hsu, E N Maslen and V A Streltsov, *Crystallography Centre, University of Western Australia, Nedlands, WA 6907, Australia* and N Ishizawa, *Research Laboratory of Engineering Materials, Tokyo Institute of Technology, 4259 Nagatsuta, Midori-Ku, Yokohama 227, Japan*

Diffraction imaging of the deformation density ($\Delta\rho$) in $LiNbO_3$ and $LiTaO_3$, using the four-circle diffractometer on BL14A at the Photon Factory in Tsukuba, Japan, has clarified the relationship of ferroelectricity to structure, atomic vibrations and deformation density. Both analyses indicate substantial exchange transfer of electron density from the Nb(Ta) atom to a more open region of the structure within the large O_3 triangle near the Li atom. Hirshfeld partitioning of $\Delta\rho$ indicates that approximately two electrons are transferred to the Li atom, whereas the O atoms carry a charge of only -0.3 electrons. The Nb(Ta) atoms carry a positive charge of approximately 3 e. Spontaneous polarisations $P_{LiNbO_3} = 43$ and $P_{LiTaO_3} = 33$ ($\times10^{-2}Cm^{-2}$) calculated from these charges agree qualitatively with the experimental values of 71 and 50 ($\times10^{-2}Cm^{-2}$) respectively. The calculated and experimental ratios P_{LiNbO_3}/P_{LiTaO_3} are similar. The Li atom' role in the polarisation process is pivotal. In the high temperature paraelectric phase the Li atom forms three short Li-O bonds to coplanar O atoms, whereas the Nb(Ta) atom is the central metal atom in a regular MO_6 octahedron. In the low temperature ferroelectric phase both the Li and the Nb(Ta) atoms move from the ideal paraelectric positions to off-centre positions in irregular MO_6 octahedra. The O atoms have limited influence on the deformation density in both compounds, which has strong but approximate symmetry determined by the cation lattices. The two strongest Li–Nb(Ta) vectors in the structures are both markedly shorter than all Li-Li, Nb-Nb or Ta-Ta vectors, as would be expected if the A and B cations in the distorted perovskite structure carry charges of opposite sign.

Structure factors for small flux grown $LiNbO_3$ crystals measured using focused $\lambda = 0.7$ Å synchrotron X-radiation (Tsukuba, Japan). Space group *R3c*, rhombohedral, $M_r = 147.8$, $a = 5.493$ (2) Å, $\alpha = 55.89°$ (3), $V = 318.2(3)$ Å^3, $Z = 2$, $D_x = 4.629$ Mg m^{-3}, $\mu 0.7 = 5.01$ mm^{-1}, $F(000) = 136$, $T = 293$ K, $R = 0.015$, $wR = 0.015$, S = 3.276 (84), $y_{min} = 0.27$ for 773 unique reflections.

3P43

TOPOLOGICAL STUDY ON THE ELECTRON DENSITY DISTRIBUTION OF BIS(DIIMINOSUCCINONITRILO)NICKEL, NI($C_4N_4H_2$)$_2$

Tsong-Song Hwang and Yu Wang*, Department of Chemistry, National Taiwan University, Taipei, Taiwan

Planar molecule Ni($C_4N_4H_2$)$_2$ is roughly in D_{2h} symmetry and its electronic structure can be written as a combination of several resonance forms. Its bonding character is very interesting and suitable to be analyzed via low temperature x-ray diffraction experimentally and molecular orbital calculation theoretically. Deformation density distribution using these two methods give solid confirmation on π-delocalization phenomena on the ligand. The asphericity on electron density around Ni atom conforms to the crystal field theory. Topological study based on the total electron density of the molecule gives also valuable information about chemical bond. Atom domains, bond paths and bond critical points can be deduced both experimentally and theoretically. There are two ring critical points(RCP) located at the center of each ligand. Bond critical points(BCP) are formed along Ni-N, N-H, N-C, C-C, C=C, C≡N bonds. From the charge density (ρ), the laplacian ($\nabla^2\rho$) and the three hessian eigenvalues($\lambda 1,\lambda 2,\lambda 3$) at the bond critical points, the bonding characters are quantitatively described. According to these values, the bond strength as well as σ, π-characters can be compared. It is apparent that C≡N bond is the strongest bond and the electron density along the bond is cylindrically distributed, characterized as triple bond. Each atom in molecule is enclosed by a zero-flux surface called atom domain. It contains constant charge, dipole, quadrupole and higher moment within this atom domain. The bond path is the maximum density line between two bonded atoms. The collection of all these bond paths in molecule should give the shape of the molecule. The gradient vector of charge density ρ helps to locate the critical point and atom domain. The agreement on the topological properties derived from experiment and theory is very good. This means that the experimental multipole model and the molecular orbital calculation are complementary with each other.

3P44

Electron Density Studies of Cobalt(II) Octaaza Bis - α - diimine Macrocyclic Complex $[Co(C_{10}H_{20}N_8)(H_2O)_2]^{2+}[ClO_4]_2^{2-}$

Jey-Jau Lee, Yuan-Shyane You , Gene-Hsiang Lee, Yu Wang.,
Department of Chemistry, National Taiwan University, Taipei, Taiwan

Abstract:

The Crystal and molecular structure of $[Co(C_{10}H_{20}N_8)(H_2O)_2]^{2+} \cdot [ClO_4]_2^{2-}$ has been determined by single - crystal X-ray diffraction method at 295 and 125 K. It crystallizes in the space group of P bca at 125 K with cell parameter a=11.655(2), b=16.930(4), c=10.508(2)Å, Mw=556.27, V=2073.4(6)($Å^3$), Z=4. The final agreement index R is 0.033 and Rw is 0.037 based on 5547 observed reflections ; the site symmetry of cobalt is at -1 .

The Cobalt is in the same plane of the macrocyclic ring , the two axial directions are coordinated by two water molecules. The Co-N distances of the macrocyclic ring plane is 1.9026(7)Å and 1.9153(7)Å, the axial Co-O distance is 2.2854(9)Å. The CoN_4O_2 can be associated as a tetragonal distorted octahedron due to Jahn - Teller distortion . The ligand is a partially π-delocalized α - diimine, the C–N bond distance is 1.301(1),indicating a double bond character .

Electron density distribution based on multipole refinement confirms the predication on the asphericity in electron density around Cobalt. The bonding between α - diimine nitrogen and Co can be described as a weak covalent bond with N at the ligand served as a σ - donor. The d-orbital populations are derived from the multipole model, the populations in d_π orbitals are more than those on d_σ orbitals. This gives a low spin d^7 configuration. the C-C,C-N bond of the ligand are showing strong covalent bond character as indicated in the electron density distribution. Further analyses on the bond characterization will be made by comparative study on molecular orbital calculation.

EFFECT OF A MAGNETIC FIELD ON NICKEL-PLATINUM ALLOYS

D. K. Saha, Atomic Energy Centre, P. O. Box - 164, Dhaka 1000, Bangladesh and K. Ohshima, Institute of Applied Physics, University of Tsukuba, Tsukuba 305, Japan.

Magnetic properties of $Ni_{1-x}Pt_x$ alloys were studied in both the disordered and ordered states for x=0.25, 0.35, 0.44 and 0.50. Different magnetic fields were applied in the range from 0 to 800 Oe for the disordered state and from 0 to 10 kOe for the ordered state under the zero-field cooling condition with the temperature range from 5 to 400 K. For x=0.25 and 0.35 alloys, a ferromagnetic moment was observed in both the disordered and ordered states for the whole magnetic-field range. In the ordered state, an unusal behavior of the magnetic moment was observed, which is independent of magnetic field. For the x=0.44 alloy, a ferromagnetic moment was observed in the disordered state, but peculiar results were observed in the ordered state. A weak ferromagnetic moment appeared at 0 to 10 Oe magnetic field but from 50 up to 1000 Oe magnetic field, an antiferromagnetic-type feature is seen, where the antiferromagnetic-paramagnetic transition temperature T_N decreases momotonically with increasing magnetic field. Further, from 1200 Oe up to 10 kOe , the paramagnetism is evident. Hysteresis-loop data and the curve of the inverse of the magnetic susceptibility confirmed antiferromagnetism in the alloy. This is the first observation to our knowledge for such a change under an applied magnetic field in the binary alloys. For the x=0.50 alloy, a ferromagnetic mement in the disordered state and a clear paramagnetic moment in the ordered state observed for the whole magnetic-field range.

3P46

ATOMIC RADII FROM ELECTRON DENSITIES

E. N. Maslen and B.E. Etschmann
Crystallography Centre, University of Western Australia, Nedlands, 6907, Australia

In principle the radius of an atom is a physical property that can be defined uniquely, but the values obtained by partitioning bonds between identical atoms [1] are not necessarily appropriate to bonds between different atoms [2]. In practice different scales proposed for radii reflect alternative methods for partitioning interatomic distances. We have tested the existence of a well defined relationship between the ground state electron configuration for free atoms, the corresponding one-electron density and the atomic radii invoked when predicting structural geometry.

The invariant component of the radius associated with the atomic cores can be equated quite accurately to the value at which the integral of the density equals the number of core electrons. The most significant additional contributions is from the valence electrons which, unlike the cores, must be treated as penetrable when determining their contribution to the radius. The main requirement when evaluating atomic radii from atomic electron densities is to evaluate the penetrability of the valence subshells. Sub-shell penetrability increases with bond order, and decreases with the angular momentum quantum number. The investigation so far indicates that the effect of the principle quantum number on the penetrability of the valence sub-shells is small. Interatomic distances can be represented only approximately as sums of invariant atomic radii. The distances are affected to second order by exchange interactions with electrons that do not participate directly in bonding, including those in other neighbouring atoms. Predicting accurate bond lengths requires the development of formulae which specify those second order corrections. The approaches have been tried out so far on diatomic molecules, where the results are promising. It is likely that they will extend successfully to poly-atomic molecules and crystalline materials.

[1] Shannon, R.D. & Prewitt, C.T. (1969). *Acta Cryst* **B25**, 925-946

[2] Slater J.C. (1965) *Quantum Theory of Molecules and Solids*. Vol II, McGraw-Hill: New York

3P47

Crystal Structure Refinement of Silk Fibroin:*Bombyx mori*

Yasuhiro Takahashi, Department of Macromolecular Science, Faculty of Science, Osaka University, Toyonaka, Osaka 560, Japan

In 1955, the crystal structure of silk fibroin was proposed by Marsh et al.[1] Their model was based on quantitative intensity estimation of six equatorial reflections and qualitative intensity comparison of the layer line reflections. In the previous papers,[2, 3] the crystal structure analysis of silk was reexamined based on 35 reflections newly collected by using the drum scan densitometer. And it was clarified that the crystal region is composed of rather irregular stacking of the sheet structures formed by hydrogen bonds, in which the pleated-sheet molecules are arranged in the different antiparallel manner (antipolar-) from the one proposed by Marsh et al. (polar-). Silk assumes the crystal structure in which two antipolar-antiparallel sheets related by a two-fold rotation axis parallel to the b-axis statistically occupy a crystal site with different probabilities. The refinement was made by using the constrained least-squares method,[4] where the bond lengths and bond angles were fixed on the accepted values, the same conformation was assumed for the symmetrically independent molecules, and the anisotropic temperature factor $\exp\{-[(ha^*/2)^2 B_x + (kb^*/2)^2 B_y + (lc^*/2)^2 B_z]\}$ was adopted. The R-factor reduced to 7.5 %. The crystal structure is shown in Figure.

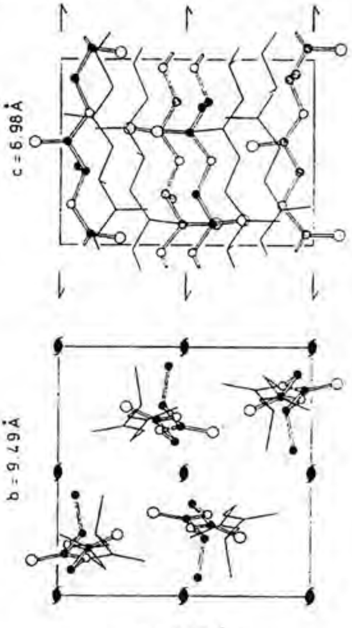

1. Marsh, R. E. et al. (1955). *Biochim. Biophys. Acta* **16**, 1.
2. Takahashi, Y. et al. (1991). *J. Polym. Sci. Polym. Phys. Ed.* **29**, 889.
3. Takahashi, Y. *ACS Symposium Series* **544** *"Silk Polymers"*, Chapter 15, 1993.
4. Takahashi, Y. et al. (1973). *J. Polym. Sci. Polym. Phys. Ed.* **11**, 233.

3P48

Physicochemical investigations on natural spinel ($MgAl_2O_4$)

C. P. Udawatte, Institute of Fundamental Studies, Kandy, Sri Lanka
R. P. Gunawardena, University of Peradeniya, Peradeniya, Sri Lanka
H. Annersten, University of Uppsala, Uppsala, Sweden

The spinel structure is described as a double oxide, AB_2O_4, where A and B occupy tetrahedral and octahedral sites respectively. Such an arrangement is known as the "ordered" cation distribution denoted by $(A)[B_2]O_4$. The opposite extreme is the "disordered" arrangement $(B)[AB]O_4$ which is frequently found in natural spinels. Other distributions between these two extremes are also possible.

The chemical analyses of natural spinels has been performed by using a Cameca SX 50 automated electron microprobe. The lattice constants and the distribution of Al among the octahedral and tetrahedral sites in the spinels were determined using a Phillips PW 1710 X-ray powder diffractometer and a ^{27}Al-MAS-NMR spectrometer respectively. Mössbauer spectroscopic technique was used to obtain further information on the nature of the site of iron in the natural spinels. The variation of the lattice constants with temperature was studied by x-ray powder diffraction.

Spinels contain high amounts of FeO (0.6-3.5 wt%) and ZnO (0.07-4.50 wt%) besides the major consistents of Al_2O_3 and MgO. Among the other transition metals ions, iron is the predominant element and its concentration was found to be in the range 0.5-1.8% by weight. In most samples iron is found predominantly as Fe^{2+} in the tetrahedral sites.

The spinels belonging to the cubic space group have cell parameters ($a=b=c$) in the range 8.087-8.091 Å. The observed decrease in the cell edge with increasing temperature is in general agreement with the expected behavior of cell parameters with increasing disorder in the spinel structure. The results also indicate that, complete ordering of natural spinels occurs at 280±175°C. Disorder in the cation distribution as measured by the fraction of Al in the tetrahedral site described by the inversion parameter, x, increased with temperature from 0 to 0.13 at 1000°C.

This study indicate that, the natural spinels have ordered cation distribution as regard to Al^{3+}, Fe^{3+}, Fe^{2+} and Cr^{3+}. Cation distribution also depends on the heat treatment of the crystals.

3P49

STRUCTURAL STUDIES ON α- AND β-FORMS OF POLY (TETRAMETHYLENE SUCCINATE)

K. Noguchi, Y. Igarashi, and K. Okuyama, Faculty of Technology, Tokyo University of Agriculture and Technology, Koganei Tokyo 184, Japan
Y. Ichikawa, M. Imaizumi, and Y. Moteki, Showa Denko K. K., Kawasaki Plastics Laboratory, Chidori-cho, Kawasaki-ku Kawasaki 210, Japan
T. Fujimaki, Showa High Polymer Co. Ltd., Kanda-Nishiki-cho, Chiyoda-ku Tokyo 101, Japan

Recently, much attention is being denoted to biodegradable polymers, especially from the ecological viewpoint. It is well known that some of synthetic aliphatic polyesters, such as poly(tetramethylene succinate) (PTMS), poly(ethylene succinate) and their copolymers, show excellent biodegradability. These are crystalline polymers. Physical properties of crystalline polymers, in general, depend strongly on their crystal structure. The molecular conformation and crystal structure of PTMS (α-form) were first investigated by Chatani and coworkers (1971). Recently, we found that the new crystal modification of PTMS (β-form) was induced by strain (Y. Ichikawa et al. 1994). The solid-state crystal transition from the α-form to the β-form and *vice versa* was found to be reversible with respect to the repeated application and removal of strain. In order to clarify the crystal transition mechanisms of PTMS, their crystal structures have been investigated by an X-ray diffraction method. Diffraction patterns were recorded using an Imaging Plate system (DIP-100S, Mac Science) with graphite monochromatized CuKα radiation. All the 36 observed reflections of α-form could be indexed in terms of a monoclinic cell with cell dimensions of $a = 5.23(2)$, $b = 9.12(3)$, c(fiber axis) = 10.90(5) Å, and $\beta = 123.9(2)°$. Two plausible structural models were obtained for α-form (model A, $R = 0.14$; model B, $R = 0.20$). Model A was essentially the same as that proposed by Chatani and coworkers. Its chain conformation is T_7GTG. On the other hands, the observed fiber period of β-form (11.90 Å) indicates that the chain conformation is planar zigzag (all *trans*, T_{10}). The detailed structure analysis of β-form is now in progress.

Chatani, Y., Hasegawa, R., & Tadokoro, H., (1971). A. Meet., Soc. Polym. Sci. (Japan), page 420.
Ichikawa, Y., Suzuki, J., Washiyama, J., Moteki, Y., Noguchi, K. & Okuyama, K., (1994). *Polymer* **35**, 3338-3339.

3P50

ON THE INTERPRETATION OF SMALL ANGLE SCATTERING DATA

T M Sabine, W K Bertram and L P Aldridge
Advanced Materials Program, ANSTO, Menai, NSW 2234, Australia

The results of a small angle scattering experiment are usually presented as a graph of I(q) versus q. This graph is then compared with calculations of the scattering profile to be expected from inhomogeneities of different shapes and sizes to obtain information about the micro-structure of the specimen. The shape of the profile is determined by the square of the form factor of the scattering object which is designated F(q) and normalised so that F(0) equals unity.

It is proposed that $[F(q)]^2$ is expanded in powers of the variable x_j which is defined by the equation

$$x_j = \frac{1}{\sqrt{1+\frac{1}{3}(qR_j)^2}}$$

R_j is a parameter with the dimensions of length specifying an average size or correlation length in the scattering object. In the Guinier region, ($q \to 0$), $x_j \to \exp(-\frac{1}{6}(qR_j)^2)$ while in the Porod region, $(q \to \infty)$, $x_j \to \frac{\sqrt{3}}{qR_j}$.

It will be demonstrated that the first, second and fourth powers of x_j give excellent approximations to the classical solutions for the rod, the disc and the sphere respectively while non-integral powers provide the modern fractal type solutions.

The use of this method for the interpretation of small angle neutron scattering data from hydrating cement will be described.

3P52

Crystal Structures of the copper complexes toward the functional model compound of Dopamine β-Hydroxylase

C. Li; N. Kanehisa; Y. Kai; S. Itoh; T. Kondo; M. Komatsu; Y. Ohshiro; S. Fukuzumi, Department of Applied Chemistry, Faculty of Engineering, Osaka University, Suita 565, JAPAN

Dopamine β-hydroxylase catalyzes the ascorbate dependent benzylic hydroxlation of phenyethylamines such as dopamine to the corresponding norepinephrine. However its functional models are very rare up to now. In order to mimic the enzyme active center, we synthesized [Cu(II)(py2phe)(ClO_4)$_2$] (py2phe =N, N-bis[2-(2-pyridyl)ethyl 2-phenylethylamine) in which a phenethylamine (substrate) moiety is in corporated into the ligand. After [Cu(II)(py2phe)(ClO_4)$_2$] was treated with an equimolar amount of benzoin and triethylamine in CH_2Cl_2(5ml) at room temperature, its product was found to be a dimer. The ligand hydroxylation occurred selectively at the benzylic position of the substrate moiety, which was confirmed by its x-ray crystal structure analysis. Crystal structure analysis also found its crystal belongs to monoclinic system, space group *P21/c*, a=16.176(2), b=15.082(2), c=41.608(2)Å, β=96.54(1)°, V=10084(1)Å^3, Z=8, Dc=1.51gcm^{-3}. Two molecules were found in the asymmetric unit. Final R and Rw values were 0.070 and 0.069, respectively. The dimer(ORTEP) has an approximate C_2 symmetry, and both copper ions also have nearly square pyramidal structures. Details of its structure information and comparison with other enzyme structures will be discussed in our report.

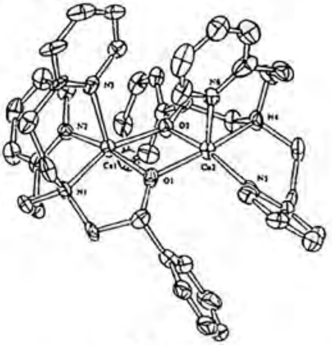

ORTEP

1)Stewart, L. C.; Klinman, J. P. *Annu. Rev. Biochem.* 1988, 57, 551
2)Thompson, J. S. *J. Am. Chem. Soc.* 1984, 106, 8308
3)Amadei, E. *et al. J Chem. Soc., Chem. Commun.* 1992, 1782
4)Itoh, S et al. *J. Am. Chem. Soc.* 1995, 117, 4714

OP53

[illegible]

[illegible] Department of Applied [illegible] Faculty of [illegible]

[illegible]

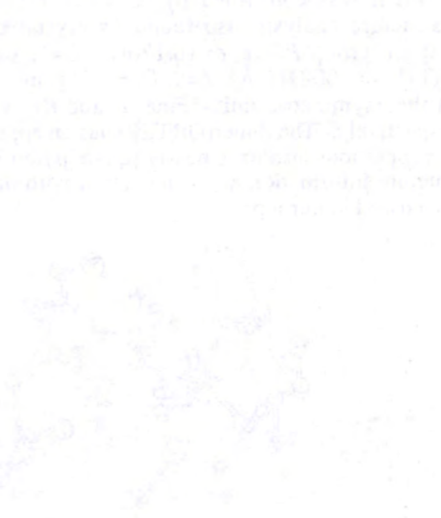

[illegible]

[illegible]

Author Index

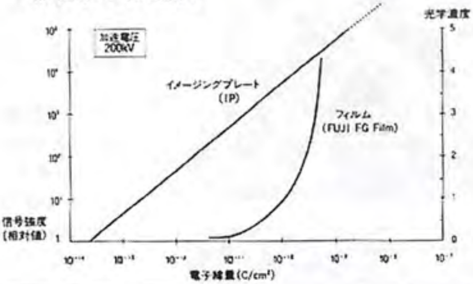
加速電圧
200kV
イメージングプレート
(IP)
フィルム
(FUJI FG Film)
信号強度
(相対値)
1
10^1
10^2
10^3
10^4
10^5
光学濃度
0
1
2
3
4
5
10^{-14}
10^{-13}
10^{-12}
10^{-11}
10^{-10}
10^{-9}
10^{-8}
10^{-7}
電子線量(C/cm²)

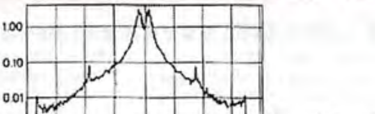
1.00
0.10
0.01
0.0
10.0
20.0
30.0
40.0
50.0
60.0
70.0
80.0
mm

PW3050

全自動多目的X線回折装置

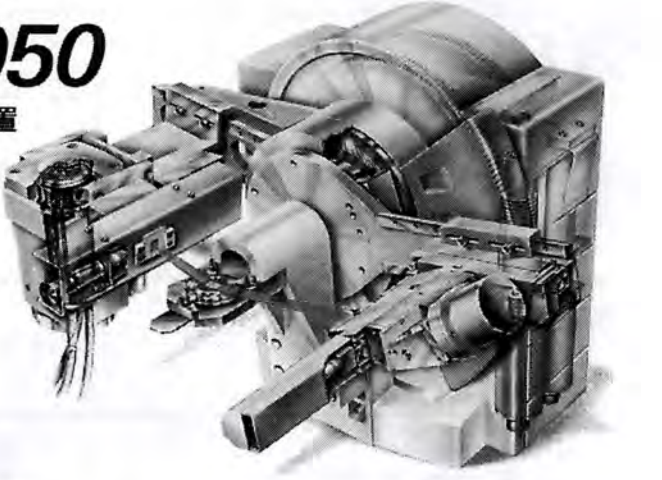

セラミック絶縁X線回折管球

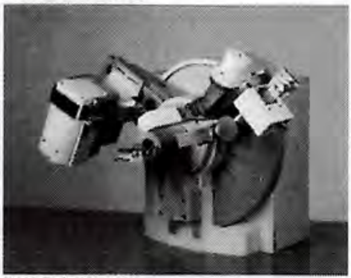

試料水平ゴニオメータ

PW3050システム

ウィンドウズ対応PC-APDソフトウェア

試料を中心に発想すると、X線回折装置はこうなります。

- ●試料に制約を与えません。
- ■傾けると測定に不都合を与える試料（液体、高温加熱試料、粉体）、温度可変、真空排気、ガス排気接続のため試料ステージを水平に保持が条件の試料も、容易に測定
- ■大型試料も容易に装着可能
- ●試料水平ゴニオメータで角度設定再現性0.0001°、小型軽量セラミックス管球との組み合わせで高精度測定を実現しました。
- ●各種アプリケーションに最適な光学系を、自動切り換え、調整します。
- ■全スリット（発散スリット、散乱スリット、受光スリット）はDCモータ駆動の自動スリットのため、バックグラウンドが低く、高分解能で、高いS/Nのデータ測定が可能
- ■ダブル検出器アームはスリットやモノクロメータの調整、交換の必要なしに、平行ビーム法と集中法が切り換えられる方式で、通常の測定から薄膜測定にワンタッチで切り換え可能

日本フィリップス株式会社 産業機器事業部/X線分析営業部

本　　社　〒108 東京都港区港南2-13-37（フィリップスビル） TEL（03）3740-5171（直通）
大阪支店　〒532 大阪市淀川区宮原3-5-36（新大阪第2森ビル） TEL（06）350-3814（直通）
九州支店　〒812 福岡市博多区綱場町8-2（朝日生命福岡昭和通りビル） TEL（092）282-8108（直通）
筑波営業所　〒305 茨城県つくば市竹園2-8-6（つくしビル） TEL（0298）52-9940（代表）
アプリケーションラボラトリー　〒108 東京都港区港南2-13-34（フィリップステクニカルセンター） TEL（03）3740-5370（代表）

Philips
Analytical
X-Ray

PHILIPS

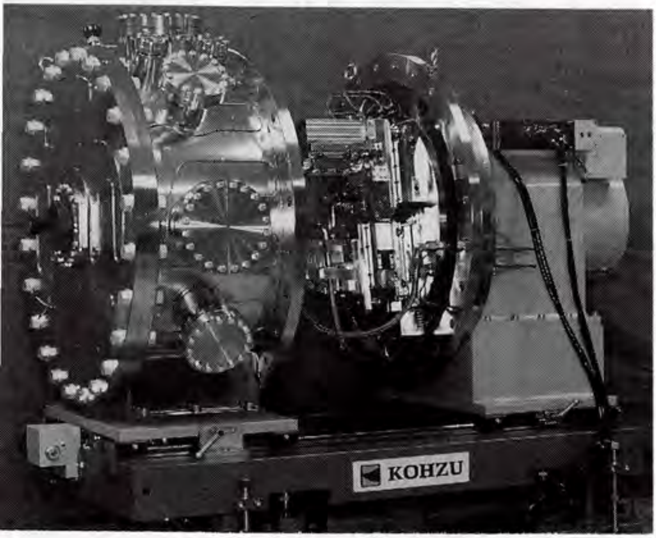

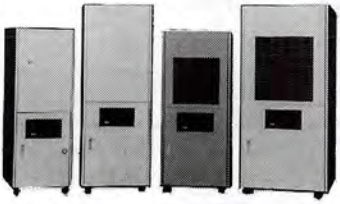

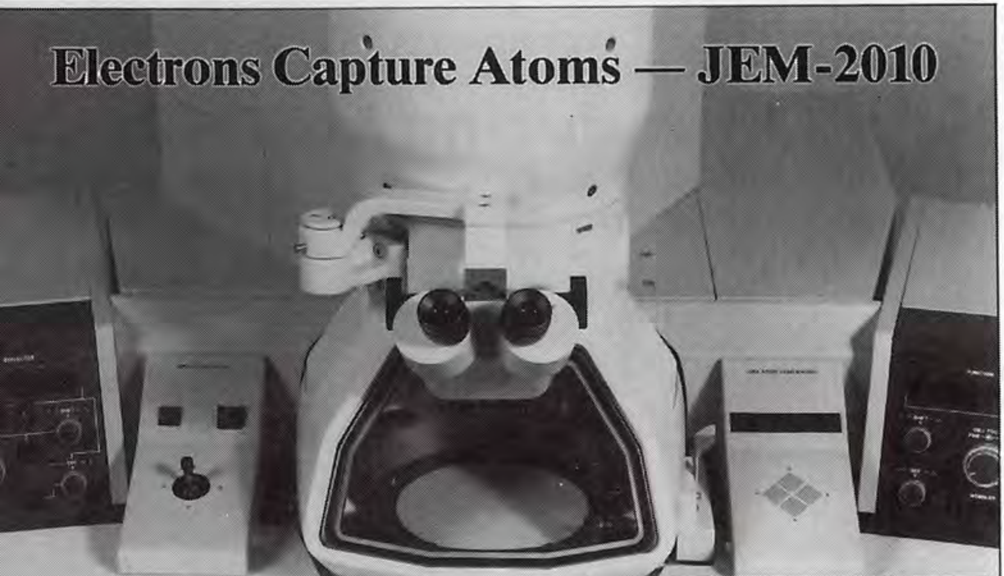

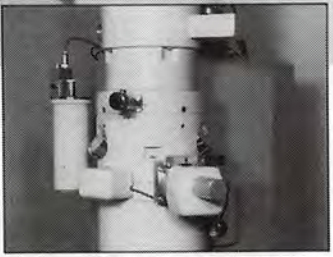

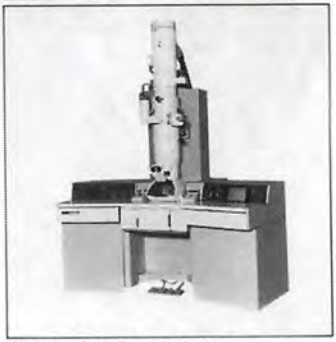

Optional functions included

The NONIUS FR591 ROTATING ANODE X-RAY GENERATOR

Power, ease of use and reliability

Analytical and research scientists applying a strong laboratory X-ray source, need a powerful, easy to use, safe and very reliable rotating X-ray generator. Knowing this, NONIUS now offers: the NONIUS FR591 Rotating Anode X-ray Generator.

Power-features:

- maximum 18 kW;
- high flux / high brilliance X-ray beam of proven unparalleled stability (< 0.01%);
- wide choice of target material and focal dimensions.

Ease-of-use-features:

- expert program for generator control supports automatic filament formation and tube conditioning;
- straight forward operator control menu;
- remote control through PC;
- perfect accessibility of sample.

Reliability-features:

- automatic self-test at start up;
- monitoring of filament current and optimized anode speed result in long operating periods without maintenance;
- integrated diagnostic menu for effective trouble shooting.

Call or fax us today for more information.

NONIUS
DELFT
INSTRUMENTS

NONIUS B.V., P.O. Box 811, 2600 AV Delft, The Netherlands,
Tel.: 31 (0)15 698300, Fax: +31 (0)15 627401.
Enraf-Nonius Ltd., UK, Tel.: 44 72 784 3939, Fax: 44 72 784 2185.
Nonius SA, France, Tel.: 33 14 509 0404, Fax: 33 14 509 2287.
Enraf-Nonius Co., USA, Tel.: 1 516 589 2885, Fax: 1 516 589 2068.
Enraf-Nonius GmbH, Germany, Tel.: 49 212 587 50, Fax: 49 212 587 549.

NONIUS
The choice for
quality & reliability


marresearch


Human lipase-colipase
LOL II · N2 fragment
Catalytic Triad Nat

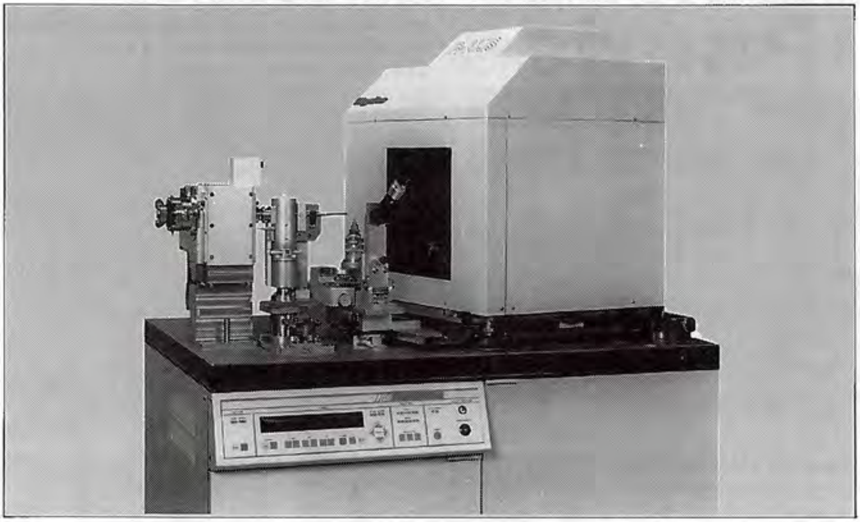

Material®
Analysis and
Characterization

Structure analysis has become
FASTER & EASIER

Highest Performance IP Systems

FASTEST *Spiral Readout*
LARGEST *10^6 Dynamic Range*
HIGHEST *Single Photon sensitivity*
GREATEST *choice suited to your needs.*

Image Plates for X-ray Diffraction

DIPseries

These highly compact dual image plate system rapidly records data for applications ranging from small molecule to the very largest macromolecular assemblies. Small moiety data can be collected in just a few hours, macromolecular data can be collected extremely rapidly due to the fast readout and high sensitivity of these systems.

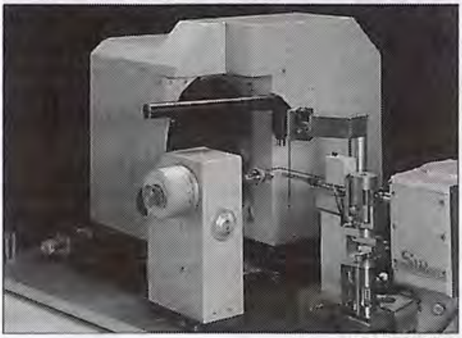

DIP-2000

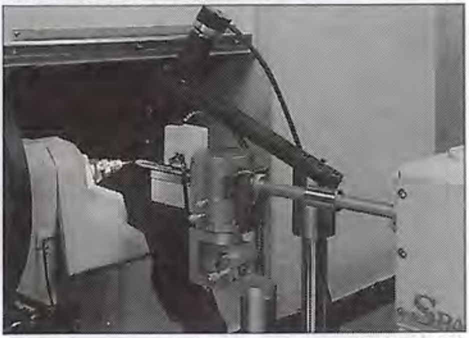

DIP-3000

MAC Science's single crystal X-ray Diffraction systems

MXCseries

MAC Science has developed these extremely fast and highly accurate single crystal diffractometers to meet the growing needs of researchers. The highly flexible data collection software allows these systems to be used for the most difficult applications.

High speed single crystal Kappa-mini diffractometer with sealed source generator : MXC3KHF

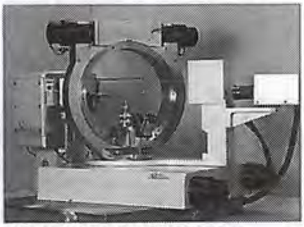

High power Eularian diffractometer and 18kW generator : MXC18HF

CRYSTAN-GM

Fully automatic structure solution package. Complete structural solution in just a few minutes. Complete user control over each step allows handling of the most difficult problems. The friendly GUI and 3D graphics with CIF and other publication outputs make structure solution and reporting fast and simple.

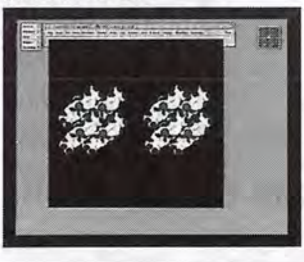

MAC Science Co., Ltd.

SALES OFFICE & RESEARCH LABORATORY
3-12-1 NAKAMACHIDAI, TSUZUKI-KU, YOKOHAMA-SHI, KANAGAWA, 224 JAPA
PHONE : 81-45-943-5855 FAX : 81-45-943-5899

SIEMENS

SMART – Siemens Molecular Analysis Research Tool

SMART's outstanding capabilities include:

- test crystal data set in 1 hr (R1=1.8 %)
- **routine** structures in 1 to 6 hrs
- **high resolution** data sets for electron density studies in less than a day
- **small crystals** down to 10 microns
- **large unit cell** up to 100 Å
- superb **absorption correction** for heavy atom containing compounds
- easy to handle **twin-** and **superlattice** studies and **variable temperature** work
- enabling analysis of **air and moisture sensitive** samples

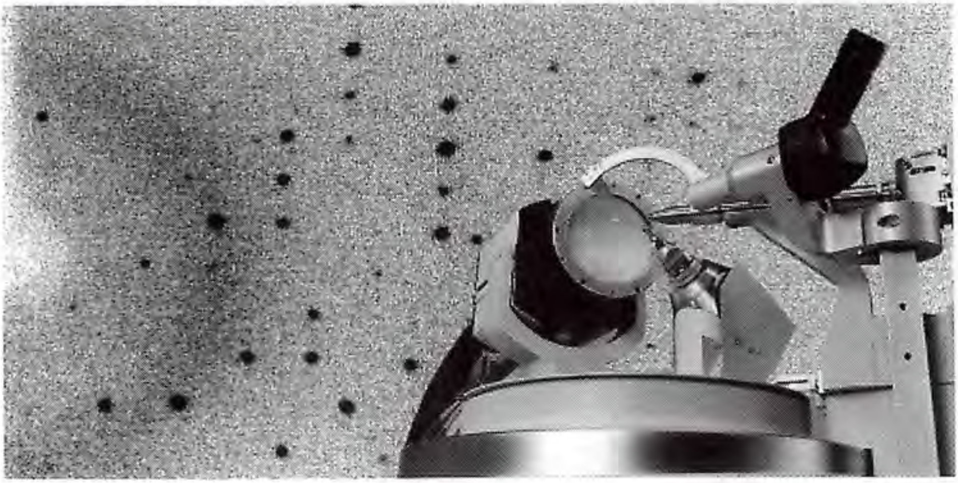

The new CCD single crystal diffraction system

- **reduces data collection time**
- **while improving data quality**

Worldwide contact:

Siemens AG
Analytical X-ray Systems, AUT 37
D-76181 Karlsruhe, Germany
Tel: (49)-721-595-6213
Fax: (49)-721-595-4506

In USA and Canada:

Siemens Industrial Automation, Inc
6300 Enterprise Lane
Madison, WI 53719
Tel: (608) 276-3000, (800) 234-XRAY
Fax: (608) 276-3006

Progress
in Automation.
Siemens